ANA INÊS LOURENÇO DE ALMEIDA

AN APPROACH TO MOLECULAR GENETICS OF THYROID CANCER: FROM NOVEL MUTATIONS TO A ZEBRAFISH MODEL

Tese de candidatura ao grau de

Doutor em Patologia e Genética Molecular

submetida ao Instituto de Ciências Biomédicas Abel Salazar

da Universidade do Porto

Orientador – Doutora Ana Paula Soares Dias Ferreira

Categoria – Professora Auxiliar, Faculdade de Medicina da Universidade do Porto e Coordenadora do Grupo Cancer Signaling & Metabolism, IPATIMUP/Instituto de Investigação e Inovação em Saúde

Afiliação – Faculdade de Medicina da Universidade do Porto e IPATIMUP/Instituto de Investigação e Inovação em Saúde

Coorientador – Miguel Godinho Ferreira

Categoria – Coordenador do Grupo Telomere and Genome Stability, Instituto Gulbenkian de Ciência

Afiliação – Instituto Gulbenkian de Ciência

Financial Support

The candidate was supported by a PhD fellowship (SFRH/BD/79135/2011) from Fundação para a Ciência e Tecnologia (FCT).

There are many people in my life

And then there's you,

To my Dad, to my Mum

Acknowledgments

Thank you to every one of you that came along on my five-year journey.

Believe me, I haven't forgotten each one of you. Yes, you!

Thank you Paula.

Thank you Miguel.

Thank you Professor Sobrinho Simões.

A BIG THANK YOU to my Dad and my Mum.

Prefácio

Eu acredito que cada pessoa tem a sua própria filosofia. Na minha filosofia há uma grande disposição para absorver a experiência da vida e com ela apreciar o mundo. Grande parte da minha satisfação pessoal provém das minhas opções profissionais. Há cinco anos atrás lancei um desafio. Candidatei-me a um programa doutoral. E tracei o meu caminho. Ao longo dele encontrei fraquezas, encontrei esperanças. E fui guardando tudo o que vi, tudo o que fiz. A minha tese reflecte o meu percurso destes cinco anos.

Comecei o meu projecto de doutoramento no grupo Cancer Biology no IPATIMUP, o qual reportou uma elevada prevalência de mutações BRAF em carcinomas papilares da tiróide esporádicos e linhas celulares derivadas destes carcinomas. A procura de factores adicionais que explicassem a tumorigénese do cancro da tiróide potencialmente relacionadas com as mutações do BRAF e a descoberta de mutações no promotor da telomerase permitiram ao grupo explorar estas últimas mutações nas várias séries existentes no banco de tumores. Entretanto, enquanto outros elementos do grupo procuravam perceber mecanisticamente o efeito das mutações no promotor da telomerase, eu foquei-me no desenvolvimento de um modelo animal que permitisse inicialmente compreender o efeito de alterações frequentemente encontradas no cancro da tiróide (mutações nos genes BRAF e p53) e futuramente estudar factores adicionais que agora se sabem terem um papel relevante na tumorigénese tais como as mutações no promotor da telomerase. Por esta altura foi estabelecida uma colaboração com o grupo Telomeres and Genome Stability no IGC passando de uma ciência translacional para uma ciência básica. O desenvolvimento de um modelo para o estudo do efeito das mutações nos genes BRAF e p53 em peixe-zebra foi o fruto dessa colaboração. Deixarei um legado de ferramentas que muitos poderão usufruir.

Publications

Ao abrigo do disposto do nº 2, alínea a) do artigo 31º do Decreto-Lei n.º 115/2013 de 7 de Agosto fazem parte integrante desta tese de doutoramento os seguintes trabalhos já publicados ou submetidos para publicação:

Artigo I - Vinagre J, **Almeida A**, Pópulo H, Batista R, Lyra J, Pinto V, Coelho R, Celestino R, Prazeres H, Lima L, Melo M, da Rocha AG, Preto A, Castro P, Castro L, Pardal F, Lopes JM, Santos LL, Reis RM, Cameselle-Teijeiro J, Sobrinho-Simões M, Lima J, Máximo V, Soares P. 2013. Frequency of TERT promoter mutations in human cancers. Nat Commun. 4:2185.

Artigo II – **Almeida A**, Sobrinho-Simões M, Ferreira MG, Soares P. (Submetido).

O seguinte capítulo de livro não faz parte do corpo principal de resultados desta tese, mas é parte integrante da mesma, tendo sido utilizado na sua Introdução e Discussão.

Appendix I - **Almeida AL**, Boaventura P, Soares P, Clinical Management of Thyroid Cancer: Etiopathogenic factors of thyroid cancer, Pages 46-62, Future Medicine. 2013

Table of contents

Abbreviations

4-OHT	4-Hydroxyl-Tamoxifen
AKAP9	A Kinase (PRKA) Anchor Protein 9
AKT	V-Akt Murine Thymoma Viral Oncogene Homolog
ALK	Anaplastic Lymphoma Receptor Tyrosine Kinase
AMP	Adenosine Monophosphate
ARAF	A-Raf Proto-Oncogene, Serine/Threonine Kinase
ATC	Anaplastic Thyroid Cancer
ATP	Adenosine Triphosphate
attL	Left End of Prophage
attR	Right End of Prophage
BAC	Bacterial Artificial Chromosome
BCL2	B-Cell Lymphoma 2
BF	Bright Field
BMI	Body Mass Index
bp	Base Pairs
BRAF	B-type Raf kinase
cAMP	Cyclic Adenosine Monophosphate
CCDC6	Coiled-Coil Domain Containing 6
CDE	Cell Cycle-Dependent Element
CDK	Cyclin-Dependent Kinases
CDKN2A	Cyclin-Dependent Kinase Inhibitor 2A
CFP	Cyan Fluorescent Protein
CHR	Cell Cycle Genes Homology
cmcl2	Cardiac Myosin Light Chain
CMV	Cytomegalovirus
CNS	Central Nervous System
CPT	Carcinoma Papilar da Tiróide
CRAF	C-Raf Proto-Oncogene, Serine/Threonine Kinase
Cre	Cre Recombinase
CreER	Cre Recombinase-Estrogen Receptor
ctsb	Cathepsin B
DBD	DNA-Binding Domain
DEPC	Diethylpyrocarbonate

dpf	Days Post Fertilization
DNA	Deoxyribonucleic Acid
dpi	Days Post Injection
EDTA	(Ethylenedinitrilo)tetraacetic Acid
EGFP	Enhanced Green Fluorescent Protein
EGTA	Ethylene Glycol Tetraacetic Acid
Erg	ETS-Related gene
ERK	Extracellular Regulated Kinase
ETS	Erythroblast Transformation-Specific
FCT	Fundação para a Ciência e Tecnologia
Fos	FBJ murine Osteosarcoma Viral Oncogene Homolog
FTC	Follicular Thyroid Carcinoma
GABP	GA-Binding Protein
GBM	Glioblastomas
GDP	Guanosine-5'-Diphosphate
GFRα	GDNF family receptor-α
GIST	Gastrointestinal Stromal Tumor
GTP	Guanosine-5'-Triphosphate
HE	Hematoxylin-Eosin
hhex	Hematopoietically Expressed Homeobox
hpf	Hours Post Fertilization
hpi	Hours Post Injection
HPT	Hypothalamus-Pituitary-Thyroid
HRP	Horseradish Peroxidase
hspl70	Heat shock cognate 70-kd protein, like
IGC	Instituto Gulbenkian de Ciência
IGFBP7	Insulin-like Growth Factor-Binding Protein 7
IgG	Immunoglobulin G
IPATIMUP	Institute of Molecular Pathology and Immunology at the University of Porto
JUN	Jun proto-oncogene
LB	Lysogeny Broth
LKB1	Tumor Suppressor Liver Kinase B1
LOF	Loss Of Function
MAPK	Mitogen-Activated Protein Kinases
mCh	Monomeric mCherry

MCS	Multicloning Site
MDM2	MDM2 proto-oncogene, E3 ubiquitin protein ligase
ME	Middle Entry Clone
MEK	MAP Kinase 1
mpf	Months Post Fertilization
mRNA	Messenger Ribonucleic Acid
MS222	Tricaine Methanesulfonate
mTOR	Mechanistic Target Of Rapamycin
mTORC1	Mammalian Target Of Rapamycin Complex 1
mTORC2	Mammalian Target Of Rapamycin Complex 2
Myc	V-Myc Avian Myelocytomatosis Viral Oncogene Homolog
NCOA4	Nuclear Receptor Coactivator 4
NICD	Notch Intracellular Domain
NIS	Sodium-Iodine Symporter
nk2-1a	NK2 Homeobox 1a
NRAS	Neuroblastoma RAS Viral (v-ras) Oncogene Homolog
NTRK1	Neurotrophic Tyrosine Kinase, Receptor, Type 1
pA	PolyA
PAX2.1	Paired Box Gene 2.1
PAX8	Paired Box 8
PCCL3	Rat Thyroid Follicular Cell Line
PCNA	Proliferating Cell Nuclear Antigen
PCR	Polymerase Chain Reaction
PDK1	Pyruvate Dehydrogenase Kinase, Isozyme 1
PDTC	Poorly Differentiated Thyroid Cancer
phf20l1	PHD Finger Protein 20-Like 1
PI3K	Phosphatidylinositol-4,5-Bisphosphate 3-Kinase
PIK3CA	Phosphatidylinositol-4,5-Bisphosphate 3-Kinase, Catalytic Subunit Alpha
PKA	Protein Kinase A
PMSF	PhenylMethylSulfonyl Fluoride
PPAR	Peroxisome Proliferator-Activated Receptor
PPARG	Peroxisome Proliferator-Activated Receptor Gamma
PRKAR1A	Protein Kinase, cAMP-Dependent, Regulatory, Type I, alpha
PSI	Pounds per Square Inch
PTC	Papillary Thyroid Carcinoma

PtdIns	Phosphatidylinositol
PTEN	Phosphatase and Tensin Homolog
PVDF	Polyvinylidene Fluoride
Rag2	Recombination Activating Gene 2
RAS	Rat Sarcoma Viral Oncogene Homolog
RET	Rearranged during Transfection
RIPA	Radioimmunoprecipitation Assay Buffer
RPM	Revolutions Per Minute
SAP	Shrimp Alkaline Phosphatase
SDS	Sodium Dodecyl Sulfate
SDS PAGE	Sodium Dodecyl Sulfate Polyacrylamide Gel Electrophoresis
Ser	Serine
SETDB1	SET Domain, Bifurcated 1
siRNA	Small Interfering Ribonucleic Acid
SL	Standard Length
slc5a5	Solute Carrier Family 5 (Sodium/Iodide Cotransporter), Member 5
SV40	Simian Vacuolating Virus 40
T2A	Thoseaasigna virus 2A
T3	Tri-Iodothyronine
T4	Thyroxine
TAE	Tris base, acetic acid and EDTA solution
T-ALL	T-cell Acute Lymphoblastic Leukemia
TAM	Tamoxifen
TBE	Tris base, boric acid and EDTA solution
TBS	Tris-Buffered Saline
TERT	Telomerase Reverse Transcriptase
tg	Thyroglobulin
TGB	Thyroxine-Binding Globulin
TGFβ	Transforming Growth Factor Beta
TH	Thyroid Hormone
Thr	Threonine
TK	Tyrosine Kinase
TPO	Thyroid Peroxidase
TRAP	Telomeric Repeat Amplification Protocol
TRH	Thyrotropin-Releasing Hormone

Tris-Cl	Tris(hydroxymethyl)aminomethane Chloride
TSH	Thyroid Stimulating Hormone
TshR	Thyroid Stimulating Hormone Receptor
WDTC	Well-Differentiated Thyroid Cancer
WHO	World Health Organization
WT	Wild-type

Abstract

Thyroid diseases are extremely frequent and are most often of benign nature. Thyroid cancer is the most common endocrine malignancy in humans and the majority of tumors harbor genetic alterations such as the *BRAF* mutation. Most of this mutation is an activating mutation in the kinase domain of the BRAF. In sporadic papillary thyroid carcinomas (PTCs), *BRAF* gene mutations are found in 29%–83% of all cases and almost never co-exist with *RAS* mutations or *RET* (*RET*/PTC) and *NTRK1* rearrangements. As a result of *BRAF* mutation, the MAPK pathway is activated and cellular processes such as proliferation, survival, motility and invasion are promoted. Recently, mutations in the telomerase reverse transcriptase (*TERT*) promoter have been described in thyroid cancer and considered one of the possible mechanisms that underlies TERT reexpression in several types of human tumors including those of the thyroid.

In the first part of the thesis, I describe the study regarding *TERT* promoter mutations in which I was deeply involved. Our study highlighted the presence of recurrent somatic mutations in the *TERT* promoter in cancers of the central nervous system (43%), bladder (59%), thyroid (follicular cell-derived, 10%) and skin (melanoma, 29%). Concerning thyroid cancer, the presence of *TERT* promoter mutations was found to be significantly associated with higher *TERT* mRNA expression and with older age of the patients. We concluded that *TERT* promoter mutations are relatively frequent in several specific types of human cancer and that such mutations may enhance expression of telomerase.

Over the years, thyroid cancer has been studied using mice models. These models have provided evidence showing that thyroid-specific expression of $BRAF^{V600E}$ induced goiter as well as invasive PTCs which progress to poorly differentiated carcinoma closely recapitulating some human thyroid tumor phenotypes. Very successful, mice models of thyroid cancer are being used to explore molecular mechanisms involved in thyroid tumorigenesis. Mice models can also be used to monitor tumors and to perform drug screening in the setting of thyroid cancer but such tasks remain time-consuming.

In the second part of the thesis, I developed a thyroid-targeted $BRAF^{V600E}$-expressing transgenic zebrafish and evaluated the thyroid tissue phenotypes

during all stages of development up to 12 months of age. I observed that thyroid-specific expression of $BRAF^{V600E}$ induced abnormal thyroid morphogenesis early in life that developed later on into hyperplasia by ~2-3 months of age and colloid goiter by 12 months of age. $BRAF^{V600E}$-expressing cells disclosed upregulation of proliferation, concomitant with MAPK pathway activation, and there was promotion of apoptosis. High levels of p53 suggested that this protein may be restraining progression to malignancy. Loss of WT p53 using a *tp53*^{M214K} zebrafish prevented impairment of thyroid morphogenesis induced by $BRAF^{V600E}$ and surprisingly no evidence of thyroid hyperplasia, goiter and/or neoplasia was detected in those animals up to 12 months of age. *tp53*^{M214K} $BRAF^{V600E}$-expressing cells were low proliferative, consistent with downregulation of the MAPK pathway; suppression of apoptosis was also observed.

In conclusion, my work showed that *TERT* promoter mutations are relatively frequent in specific types of human cancer, including those of the thyroid, and that may enhance telomerase expression. Also, thyroid-specific expression of $BRAF^{V600E}$ induces hyperplasia and colloid goiter in zebrafish and together with the absence of WT p53, $BRAF^{V600E}$ was not able to develop thyroid cancer. This data provides evidence that BRAF activation is sufficient for thyroid cell transformation and that BRAF and p53 pathways must interact genetically in zebrafish thyroid.

Resumo

As doenças na tiróide são extremamente frequentes e são geralmente de natureza benigna. O cancro da tiróide é o tumor endócrino maligno mais comum em humanos e a maioria destes tumores possui alterações genéticas tais como a mutação no gene *BRAF*. A maioria das mutações do *BRAF* activam o domínio de cinase da proteína BRAF. Em carcinomas papilares da tiróide (CPT) esporádicos, as mutações no gene *BRAF* são encontradas em 29% a 83% do total de casos e quase nunca co-existem com as mutações do *RAS* e rearranjos do *RET* (*RET*/PTC) e *NTRK1*. Como resultado das mutações do *BRAF*, a via de sinalização das MAP cinases é activada e processos celulares, tais como proliferação, sobrevivência, motilidade e invasão, são promovidos. Recentemente, foram descritas mutações no promotor da telomerase transcriptase reversa (*TERT*) e estas são consideradas um dos possível mecanismos de reexpressão da telomerase em vários tipos de cancro humano incluindo os da tiróide.

Na primeira parte da tese eu descrevo o estudo relativo às mutações no promotor da *TERT* no qual eu estive envolvida. O nosso estudo realçou a presença de mutações somáticas recorrentes no promotor da *TERT* em tumores como os do sistema nervoso central (43%), da bexiga (59%), da tiróide com origem nas células foliculares (10%) e da pele (melanoma) (29%). Relativamente ao cancro da tiróide, foi encontrada uma associação significativa entre a presença de mutações no promotor da *TERT* e níveis elevados de expressão de mRNA e também uma associação com pacientes mais velhos. Concluímos que as mutações no promotor da *TERT* são relativamente frequentes em determinados tipos de cancro humanos e que estas mutações podem aumentar a expressão da TERT.

Ao longo dos anos, o cancro da tiróide tem sido estudado usando modelos de ratinho. Estes modelos deram evidências que demonstram que a expressão específica de $BRAF^{V600E}$ induziu bócio bem como CPT invasivos que progrediram para carcinomas pouco diferenciados recapitulando alguns dos fenótipos dos tumores de tiróide humanos. Os modelos de ratinho ainda são usados para explorar mecanismos moleculares envolvidos na tumorigénese da tiróide. Estes modelos podem também ser usados para monitorizar tumores e para realizar ensaios de drogas no contexto do cancro da tiróide mas estas tarefas são morosas.

Na segunda parte do tese eu desenvolvi uma linha transgénica com expressão específica de $BRAF^{V600E}$ na tiróide de peixe-zebra e avaliei os fenótipos na tiróide durante todos os estádios de desenvolvimento e até aos doze meses de idade. Observei que a expressão específica de $BRAF^{V600E}$ na tiróide induziu uma morfogénese anormal deste tecido em estádios iniciais que se desenvolvem em hiperplasia aos 2-3 meses de idade e bócio colóide ao fim de 12 meses. Células da tiróide que expressavam $BRAF^{V600E}$ tinham uma sobreregulação da proliferação, concomitante com a activação da via de sinalização das MAP cinases, e foi observada indução da apoptose. Nível elevados de p53 sugerem que esta proteína pode ter contido a progressão para malignidade. Perda da proteína selvagem de p53, usando uma linha homozigota para a mutação *M214K* do *tp53*, preveniu morfogénese anormal da tiróide induzida pelo $BRAF^{V600E}$ e surpreendentemente não foram encontradas evidências de hiperplasia, bócio e/ou carcinomas em peixes até doze meses de idade. Células da tiróide que expressavam $BRAF^{V600E}$ eram pouco proliferativas, consistente com desregulação da via de sinalização das MAP cinases, e foi observada supressão da apoptose.

Em conclusão, o meu trabalho demonstrou que as mutações no promotor da *TERT* são relativamente frequentes em determinados tipos de cancro humanos, incluindo os da tiróide, e podem aumentar a expressão da TERT. A expressão específica de $BRAF^{V600E}$ induziu hiperplasia e bócio colóide em peixe-zebra e que em conjunto com a ausência da proteína p53, o $BRAF^{V600E}$ não foi capaz de induzir cancro na tiróide. Estas observações demonstram evidências de que a activação do BRAF é suficiente para a transformação de células da tiróide e que as vias de sinalização da qual fazem parte o BRAF e o p53 devem interagir geneticamente na tiróide do peixe-zebra.

Chapter I

Introduction

THE HUMAN ENDOCRINE SYSTEM comprises part of the body's communication system connecting the brain to the organs which in turn control the metabolism, growth and reproduction. Tight control of the system is possible through complex feedback mechanisms that maintains homeostasis. Any disruption to an endocrine gland or to the feedback mechanisms may result in endocrine disturbance. Ultimately, cancer may either contribute or be the outcome of such disturbance.

I.1 Thyroid gland

The human thyroid gland is a butterfly-shaped gland located on the trachea and comprises two lobes connected by an isthmus (VanPutte et al., 2010). The gland is highly vascularized and is one of the largest endocrine glands in the human body (VanPutte et al., 2010). The thyroid gland comprises numerous and varying sized follicles consisting of a thin-layer of cuboidal epithelial cells and a central lumen. The lumen is filled with a homogeneous protein-rich colloid named thyroglobulin which is essential to thyroid hormone (TH) synthesis (Manson et al., 1973; VanPutte et al., 2010). Two hormones are produced in the thyroid gland by the follicular cells in response to thyroid-stimulating hormone (TSH) released from the pituitary: tri-iodothyronine (T3) and thyroxine (T4). These hormones have an effect on all body systems at all stages of life regulating the basal metabolic rate and tissue growth and maturation (Manson et al., 1973; Kumar et al., 2005; VanPutte et al., 2010). Parafollicular cells secreting calcitonin are also found in clusters surrounding the follicles and in the connective tissue (VanPutte et al., 2010).

I.1.1 Thyroid physiology

Thyroid follicles are the factory and the storage of THs. The presence of TSH is indispensable for the synthesis and secretion of THs as well as an adequate iodide nutrition.

The first step in the synthesis of THs is the uptake of iodide by sodium-iodine symporter (NIS) which is converted to iodine and then condensed onto tyrosine residues from the backbone of thyroglobulin, a protein produced inside the thyroid cells. The newly formed iodothyroglobulin can be either mono-iodinated or di-iodinated. When coupled, two di-iodotyrosine molecules result in the formation of

T4 whereas a di-iodotyrosine coupled with a mono-iodotyrosine results in T3. Although the T3 is more biologically active than the T4, the production of T3 occurs preferentially outside the thyroid gland by peripherical conversion from T4. THs are stored inside the thyroid follicles composing the majority of the colloid material. T3 and T4 are released by proteolysis from the thyroid to the bloodstream where they bind to TH binding proteins namely the thyroxin binding globulin (TBG) (Figure 1) (Kumar et al., 2005; Brix et al., 2011).

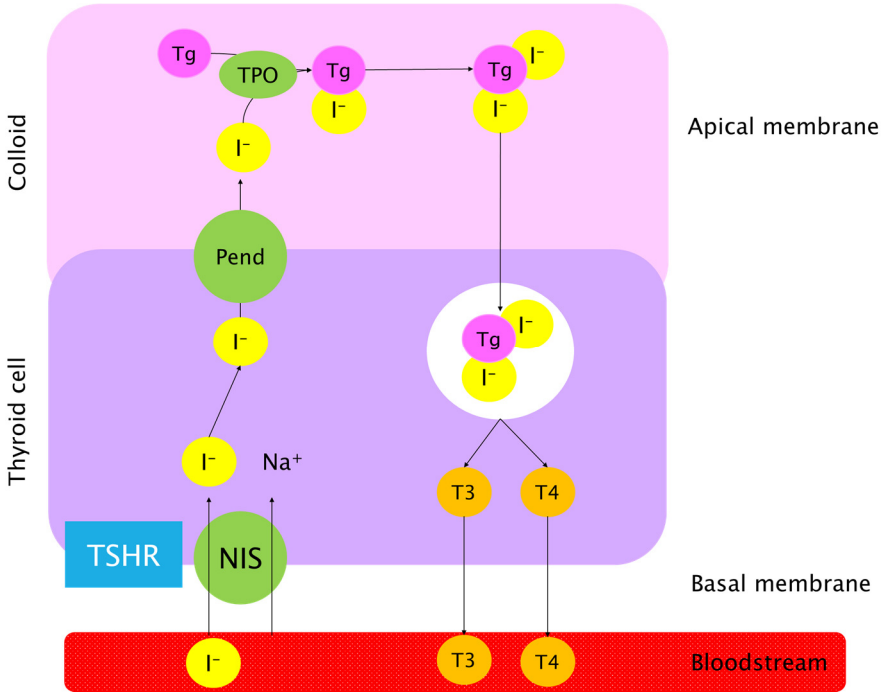

Figure 1. **TH synthesis.** TSH signaling via the TSH receptor controls TH synthesis. NIS at the basolateral membrane takes up iodide from the blood. Iodide is organified in the tyrosyl residues of *tg* in a reaction catalyzed by thyroid peroxidase (TPO). T_3, and T_4 are stored in colloid until they are released into the blood.

I.1.2 Thyroid disorders

Thyroid disorders can range from an enlarged thyroid gland that does not need treatment to thyroid cancer. The most common thyroid problems include goiter and benign thyroid nodules. Also relatively frequent, and clinically more evident, is the abnormal production of TH that can be classified into two groups: hyperthyroidism and hypothyroidism (Manson et al., 1973; VanPutte et al., 2010).

In hyperthyroidism, the thyroid gland is overactive producing high levels of thyroid hormones and speeding up the metabolism. Graves' disease also known as toxic diffuse goiter is the most common cause of hyperthyroidism (Manson et al., 1973; VanPutte et al., 2010). In hypothyroidism, the thyroid gland is underactive producing inadequate levels of thyroid hormones and slowing down the metabolism. Hashimoto's thyroiditis, congenital hypothyroidism and irradiation are some of the causes of hypothyroidism (Manson et al., 1973; VanPutte et al., 2010).

The proper treatment of hyperthyroidism and hypothyroidism depends on the symptoms of the disease and the aetiology. In hyperthyroidism, treatments include thiouracils or thioamides, radioiodine therapy, thyroidectomy, radioactive iodine and/or beta blockers. In hypothyroidism, levothyroxine is a hormone replacement used for treatment (VanPutte et al., 2010).

I.1.2.1 Goiter

A goiter is an enlarged thyroid gland, it can be either diffuse or nodular and it may extend into the retrosternal space with or without substantial anterior enlargement (Kumar et al., 2005; Lam et al., 2014).

A deficiency in iodine intake or in TH synthesis leads to an increased TSH production which in turn sustains increased cellularity and hyperplasia of the thyroid gland as an attempt to normalize the levels of the TH. TH deficiency can be due to defects on hormone synthesis, iodine deficiency and goitrogens (Figure 2). Also, a goiter may appear as a result of the stimulation of the thyroid gland by thyroid stimulating hormone receptor (TshR) agonists such as TSH receptor antibodies, pituitary resistance to thyroid hormone, adenomas of the hypothalamus or pituitary gland and human chorionic gonadotropin-producing tumours (Kumar et al., 2005; Lam et al., 2014).

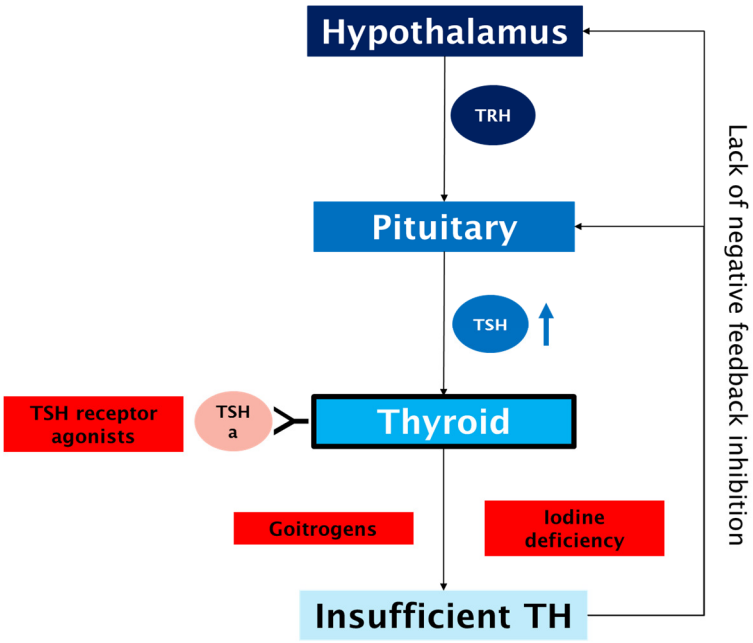

Figure 2. **Relation between hypothalamus-pituitary-thyroid (HPT) axis and human goiter development**. Iodine deficiency and/or goitrogens disrupt the TH synthesis in many ways. Upon insufficient TH levels, the negative feedback inhibition is lost resulting in increased secretion of tropic hormones (TRH and TSH). High TSH levels stimulate thyroid cells promoting goiter. Also, TSH receptor agonists can ilicitly mimick the biological activity of TSH.

Small benign euthyroid goiters do not require any treatment, however their size may be reduced with levothyroxine suppressive therapy. Large and complicated goiters usually require surgical and/or radiation treatment followed by TH replacement (Kumar et al., 2005; Lam et al., 2014).

I.1.2.2 Neoplasias

Thyroid cancer is the 16th most common cancer worldwide and accounts for approximately 2% of total of human malignancies with around 298.000 new cases diagnosed in 2012 worldwide (latest data reported) (Nikiforov, 2012; Ferlay et al., 2013). Incidence rates of thyroid cancer are highest in Northern America and other developed countries and lowest in western Africa but this is partly due to data quality and reflects different prevalence of risk factors and screening and

diagnostic methods used (Nikiforov, 2012; Ferlay et al., 2013). Although incidence rates have increased in most countries, mortality rates have decreased and remained low. There were approximately 37.800 deaths worldwide from thyroid cancer in 2012 corresponding to 0.5% of total cancer deaths (Nikiforov, 2012; Ferlay et al., 2013).

Thyroid cancer represents the most common type of endocrine malignancy although it is relatively rare when compared to benign thyroid tumors. Thyroid cancer occurs primarily in youngsters and middle aged adults whilst in children is rare. The incidence of thyroid cancer is four times higher in females than in males and this sex difference it less pronounced in children and older adults (DeLellis et al., 2004; Nikiforov, 2012).

According to the current World Health Organization (WHO) classification, thyroid tumors can be subdivided into primary and secondary or metastatic tumors (DeLellis et al., 2004). While most of the primary tumors are epithelial and originated from the thyroid follicular cells, a lower number of cancers derive from neural crest-derived parafollicular C cells. Follicular thyroid cell-derived tumors can be benign (follicular adenomas) or malignant (well differentiated follicular and papillary carcinomas, poorly differentiated and undifferentiated/anaplastic carcinomas) and tumors with an uncertain malignant potential (Soares et al., 2011; Nikiforov, 2012) (Figure 3). Also found are the medullary carcinomas which have a C-cell origin (DeLellis et al., 2004). Among malignant tumors, papillary thyroid carcinomas (PTC) constitute about 80% of all thyroid cancer cases and the increased incidence observed in thyroid cancer is mostly due to PTCs. The follicular thyroid carcinomas (FTC) represent 15% and medullary and anaplastic carcinomas about 3% and 2%, respectively, of all thyroid cancer cases. For these tumors, the incidence has not changed significantly (DeLellis et al., 2004; Nikiforov, 2012).

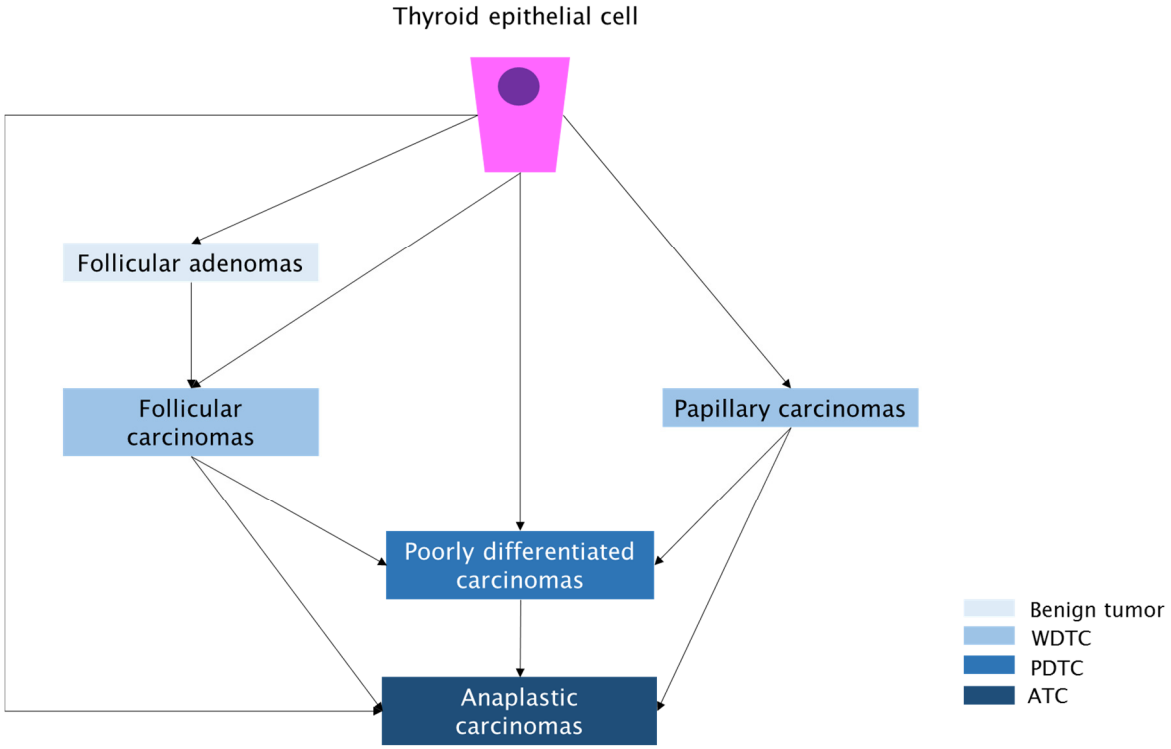

Figure 3. **Follicular thyroid cell-derived tumors and its putative progression.** Scheme of step-wise dedifferentiation of follicular cell-derived thyroid cancer from benign to malignant tumors.

Conventional surgical thyroidectomy and adjuvant ablation by radioiodine treatment are the standard treatments for follicular thyroid cell-derived tumors. These treatments are not curative in all cases and a big effort is still being made towards understanding the molecular pathogenesis of thyroid cancer, namely of those that show clinical progression (DeLellis et al., 2004; Nikiforov, 2008; Nikiforov, 2012).

Papillary thyroid cancer

The PTC is a malignant epithelial tumor that shows evidence of follicular cell differentiation and is characterized histologically by distinctive nuclear features (DeLellis et al., 2004; Kumar et al., 2005; Nikiforov, 2012).

PTCs are rare in childhood but still are the most common pediatric thyroid tumor. Incidence of PTCs begins to rise in the second decade of life up to the fifth and

sixth decades. Female to male ratio is as high as 4:1 but in older adults the prevalence for females is less pronounced (DeLellis et al., 2004; Kumar et al., 2005; Nikiforov, 2012). Increased accuracy in the diagnosis and changes in the histological WHO criteria have contributed to a very high prevalence of the papillary type among other thyroid carcinomas (DeLellis et al., 2004). Nevertheless, one cannot exclude a real increase in the incidence of PTCs due to iodine supplementation or exposure to radiation and endocrine disruptors especially during childhood (Farahati et al., 2004; Tronko et al., 2006; Frasca et al., 2008; Almeida et al., 2013). Indeed, development of PTC is linked to environmental (mainly radiation exposure), genetic, hormonal factors and interactions between them. Radiation either external or internal from radioactive iodine is a major risk factor and children are the most susceptible as thyroid gland grows during childhood (DeLellis et al., 2004; Kumar et al., 2005; Nikiforov, 2012; Almeida et al., 2013).

PTC is presented as a cold mass on radioactive scan or as a cervical lymphadenopathy. On gross examination, PTCs present a variety of patterns but most masses are grey-white and firm with irregular borders that may infiltrate the surrounding thyroid tissue. Tumor size ranges from less than 1mm to several centimeters and multicentricity and cystic change are commonly observed (DeLellis et al., 2004; Kumar et al., 2005; Nikiforov, 2012).

The diagnosis of a PTC relies mainly in the cytological features observed in the nuclei and on the architecture. This includes enlargement, oval shape, elongation and overlapping of the nuclei, chromatin clearing, irregular nuclear contours, nuclear pseudoinclusions and nuclear grooves. Papillary growth pattern with branching is frequently seen but not required for diagnosis. Also found are intratumoral sclerosis, peritumoral lymphocytic infiltration and psamomma bodies (DeLellis et al., 2004; Kumar et al., 2005; Nikiforov, 2012).

Some PTCs present particular features which represent specific histological variants. The two most frequent variants are the papillary microcarcinomas (30-40%) usually found incidentally and with a tumor size less than 1cm and the follicular variant (15-20%) which has a follicular pattern instead of a papillary pattern, very often absent. Other variants, exhibiting variable clinical behaviors, are less prevalent (solid, tall-cell, sclerosing, etc.) (DeLellis et al., 2004; Kumar et al., 2005; Lloyd et al., 2011; Nikiforov, 2012).

Prognosis is overall excellent with a 20-year survival of 98% and a mortality rate of less that 1% (DeLellis et al., 2004). However, rate of recurrence is highly variable ranging from 5% to 40%. Commonly, PTCs metastasize *via* lymphatic vessels often in the cervical lymph nodes and rarely to the lungs and bones as bilateral, small and diffuse lesions (DeLellis et al., 2004; Kumar et al., 2005; Nikiforov, 2012).

Treatment of PTCs remains surgical. Total thyroidectomy is advised for tumors greater that 1cm and since well-differentiated PTCs are radiosensitive, iodine-131 ablation may be employed as adjuvant therapy (DeLellis et al., 2004; Kumar et al., 2005; Nikiforov, 2012).

Molecular genetics of papillary thyroid cancer

The rapidly understanding of cancer molecular genetics has led not only to a deep insight of cell biology but also to seek prevention and new treatments for cancer. In thyroid cancer as in other human cancers, the success of molecular genetics to further contribute with novel therapeutic approaches, such as targeted molecular therapy, is yet to be fully achieved.

PTCs are characterized by nonoverlapping genetic alterations in more than 70% of the cases. These alterations include rearrangements in the tyrosine kinase (TK) receptors Rearranged-during-transfection (*RET*), Neurotrophic Tyrosine Kinase, Receptor, Type 1 (*NTRK1*), Anaplastic Lymphoma Receptor Tyrosine Kinase (*ALK*) and A Kinase (PRKA) Anchor Protein 9/B-type Raf kinase (*AKAP9*/*BRAF*) and also point mutations in Rat Sarcoma Viral Oncogene Homolog (*RAS*) and *BRAF* genes. Ultimately, most cases will lead to an aberrant activation of the RAS-RAF-MEK-ERK kinase pathway (DeLellis et al., 2004; Kumar et al., 2005; Nikiforov, 2012).

Despite the high frequency of chromosomal rearrangements in PTCs, the predisposition of follicular thyroid cells to undergo those rearrangements is not fully understood. Chromosomal rearrangements are likely to reflect the sensitivity of the follicular thyroid cells to ionizing radiation and/or the intrinsic capacity of cells to repair radiation-induced deoxyribonucleic acid (DNA) double-strand breaks and proneness to aberrant DNA repair instead of apoptosis (Galleani et al., 2014).

BRAF mutations BRAF serine-threonine kinase belongs to the RAF family together with A-Raf Proto-Oncogene, Serine/Threonine Kinase (ARAF) and C-Raf Proto-Oncogene, Serine/Threonine Kinase (CRAF). BRAF is an intracellular effector mediating the response to growth factor signaling through the Mitogen-Activated Protein Kinases (MAPK) pathway which controls cell proliferation and differentiation (McKay et al., 2007). From all the RAF proteins, BRAF has the highest basal kinase activity and it is the most potent activator of the MAPK signaling pathway (Marais et al., 1997).
Most mutations in *BRAF* are activating mutations in the kinase domain. In sporadic PTCs, *BRAF* gene mutations are found in 29%-83% of the cases and are almost exclusive to *RAS* mutations, *RET* (*RET*/PTC) and *NTRK1* rearrangements (Soares et al., 2003; Xing, 2005; Frasca et al., 2008).

Up to 90% of the *BRAF* gene mutations are a thymine-to-adenosine transversion at position 1799 in exon 15 of the *BRAF* gene leading to the substitution of a valine (V) by glutamic acid (E) at the residue 600 (V600E) of the protein (Garnett et al., 2004; Frasca et al., 2008). When BRAF is in its inactive and dephosphorylated conformation, the adenosine triphosphate (ATP)-binding site and the phosphoregulatory activation loop are bound through hydrophobic interactions and the kinase domain of BRAF is closed. In the mutant form of BRAF, glutamic acid introduces a negative charge adjacent to the Thr599 residue mimicking phosphorylations at Thr599 and Ser602 residues. This disrupts the hydrophobic interactions and allows new interactions that maintain the protein in a catalytically competent conformation resulting in a continuous phosphorylation of MAP Kinase 1 (MEK), a downstream effector (Dhillon et al., 2004; Wan et al., 2004).

$BRAF^{V600E}$ mutation are highly frequent in classical PTCs and in the tall-cell variant but rare in the follicular variant of PTCs. Additionally, $BRAF^{V600E}$ mutation is found in poorly differentiated and undifferentiated carcinomas arising from preexisting PTCs which may still contain well-differentiated areas (Nikiforova et al., 2003; Begum et al., 2004; Soares et al., 2004; Frasca et al., 2008).

$BRAF^{V600E}$ mutation is also found in many other human cancers with a high prevalence in cutaneous melanoma and in a smaller subset of serous ovarian carcinoma and colorectal carcinoma (Davies et al., 2002).

Besides the $BRAF^{V600E}$ mutation, other rare *BRAF* mutations are found comprising nucleotides around the codon 600 which also constitutively activate the BRAF kinase (Soares et al., 2003; Xu et al., 2003). One example is the $BRAF^{K601E}$ mutation

which lead to the substitution of a lysine (K) by glutamic acid (E) at the residue 601 (K601E). This mutation has a higher prevalence in the follicular variant of PTCs (Trovisco et al., 2005).

$BRAF^{V600E}$ and thyroid tumorigenesis The initial evidence that $BRAF^{V600E}$ is required for the cell proliferation, transformation and tumorigenicity of follicular thyroid cells was demonstrated in a xenograft mice model (Liu et al., 2007) although many studies had already supported the role of that *BRAF* mutation in tumor initiation.

By stably and specifically knocking down BRAF using small interfering ribonucleic acid (siRNA) expression vectors in BRAF mutation-harboring papillary thyroid cells, suppression of cell proliferation, colony formation in monolayer culture and anchorage-independent cell growth in soft agar was achieved (Liu et al., 2007). Furthermore, it was observed inhibition of *in vivo* tumorigenicity and tumor growth of BRAF mutation-harboring papillary thyroid cells after stable knockdown of BRAF and xenografted in nude mice. These data suggest that $BRAF^{V600E}$ is a maintainer of PTCs phenotype (Liu et al., 2007).

Targeted expression of the $BRAF^{V600E}$ in follicular thyroid cells of transgenic FVB/N mice with a bovine thyroglobulin promoter was also studied. BRAF induced thyroid dysfunction which was compensated by increased levels of TSH and goiter development. In this model, multifocal tumors involving both lobes of the thyroid gland with mixed papillary and follicular growth pattern were observed in 12 and 22-week-old mice. PTCs presented the classical architecture, tall-cell features and a high potential for invasiveness. Tumors from one of the transgenic lines progressed into poorly differentiated carcinomas (Knauf et al., 2005).

PTCs were also observed in a thyrocyte-specific knock-in of $BRAF^{V600E}$ in mice but with a very short latency and complete penetrance by 3 weeks. When this model was crossed with a TshR knockout mice to genetically ablate TSH signaling, thyroid growth was reduced and low-grade PTCs were only observed by 9 weeks of age (Franco et al., 2011).

Along with these observations, a study has explored the consequences of induced $BRAF^{V600E}$ expression in the thyroid of adult mice. Shortly after inducing $BRAF^{V600E}$ expression, one-month-old mice developed hypothyroidism and a dramatically enlarged, goiterous and hypercellular thyroid gland that was 10 times larger than controls and up to 300 times larger by 12 months. Only after 6-to-9 months, all

mice developed PTC that closely recapitulated the phenotype in humans. Strikingly, treatment of these mice with a MEK inhibitor reduced thyroid size, restored the production of THs and inhibited tumorigenesis (Charles et al., 2011).

More evidence of $BRAF^{V600E}$ involvement in mice thyroid tumorigenesis was observed when $BRAF^{V600E}$ expression was induced in follicular thyroid cells in a doxycycline-inducible manner. As early as one week after doxycycline treatment, development of highly penetrant and high-grade PTCs with poorly differentiated features and a reversible activation of the MAPK pathway were observed. Upon doxycycline withdrawal, follicular architecture was reestablished but a second induction not only resulted in hypothyroidism but also reduced thyroid-specific genes expression (Chakravarty et al., 2011).

It is reasonable to assume that $BRAF^{V600E}$ is an early event in thyroid tumorigenesis due to a high prevalence of $BRAF^{V600E}$ in papillary microcarcinomas and development of tumors with histological features of human PTCs induced by expression of $BRAF^{V600E}$ in transgenic mice in the absence of any other genetic alterations (Park et al., 2010).

Intriguingly, it has been showed that some human PTCs have intratumor heterogeneity of the BRAF genotype as there are two distinct cell populations either with the wild-type (WT) or the $BRAF^{V600E}$. This may suggest that the clonal occurrence of BRAF mutation is a rare event, occuring only in a subpopulation of cells, and BRAF mutations are rather a late subclonal event in PTCs (Guerra et al., 2012).

Also, genome-wide allelotyping and *BRAF* mutation analysis of foci in multifocal human PTCs showed that $BRAF^{V600E}$ mutation is an early event during clonal evolution in most but not all cases. In fact, $BRAF^{V600E}$ is not always present in all tumor foci which suggests that other genetic factors in the primary tumor clone may have triggered neoplastic transformation (Jovanovic et al., 2008).

Nonetheless, in most mice studies $BRAF^{V600E}$ is expressed in all thyroid cells very early in life (fetal or during the first month) and BRAF-induced suppression of thyroid function led to TSH elevation which in turn promoted thyroid tumorigenesis. One particular study generated a model in which $BRAF^{V600E}$ expression was temporally and spatially restricted so that it can recapitulates the human sporadic PTC that usually arises postnatally from follicular cells under physiological serum TSH concentrations. With this approach, thyroid carcinomas under normal TSH levels were not found (Shimamura et al., 2013). This shows that

the timing of BRAF activation may be the key to determine cell transformation as the induction of an oncogene in poorly dividing cells, such as the follicular thyroid cells, during adulthood may not trigger tumorigenesis (Shimamura et al., 2013).

These data questions whether $BRAF^{V600E}$ initiates thyroid tumorigenesis or $BRAF^{V600E}$ is a consequence of tumor development and not a driver mutation. An alternative scenario is that $BRAF^{V600E}$ does initiate the formation of a PTC however as secondary genetic alterations and/or epigenetic changes take over to maintain tumor sustainability, $BRAF^{V600E}$ is no longer selected and/or important for tumor maintenance (Xing, 2012).

RET/PTC and NTRK1 rearrangements The *RET* gene is a member of the cadherin superfamily and encodes one of the first TK receptors that were found to have a role in human cancer (Phay et al., 2010). RET ligands belong to the glial cell-derived neurotrophic factor family and, when bound to RET co-receptors (GFRα-1), brings together two RET molecules leading to the autophosphorylation of the intracellular tyrosine portion (Manie et al., 2001; Airaksinen et al., 2002; Trovisco et al., 2007). In turn, there is the recruitment and binding of adaptor proteins and subsequent activation of signaling pathways such as the MAPK pathway which are able to control cell proliferation, differentiation, motility and survival (Manie et al., 2001; Airaksinen et al., 2002; Trovisco et al., 2007).

NTRK1 gene encodes a member of the neurotrophic TK receptor family. Upon neurotrophin binding, this membrane-bound receptor auto-phosphorylates and activates other members of the MAPK signaling pathway leading to cell differentiation (Teng et al., 2004; Trovisco et al., 2007).

Rearrangements of *RET* and *NTRK1* usually involve the fusion with heterologous genes resulting in *RET*/PTC and *NTRK1* chimeric transcripts. The chimeric proteins have an aberrant and persistent activation of their TK domains (Trovisco et al., 2007).

Somatic rearrangements of *RET* gene are found in 3% and up to 60% of sporadic PTCs and lead to a *de novo* expression of the TK on RET domain in the cytoplasm of follicular thyroid cells (Nikiforov, 2002; Santoro et al., 2002; Frasca et al., 2008). The most common *RET* rearrangements are the *RET*/PTC1 and *RET*/PTC3. *RET*/PTC1 is by far the most prevalent type comprising 60-70% of all the

rearrangements however *RET*/PTC3 is the most frequent rearrangement found early after radiation exposure. *RET*/PTC1 and *RET*/PTC3 are paracentric rearrangements with *CCDC6* (coiled-coil domain containing 6) and *NCOA4* (nuclear receptor coactivator 4) genes, respectively (Trovisco et al., 2007). Another rearrangement, *RET*/PTC2, involves reciprocal translocations with the protein kinase, cAMP-dependent, regulatory, type I, alpha *(PRKAR1A*) gene. *RET* gene can still be involved in other rearrangements but it is mainly associated with radiation (Trovisco et al., 2007). *RET*/PTC fusions leave intact the TK domain of the RET receptor enabling the protein to induce activation of signaling cascades including MAPK and phosphatidylinositol-4,5-bisphosphate 3-kinase (PI3K)-V-Akt murine thymoma viral oncogene homolog (AKT) pathways (Kuroda et al., 2003; Knauf et al., 2009).

Rearrangements of *NTRK1* gene are rare and are found in less than 10% of sporadic PTCs (Trovisco et al., 2007).

RAS mutations The *RAS* gene encodes for a family of related proteins that stay at the center of a cascade of molecular interactions. Most proteins are activated by RAS upon phosphorylation as Ras switches between its "on" and "off" state. Usually, RAS binds to guanosine-5'-diphosphate (GDP) but upon a receptor activation, GDP is expelled allowing guanosine-5'-triphosphate (GTP) to bind. In turn, GTP causes a subtle rearrangement of the RAS protein ultimately leading to the activation of MAPK signaling pathway. As GTP is hydrolyzed to GDP, RAS turns itself "off", self-limiting its activity (Lodish et al., 2000).

RAS mutations lead to a loss of the GTPase activity in RAS protein in such a way that it locks RAS in a constitutively active GTP-bound state which potentiate uncontrolled proliferative signals (Lodish et al., 2000).

In PTCs, *RAS* gene mutations are more frequently found in the follicular variant of PTC (Zhu et al., 2003, Giordano et al., 2005, Frasca et al., 2008). The prevalence of *RAS* mutations in PTCs ranges from 0% to 16% and neuroblastoma RAS viral (v-ras) oncogene homolog (*NRAS*) gene is the most predominantly mutated namely on codon 61 (Zhu et al., 2003; Trovisco et al., 2007).

PAX8-PPAR gamma rearrangements The paired box 8 (*PAX8)* gene encodes for a member of the paired box family of transcription factors involved in follicular

thyroid cell development and expression of thyroid-specific genes (Kimura, 2011). Peroxisome proliferator-activated receptor gamma (*PPARG*) gene encodes for a peroxisome proliferator-activated receptor that regulates the expression of target genes involved in cell proliferation, differentiation and immune and inflammatory responses (Kroll et al., 2000).
PAX8-PPAR gamma rearrangements are tipically found in follicular thyroid adenomas, FTCs and on the follicular variant of PTCs, in the latter with a prevalence up to 38% (Castro et al., 2006).

PTEN and PIK3CA mutations The phosphatase and tensin homolog (*PTEN*) gene encodes for a phosphatidylinositol-3,4,5-triphosphate 3-phosphatase which regulates dephosphorylation of phosphoinositide substrates thereby negatively regulating the PI3K-AKT signaling pathway (Sun et al., 1999; Hou et al., 2007). *PTEN* mutations are found in 1-2% of PTCs and mutations in this tumor suppressor gene activate the PI3K-AKT pathway (Hou et al., 2007).
Phosphatidylinositol-4,5-bisphosphate 3-kinase, catalytic subunit alpha (*PIK3CA*) encodes for a catalytic subunit that uses ATP to phosphorylate phosphatidylinositol-4-monophosphate and phosphatidylinositol-4,5-diphosphate (Samuels et al., 2004). PIK3CA mutations have also a very low prevalence in PTCs (1-3%) and most are found in the helical and kinase domains of the p110α protein producing variants that are independent of the regulatory subunits and are capable of inducing cell proliferation, invasiveness and resistance to apoptosis (Gymnopoulos et al., 2007; Santarpia et al., 2010). *PIK3CA* copy gain prevalence goes up to 14% (Wang et al., 2007; Hou et al., 2007). Either mutations in the *PIK3CA* gene or increase in copy number result in the gain of function reflected by high or constitutive activation of the PI3K activity and promotion of tumorigenesis (Santarpia et al., 2010).

p53 mutations The *TP53* gene encodes for a protein that maintains genome integrity by binding specifically to a DNA consensus sequence to induce growth inhibitory genes or nonspecifically to damaged sites leading to DNA repair or apoptosis (Liu et al., 2001). The levels of p53 in normal cells are very low but upon p53 activation in response to environmental challenges such as cellular stress, p53 protein is accumulated and stabilized (Liu et al., 2001). p53 is capable of arresting the cell cycle at G1, G2 or in S-phase by inducing p21 which in turn blocks the

cycling-dependent kinases (CDKs) responsible for checkpoint regulation and progression of the cell cycle (Bai et al., 2006). This allows time to repair damaged DNA or induce cell death (Bai et al., 2006). p53 is also an activator of the MDM2 proto-oncogene, E3 ubiquitin protein ligase (*MDM2*) gene which negatively auto-regulates p53 maintaining low levels of the p53 protein in normal cells (Bai et al., 2006).

At variance with other human tumors, *TP53* mutations are not frequent in thyroid cancer (only 10%) and most have been documented in anaplastic carcinomas. Indeed, well-differentiated thyroid cancers do not harbor mutations in *TP53* suggesting a role on thyroid cancer progression to poorly differentiated and aggressive phenotypes (Morita et al., 2008). Of note, studies on thyroid tumor samples revealed an accumulation of p53 in poorly differentiated and anaplastic forms but also well-differentiated tumors in the absence of any p53 mutation suggesting that p53 inactivation may result from loss of interaction with MDM2 (Soares et al., 1994). In thyroid cancer, *TP53* mutations are commonly found at codons 213 and 238 and in anaplastic carcinomas are also found at codons 248 and 273 (Bai et al., 2006).

Modeling thyroid cancer in mice have shown that acquired mutations drive tumor progression and in general $BRAF^{V600E}$ is sufficient to initiate PTCs. Already demonstrated is evidence that p53 constrains progression from papillary to anaplastic thyroid carcinoma (Preto et al., 2004). By generating a thyroid-specific Cre recombinase-estrogen receptor (CreER) transgenic mouse and using a Cre-regulated $BRAF^{V600E}$ and a conditional *Trp53*, it was found that p53 loss does enable progression to aggressive anaplastic thyroid cancer but additional events may be required for full anaplastic conversion (McFadden et al., 2014).

Telomerase promoter mutations Telomerase is a ribonucleoprotein complex that adds telomeres repeats sequences to the ends of telomeric DNA. The protein component has reverse transcriptase (TERT) activity while the RNA component serves as a template for the telomere repeat (Capezzone et al., 2009; Hanahan et al., 2011).

Telomerase is active in the vast majority of human cancer cells (80-90%) enabling their replicative immortality (Figure 4) (Hanahan et al., 2011) and sporadic thyroid carcinomas are no exception. In PTCs, telomerase activity measured by TRAP assay

ranged from 20% to 87.5% (Capezzone et al., 2009) but the high levels reported in some studies may be due to the presence of lymphocytic infiltration coexisting with the neoplasia (Brousset et al., 1997; Umbricht et al., 1997; Saji et al., 1999). Of note, telomerase activity in normal thyroid tissue is almost absent (Capezzone et al., 2009).

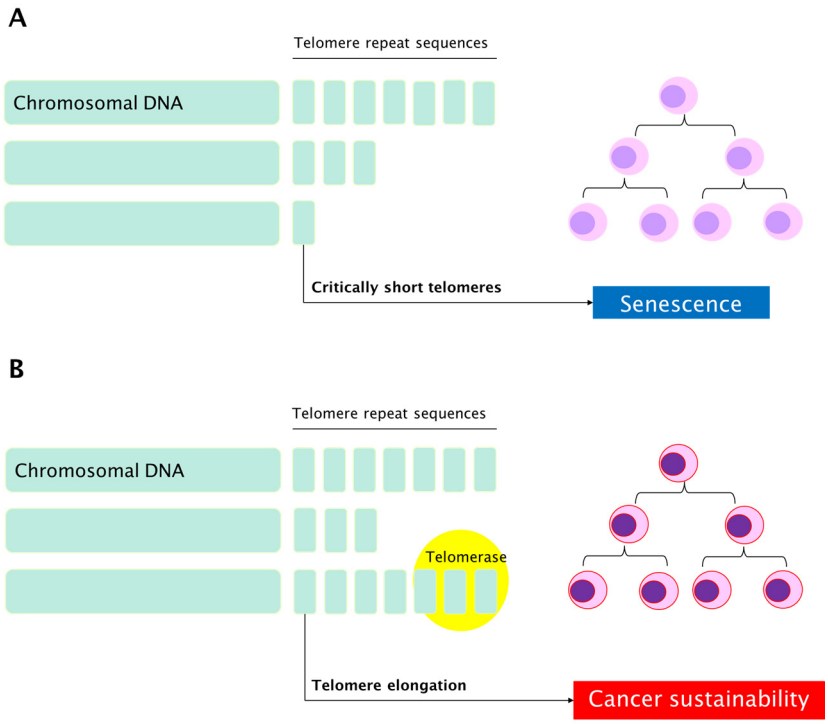

Figure 4. **Regulation of telomere length by telomerase.** (A) In normal somatic cells, telomerase is absent and the telomere repeat sequence (light blue boxes) is lost everytime the cell divides. After many cell divisions, telomeres reach a critically short length triggering senescence and cessation of proliferation. (B) In cancer cells, reexpression of the telomerase expression bypasses senescence and telomere length is compatible with proliferation. Telomere elongation sustains cancer.

Telomerase activity is considered the result of clonal selection as telomeres become critically shortened (Skvortzov et al., 2009). It was shown that genetic mechanisms that promote telomerase reactivation in human tumors include *TERT* alternative splicing, *TERT* gene amplification and *TERT* promoter mutations (Figure 5) (Skvortzov et al., 2009). As recently reported two recurrent, non-overlapping somatic mutations on chromosome 5, -124C>T (C228T) and -146C>T (C250T) (where -1 is the base just upstream of the ATG translation start site of the *TERT*

gene), in the *TERT* promoter are very frequent in sporadic melanoma (Huang et al., 2013, Horn et al., 2013). These mutations were subsequently found in several tumors including thyroid cancer lines and either well-differentiated or poorly and anaplastic thyroid carcinomas (Vinagre et al., 2014).

TERT promoter mutations create an eleven-base nucleotide stretch 5'-CCCCTTCCGGG3' which contains a new consensus binding site GGAA, generating *de novo* consensus binding motifs for E-twenty-six (erythroblast transformation-specific -ETS- transcription factors). It was shown that it increases the transcriptional activity of the telomerase promoter by two-to-six-fold in human cancer cell lines (Huang et al., 2013; Horn et al., 2013; Liu et al., 2013). This is consistent with a mildly enhanced TERT expression with respect to normal tissues (Muzza et al., 2015). One of the transcription factors found to be recruited specifically to the mutant promoter is the multimeric GA-binding protein (GABP) (Bell et al., 2015).

TERT promoter mutations are found in 8% to 22% of PTCs, being the -124C>T mutation more prevalent (Liu et al., 2013; Landa et al., 2013; Vinagre et al., 2013; Melo et al., 2014; Liu et al., 2014; Wang et al., 2014; Muzza et al., 2015). Noticeably, 33% of PTCs with distant metastasis harbored *TERT* promoter mutations (Melo et al., 2014; Xing et al, 2014; Gandolfi et al., 2015).

It was proposed that *TERT* promoter mutations may be more common in cancers derived from terminally differentiated cells which have a low self-renewing capacity. Indeed, follicular thyroid cells have a very low mitotic rate postnatally (proliferative rate lower than 0.1 in adults). Also, well-differentiated PTCs are usually indolent lesions with low rate of growth. A significant rate of *TERT* promoter mutations in those carcinomas suggests that thyroid cancer cells may benefit from this mechanism to maintain telomerase lengthening (Saad et al., 2006; Killela et al., 2013).

Moreover, it was found a significant overrepresentation of *TERT* promoter mutations in thyroid tumors harboring alterations in *BRAF* or *RAS* genes. *TERT* promoter mutations seemed to be more frequent in $BRAF^{V600E}$ that in $BRAF^{WT}$-PTCs (Liu et al., 2013; Melo et al., 2014; Xing et al., 2014).

In differentiated thyroid carcinomas, *TERT* promoter mutations are associated with older age at diagnosis, tumor size and male gender and are correlated with a

reduced progression free survival and overall survival (Vinagre et al., 2013; Xing et al., 2014; Melo et al., 2014).

This comes as no surprise that *TERT* promoter mutations are associated with older age at diagnosis which is consistent with a progressive shortening of telomeres in follicular cells during lifetime. When these cells acquire genetic alterations, such as the $BRAF^{V600E}$ mutation, and begin to reply to the oncogenic stimuli by inducing proliferation, very short telomeres also trigger telomere dysfunction which may be compensated by telomerase reactivation via *TERT* promoter mutations (Londoño-Vallejo, 2008; Muzza et al., 2015). Furthermore, *BRAF* mutations leading to MAPK activation can be conceived as inducers of expression of members of the ETS transcription factor family. Having *de novo* consensus binding sites for ETS factors promoted by *TERT* promoter mutations, the lifespan of BRAF-driven clones is extended. Further accumulation of additional genetic defects is promoted which in turn allows progression to advanced tumor stages (Pratilas et al., 2009; Huang et al., 2013; Horn et al., 2013; Liu et al., 2013).

These hypothesis could explain why well differentiated PTCs harboring *BRAF* mutations are more likely to harbor *TERT* promoter mutations than those PTCs without *BRAF* mutations. It is also consistent with an enrichment of *TERT* promoter mutations in poorly differentiated thyroid carcinomas and anaplastic thyroid carcinomas which have partially and completely lost differentiation, respectively, and are the most aggressive thyroid carcinomas (Landa et al., 2013; Liu et al., 2013). Of note, *TERT* promoter mutations must be only one of the several mechanisms that illegitimately activate telomerase in human cancer.

Signaling pathways altered in papillary thyroid carcinomas

MAPK signaling pathway The MAPK pathway comprises evolutionarily conserved kinase modules that join extracellular signals to the machinery responsible for cell growth, proliferation, differentiation, migration and apoptosis. One of the groups of MAPK characterized in mammals is the extracellular signal-regulated kinase (ERK)1/2 (Dhillon et al., 2007).

Constitutive activation of the MAPK signaling pathway is a frequent event in human cancers particularly in PTCs and melanomas (Xing, 2013).

For most cancers, constitutive activation of ERK signaling is established by sustained autocrine or paracrine production of activating ligands, overexpression and activating mutations of the TK receptor and activating mutations in RAS and BRAF (Dhillon et al., 2007; Knauf et al., 2009). In thyroid cancers, besides *RAS* and *BRAF* mutations, *RET*-PTC, *NTRK1* and *ALK* mutations also mediate tumorigenesis via the MAPK pathway (Xing, 2013).

In this pathway, ligand-mediated activation of TK receptor promote RAS GTPase conversion which recruits and activates RAF kinases to the plasma membrane. ERK1 and ERK2 are activated upon phosphorylation by MEK1 and MEK2 which are themselves activated when phosphorylated by RAF proteins. Activated ERKs phosphorylate cytoplasmic and nuclear targets including kinases, phosphatases, transcription factors and cytoskeletal proteins (Figure 5) (Dhillon et al., 2007).

The effect of ERK signaling activation is consistent to the cellular processes that itself regulates. Sustained ERK signaling promotes phosphorylation and stabilization of FBJ murine osteosarcoma viral oncogene homolog (Fos), Jun proto-oncogene (Jun), V-Myc avian myelocytomatosis viral oncogene homolog (Myc) and ETS-Related (Erg-1) genes and also cyclin D1 thereby promoting cell-cycle entry and can repress genes responsible for inhibiting proliferation (Yamamoto et al., 2006). On the other hand, high levels of ERKs can induce cell-cycle arrest by expression of CDK-inhibitor proteins such as p21 and p27 that must be counteracted by elevated RhO signaling or activation of AKT so that cells continue to proliferate (Dhillon et al., 2007).

PI3K-AKT signaling pathway PI3Ks represent a family of kinases that phosphorylate the 3'-hydroxyl group of phosphatidylinositol inositides that are activated by many TK receptors. Class I of PI3Ks consists of heterodimers of regulatory (p85) and catalytic (p110) subunits. p110α and p110β subunits have an important role in tumorigenesis as RAS function is mediated by its interaction with the RAS-binding site present in those subunits. Also, activation of TK receptor by extracellular signals is itself sufficient to activate p110 subunits which in turn phosphorylates phosphatidylinositol (PtdIns)-3,4-P2 producing PtdIns-3,4,5-P3 leading to the recruitment of AKT to the cytosolic membrane. AKT is then phosphorylated and activated by PDK1 resulting in the phosphorylation of downstream effector such as the mammalian target of rapamycin (mTOR) (Figure

5). This result in a broad cascade of signaling responsible for cell growth and proliferation, glucose uptake, migration and apoptosis resistance (Saji et al., 2010).

Constitutive activation of the PI3K-regulated signaling pathway is relevant in a wide variety of human tumors including thyroid cancer. This is particularly valid in Cowden's syndrome, that present thyroid carcinomas, which is characterized by mutations in the *PTEN* gene that encodes a phosphatase that dephosphorylate PtdIns-3,4,5-P3 and thereby negatively regulates the PI3K-AKT pathway. Additionally, *RAS* mutations, *RET*/PTC rearrangements and *PIK3CA* and *AKT1* mutations are further evidences that PI3K signaling pathway has a fundamental role in thyroid tumorigenesis (Saji et al., 2010, Xing, 2010).

mTOR signaling pathway mTOR is a serine/threonine kinase that belongs to the phosphoinositide 3-kinase (PI3K)-related kinase family and functions as a regulator of cell growth-related processes. mTOR can form two distinct complexes with other proteins, mTOR complex 1 (mTORC1) and complex 2 (mTORC2), that have different upstream inputs and downstream outputs. Regulation of mTOR by growth factors occurs through the PI3K/AKT pathway which is counteracted by PTEN. There is evidence of overactivation of AKT/mTOR pathway in PTCs when compared to other differentiated thyroid carcinomas and correlation with $BRAF^{V600E}$ mutation which could be explained by BRAF-induced phosphorylation of tumor suppressor liver kinase B1 (LKB1) Ser428, a main upstream kinase of AMP-activated protein kinase (Faustino et al., 2012).

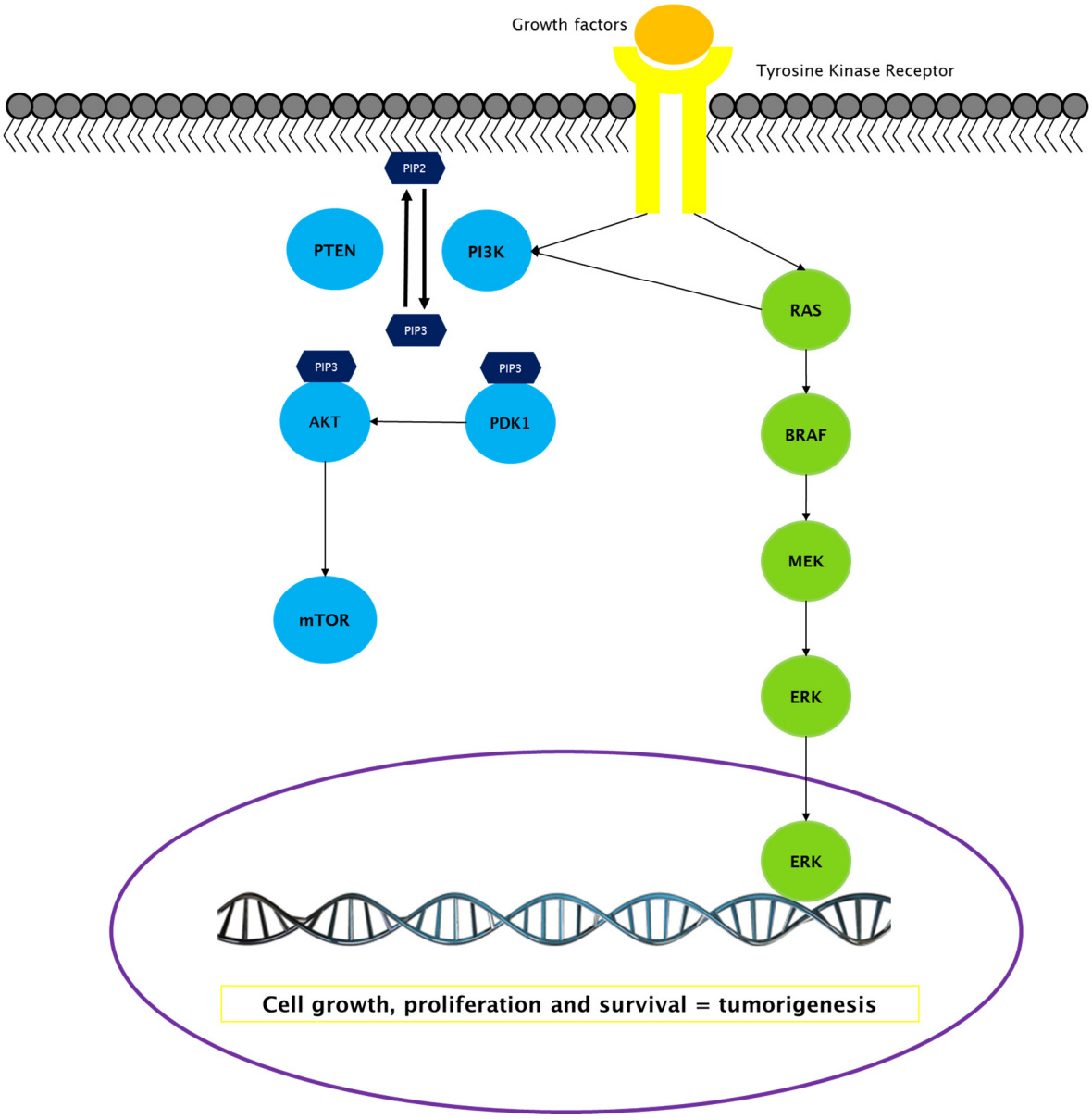

Figure 5. **MAPK and PI3K-AKT-mTOR signaling pathways.** In green are the proteins from the MAPK pathway; in blue those belonging to the PI3K-AKT-mTOR pathway. These two classical pathways are associated to TK receptors at the cell membrane that transduces extracellular growth signals into intracellular signals downstream of the pathways. RAS protein can couples the signaling from the receptor to both MAPK and PI3K-AKT-mTOR pathways. These two pathways, driven by genetic alterations in one or more of their components, have a fundamental role in thyroid tumorigenesis.

THROUGHOUT HISTORY, ethical and religious considerations have prevented experimental studies of human biology. Most of the knowledge of human biology, physiology, endocrinology and pharmacology has come first from studies in animal models. Often practical, economical and scientific reasons are also crucial in understanding why animals are the best models for studies of biological phenomena.

I.2 Zebrafish as a model system

Zebrafish is a freshwater fish that was originally found in slow streams and rice paddies and in the Ganges River in East India and Burma. In these water, zebrafish rarely grow larger than 4 centimeters long (Clark et al., 2013).

In comparison to other animal models, zebrafish has a far shorter relationship with research. Zebrafish started to be studied for developmental genetics by George Streisinger from the University of Oregon in the late 1960s. His idea was to apply mutational analysis to study zebrafish embryonic development as he thought this analysis was needed in vertebrates. Initially studies were set to study features of the organization and embryological development of the nervous system using mutant vertebrate strains (Grunwald et al., 2002; Clark et al., 2013).

Zebrafish was and it still is an attractive model due to its brood size, short life cycle, transparent embryos, *ex utero* development of embryos, ease of keeping many fish in a small space, frequent mating possibility, sexual maturity at 3 months post fertilization (mpf) and conservation of vertebrate tissues (White et al., 2013; Liu et al., 2011). Zebrafish was only later used in large forward genetic screens that produced genetic mutants for virtually any phenotype (Dooley et al., 2000; Liu et al., 2011) and nowadays this model reached its full potential to study vertebrate biology and physiology as well as human diseases (Dooley et al., 2000).

I.2.1 Zebrafish in Cancer Research

The cancer field is heading towards a post-genomic state and, as most human cancers are being extensively sequenced, new tools are required so that the extensive genomic alterations found can be studied in a biological context and be translated into a more effective therapy (Mione et al., 2010; Liu et al., 2011; White et al., 2013).

Although no single model can fully reflect the complexity of cancer biology *in vivo*, zebrafish has been considered a great addition to animal models of human disease (Liu et al., 2011; White et al., 2013).

In 1982, zebrafish was first proposed as a model for cancer with a study showing that exposure to carcinogens induced low-penetrance tumors (Pliss et al., 1982). Remarkably, despite over 300 million years of divergence between fish and humans, tumors in zebrafish strongly resemble human tumors at the histological, gene expression and genomic levels. Moreover, crucial genes and pathways involved in tumorigenesis are highly conserved between fish and humans (Amatruda et al., 2002).

Two decades later more studies were able to demonstrate various neoplasms in zebrafish after mutagen exposure but the breakthrough came when T-cell leukemia was induced by expressing oncogenic myc under the control of rag2 in transgenic animals (Langenau et al., 2003).

Since then, many zebrafish models of cancer expressing dominant-acting oncogenes have been established using various technologies. The two main approaches are either to select genetic alterations in human tumors and then test it in transgenic animals or to identify evolutionarily drivers conserved between human tumors and those tumors arising in transgenic animals (Liu et al., 2011; White et al., 2013).

Taking into account the first approach, probably the most extensively studied transgenic zebrafish model of cancer is the melanoma model. Human melanoma is a lethal form of skin cancer with an incidence and mortality rates that are rapidly increasing (Wangari-Talbot, 2012). Molecular genetic analysis of precursor lesions such as the nevi and melanoma tumors have pointed to alterations in key genes of the RAS-RAF-MEK-ERK and PI3K-AKT pathways regulating signal transduction and other genes involved in cell cycle regulation such as the cyclin-dependent kinase inhibitor 2A (*CDKN2A*) (Wangari-Talbot, 2012). The majority of human melanomas exhibit mutations in *BRAF*, the same found in PTCs, and this may have a critical role in melanoma initiation (Wangari-Talbot, 2012).

To study the role of activated BRAF, a transgenic zebrafish expressing $BRAF^{V600E}$ under the control of a melanocyte promoter was generated. Expression of the oncogene in the melanocytes lead to nevi which rapidly develop into invasive melanomas only in the absence of WT p53 (Patton et al., 2005). Furthermore, to

test for the ability of genes in a region of chromosome 1 (1q21) amplified in human melanomas to cooperate with $BRAF^{V600E}$, the melanoma model described above was used to inject a rescuing-plasmid containing any of the genes present in the 1q21 region. A single gene (SET Domain, Bifurcated 1-*SETDB1*) was found to cooperate with $BRAF^{V600E}$ in mediating melanoma growth in zebrafish and increase tumor aggressiveness (Ceol et al., 2011).

An approach to compare common genetic alterations in human and zebrafish tumors is highlighted by the zebrafish T-cell acute lymphoblastic leukemia model (T-ALL). Almost 900 genes were found to have copy number alterations in zebrafish leukemia and when compared to human leukemia ten genes, that seemed to be true drivers of T-ALL, were repeatedly altered in the two species (Rudner et al., 2011).

Besides classic transgenesis and comparative genomic studies, zebrafish has also the potential for tumor transplantation and xenotransplantation of human cells. In fact, transplantation models in zebrafish are being used to study cancer-related events such as invasion, metastasis, angiogenesis and cancer stem cell renewal which rely on *in vivo* imaging. More recently, zebrafish models were considered candidates for large-scale reverse genetics to identify tumor suppressors, for modeling multigenic alterations and epigenetic changes and for studying the immunological response and microenvironment (Liu et al., 2011; White et al., 2013).

I.2.2 Studies on zebrafish thyroid physiology and function

The thyroid gland is responsible for producing THs in all vertebrates in order to regulate metabolism in the adult organism but also to control many processes during development (VanPutte et al., 2010). Despite some anatomical differences between fish and mammals, the hypothalamus-pituitary-thyroid (HPT) axis is conserved (VanPutte et al., 2010).

The functional unit of teleost thyroid is the follicle (Fournie et al., 2005; Wendl et al., 2002). Thyroid follicles are scattered predominantly throughout the connective tissue of the pharyngeal region between the first gill arch and the bulbus arteriosus along the ventral aorta within the mesenchyme of the ventral head region. Adjacent muscle, cartilage or bone may also be surrounded by random follicles. Normal-appearing thyroid follicles may also be found in the ocular choroid, kidney, spleen,

intestine, liver and heart. Indeed, this ectopic distribution could be due to the absence of a connective tissue barrier. Histologically, each thyroid follicle resembles that of other vertebrates (Fournie et al., 2005; Wendl et al., 2002). The follicles are usually round to oval and are lined by a single-layered epithelium consisting of endoderm-derived flat or cuboidal thyroid cells. Follicles are filled with colloid and the amount of colloid depends on the metabolic activity of thyroid cells and the extent of TSH production (Fournie et al., 2005; Wendl et al., 2002). Teleost follicles produce THs (T3 and T4) and their synthesis follows the iodine uptake and iodination of thyroglobulin and the release of the hormones into the blood stream (Wendl et al., 2002).

Follicular thyroid cells in zebrafish, as in other vertebrates, express the orthologous transcription factors NK2 Homeobox 1a (*nk2-1a*) (Rohr et al., 2000), paired box gene 2.1 (*pax2.1)*, *pax8* and hematopoietically expressed homeobox (*hhex*) (Wendl et al., 2002) for thyroid differentiation and orthologous proteins such as solute carrier family 5 (sodium/iodide cotransporter), member 5 (*slc5a5*) and cathepsin B (*ctsb*) (Alt et al., 2006) important in TH synthesis, produce thyroglobulin (Wendl et al., 2002; Alt et al., 2006) and accumulate iodine (Elsalini et al., 2003).

Development of thyroid in zebrafish In zebrafish development, classical steps shared with mammals include specification of follicular thyroid cells progenitors, budding of a thyroid anlage, migration of thyroid primordium and late thyroid morphogenesis and functional differentiation of follicles (Figure 6) (Alt et al., 2006; Porazzi et al., 2009).

TH immunoreactivity appears faint at around 55 hours post fertilization (hpf) when the embryo hatches from the chorion. However, expression of thyroglobulin (*tg*) is first observed in the thyroid primordium as early as 32hpf (Alt et al., 2006). As the primordium grows along the midline of the ventral pharyngeal area, expression of *slc5a5* and *ctsb* also initiates. T4 immunoreactivity is observed at about 80hpf in a group of cells that are not organized as follicles but lay at the base of the larva lower jaw (Alt et al., 2006). At 96hpf, the immunoreactivity increases as well as the number of cells which are localized caudally along the ventral aorta (Alt et al., 2006). At 5 days post fertilization (dpf), three to five follicles can be observed and at 7dpf up to seven follicles arise. Larval follicles have a lumen filled with colloid

and vesicles at the apical surface of the follicular cells. These cells are usually round and their size is 5-10μm in diameter (Alt et al., 2006).

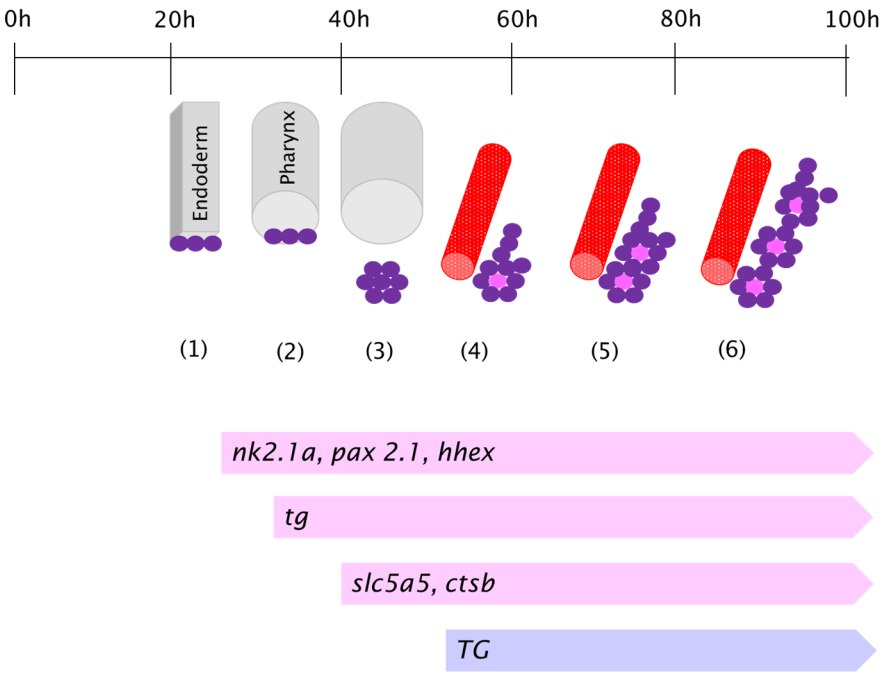

Figure 6. **Embryonic thyroid growth in zebrafish.** The main steps are the following: (1) expression of developmental markers (nk2.1, hhex, pax2.1) in a field of the endoderm before a pharynx has formed; (2) and (3) evagination of the middle diverticulum; (4) differentiation of the first follicle at around 55hpf; (5) and (6) follicle growth with tissue added caually. The scale bar shows time of development in hpf. (Pink arrows indicate the onset of developmental gene expression and differentiation markers and blue arrows mark the onset of thyroid function judged by production of T4.

The yolk of the larva contains maternal THs which explain the early onset of T4 and fast development (Wendl et al., 2002). Follicular thyroid cells do not fuse with the calcitonin-producing cells (Alt et al., 2006).

I.3 Aims

Not so long ago cancer was seen as arising owing to the accumulation of mutations in critical genes that altered the normal programme of cell proliferation, differentiation and death. But the impact of such mutations, including those in the BRAF gene, is only part of the cancer paradigm, indeed many other mechanisms mediate tumorigenesis.

One of the most novel mechanism is related to *TERT* promoter mutations. *TERT* promoter mutations were initially found at high frequency in human melanoma but not in nevi and are believed to illicitly contribute to telomerase reactivation in melanoma as in other cancers. I was involved in a study to investigate whether *TERT* promoter mutations were present in cancer types other than melanomas: thyroid, kidney, bladder, gastrointestinal stromal tumors (GIST), adrenal medulla and central nervous system (CNS) tumors. The frequency of *TERT* promoter mutations was assessed in the above-mentioned cancers and contributed to further studies to understand why those mutations are important in some cancers but not in others and how do they relate with additional genetic alterations.

Virtually every breakthrough in the study of human diseases has been the direct result of using animal models. Although many alternative animal-replacing methods are also used, living systems remain a necessity in research.

In thyroid cancer studies, mice models have provided enough evidence that thyroid-specific expression of $BRAF^{V600E}$ induced goiter and invasive PTCs which progress to poorly differentiated carcinomas that closely recapitulated the human PTC phenotypes. Those mice models are still used nowadays to disclose new mechanisms of thyroid tumorigenesis, however tumor imaging and translational studies namely drug screening are difficult and time-consuming.

In the last years, zebrafish has proved to be a good addition to animal models of human cancer not only because they develop cancer spontaneously, after mutagen exposure or through transgenesis but also because tumors that arise resemble those of the humans at the histological, genetic and genomic levels. Taking advantage of this versatile animal model, I developed a novel transgenic line that expressed $BRAF^{V600E}$ specifically in thyroid cells of zebrafish to understand the effect of $BRAF^{V600E}$ in this tissue and validate a model useful to study thyroid disease. Upregulation of p53 was found to play an important role in the $BRAF^{V600E}$-induced phenotype in that line. Also, human and mice data showed that p53 loss is essential

in tumor progression. Therefore, I developed a transgenic line that expressed $BRAF^{V600E}$ specifically in thyroid cells of *tp53*^{M214K} zebrafish to understand whether the absence of WT p53 would promote cancer or at least exacerbate the $BRAF^{V600E}$ effect on thyroid. Finally, to closely recapitulate the timing of BRAF activation in sporadic thyroid carcinomas, I developed a transgenic model that allowed temporally restricted expression of $BRAF^{V600E}$ in thyroid cells of zebrafish.

Chapter II

Material & Methods

The material and methods from the "Frequency of *TERT* promoter mutations in human cancers" work are exclusively described in chapter III.1. The material and methods from the studies in zebrafish are described in detail in this chapter and briefly in chapter III.2

II.1 Plasmid cloning

II.1.1 p5E-*tg* promoter plasmid

The (-2041; -1) region, being -1 the position immediately upstream of the ATG sequence of the zebrafish thyroglobulin (*tg*) gene, was amplified by polymerase chain reaction (PCR) from bacterial artificial chromosome (BAC) genomic clone DKEY-97I18 BAC, GenBank CR855311.15 (SourceBioScience) using the following primers: forward primer 5'-CAGCTGGTACTCTAAATGTGAGAAA-3' and reverse primer 5'-TGTTTAAAAGGGACGATGTAGC-3'. The fragment was initially cloned into a pCR™-BluntII-TOPO® plasmid (Thermo Fisher Scientific Inc.). The insert was then excised using restriction sites from the backbone plasmid and cloned into the *Kpn*I (Thermo Fisher Scientific Inc.) and *Xho*I (Thermo Fisher Scientific Inc.) restriction sites on the multicloning site (MCS) of a p5E-MCS plasmid, containing attL4 and attR1 recombination sites and provided by the Tol2Kit (Kwan et al., 2007). Ligation product was transformed into One Shot® TOP10 Chemically Competent Cells (Thermo Fisher Scientific Inc.). The full-length construct was sequenced for accuracy.

II.1.2 pME-mCherry and p3E-polyA plasmids

pME-mCherry is a middle entry (ME) clone containing attL1 and attL2 recombination sites. p3E-polyA is a 3' entry clone containing simian vacuolating virus 40 (SV40) late polyA signal and attR2 and attL3 recombination sites. Both entry clones were provided by the Tol2Kit (Kwan et al., 2007). pME-mCherry and p3E-polyA plasmids were transformed into One Shot® TOP10 Chemically Competent Cells (Thermo Fisher Scientific Inc.). The full-length constructs were sequenced for accuracy.

II.1.3 pME-mCherry-T2A-BRAF^{WT} and pME-mCherry-T2A-BRAF^{V600E} plasmids

Full-length human B-type Raf kinase (BRAF)^{WT} and BRAF^{V600E} coding sequences were amplified by PCR from expression vectors previously generated in my lab: p*CMV*-BRAF^{WT} and p*CMV*-BRAF^{V600E}, respectively (Faustino et al., 2012) using the following primers: forward primer 5'-CCGGCCCTATGGCGGCGCTGAGC-3' and reverse primer 5'- GTTTCCTGTCCACTGATGATATCG-3'. mCherry coding sequence was amplified by PCR from pME-mCherry (Kwan et al., 2007) using the following primers: forward primer 5'-GGGCCCCCCCTCGAGGGCCGCCACCATGGTG-3' and reverse primer 5'-GAGAATCCCGGCCCTATGGCGGC-3'. T2A sequence (5'-GAGGGCAGAGGAAGTCTTCTAACATGCGGTGACGTGGAGGAGAATCCCGGCCCT-3') was synthetized as an oligomer of 54bp and amplified by PCR. All PCR products generated were purified individually and assembled in frame into a previously linearized pME-MCS (containing attL1 and attL2 recombination sites) using the GeneArt® Seamless Assembly Kit (Thermo Fisher Scientific) and according to the following order: (1st) mCherry – (2nd) T2A – (3rd) BRAF^{WT} or BRAF^{V600E}. Ligation product was transformed into One Shot® TOP10 Chemically Competent Cells (Thermo Fisher Scientific Inc.). The full-length constructs were sequenced for accuracy.

II.1.4 pTol2A2-*tg*:mCherry-pA and pTol2CG2-*tg*:mCherry-pA plasmids

p5E-*tg* promoter, pME-mCherry and p3E-polyA were assembled into a pDestTol2pA2, containing attR4 and attR3 recombination sites and provided by the Tol2Kit (Kwan et al., 2007), using a Gateway LR Clonase II Enzyme Mix (Thermo Fisher Scientific Inc.) and according to the manufacturer's instructions. Ligation product was transformed into One Shot® TOP10 Chemically Competent Cells (Thermo Fisher Scientific Inc.). The full-length pTol2A2-*tg*:mCherry-pA construct was sequenced for accuracy. Same protocol was performed to generate the pTol2CG2-*tg*:mCherry-pA, however the three entry clones were assembled into a pDestTol2CG2, containing the *cmlc2*:EGFP cassette and the attR4 and attR3 recombination sites, provided by the Tol2Kit (Kwan et al., 2007) (Figure 1). The full-length pTol2CG2-*tg*:mCherry-pA construct was sequenced for accuracy.

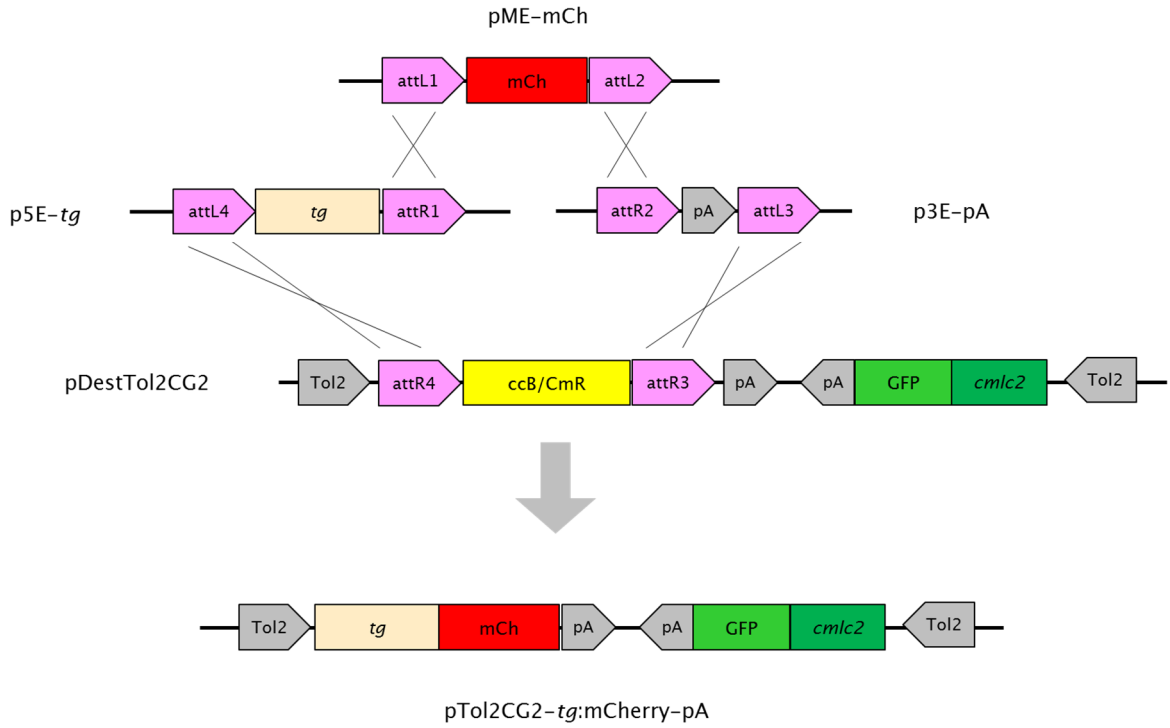

Figure 1. **Gateway cloning strategy to generate the pTol2CG2-*tg*:mCherry-pA plasmid.** Schematic of the three-part LR recombination reaction used to generate pTol2CG2-*tg*:mCherry-pA. Entry clones (p5E-tg, pME-mCh and p3E-pA) containing attL sites and pDestTol2CG2 destination plasmid containing attLR sites recombined when LR clonase was added to the reaction.

II.1.5 pTol2CG2-*tg*:mCherry-T2A- BRAF^{V600E}-pA plasmids

p5E-*tg* promoter, pME-mCherry-T2A-BRAF^{V600E} and p3E-polyA were assembled into a pDestTol2CG2, containing the cardiac myosin light chain (*cmlc2*): enhanced green fluorescent protein (EGFP) cassette and containing attR4 and attR3 recombination sites, provided by the Tol2Kit (Kwan et al., 2007) using a Gateway LR Clonase II Enzyme Mix (Life Technologies) and according to the manufacturer's instructions (Figure 2). Ligation product was transformed into One Shot® TOP10 Chemically Competent Cells (Thermo Fisher Scientific Inc.). The full-length pTol2CG2-*tg*:mCherry-T2A-BRAF^{V600E}-pA construct was sequenced for accuracy.

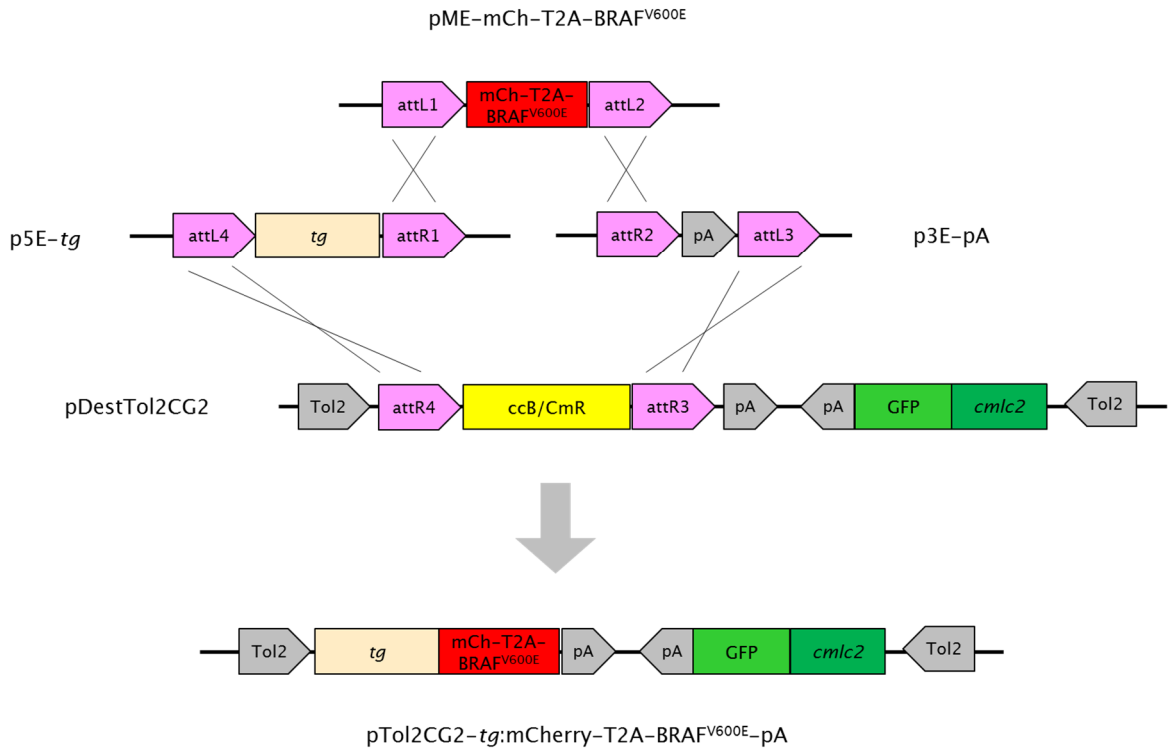

Figure 2. **Gateway cloning strategy to generate the pTol2CG2-*tg*:mCherry-T2A-BRAF^{V600E}-pA plasmid.** Schematic of the three-part LR recombination reaction used to generate pTol2CG2-*tg*:mCherry-T2A-BRAF^{V600E} -pA. Entry clones (p5E-tg, pME-mCh-T2A-BRAF^{V600E} and p3E-pA) containing attL sites and pDestTol2CG2 destination plasmid containing attLR sites recombined when LR clonase was present in the reaction.

II.1.6 pTol2CG2-*tg*:loxP-CFP-loxP-mCherry-pA and pTol2CG2-*tg*:loxP-CFP-loxP-mCherry-T2A-BRAF^{V600E}-pA plasmids

pTol2CG2-*tg*:mCherry-pA was cut with *Sal*I (Thermo Fisher Scientific Inc.), gel purified and dephosphorylated with Shrimp Alkaline Phosphatase (SAP) (Thermo Fisher Scientific Inc.). loxP-cyan fluorescent protein (CFP)-loxP was amplified from a donor plasmid generated in the lab (unpublished plasmid) using the following primers: forward primer 5'-CAAGCTTATCGATACCGCCCGGGATAACTTCGTATAATGTATGCTATACGAAGTTATC TTG-3' and reverse primer 5'-CTAGAGAAGCTGAGGACAGGGATCCGGCCGGCC-3'. These primers were engineered for recombination deoxyribonucleic acid (DNA) assembly and the PCR product was gel purified. Plasmid and insert were ligated using the Gibson Assembly Cloning Kit (New England Biolabs) and ligation product

was transformed into One Shot® TOP10 Chemically Competent Cells (Thermo Fisher Scientific Inc.). The full-length pTol2CG2-*tg*:loxP-CFP-loxP-mCherry-pA construct was sequenced for accuracy. Same protocol was performed to generate the pTol2CG2-*tg*:loxP-CFP-loxP-mCherry-T2A-BRAF^{V600E}-pA however pTol2CG2-*tg*:mCherry-T2A-BRAF^{V600E}-pA was used as a backbone. The full-length pTol2CG2-*tg*:loxP-CFP-loxP-mCherry-T2A-BRAF^{V600E}-pA construct was sequenced for accuracy.

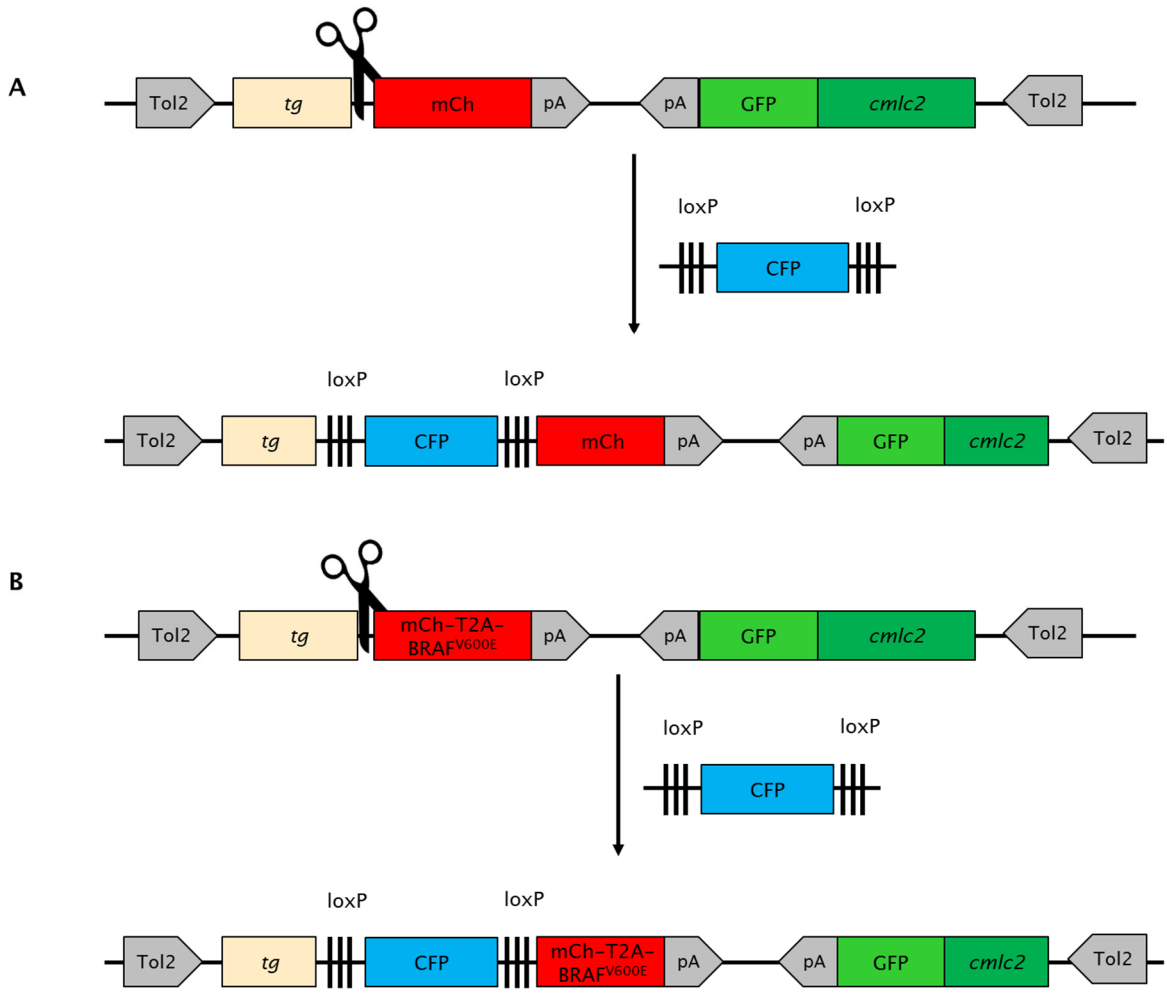

Figure 3. **Cloning strategy to generate conditional constructs.** (A) pTol2CG2-*tg*:loxP-CFP-loxP-mCherry-pA and (B) pTol2CG2-*tg*:loxP-CFP-loxP-mCherry-T2A-BRAF^{V600E}-pA plasmids. The loxP-CFP-loxP cassette was inserted into previously generated constructs. Scissor represent *Sal*I cut.

II.1.7 pCS2-*CMV*:mCherry-pA plasmid

pTol2-*tg*:mCherry-pA and pCS2-*CMV* plasmid were excised with *Bam*I (Thermo Fisher Scientific Inc.). mCherry insert was gel purified and linearized pCS2-*CMV* was dephosphorylated with SAP (Thermo Fisher Scientific Inc.). Plasmid and insert were ligated using T4 ligase (Thermo Fisher Scientific Inc.) and ligation product was transformed into One Shot® TOP10 Chemically Competent Cells (Thermo Fisher Scientific Inc.) (Figure 3). The full-length pCS2-*CMV*:mCherry-pA construct was sequenced for accuracy.

II.1.8 pCS2-*CMV*:mCherry-T2A-BRAF^{WT}-pA and pCS2-*CMV*:mCherry-T2A-BRAF^{V600E}-pA plasmids

pME-mCherry-T2A-BRAF^{WT} and pCS2-*CMV* plasmid were excised with *Xba*I (Thermo Fisher Scientific Inc.) and *Xho*I (Thermo Fisher Scientific Inc.). mCherry-T2A-BRAF^{WT} insert was gel purified and linearized pCS2-*CMV* was dephosphorylated with SAP (Thermo Fisher Scientific Inc.). Plasmid and insert were ligated using T4 ligase (Life Technologies) and ligation product was transformed into One Shot® TOP10 Chemically Competent Cells (Thermo Fisher Scientific Inc.). The full-length pCS2-*CMV*:mCherry-T2A-BRAF^{WT}-pA construct was sequenced for accuracy. Same protocol was performed to generate the pCS2-*CMV*:mCherry-T2A-BRAF^{V600E}-pA however pME-mCherry-T2A-BRAF^{V600E} was used to excise the mCherry-T2A-BRAF^{V600E} insert (Figure 4). The full-length pCS2-*CMV*:mCherry-T2A-BRAF^{V600E}-pA construct was sequenced for accuracy.

II.1.9 Summary of the plasmids generated

Table 1 summarizes the plasmids generated in this work.

Name	Insert	Size
5' entry clones (kanamycin resistant)		
p5E-*tg* promoter	2.0 kb *tg* promoter	4843
Middle entry clones (kanamycin resistant)		
pME-mCherry	mCh	3261
pME-mCherry-T2A-$BRAF^{WT}$	mCh and $BRAF^{WT}$ separated by T2A sequence	5818
pME-mCherry-T2A-$BRAF^{V600E}$	mCh and $BRAF^{V600E}$ separated by T2A sequence	5818
3' entry clone (kanamycin resistant)		
p3E-polyA	SV40 late polyA signal	2838
Destination vector (ampicillin resistant)		
pTol2-*tg*:mCherry-pA	*tg* promoter and mCh reporter*†	7385
pTol2CG2-*tg*:mCherry-pA	*tg* promoter and mCh reporter*†	9298
pTol2CG2-*tg*:mCherry-T2A-$BRAF^{V600E}$-pA	*tg* promoter, mCh reporter and $BRAF^{V600E}$ separated by T2A sequence*†	11855
pTol2CG2-*tg*:loxP-CFP-loxP-mCherry-pA	*tg* promoter, CFP flanked by loxP inverted sequences and mCh reporter*†	10604
pTol2CG2-*tg*:loxP-CFP-loxP-mCherry-T2A-$BRAF^{V600E}$-pA	*tg* promoter, CFP flanked by loxP inverted sequences and mCh reporter and $BRAF^{V600E}$ separated by T2A sequence*†	13161
Plasmids for *in vitro* RNA transcription		
pCS2-*CMV*: mCherry-pA	CMV/SP6 cassette with mCh reporter *	4934
pCS2-*CMV*: mCherry-T2A-$BRAF^{WT}$-pA	CMV/SP6 cassette with mCh reporter and and $BRAF^{WT}$ separated by T2A sequence*	7203
pCS2-*CMV*: mCherry-T2A-$BRAF^{V600E}$-pA	CMV/SP6 cassette with mCh reporter and and $BRAF^{V600E}$ separated by T2A sequence*	7203

Table 1. List of plasmids generated for transgenesis or *in vitro* RNA transcription.

* with SV 40 polyA; † flanked by Tol2 inverted repeats

II.2 Cloning-auxiliary techniques

II.2.1 PCR

To produce small PCR products, standard PCR protocols using non-proofreading enzymes (DreamTaq™ DNA polymerase, Thermo Fisher Scientific Inc. and GoTaq® DNA Polymerase, Promega) were performed according to manufacturer's instructions. To produce large PCR products for cloning, PCR protocols using high proofreading enzymes (iProof™ High-Fidelity DNA Polymerase, BioRad and Phusion High-Fidelity DNA Polymerase, Thermo Fisher Scientific Inc.) were performed according to manufacturer's instructions. PCR reactions were optimized to generate none or very few unspecific amplicons and specific PCR products were sequenced for accuracy.

II.2.2 DNA sequencing

PCR products or DNA plasmids to be sequenced were processed using the BigDye® Terminator v3.1 Cycle Sequencing Kit (Thermo Fisher Scientific Inc.) and according to the manufacturer's instructions. Cycle sequencing include the following conditions: initial denaturation step at 96ºC for 2 minutes followed by 35 cycles at 96ºC for 10 seconds, 55ºC (or more according to the primer annealing temperature) for 30 seconds and 60ºC for 2 minutes and a final extension cycle at 60ºC for 10 minutes. Samples were centrifuged and purified using Sephadex™ G-50 (GE Healthcare) columns and denatured with an equal volume of formamide (GE Healthcare). Sequencing products were resolved by capillary electrophoresis at the Institute of Molecular Pathology and Immunology at the University of Porto (IPATIMUP) Sequencing Service Unit and analyzed using the ABI PRISM® BigDye® v3 Software (Thermo Fisher Scientific Inc.).

II.2.3 DNA quantification

DNA quantification was determined by spectrophotometry using the Nanodrop 2000 spectrophotometer (Thermo Fisher Scientific Inc.). The purity of the nucleic acid preparation was estimated by the ratio between the readings obtained at 260 nm and 280 nm (pure preparations of DNA show ratio values of 1.8-2.0).

II.2.4 Restriction digestion and ligation

Restriction digestions of plasmid DNA were performed using commercial restriction enzymes and buffers and according to manufacturer's instructions. For most restriction digestions, overnight incubations at 37ºC were performed and the volume of enzyme used in each reaction never exceeded 10% of the final reaction volume.

Ligation was performed using a commercial T4 ligase and buffer (Thermo Fisher Scientific Inc.) and according to manufacturer's instructions. All reactions were carried out in a final volume of 10μL unless otherwise specified by the manufacturer.

II.2.5 Isolation of DNA by agarose gel electrophoresis

To isolate DNA by agarose gel electrophoresis, agarose gels were prepared with 1x Tris base, acetic acid and EDTA solution (TAE) buffer or Tris base, boric acid and EDTA solution (TBE) buffer. The final agarose concentration (ranging from 0.8% to 2.0%) was dependent on the size of the DNA fragments to be isolated. Samples were stained with a GelRed working solution prior to loading into the gel. DNA fragments were manually excised from the gel and purified using the Wizard® SV Gel and PCR Clean-Up System (Promega) and following the manufacturer's instructions.

II.2.6 Plasmid transformation in competent E. Coli

All plasmids described in this chapter except the pDest plasmids had either ampicillin or kanamycin resistance genes and they were transformed and grown in ampicillin or kanamycin, respectively, using One Shot® TOP10 Chemically Competent Cells (Thermo Fisher Scientific Inc.). pDest-plasmids had ampicillin and chloramphenicol resistance genes and they were transformed and grown in ampicillin/chloramphenicol using One Shot® ccdB Survival™ 2 T1R Chemically Competent Cells (Thermo Fisher Scientific Inc.). For plasmid transformation, frozen aliquots of competent cells were thawed on ice. Plasmid DNA (10-50ng/uL) was added directly into 50-100μL of cells followed by incubation on ice for 30 minutes. The cells/DNA mix was heatshocked for 42 seconds at 42 ºC and then incubated on ice for 2 minutes. 150μL of pre-warmed Super Optimal Broth (0.5% Yeast

Extract, 2% Tryptone, 10 mM NaCl, 2.5 mM KCl, 10 mM $MgCl_2$, 10 mM $MgSO_4$ and 20 mM Glucose) was added to the mix and incubated at 37 ºC for 60 minutes at 225rpm. This last step was always performed for kanamycin and ampicillin/chloramphenicol resistant plasmids and for larger ampicillin resistant plasmids.

II.2.7 Plasmid growth in solid and liquid cultures

Competent E.coli used for plasmid transformation was spread on plates containing a solid medium of lysogeny broth (LB) and agar (10g Bacto-tryptone, 5g yeast extract, 10g NaCl and 15g agar, pH 7.5). Liquid cultures containing LB medium were prepared by picking single colonies from LB-agar plates. Solid and liquid media were supplemented with the appropriate antibiotic: ampicillin (50-100μg/mL), kanamycin (50μg/mL) and chloramphenicol (30μg/mL). Cultures were grown overnight (12-16 hours) at 37ºC (shaking was only required for liquid cultures).

II.2.8 Plasmid purification

For small scale extraction and purification of plasmid DNA, 5mL-liquid culture (previously screened by colony PCR) was prepared from single colonies. The culture was pelleted for 5 minutes at 5000g and the supernatant was discarded. The purification was performed using the NZYMiniprep (Nzytech) according to the manufacturer's instructions. For large scale extraction and purification of plasmid DNA, 100mL-liquid culture was prepared from pre-innoculated 5mL-liquid cultures. The culture was pelleted for 30 minutes at 3000g at 4ºC and the supernatant was discarded. The purification was performed using the NZYMidiprep (Nzytech) according to the manufacturer's instructions.

II.3 Capped messenger ribonucleic acid (mRNA) synthesis

II.3.1 Capped transposase mRNA synthesis

pCS2FA-transposase plasmid was provided by the Tol2Kit (Kwan et al., 2007). The plasmid was linearized using *Not*I (Thermo Fisher Scientific Inc.) and gel-purified. *In vitro* capped transcription was performed using Ambion mMessage mMachine

SP6 Kit (Thermo Fisher Scientific Inc.) and according to the manufacturer's instructions. *In vitro* transcribed transposase mRNA was purified using Illustra Microspin G-50 (GE Healthcare) columns and run on an agarose gel to confirm its integrity.

II.3.2 Capped mCherry mRNA, mCherry-T2A-BRAF^{WT} mRNA and mCherry-T2A-BRAF^{V600E} mRNA synthesis

pCS2-*CMV*:mCherry was linearized using *Hpa*I (Thermo Fisher Scientific Inc.) and gel-purified. *In vitro* capped transcription was performed using Ambion mMessage mMachine SP6 Kit (Thermo Fisher Scientific Inc.) and according to the manufacturer's instructions. *In vitro* transcribed mCherry mRNA was purified using Illustra Microspin G-50 columns (GE Healthcare) and run on an agarose gel to confirm its integrity. Same protocol was used to synthesize capped mCherry-T2A-BRAF^{WT} and mCherry-T2A-BRAF^{V600E} mRNAs using the pCS2-*CMV*:mCherry-T2A-BRAF^{WT} and pCS2-*CMV*:mCherry-T2A-BRAF^{V600E} plasmids, respectively.

II.4 Microinjections

Microinjections were performed to establish transgenic lines and in mRNA experiments.

II.4.1 DNA plasmid microinjections

pTol2-*tg*:mCh-pA, pTol2CG2-*tg*:mCh-pA, pTol2CG2-*tg*:mCh-T2A-BRAF^{V600E}-pA, pTol2CG2-*tg*:loxP-CFP-loxP-mCh-pA and pTol2CG2-*tg*:loxP-CFP-loxP-mCh-T2A-BRAF^{V600E}-pA plasmids were used to generate the transgenic lines described in this thesis. Plasmid DNA was co-injected with capped transposase mRNA into one-cell stage wild-type (WT) or tg(*hsp70l*:mCherry-T2A-CreER^{T2}) embryos at a final concentration of 30ng/μL and 25ng/μL, respectively. Diethylpyrocarbonate (DEPC)-water was used to bring the injection mix to a final volume of 10μL. Microinjections were performed using the following apparatus: SZX10 Stereo Microscope (Olympus), PV820 Pneumatic PicoPump (World Precision Instruments, Inc.), MN-153 Micromanipulator (Narishige) and MPH6S Microelectrode holder (World Precision Instruments, Inc.). The following injection settings were used: hold

pressure set for 3PSI (vent port), eject pressure set for 20PSI (vent port), range set for 100ms, duration set for gated, period dial set for 7.0. The needle was calibrated to a final drop volume of 1.4nL.

II.4.2 Capped mRNA microinjections

Capped mCherry, mCherry-T2A-BRAF^{WT} mRNA or mCherry-T2A-BRAF^{V600E} mRNAs were microinjected into the yolk of one-cell stage WT or *tp53*^{M214K} embryos at a final concentration of 35ng/μL. DEPC-water was used to bring the injection mix to a final volume of 10μL. Microinjections were performed using the following apparatus: SZX10 Stereo Microscope (Olympus), PV820 Pneumatic PicoPump (World Precision Instruments, Inc.), MN-153 Micromanipulator (Narishige) and MPH6S Microelectrode holder (World Precision Instruments, Inc.). The following injection settings were used: hold pressure set for 3PSI (vent port), eject pressure set for 20PSI (vent port), range set for 100ms, duration set for gated, period dial set for 7.0. The needle was calibrated to a final drop volume of 1nL.

II.5 Transgenesis

To generate transgenic lines, the following general protocol was used: (1) co-microinjection of plasmid DNA and capped transposase mRNA as describe in II.4.1; (2) screening of injected embryos/larvae for the reporters expressed by the transgene; (3) raising injected larva to adulthood; (4) screening mosaic fish and select founders (germline transmission of the transgene) by PCR screening of sperm/eggs and/or progeny screening; (5) outcrossing with WT and/or *tp53*^{M214K} fish and; (6) screening the transgenic progeny and raise to adulthood (Figure 4).

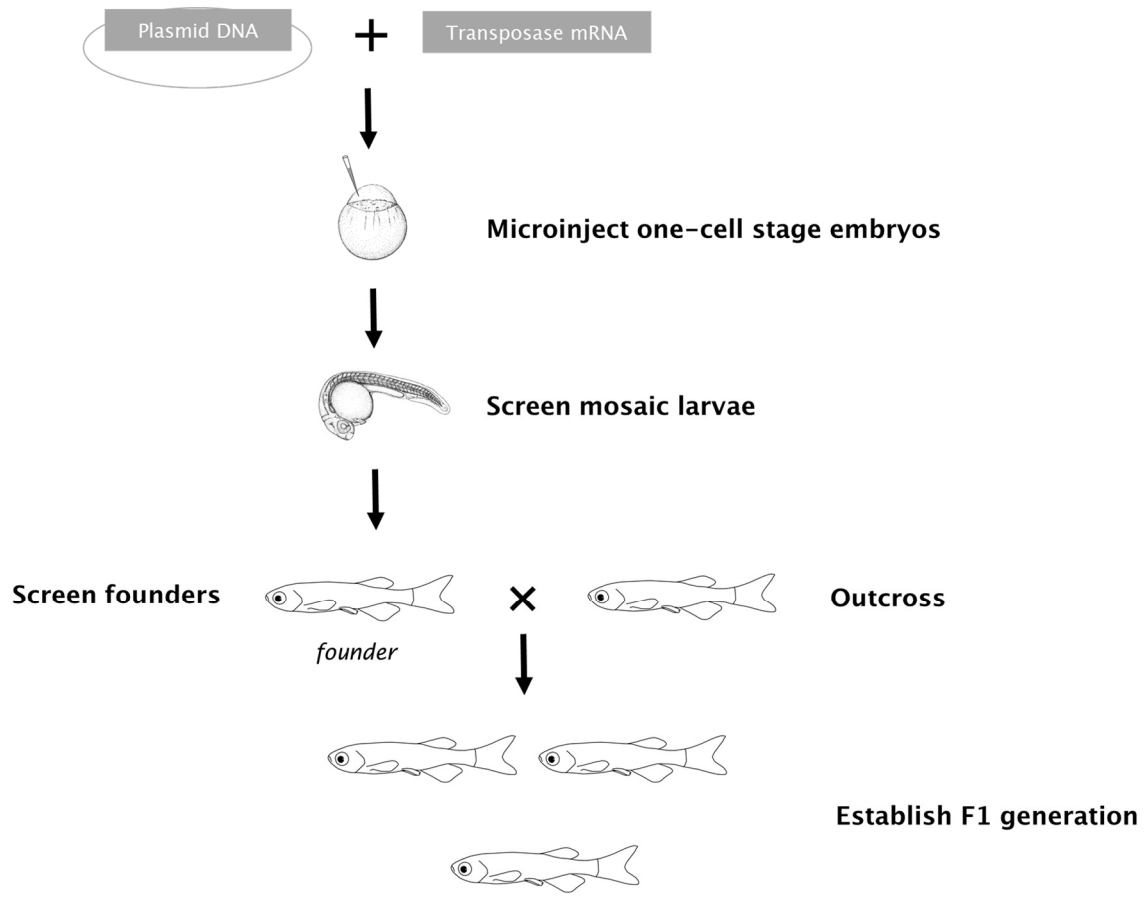

Figure 4. **Transgenesis.** General transgenesis strategy to generate the transgenic lines used in this work: from plasmid injections to F1 generations.

II.5.1 WT lines

tg(*tg*:mCh) Embryos from AB strain were injected with pTol2-*tg*:mCherry-pA plasmid to generate mosaic tg(*tg*:mCh) fish. Founder fish were crossed with WT fish to generate the tg(*tg*:mCh) line. These lines were selected for mCh reporter.

tg(*tg*:mCh;*cmlc2*:EGFP) lines Embryos from AB strain were injected pTol2CG2-*tg*:mCherry-pA plasmid to generate mosaic tg(*tg*:mCh;*cmlc2*:EGFP) fish. Founder fish were crossed with WT fish to generate the tg(*tg*:mCh;*cmlc2*:EGFP) line. These lines were selected for mCh and EGFP reporters, respectively.

tg(*tg*:mCh-T2A-BRAF^{V600E};*cmlc2*:EGFP) line Embryos from AB strain were injected with pTol2CG2-*tg*:mCherry-T2A-BRAF^{V600E}-pA plasmid to generate mosaic tg(*tg*:mCh-T2A-BRAF^{V600E};*cmlc2*:EGFP) fish. Founder fish were crossed with WT fish to generate the tg(*tg*:mCh-T2A-BRAF^{V600E};*cmlc2*:EGFP) line. This line was selected for mCh and EGFP reporters.

tg(*tg*:mCh*; tg*:mCh-T2A-BRAF^{V600E};*cmlc2*:EGFP) line *tg*:mCh fish were crossed with tg(*tg*:mCh-T2A-BRAF^{V600E};*cmlc2*:EGFP) fish to produce the tg(*tg*:mCh*; tg*:mCh-T2A-BRAF^{V600E};*cmlc2*:EGFP) line. This line was selected for mCh and EGFP reporters.

tg(*hsp70l*:mCh-T2A-CreER^{T2}; *tg*:loxP-CFP-loxP-mCh; *cmlc2*:EGFP) line tg(*hsp70l*:mCh-T2A-CreER^{T2}) fish were used to provide embryos to inject the pTol2CG2-*tg*:loxP-CFP-loxP-mCherry-pA plasmid and generate mosaic tg(*hsp70l*:mCh-T2A-CreER^{T2}; *tg*:loxP-CFP-loxP-mCh; *cmlc2*:EGFP) fish. Founder fish were crossed with WT fish if they carried the *hsp70l*:mCh-T2A-CreER^{T2} allele or tg(*hsp70i*:mCh-T2A-CreER^{T2}) fish if they did not. This line was selected for CFP and EGFP reporters and the *hsp70l*:mCh-T2A-CreER^{T2} allele.

tg(*hsp70l*:mCh-T2A-CreER^{T2}; *tg*:loxP-CFP-loxP-mCh T2A-BRAF^{V600E}; *cmlc2*:EGFP) line tg(*hsp70l*:mCh-T2A-CreER^{T2}) fish were used to provide embryos to inject the pTol2CG2-*tg*:loxP-CFP-loxP-mCherry-T2A-BRAF^{V600E}-pA plasmid and generate mosaic tg(*hsp70l*:mCh-T2A-CreER^{T2}; *tg*:loxP-CFP-loxP-mCh T2A-BRAF^{V600E}; *cmlc2*:EGFP) fish. Founder fish were crossed with WT fish if they carried *hsp70l*:mCh-T2A-CreER^{T2} allele or tg(*hsp70i*:mCh-T2A-CreER^{T2}) fish if they did not. This line was selected for CFP and EGFP reporters and the *hsp70l*:mCh-T2A-CreER^{T2} allele.

II.5.2 *tp53^{M214K}* lines

***tp53^{M214K}* tg(*tg*:mCh) line** *tp53^{M214K}* fish were crossed with tg(*tg*:mCh) fish to produce heterozygous *tp53^{M214K}* tg(*tg*:mCh). This line was crossed again with *tp53^{M214K}* fish to produce homozygous *tp53^{M214K}* tg(*tg*:mCh) fish. All lines were

selected for mCh reporter. *tp53*^{M214K} mutation was confirmed by genotyping the fin of selected fish.

***tp53*^{M214K} tg(*tg*:mCh;*cmlc2*:EGFP) line** *tp53*^{M214K} fish were crossed with tg(*tg*:mCh;*cmlc2*:EGFP) fish to produce heterozygous *tp53*^{M214K} tg(*tg*:mCh;*cmlc2*:EGFP). This line was crossed again with *tp53*^{M214K} fish to produce homozygous *tp53*^{M214K} tg(*tg*:mCh;*cmlc2*:EGFP) fish. All lines were selected for mCh and EGFP reporters. *tp53*^{M214K} mutation was confirmed by genotyping the fin of selected fish.

***tp53*^{M214K} tg(*tg*:mCh-T2A-BRAF^{V600E};*cmlc2*:EGFP) line** *tp53*^{M214K} fish were crossed with tg(*tg*:mCh-T2A-BRAF^{V600E};*cmlc2*:EGFP) fish to produce a heterozygous *tp53*^{M214K} tg(*tg*:mCh-T2A-BRAF^{V600E};*cmlc2*:EGFP) line. This line was crossed again with *tp53*^{M214K} fish to produce a homozygous *tp53*^{M214K} tg(*tg*:mCh-T2A-BRAF^{V600E};*cmlc2*:EGFP) line. All lines were selected for mCh and EGFP reporters. *tp53*^{M214K} mutation was confirmed by genotyping the fin of selected fish.

***tp53*^{M214K} tg(*tg*:mCh*; tg*:mCh-T2A-BRAF^{V600E};*cmlc2*:EGFP) line** *tp53*^{M214K} tg(*tg*:mCh) fish were crossed with *tp53*^{M214K} tg(*tg*:mCh-T2A-BRAF^{V600E};*cmlc2*:EGFP) fish to produce the *tp53*^{M214K} tg(*tg*:mCh*; tg*:mCh-T2A-BRAF^{V600E};*cmlc2*:EGFP) line. This line was selected for mCh and EGFP reporters. *tp53*^{M214K} mutation was confirmed by genotyping the fin of selected fish.

II.6 Fish strains and husbandry

AB wild-type fish was the zebrafish strain used throughout the work. Embryos and larvae <7dpf/dpi were collected from pair mating or outcrosses and kept in embryo medium (5.0mM NaCl, 0.17mM KCl, 0.33mM CaCl, 0.33mM $MgSO_4$, 0.05% methylene blue, pH 7.4) at 28°C on a 14 hour light/10 hour dark cycle. Zebrafish ≥7dpf/7dpi were kept in a recirculating system at 28°C on a 14 hour light/10 hour dark cycle according to Westerfield et al., 2000. Fish were kept in standard densities (10-12 fish/liter of water).

II.7 Screening and Imaging

The transgenic lines generated expressed mCherry, EGFP and/or CFP reporters. Screening of embryos, larvae and adult fish was performed on a Zeiss Stereo LUMAR stereoscope. Images were acquired on the Zeiss Stereo Lumar.V12 stereoscope equipped with a Hamamatsy Orca-ER CCD Camera, controlled with the MicroManager v1.14 software. Bright field (BF) images were acquired using the Lumar filter LP420 and fluorescence images were acquired with Lumar filters for Texas Red®, EGFP and CFP.

II.8 Fin clip and gDNA extraction

Fish were fasten, prior to anesthesia, in tricaine methane sulfonate (MS222) (168ug/L, Sigma). The fin was clipped with a sharp scalpel at a point not greater than halfway between the tip of the fin and the point where the scales end. Fish were then immediately transferred to a container with fresh system water and monitored until they recovered and regained swimming ability. Fin tissue was placed in an eppendorf tube containing 100μL of 50mM NaOH. The sample was heated at 95ºC for 15 minutes or until the tissue was noticeably friable. The sample was cooled to 4ºC and 1/10th volume of 1M Tris-HCl, pH 8.0 was added to neutralize the basic solution. A centrifugation to pellet the debris was performed at maximum speed for 10 minutes at room temperature. The supernatant containing the genomic DNA was collected to a new tube and stored at 4ºC or longer at -20ºC.

II.9 Genotyping

tp53^{M214K} mutation was genotyped using primers to amplify the loss-of-function (LOF) point mutation on exon 7 of the zebrafish *tp53* gene (homozygous fish were selected if T>A was in both alleles; heterozygous fish were selected if T>A was in one allele) as described by Berghmans et al., 2005. The following primers were used: forward primer 5'-CACAAGTGTCCTGTTATCGAT-3' and reverse primer 5'-CATGGCAAGGCAACTGAACTGT-3'.

Conditional lines were also genotyped for the *hsp70l*:mCh-T2A-CreER^{T2} allele using primers to amplify the Cre recombinase (Cre) coding sequence. The

tg(*hsp70l*:mCherry-T2A-CreER^{T2}) line (Hans et al., 2011) does not have a transgenesis marker and progeny from this line can result in WT or transgenic fish. It was only possible to genotype adults. The following primers were used: forward primer 5'-GCATTTCTGGGGATTGCTTA-3' and reverse primer 5'-CCCGGCAAAACAGGTAGTTA-3'.

II.10 Histopathology

7dpf larvae were euthanized by submersion in ice water (5 parts of ice/1 part of water, 0-4ºC) for at least twenty minutes to ensure death by hypoxia. Larvae ≥8dpf were euthanized by an overdose of MS222 (200mg/L, Sigma) by prolonged immersion. Larvae 7-14dpf were fixed in formaldehyde (Sigma-Aldrich) for one day and larvae ≥15dpf were fixed in formaldehyde (Sigma-Aldrich) for two days and then decalcified in 0.5M ethylenediaminetetraacetic acid (EDTA) for one or two more days before paraffin embedding and sectioning. 3μm longitudinal sections representative of the whole larvae or representative of the adult head were performed. Hematoxylin-Eosin (HE) staining were performed according to standard techniques by the HistopathUnit at Instituto Gulbenkian de Ciência (IGC).

Images were acquired on a Leica DM LB2 upright microscope equipped with an IDS color CCD camera using the following objectives: 10x 0.25NA and 40x 0.75NA and using the uEye Cockpit software (Imaging Development Systems GmbH, Germany).

II.11 Measurement of standard length in larvae

Parichy et al., 2009 proposed standard length (SL), defined by the distance from the snout to the caudal peduncle, as a readout of developmental stage (Parichy et al., 2009). SL was measured at 7dpf in larvae anesthetized in tricaine methane sulfonate (MS222 168ug/L, Sigma). Images were acquired on the Zeiss Stereo LUMAR stereoscope equipped with a Hamamatsy Orca-ER CCD Camera and EGFP and Texas Red® filtersets, controlled with the MicroManager v1.14 software. Measurements were performed using the LAS AF Lite software (Leica Microsystems).

II.12 Measurement of body mass index (BMI)

Body weight (kg) and body length (m) of adult fish were measured at 3 months post fertilization (mpf) and 12mpf. Fish were fasten prior to anesthesia in MS222 (168ug/L, Sigma). Body length was measured from the head to the end of the caudal fin. Body weight and body length were used to calculate the BMI according to the formula: BMI = (body weight kg)/(body length m^2).

II.13 Measurement of thyroid volume in adult fish

Paraffin blocks were exhaustively sectioned into 3-µm-thick sections covering the whole thyroid of the adult fish as previously described. Thyroid middle sections were determined according to the distance between the first and the last sections displaying thyroid tissue and the ventral aorta position. 5 longitudinal sections of each fish were chosen (middle section, 1/3 and 2/3 of total thyroid sections starting from the middle section) (Figure 5). Images were acquired on a Leica DM LB2 upright microscope equipped with an IDS color CCD camera using the following objectives: 10x 0.25NA and 20x 0.5NA and using the uEye Cockpit software (Imaging Development Systems GmbH, Germany). To measure the follicle area, measurements were performed on ImageJ2 (National Institutes of Health, USA) and for each fish total follicle area was calculated by the sum of all individual areas. To calculate a representative total thyroid volume, total follicle area and thickness were multiplied.

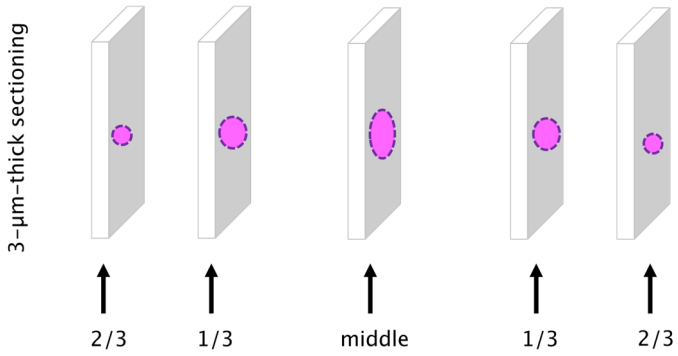

Thyroid volume = (Σ Follicle area) x section thickness

Figure 5. **Measurement of thyroid volume in adult fish using five 3-µm-thick sections that would be representative of the volume.** Pink circles outlined by purple dashes represent thyroid follicles and grey boxes represent 3µm-tissue sections.

II.14 Preparation of embryo lysates

Embryos from mRNA experiments were manually dechorionated and deyolked at 4hpf/4hpi (n=50) as described by Link et al., 2006. Embryo lysates were prepared by adding 100µL of radioimmunoprecipitation assay buffer (RIPA) Buffer (10 mM Tris-Cl pH 8.0, 1 mM EDTA, 0.5 mM EGTA, 1% Triton X-100, 0.1% sodium deoxycholate, 0.1% SDS, 140 mM NaCl and 1 mM PhenylMethylSulfonyl Fluoride-PMSF) supplemented with 1x phosphatase and 1x protease inhibitors (ThermoFisher Scientific). Embryos were mashed with a cell pestle for 30 seconds on ice. Protein extracts were incubated for 30 minutes on ice and centrifuged at 13.000rpm for 10 minutes at 4ºC. The supernatant was collected to a new eppendorf tube and stored at -80ºC prior to use.

II.15 Dissection of thyroid tissue in adult zebrafish

Adult zebrafish was euthanized by an overdose of MS222 (200mg/L, Sigma, MI, USA) by prolonged immersion, rinse in water and then dried on a paper towel. Thyroid tissue was dissected with the help of a Zeiss Stereo LUMAR stereoscope and immediately transferred to an eppendorf placed on dry ice until preparation of tissue lysates.

II.16 Preparation of tissue lysates

Tissue lysates were prepared by adding 100µL of RIPA Buffer (10 mM Tris-Cl pH 8.0, 1 mM EDTA, 0.5 mM EGTA, 1% Triton X-100, 0.1% sodium deoxycholate, 0.1% SDS, 140 mM NaCl and 1 mM PMSF) supplemented with 1x phosphatase and 1x protease inhibitors (ThermoFisher Scientific). Dissected tissue was mashed with a cell pestle for 45 seconds on ice. Protein extracts were incubated on ice for 30 minutes and centrifuged at 13000rpm for 10 minutes at 4ºC. The supernatant was collected to a new eppendorf tube and stored at -80ºC prior to use.

II.17 Immunoblotting

Total protein extracts from tissue or embryo lysates were thawed and prepared by adding an equal volume of 2x Laemmli sample buffer (100 mM Tris-Cl pH 6.8, 2% SDS and 20% glycerol supplemented with 1/10 volume of B-mercaptoethanol). Samples were heated at 95ºC for 5 minutes and immediately run in 10% sodium dodecyl sulfate polyacrylamide gel electrophoresis (SDS PAGE) gels. After proper resolution, samples were transferred to HyBond-P PVDF membranes (GE Healthcare) previously activated with methanol. Following the transfer, the membranes were stained with Ponceau Red to confirm protein loading. Membranes were blocked with 5% non-fat milk in 1x tris-buffered saline (TBS)-t20 for 60 minutes in slow shaking. Then, membranes were probed overnight at 4ºC with primary antibodies. The following primary antibodies and dilutions were used: Living Colors® DsRed Polyclonal Antibody (dilution 1:1000 in 5% non-fat milk in 1x TBS-t20, Clontech Lab), Raf-B Antibody - C19 sc:166, (dilution 1:500 in 5% non-fat milk in 1x TBS-t20, Santa Cruz Biotechnology), phospho p44/42 MAPK (ERK1/2) (Thr202/Tyr 204) Antibody (dilution 1:1000 in 5% non-fat milk in 1x TBS-t20, Cell Signaling), PCNA Antibody FL-261 (dilution 1:1000 in 5% non-fat milk in 1x TBS-t20, Santa Cruz Biotechnology), CDKN2a/p16 (F12) Antibody (dilution 1:1000 in 5% non-fat milk in 1x TBS-t20, Santa Cruz Biotechnology), p53 Antibody (dilution 1:500 in 5% non-fat milk in 1x TBS-t20, Anaspec), Anti-active caspase 3 Antibody (dilution 1:500 in 5% non-fat milk in 1x TBS-t20, Abcam), Anti-pan-Akt (Phospho T308) Antibody (dilution 1:1000 in 5% non-fat milk in 1x TBS-t20, Abcam), Phospho-Akt (Ser 473) (D9E) XP® Antibody (dilution 1:1000 in 5% non-fat milk in 1x TBS-t20, Cell Signaling) and Phospho-p38 MAPKinase (Thr180/Tyr182) Antibody (dilution 1:1000 in 5% non-fat milk in 1x TBS-t20, Cell Signaling). Overnight probing was followed by washes in 1x TBS-t20 and by incubation for 1-3 hours at room temperature with species-specific horseradish peroxidase (HRP)-conjugated antibodies. The following secondary antibodies and dilutions were used: goat anti-mouse IgG-HRP Antibody (dilution 1:1000 or 1:2000 in 5% non-fat milk in 1x TBS-t20, Santa Cruz Biotechnology) and goat anti-rabbit IgG-HRP Antibody (dilution 1:1000/1:2000 in 5% non-fat milk in 1x TBS-t20, Santa Cruz Biotechnology, USA). Membranes were washed in 1x TBS-t20 and developed manually using the Pierce™ ECL Plus Western Blotting Substrate detection system (ThermoFisher Scientific). Protein expression levels from western blot band densities were quantified on ImageJ2 and normalized for tubulin.

II.18 Heatshock and drug treatment

2 ½ mpf fish were heat-shocked in a 37ºC water bath for 30 minutes and immediately a drug treatment was carried out. 4-hydroxyl-tamoxifen (4-OHT) (H7904, Sigma) was dissolved at 10mM in 100% ethanol and stored at -20ºC (protected from light). Subsequent dilutions to prepare working solutions were made immediately before use, in embryo medium, to 2.5μM. Controls were treated with an equivalent amount of 100% ethanol diluted in embryo medium. Fish received treatment at 28ºC for 5 hours in the dark followed by a recovery period in fresh water for 12 hours.

II.19 Statistical analysis

Statistical analysis was performed using GraphPad Prism version 6.0 (GraphPad Software Inc, San Diego, CA) using T-Student test and Mann-Whitney U test. Results were considered statistically significant when $p<0.05$ (*$p<0.05$; **$p<0.01$; ***$p<0.001$ and ****$p<0.0001$) and not statistically significant when $p\geq0.05$.

Chapter III

Results

III.1 Frequency of *TERT* promoter mutations in human cancers

nature COMMUNICATIONS

ARTICLE

Received 19 Apr 2013 | Accepted 25 Jun 2013 | Published 26 Jul 2013

DOI: 10.1038/ncomms3185

Frequency of *TERT* promoter mutations in human cancers

João Vinagre[1,2,*], Ana Almeida[1,2,*], Helena Pópulo[1,*], Rui Batista[1], Joana Lyra[1,3], Vasco Pinto[1,3], Ricardo Coelho[1,2], Ricardo Celestino[1], Hugo Prazeres[1,4], Luis Lima[2,5,6,7], Miguel Melo[8,9], Adriana Gaspar da Rocha[1,3], Ana Preto[1,10], Patrícia Castro[1], Ligia Castro[3,11], Fernando Pardal[12], José Manuel Lopes[1,3,11], Lúcio Lara Santos[5], Rui Manuel Reis[13,14], José Cameselle-Teijeiro[15], Manuel Sobrinho-Simões[1,3,11], Jorge Lima[1,3], Valdemar Máximo[1,3] & Paula Soares[1,3]

Reactivation of telomerase has been implicated in human tumorigenesis, but the underlying mechanisms remain poorly understood. Here we report the presence of recurrent somatic mutations in the *TERT* promoter in cancers of the central nervous system (43%), bladder (59%), thyroid (follicular cell-derived, 10%) and skin (melanoma, 29%). In thyroid cancers, the presence of *TERT* promoter mutations (when occurring together with *BRAF* mutations) is significantly associated with higher *TERT* mRNA expression, and in glioblastoma we find a trend for increased telomerase expression in cases harbouring *TERT* promoter mutations. Both in thyroid cancers and glioblastoma, *TERT* promoter mutations are significantly associated with older age of the patients. Our results show that *TERT* promoter mutations are relatively frequent in specific types of human cancers, where they lead to enhanced expression of telomerase.

[1] Institute of Molecular Pathology and Immunology of the University of Porto (IPATIMUP), 4200-465 Porto, Portugal. [2] Institute of Biomedical Sciences of Abel Salazar, University of Porto, 4050-313 Porto, Portugal. [3] Medical Faculty, University of Porto, 4200-319 Porto, Portugal. [4] Portuguese Institute of Oncology—Coimbra Centre (IPOFG, EPE), 3000-075 Coimbra, Portugal. [5] Experimental Pathology and Therapeutics Group, Portuguese Institute of Oncology, 4200-072 Porto, Portugal. [6] Nucleo de Investigação em Farmácia, Centro de Investigaçãoem Saúde e Ambiente (CISA), Health School of the Polytechnic Institute of Porto, 4400-330 Vila Nova de Gaia, Portugal. [7] Research Department, Portuguese League Against Cancer (Norte), 4200-177 Porto, Portugal. [8] Department of Endocrinology, Diabetes and Metabolism, University Hospital of Coimbra, 3000-075 Coimbra, Portugal. [9] Unit of Endocrinology, Medical Faculty, University of Coimbra, 3000-548 Coimbra, Portugal. [10] Centre of Molecular and Environmental Biology (CBMA), Department of Biology, University of Minho, Campus de Gualtar, 4710-057 Braga, Portugal. [11] Department of Pathology, Hospital S. João, 4200-319 Porto, Portugal. [12] Department of Pathology, Hospital de Braga, 4710-243 Braga, Portugal. [13] Life and Health Sciences Research Institute (ICVS), School of Health Sciences, University of Minho, 4710-057 Braga, Portugal. [14] Molecular Oncology Research Center, Barretos Cancer Hospital, CEP 14784-400 São Paulo, Brazil. [15] Department of Pathology, Clinical University Hospital, SERGAS, Medical Faculty, University of Santiago de Compostela, IDIS, 15706 Santiago de Compostela, Spain. * These authors contributed equally to this work. Correspondence and requests for materials should be addressed to P.S. (email: psoares@ipatimup.pt).

Reactivation or re-expression of telomerase is referred to be a widespread feature in human cancers, although the genetic basis remains poorly understood in many cancer types. Somatic mutations in the coding region of *TERT* (human telomerase reverse transcriptase) are infrequent in human tumours, but germline and somatic mutations in *TERT* promoter were recently found in a high percentage of human melanomas and human cancer cell lines[1,2]. Such mutations occurred in two hotspot positions, located −124 and −146 bp upstream from the ATG start site (−124 G>A and −146 G>A, C>T on opposite strand) and conferred enhanced *TERT* promoter activity[1,2], by putatively generating a consensus binding site (GGAA) for ETS transcription factors within the *TERT* promoter region[1,2].

Our aim was to investigate whether the aforementioned *TERT* promoter mutations were present in cancer types other than melanoma, having for that matter screened 741 primary tumours from the thyroid, kidney, bladder, gastrointestinal stromal tumour (GIST), adrenal medulla (phaeochromocytomas) and central nervous system (CNS). Besides skin melanoma, we have also included ocular melanoma (not studied in the previous reports), benign lesions of the thyroid and skin and 58 human cancer-derived cell lines. Our results highlight *TERT* promoter mutations as frequent events in specific types of human cancers.

Results

TERT mutations in tumours and cell lines. Overall, *TERT* promoter mutations were found in 142 (19%) human tumour samples (Table 1; Fig. 1a) and 14 (24%) human cell lines (Fig. 1b; Supplementary Tables S1 and S2). The −124-bp mutation was the most frequent, being present in 99 cases, whereas the −146-bp mutation was present in 43 cases. The −124 G>A and −146 G>A mutations were found in a mutually exclusive fashion. Two tandem GG>AA mutations at positions −124/−125 and −138/−139 bp were observed in one cell line each (Supplementary Fig. S1 and Supplementary Table S1). *TERT* promoter mutations were not detected in normal thyroid tissue nor in benign lesions (nevi, thyroiditis, goitres and adenomas). No mutations were detected in 26 kidney cancers, 17 phaeochromocytomas and 36 GISTs.

TERT mutations in melanoma. We have analysed both skin and ocular melanomas, a type of melanoma that was not previously studied[1,2]. *TERT* mutations were present in 16 out of 56 (29%) skin melanomas, but absent in the 25 ocular melanomas (Table 1). All the four skin melanoma-derived cell lines but none of the six ocular melanoma-derived cell lines harboured *TERT* mutations (Fig. 1b and Supplementary Table S1). Ten out of 16 (63%) skin melanomas with *TERT* mutation also harboured the *BRAFV600E* mutation, whereas the *BRAF* mutation was present in 9 out of 38 (24%) melanomas without *TERT* mutation ($P=0.01$, Fisher's exact test, two-sided) (Supplementary Fig. S2 and Supplementary Table S3).

TERT mutations in CNS tumours. In CNS tumours, *TERT* promoter mutations were found in 43% (51/118) of all cases with an equal prevalence of both mutations (Table 1 and Supplementary Table S4). The frequency of *TERT* mutations was different according to the tumour histology and grade (Fig. 1c): although pilocytic astrocytomas (World Health Organization (WHO) grade 1) and diffuse astrocytoma (WHO grade 2) showed a lower frequency of mutations (8% and 15%, respectively), the most aggressive form, glioblastoma multiforme (GBM; WHO grade 4), present the highest frequency of *TERT* mutations (62%). Oligodendrogliomas (WHO grade 2) and anaplastic oligodendrogliomas (WHO grade 3) also harboured a high frequency of *TERT* mutations (45% and 54%, respectively).

Table 1 | Prevalence of *TERT* promoter recurrent mutations in human cancers.

Organ/tissue	Number	*TERT* mutation, *N* (%)
Melanocytes		
Nevi	9	0
Skin melanoma	56	16 (29%)
Ocular melanoma	25	0
CNS		
Pilocytic astrocytoma	13	1 (8%)
Diffuse astrocytoma	20	3 (15%)
Oligodendroglioma	22	10 (45%)
Anaplastic oligodendroglioma	24	13 (54%)
Glioblastoma	39	24 (62%)
Thyroid		
Benign	81	0
PTC	169	13 (8%)
FTC	64	9 (14%)
PDTC	14	3 (21%)
ATC	16	2 (13%)
MTC	28	0
Bladder		
Low grade	21	14 (67%)
High grade	61	34 (56%)
Kidney		
CCRCC	12	0
CromRCC	4	0
PRCC	10	0
Adrenal		
Phaeochromocytoma	17	0
GI		
GIST	36	0
Total	741	142 (19%)

ATC, anaplastic thyroid carcinoma; CCRCC, clear cell renal cell carcinoma; CNS, central nervous system; CromRCC, chromophobe renal cell carcinoma; FTC, follicular thyroid carcinoma; GI, gastrointestinal; GIST, gastrointestinal stromal tumour; MTC, medullary thyroid carcinoma; PDTC, poorly differentiated thyroid carcinoma; PRCC, papillary renal cell carcinoma; PTC, papillary thyroid carcinoma.

The presence of *TERT* mutations was significantly associated with a higher mean age at diagnosis (Supplementary Table S5) in CNS patients as a whole ($P<0.0001$; Mann–Whitney test, two-tailed) and also in GBM patients only ($P=0.0247$; Mann–Whitney test, two-tailed); in oligodendroglioma patients, we found the same trend, although not statistically significant ($P=0.0709$; Mann–Whitney test, two-tailed). In addition, we observed that, in a subset of 14 GBM (8 *TERT* wild-type tumours and 6 *TERT*-mutated tumours), the tumours with *TERT* mutations showed a trend to increased immunohistochemistry (IHC) expression of telomerase, although this difference was not statistically significant ($P=0.4250$; Mann–Whitney test, two-tailed) (Fig. 2).

TERT mutations in thyroid cancer. We analysed a large series of follicular cell-derived thyroid samples including normal thyroid ($n=27$), benign ($n=81$) and malignant lesions ($n=263$) (Table 1 and Supplementary Table S6). *TERT* mutations were only detected in malignant tumours (10%) (Fig. 1d), namely in

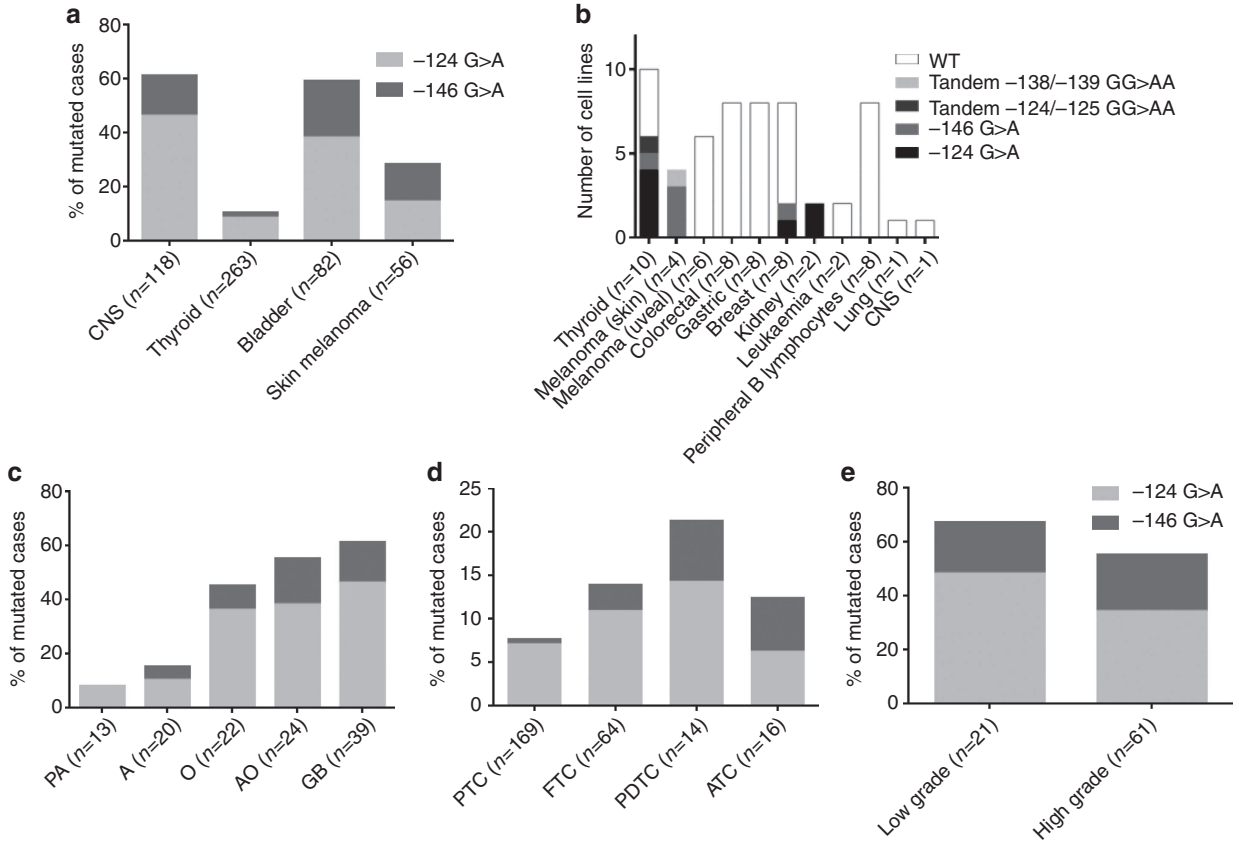

Figure 1 | Frequency and schematic illustration of *TERT* promoter mutations in human cancers. Graphics depict the overall frequency of *TERT* mutations in the four tumour types where *TERT* mutations were detected (**a**) and a bar plot showing the number of cell lines of different origin that harbour *TERT* mutations (**b**). The frequency and type of *TERT* mutations in different histological subtypes of CNS (**c**), thyroid (**d**) and bladder (**e**) tumours is also shown. A, diffuse astrocytoma; AO, anaplastic oligodendroglioma; ATC, anaplastic thyroid carcinoma; GB-glioblastoma; FTC, follicular thyroid carcinoma; O, oligodendroglioma; PA, pilocytic astrocytoma; PDTC, poorly differentiated thyroid carcinoma.

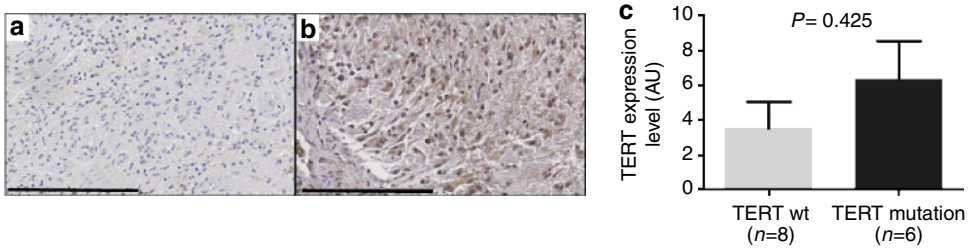

Figure 2 | IHC for TERT in two glioblastomas. (**a**)A tumour without TERT expression and without *TERT* mutation. (**b**) A tumour with positive staining both in nucleus and cytoplasm that also harboured a *TERT* mutation. The graph (**c**) displays quantification of TERT nuclear expression level (IHC) in glioblastomas with and without *TERT* mutation. We have measured the extent (<25%, 25–50%, 50–75% and >75%) and the intensity (absent, faint, moderate or strong) of TERT nuclear staining in 14 glioblastomas (eight *TERT* wild type and six *TERT* mutant). The scoring was performed by two independent observers and is the product of extent and intensity of the staining (Methods). Scale bar, 200 μm. There is a trend to higher TERT expression in *TERT*-mutated gliomas, although the difference was not statistically significant ($P = 0.4250$; Mann–Whitney test, two-tailed). Bars represent s.e.m.

11% of papillary thyroid carcinomas (PTCs), 14% of follicular thyroid carcinomas, 21% of poorly differentiated thyroid carcinomas and 13% of the anaplastic thyroid carcinomas. Within the group of PTC, *TERT* mutations were detected to be associated to the so-called conventional PTC (cPTC) (11%).The majority of *TERT*-mutated thyroid cancers harboured the −124 G>A mutation (22 out of 27 cases) (Fig. 1d and Supplementary Table S7). In thyroid cancer patients, *TERT* mutations were significantly associated with guarded prognosis features such as larger tumours ($P = 0.008$; Mann–Whitney test, two-tailed), older patients ($P < 0.0001$; Mann–Whitney test, two-tailed) and male gender ($P = 0.0312$; Fisher's exact test, two-sided) (Supplementary Table S5). After histotype stratification, such correlations were only kept in the group of cPTC where we also found significant associations with lymph node metastasis ($P = 0.0318$; Fisher's exact test, two-sided) and *BRAFV600E* mutation ($P = 0.001$; Fisher's exact test, two-sided) (Supplementary Fig. S2 and Supplementary Table S8). Accordingly, we verified by quantitative RT-PCR (qPCR) that *TERT* mRNA is expressed at variable amounts in thyroid tumours, and

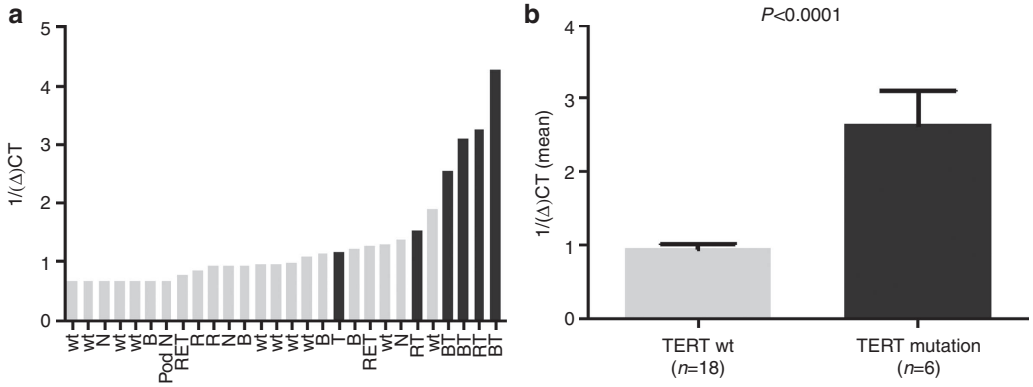

Figure 3 | Quantification of *TERT* mRNA expression level in thyroid tumours. We have performed qPCR in normal thyroid tissue (N), a pool of mRNA of nine normal thyroids (pool N) and thyroid tumours with different genetic backgrounds: without known genetic alterations (wt), with *BRAF* mutation (B), with *RET* rearrangement (RET), with *RAS* mutation (R), with *TERT* mutation (T), with *TERT* and *BRAF* mutations (BT) or with *RAS* and *TERT* mutations (RT). (**a**) Each bar represents *TERT* mRNA expression in an individual tumour measured in triplicate. *TERT* mRNA levels were normalized against *TBP* mRNA levels. (**b**) Quantification of *TERT* mRNA mean expression level in thyroid tumours with and without *TERT* mutation. Error bars represent s.e.m. The difference is statistically significant ($P<0.0001$, unpaired *t*-test).

the ones with coexistent *TERT* and *BRAF* mutations showed the highest levels of *TERT* mRNA expression ($P=0.0001$, unpaired *t*-test; Fig. 3).

TERT mutations in bladder cancer. In bladder cancer, *TERT* mutations were frequently detected (48/82; 59%) both in low-grade tumours (14/21; 67%) and high-grade tumours (34/61; 56%) (Table 1 and Fig. 1e; Supplementary Table S9). The -124 G>A mutation was present in 30 cases, whereas the -146 G>A was found in 18 cases. No association was found between the presence of the mutation and the age of the patients.

No mutations were detected in 26 kidney cancers, 17 phaeochromocytoma and 36 GISTs (Supplementary Tables S10, S11 and S12, respectively).

Discussion

Recent findings have described that *TERT* promoter mutations arise as a novel mechanism of telomerase reactivation/expression in human cancers[1,2]. In this work, we report for the first time the presence of these mutations in different histotypes of thyroid cancer, and our results validate the findings reported by others in melanoma, bladder and gliomas[1–3]. Furthermore, we present for the first time evidence showing that *TERT* promoter mutations are significantly associated with increased *TERT* mRNA expression in thyroid cancers. We also found a trend for increased telomerase expression in cases of GBM harbouring *TERT* promoter mutations. In thyroid cancers, *TERT* mRNA was particularly high in cases harbouring both *TERT* and *BRAF* mutations.

The location of these mutations in the *TERT* promoter, rather than the coding region of the gene, creating additional binding sites for transcription factors, represents also a novel mechanism of genetic activation in cancer.

The frequency of *TERT* mutations we detected in skin melanomas is similar to that reported by Horn *et al.*[1] in primary melanomas (33%), but lower than the frequency found by the same authors in metastatic melanomas (85%) and by Huang *et al.*[2] in a series of 70 melanomas and short-term cultures[1,2]. In our series, we have analysed few metastatic melanomas that did not show a significantly higher percentage of *TERT* mutations. As our series is too small to allow a conclusion, it remains to be verified if there is an increased frequency of *TERT* mutations in metastatic melanomas, as suggested by previous reports[1,2].

We have confirmed, in skin melanomas, the significant association between *TERT* and *BRAF* mutations, as previously advanced by Horn *et al.*[1], which we now also demonstrate in thyroid cancers. Interestingly, in benign nevi, which frequently harbour *BRAF* mutations, we did not detect *TERT* mutations. This finding, together with the high frequency of *TERT* mutations in metastatic melanomas[1], suggests that, although *BRAF* mutations are thought to be an early event in melanoma genesis, *TERT* mutations may occur at a later stage.

No *TERT* promoter mutations were found in ocular melanomas, which, at variance with skin melanomas, harbour *GNAQ* mutations instead of *BRAF* mutations[4,5]. Our results further support the assumption that ocular melanomas result from different etiopathogenic mechanism than skin melanomas[5,6].

Our data on CNS tumours indicate that *TERT* promoter mutations are frequent events in gliomas, particularly in GBM where the highest mutation frequency was found. It has been shown that TERT mutations conferred enhanced TERT promoter activity *in vitro*[1,2]; our findings fit with this assumption because we observed that GBM with TERT promoter mutations appear to display increased telomerase expression, despite the limited sensitivity of IHC and the low number of cases analysed. Our results are also in concordance with those of Lotsch *et al.*[7] who reported that 60% of GBMs were positive for *TERT* mRNA and telomerase activity[7]. It will be interesting to assess whether the GBM positive for telomerase activity described by Lotsch *et al.*[7] also harbour *TERT* promoter mutations. Our findings also indicate that *TERT* mutations are associated with older patients, in accordance with a recent report[3]. The high frequency of *TERT* mutations in CNS tumours, particularly in intermediate and high-grade tumours, opens a window for new approaches in the therapy of CNS tumours.

In thyroid cancer, *TERT* mutations were only found in follicular cell-derived cancers (PTC, follicular thyroid carcinoma, poorly differentiated thyroid carcinoma and anaplastic thyroid carcinoma). No mutations were detected in medullary thyroid carcinomas, as described by Killela *et al.*[3], nor in normal thyroid and benign lesions, such as goitre, adenomas or thyroiditis; this finding fits with previous studies that reported telomerase expression in malignant lesions and not in normal tissue or hyperplastic lesions[8,9]. *TERT* mutations were associated with clinicopathological features (older age, increased tumour size and

male gender), but, after histotype stratification, these associations were only maintained in cPTC. Studies in larger series will be necessary to clarify these associations. In cPTC, *TERT* mutations were associated with *BRAF* mutation, highlighting the coexistence of activation of *BRAF* and *TERT*, previously reported in melanoma[1] (Supplementary Fig. S2). Our results reinforce the hypothesis of a link between *BRAF* activation and telomerase expression, which can be mediated by transcription factors binding to the newly created consensus binding sites, as previously advanced by Horn *et al.*[1]. Both in thyroid carcinoma and melanoma, it seems that a 'background' status of activated *BRAF* enhances the effects of *TERT* promoter mutation. Our results in *TERT* mRNA expression strengthen this assumption, showing, for the first time, an increased *TERT* expression in tumours harbouring *BRAF* and *TERT* mutation (Fig. 3). Further observational and mechanistic studies are needed to clarify these points.

TERT alterations seem to constitute an early and frequent event in bladder cancer. These findings fit with the high prevalence of telomerase activity previously described in bladder tumours[10]. The recurrent hotspot mutations in *TERT* were advanced to be, in melanomas, induced by ultraviolet radiation[2]. Bladder is a target for several chemical carcinogens; it remains to be found whether *TERT* mutations can also result from the action of such agents. The identification of *TERT* mutations in urine may provide a biomarker for early diagnosis and monitoring of bladder cancer.

No *TERT* mutations were detected in kidney cancers, nor in 17 phaeochromocytoma and 36 GISTs. The underlying reasons for the tissue specificity of *TERT* mutations remain to be clarified. We can hypothesize that *TERT* mutations can be present in two settings. As described by Killela *et al.*[3], *TERT* mutations can be relevant in tissues with relative low rates of self-renewal, which fits with our findings in follicular cell-derived thyroid cancer and gliomas where they are associated with the older age of the patients. On the other hand, these mutations can also result from environmental factors such as ultraviolet radiation and chemical carcinogens as suggested by their high frequency in melanoma, bladder and tongue[1–3]. In summary, our data identify *TERT* mutations as common events in human cancers and support the assumption that *TERT* promoter mutations may be one of the mechanisms that underlies telomerase reactivation in several types of human tumours.

Methods

Human cancer samples. All the procedures described in this study were in accordance with national and institutional ethical standards and previously approved by Local Ethical Review Committees. According to Portuguese law, informed consent is not required for retrospective studies.

Formalin-fixed, paraffin-embedded tissues from nine cases of sporadic nevi, 56 cases of sporadic skin melanomas and 25 cases of ocular melanoma were retrieved from the files of the Hospital S. João (HSJ)/Medical Faculty of Porto (FMUP), Porto, Portugal, the Department of Pathology of HSJ and the Department of Pathology of Hospital S. Marcos (HSM), Braga, Portugal. Clinicopathological and follow-up data were retrieved from the files of the Department of Pathology, Department of Dermatology and Oncology Registry of HSJ and Department of Pathology of HSM, and from RORENO (Oncology Registry of North Region). All skin melanoma cases were re-evaluated and staged according to the seventh edition of the American Joint Committee on Cancer[11]. The overall female:male ratio was 1.2:1. The mean age of the patients was 58 years for females (s.d. ± 17.6), with a range from 9 to 94 years, and 62 years for males (s.d. ± 13.1), with a range from 33 to 79 years.

Follow-up data were available for 53 patients, including the diagnosis of metastases, through the evaluation of the patients or direct interview with their relatives and by review of in-hospital patient files/RORENO. The mean follow-up time of patients was 41 months (range 1–170). During follow-up, 5 (9%) patients developed (lymph node, liver or brain) metastases and 8 (15%) patients died due to malignant melanoma. The remaining patients were alive and without evidence of melanoma recurrence at the last follow-up. Additional information regarding the melanoma subtype, age, gender, thickness and molecular analysis of *TERT*, *BRAF* and *NRAS* is compiled in Supplementary Table S3.

Formalin-fixed, paraffin-embedded tissues from 372 tumours and tumour-like lesions of the thyroid and 27 normal thyroids were collected from the files of IPATIMUP, HSJ/FMUP and the Portuguese Institute of Oncology, Coimbra, Portugal. The histology of all tumour samples was revised, and the final classification was made according to the WHO criteria[12]. In Supplementary Tables S6 and S7, we have summarized the information regarding histological classification of the lesions, gender, mean age of the patients, molecular data and the size of the tumours.

Representative formalin-fixed paraffin-embedded samples from 118 gliomas were retrieved from pathology archives of the Department of Pathology of HSJ/FMUP and the Department of Pathology of HSM, Braga, Portugal. The tumours were reviewed and classified according to the WHO classification of CNS tumours (2007) (ref. 13,14). This cohort includes lesions that were classified as pilocytic astrocytoma ($n = 13$), astrocytoma grade 2 ($n = 20$), oligodendroglioma ($n = 22$), anaplastic oligodendroglioma ($n = 24$) and glioblastoma ($n = 39$). Further information regarding the CNS cases is available in Supplementary Table S4.

Formalin-fixed, paraffin-embedded tissues were collected from 82 patients with non-muscle invasive bladder cancer who underwent transurethral resection of the bladder malignant tumours in the Portuguese Institute of Oncology, Porto. Haematoxylin–eosin-stained sections were reviewed according to the standard histopathological examination by two independent pathologists. Staging and grading were conducted according to the American Joint Committee on Cancer[11], and the 2004 WHO classification system[15]. Supplementary Table S9 summarizes the clinicopathological parameters.

Formalin-fixed, paraffin-embedded tissues from 26 kidney cancers were collected from the HSJ/FMUP. Cases were classified as clear cell renal cell carcinoma ($n = 12$), chromophobe renal cell carcinoma ($n = 4$) and papillary renal cell carcinoma ($n = 10$). Information addressing the diagnosis, age, gender, nuclear grade and staging is obtainable in Supplementary Table S10.

Formalin-fixed, paraffin-embedded tissues from 17 pheochromocytomas were collected from the HSJ/FMUP and IPATIMUP, Porto, Portugal. Supplementary Table S11 summarizes the clinicopathological parameters.

Formalin-fixed, paraffin-embedded tissues from 36 GIST were collected from the HSJ/FMUP and IPATIMUP, Porto, Portugal. Tumours were classified according to the WHO pathological classification[16], and the parameters analysed in each case included: age, gender and tumour size. These data and the molecular characterization of these tumours can be observed in Supplementary Table S12.

Cell lines. DNA from 58 cell lines deposited in IPATIMUP cell line bank was retrieved. All the cell lines were authenticated using DNA profile analysis, obtained with the PowerPlex 16 system (Promega, Madison, USA), according to the DNA profiles available in American Type Culture Collection and Health Science Research Resource Bank.

DNA extraction. DNA from formalin-fixed, paraffin-embedded tissues was retrieved from 10-μm cuts after careful microdissection. DNA extraction was performed using the Ultraprep Tissue DNA Kit (AHN Biotechnologie, Nordhausen, Germany) following the manufacturer's instructions.

RNA extraction. Total RNA was extracted from frozen thyroid tumours ($n = 24$) and normal tissue specimens ($n = 3$) using a Trizol commercial kit (Life Technologies, GIBCO BRL, Carlsbad, CA) according to the manufacturer's protocol. RNA was quantified spectrophotometrically, and its quality was checked by analysis of 260/280ηm and 260/230 ηm ratios.

PCR and Sanger sequencing. Coding regions of *BRAF, GNAQ HRAS, NRAS, cKIT* and *PDGFR* were screened for mutations in DNA extracted from paraffin blocks using PCR and Sanger sequencing. The genetic characterization of part of the tumours had already been previously reported. For information on primers and PCR conditions, see refs 5,17,18. To screen for *TERT* promoter mutations, we analysed the hotspots previously identified by PCR followed by Sanger sequencing. *TERT* promoter mutation analysis was performed with the pair of primers FwTERT: 5′-CAGCGCTGCCTGAAACTC-3′ and RwTERT: 5′-GTCCTGCCCC TTCACCTT-3′. Amplification of genomic DNA (25–100 ng) was performed by PCR using the Qiagen Multiplex PCR kit (Qiagen, Hilden, Germany) according to the manufacturer's instructions. Sequencing reaction was performed with the ABI Prism BigDye Terminator Kit (Perkin-Elmer, Foster City, CA), and the fragments were run in an ABI prism 3100 Genetic Analyser (Perkin-Elmer). The sequencing reaction was performed in a forward direction, and an independent PCR amplification/sequencing, both in a forward and reverse direction, was performed in positive samples or samples that were inconclusive.

Quantitative RT-PCR. qPCR for human *TERT* was performed in 28 thyroid samples, 24 tumours and 3 normal tissue specimens. We also included a normal reference that was produced by pooling RNAs from nine samples of normal thyroid tissue[19].

For cDNA preparation, 1 μg of total RNA was reverse transcribed using the RevertAid first strand cDNA synthesis kit (Fermentas, Burlington, ON, Canada). Reverse transcription products were amplified for the *TERT* by qPCR (IDT; no. HS.PT.56a.40988589) using TaqMan PCR Master Mix (Applied Biosystems, Foster City, CA, USA) with *TBP* gene (TATA-binding protein) as endogenous control (Applied Biosystems; no. 4326322E-0705006). The ABI PRISM 7500 Fast Sequence Detection System (Applied Biosystems) was used to detect the amplification level and was programmed to an initial step of 2 min at 50 °C, 10 min at 95 °C, followed by 45 cycles of 95 °C for 15 s and 60 °C for 1 min. *TBP* and *TERT* amplifications were done in triplicate using 1 μl of cDNA (~ 50 ng) for each sample. The relative quantification of target genes was determined using the ΔΔCT method, which was previously validated by Livak's Linear Regression Method (slope = 0.0696) (Sequence Detector User Bulletin 2; Applied Biosystems).

Immunohistochemistry. IHC for telomerase was performed in representative tumour tissue sections of 14 glioblastomas. Briefly, deparaffinized and rehydrated sections were subjected to microwave treatment in 10 mM sodium citrate buffer, pH 6.0, for antigen retrieval. The sections were incubated overnight at 4 °C in a humidified chamber with the primary antibody telomerase (polyclonal, rabbit, 1:500) from Rockland Immunochemicals Inc., Gilbertsville, PA. The detection was performed with a labelled streptavidin–biotin immunoperoxidase detection system (Thermo Scientific/Lab Vision, Fremont, USA), and the immunohistochemical staining was developed with 3,3′-diaminobenzidine substrate. Omission of the primary antibody incubation was used as negative control. Previously tested liver cancer case was used as positive control. IHC evaluation was performed independently by two observers (V.M. and J.L.). An IHC score was established, which corresponded to the product of the intensity of expression (absent = 0, faint = 1, moderate = 2 and strong = 3) with the tumour extent of protein expression (0–25% = 0, 26–50% = 1, 51–75% = 2 and > 75% = 3) (ref. 6).

Statistical analysis. Statistical analysis was conducted with StatView for Windows, version 5.0 (SAS Institute, Cary, NC). The results are expressed as a percentage or mean ± s.d. Statistical analysis was performed both on the whole series and considering the different groups of lesions. For the analysis of the relationship between patients' age, tumour size and *TERT* status of the tumours, we used the unpaired *t*-test, Mann–Whitney test and analysis of variance. Fisher's exact test was used in the statistical analysis of the other parameters. Graphs and figures were done in GraphPad v6.0. Results were considered statistically significant if $P < 0.05$.

References

1. Horn, S. *et al.* TERT promoter mutations in familial and sporadic melanoma. *Science* **339,** 959–961 (2013).
2. Huang, F. W. *et al.* Highly recurrent TERT promoter mutations in human melanoma. *Science* **339,** 957–959 (2013).
3. Killela, P. J. *et al.* TERT promoter mutations occur frequently in gliomas and a subset of tumors derived from cells with low rates of self-renewal. *Proc. Natl Acad. Sci. USA* **110,** 6021–6026 (2013).
4. Van Raamsdonk, C. D. *et al.* Frequent somatic mutations of GNAQ in uveal melanoma and blue naevi. *Nature* **457,** 599–602 (2009).
5. Populo, H., Vinagre, J., Lopes, J. M. & Soares, P. Analysis of GNAQ mutations, proliferation and MAPK pathway activation in uveal melanomas. *Br. J. Ophthalmol.* **95,** 715–719 (2011).
6. Populo, H., Soares, P., Rocha, A. S., Silva, P. & Lopes, J. M. Evaluation of the mTOR pathway in ocular (uvea and conjunctiva) melanoma. *Melanoma Res.* **20,** 107–117 (2010).
7. Lotsch, D. *et al.* Prognostic significance of telomerase-associated parameters in glioblastoma: effect of patient age. *Neuro. Oncol.* **15,** 423–432 (2013).
8. Soares, P. *et al.* Genetic alterations in poorly differentiated and undifferentiated thyroid carcinomas. *Curr. Genomics* **12,** 609–617 (2011).
9. Capezzone, M. *et al.* Telomere length in neoplastic and nonneoplastic tissues of patients with familial and sporadic papillary thyroid cancer. *J. Clin. Endocrinol. Metab.* **96,** E1852–E1856 (2011).
10. Sanchini, M. A. *et al.* Relevance of urine telomerase in the diagnosis of bladder cancer. *JAMA* **294,** 2052–2056 (2005).
11. Edge, S. B. *et al. AJCC Cancer Staging Manual* (Springer, 2010).
12. DeLellis, R. A., L.R., Heitz, P. U. & Eng, C. (eds) *World Health Organization Classification of Tumours. Pathology and Genetics of Tumours of Endocrine Glands* (IARC Press, 2004).
13. Kleihues, P. & Cavenee, W. K. *Pathology and Genetics of Tumours of the Nervous System* (IARC Press, 2000).
14. Louis, D. N. *et al.* The 2007 WHO classification of tumours of the central nervous system. *Acta Neuropathol.* **114,** 97–109 2007.
15. Sauter, G. *et al.* in *WHO Classification of Tumors. Pathology and Genetics of Tumors of the Urinary System and Male Genital Organs*. (eds Eble, J.N., Sauter, G., Epstein, J.I. & Sesterhenn, I.A.) (IARC Press, 2004).
16. Fletcher, C. D. *et al.* Diagnosis of gastrointestinal stromal tumors: a consensus approach. *Hum. Pathol.* **33,** 459–465 (2002).
17. Soares, P. *et al.* BRAF mutations and RET/PTC rearrangements are alternative events in the etiopathogenesis of PTC. *Oncogene* **22,** 4578–4580 (2003).
18. Celestino, R. *et al.* Molecular alterations and expression of succinate dehydrogenase complex in wild-type KIT/PDGFRA/BRAF gastrointestinal stromal tumors. *Eur. J. Hum. Genet.* **21,** 503–510 (2013).
19. Prazeres, H. *et al.* Chromosomal, epigenetic and microRNA-mediated inactivation of LRP1B, a modulator of the extracellular environment of thyroid cancer cells. *Oncogene* **30,** 1302–1317 (2011).

Acknowledgements

We thank to Mrs Mafalda Rocha for the excellent technical support in the sequencing work. This work was partially supported by the Portuguese Science and Technology Foundation (FCT) through BPD (SFRH/BPD/85249/2012 to H.P.), PhD (SFRH/BD/81940/2011 to J.V. and SFRH/BD/79135/2011 to A.A.) and BI grants, and the grant through the Program Ciência 2008 (J.L.) and the project (PIC/IC/83037/2007). Further funding was obtained from the project 'Microenvironment, metabolism and cancer' partially supported by *Programa Operacional Regional do Norte (ON.2—O Novo Norte)*, under the *Quadro de Referência Estratégico Nacional (QREN)*, and through the *Fundo Europeu de Desenvolvimento Regional (FEDER)*. IPATIMUP is an associate laboratory of the Portuguese Ministry of Science, Technology and Higher Education and is partially supported by the FCT.

Author contributions

J.V., A.A. and H.P. contributed equally to the work. P.S. and V.M. jointly supervised the research. P.S. conceived the study. P.S., V.M. and J.L. designed the experiments. J.V., A.A., H.P., J.Ly., V.P., R.C., R.Ce., R.B., P.C., H.P., M.M. and A.R. performed the DNA extraction and mutation analysis experiments. R.B. performed the qPCR experiments. H.P. performed the IHC studies. M.S.S., L.C., J.C.-T. and J.M.L. performed the tumour classification. A.P., L.L., F.P., L.L.S. and R.R. provided tumour samples, reagents and collected the clinicopathological data. P.S., V.M., J.L., J.V., H.P., R.B. and M.S.S. wrote the paper with the contribution of all the other authors.

Additional information

Supplementary Information accompanies this paper at http://www.nature.com/naturecommunications

Competing financial interests: The authors declare no competing financial interests.

Reprints and permission information is available online at http://npg.nature.com/reprintsandpermissions/

How to cite this article: Vinagre, J. *et al.* Frequency of *TERT* promoter mutations in human cancers. *Nat. Commun.* 4:2185 doi: 10.1038/ncomms3185 (2013).

SUPPLEMENTARY INFORMATION FOR JVINAGRE - NCOMMS-13-03296-A

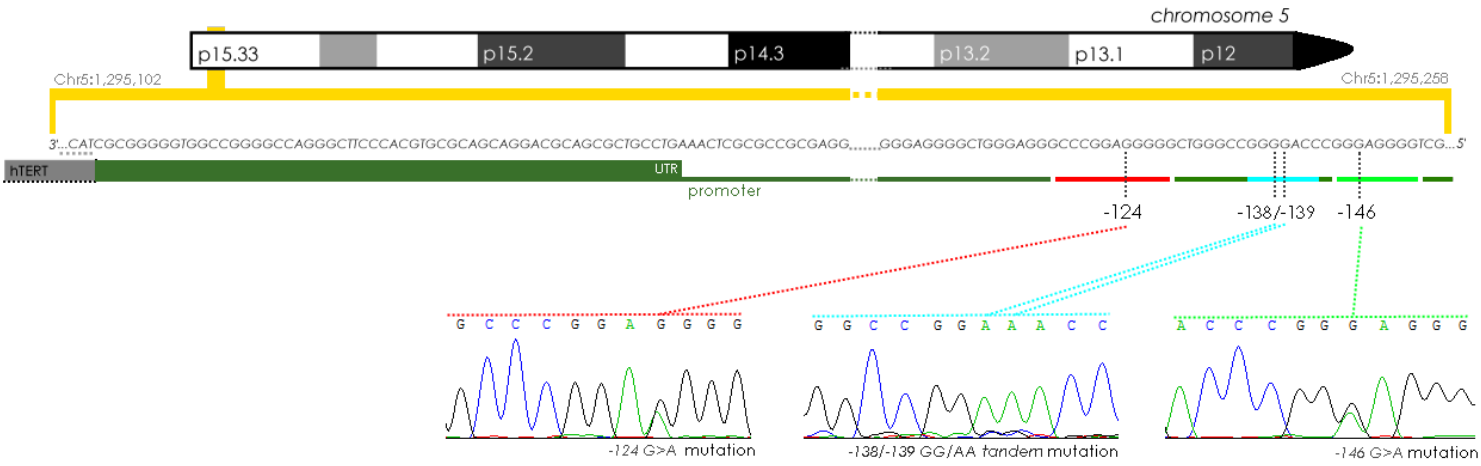

Supplementary Figure S1 - The panel illustrates the three mutations identified in this study and their location in chromosome 5 in relation to the *TERT* ATG translation start site.

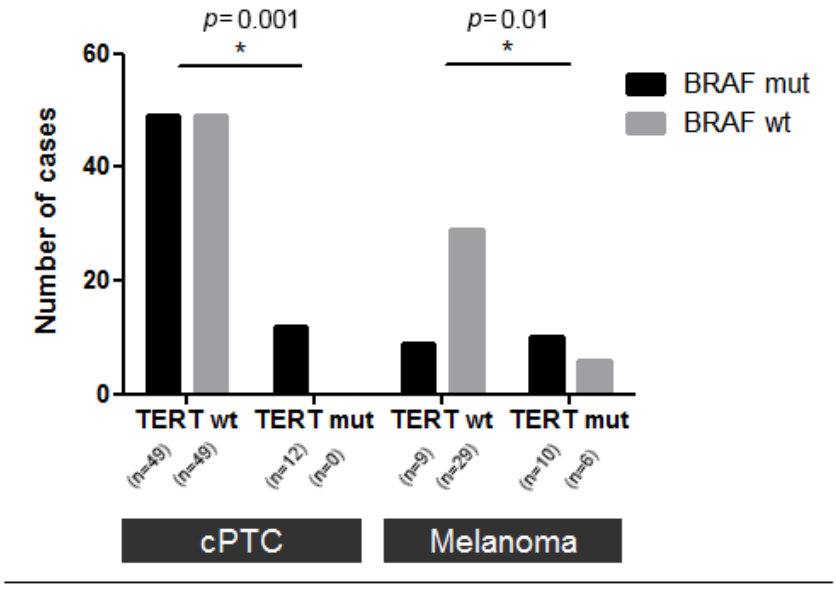

Supplementary Figure S2 - Bar plot indicating the number of cases with *TERT* mutations in *BRAF*-mutated and *BRAF*-wild-type conventional papillary thyroid carcinomas (cPTC) and melanomas. For both tumour types, the presence of *TERT* mutations is significantly associated with the presence of *BRAF* mutations (asterisks, Fisher's exact test two-sided).

Supplementary Table S1 - Genetic alterations in thyroid and melanoma cell lines

Origin	Cell line	*BRAF*	*RAS*	*RET*	*GNAQ*	*TERT*
Thyroid						
	XTC-1	WT	WT	ND	-	WT
	HTH74	V600E	WT	ND	-	-124G>A
	K1	V600E	WT	ND	-	-124G>A
	BCPAP	V600E	WT	ND	-	-124/-125GG>AA
	C643	WT	HRASG13E	ND	-	-124G>A
	8505C	V600E	WT	ND	-	-146G>A
	TPC-1	WT	WT	RET/PTC1	-	-124G>A
	T238					WT
	TT			C634W		WT
	MZ-CRC-1			M918T		WT
Skin melanoma						
	A375	V600E	WT		WT	-146G>A
	BLM	WT	WT		WT	-146G>A
	G361	V600E	WT		WT	-138/-139GG>AA
	Mewo	WT	WT		WT	-146G>A
Uveal melanoma						
	92.1	WT	WT		Q209L	WT
	OMM1	WT	WT		WT	WT
	OMM2.3	WT	WT		Q209L	WT
	Mel 202	WT	WT		Q209L	WT
	Mel 270	WT	WT		Q209P	WT
	Mel 285	WT	WT		WT	WT

*All the cell lines are deposited in the cell line bank from the IPATIMUP and were authenticated using DNA profile analysis, obtained with the PowerPlex 16 system (Promega, Madison, USA), according to ATCC and HSRRB available DNA profiles.

Supplementary Table S2 - Genetic alterations in cell lines

Origin	Derivation	Cell line	*TERT*
Colorectal	Colon adenocarcinoma	COLO-205	WT
	Colon adenocarcinoma	Caco-2	WT
	Colon adenocarcinoma	SW 480	WT
	Colon adenocarcinoma	HT29	WT
	Colon adenocarcinoma	HCT-15	WT
	Colon adenocarcinoma	HCT-116	WT
	Colon adenocarcinoma	SW48	WT
	Colon adenocarcinoma	Co-115	WT
Gastric	Gastric adenocarcinoma	AGS	WT
	Gastric adenocarcinoma	MKN28	WT
	Well-differentiated gastric carcinoma	NCI-N87	WT
	Poorly-differentiated gastric carcinoma	SNU-638	WT
	Poorly-differentiated gastric carcinoma	MKN-45	WT
	Poorly-differentiated gastric carcinoma Metastasis	KATO III	WT
	Diffuse Gastric Carcinoma	IPA220A	WT
	Diffuse Gastric Carcinoma	GP202	WT
Breast	Breast adenocarcinoma	MDA-MB-231	-124G>A
	Breast adenocarcinoma	MCF-7AZ	WT
	Breast adenocarcinoma	SKBR3	WT
	Breast adenocarcinoma	MCF-7/6	WT
	Breast adenocarcinoma	BT-549	-146G>A
	Breast adenocarcinoma	BT-20	WT
	Breast adenocarcinoma	MDA-MB-468	WT
	Breast adenocarcinoma	SUM149	WT
Kidney			
	CCRCC	Caki-2	-124G>A
	CCRCC	786-O	-124G>A
Leukemia	Acute promyelocytic leukemia	NB-4	WT
	Acute promyelocytic leukemia	HL-60	WT
Peripheral B Lymphocytes	Lymphoblastoid cell lines	GM20770	WT
	Lymphoblastoid cell lines	GM20890	WT
	Lymphoblastoid cell lines	GM11840	WT
	Lymphoblastoid cell lines	GM19782 B	WT
	Lymphoblastoid cell lines	GM20515	WT
	Lymphoblastoid cell lines	GM19777	WT
	Lymphoblastoid cell lines	GM20797	WT
	Lymphoblastoid cell lines	GM10847 B	WT
Lung	Lung Adenocarcinoma	A549	WT
CNS	Glioblastoma	SF-767	WT

*All the cell lines are deposited in the cell line bank from the IPATIMUP and were authenticated using DNA profile analysis, obtained with the PowerPlex 16 system (Promega, Madison, USA), according to ATCC and HSRRB available DNA profiles.

Supplementary Table S3 – Summary of clinico-pathological and genetic data in 56 skin melanoma

Case Code	Melanoma subtype	Age	Gender	Thickness (mm)	*BRAF*	*NRAS*	*TERT*
MEL1	Superficial spreading	74	M	1.20		Pos	
MEL2	Superficial spreading	36	F	0.95			
MEL3	Superficial spreading	NA	F	0.50	V600E		
MEL4	Superficial spreading	NA	M	1.40			-146 G>A
MEL5	Superficial spreading	46	F	3.10			
MEL6	Nodular	52	F	0.90			
MEL7	Nodular	59	M	3.20	V600E		
MEL8	Lentigo maligna	67	F	0.50	V600E		
MEL9	Nodular	54	F	16.00			
MEL10	Nodular	33	M	19.50	V600E		
MEL11	Superficial spreading	57	F	3.65			-146 G>A
MEL12	Lentigo maligna	79	F	0	V600E		-146 G>A
MEL13	Acral lentiginous	94	F	2.10			
MEL14	Acral lentiginous	50	F	1.00			
MEL15	Superficial spreading	49	M	10.00		Pos	-124 G>A
MEL16	Superficial spreading	55	M	2.30			
MEL17	Nodular	82	F	3.50	V600E		
MEL18	Nodular	35	F	2.50	V600E		-124 G>A
MEL19	Superficial spreading	58	M	7.70			
MEL20	Nodular	42	F	1.70	V600E		-124 G>A
MEL21	Nodular	61	F	4.40			-124 G>A
MEL22	Acral lentiginous	69	M	4.00			
MEL23	Superficial spreading	41	M	0	V600E		
MEL24	Acral lentiginous	72	F	0.70			
MEL25	Superficial spreading	.	M	0.50			
MEL26	Nodular	76	M	6.00			
MEL27	Superficial spreading	66	M	0			-124 G>A
MEL28	Superficial spreading	55	F	1.78			
MEL29	Acral lentiginous	67	F	4.00			
MEL30	Nodular	63	M	5.00			
MEL31	Acral lentiginous	60	M	5.40	V600E	Pos	-124 G>A
MEL32	Superficial spreading	NA	M	0.50	V600E		-146 G>A
MEL33	Acral lentiginous	71	M	5.20			
MEL34	Superficial spreading	75	F	70.00	V600E		-124 G>A
MEL35	Nodular	69	F	7.00	V600E		-146 G>A
MEL36	Acral lentiginous	9	F	3.25			
MEL37	Superficial spreading	39	F	2.30			
MEL38	Acral lentiginous	68	M	4.50			
MEL39	Acral lentiginous	NA	M	2.70			
MEL40	Superficial spreading	NA	F	1.20	V600E		-146 G>A
MEL41	Superficial spreading	59	F	3.30	V600E		
MEL42	Acral lentiginous	NA	F	4.00			
MEL43	Lentigo maligna	NA	M	5.90		Pos	

MEL44	Lentigo maligna	NA	F	0.50			
MEL45	Acral lentiginous	68	F	2.20	V600E		
MEL46	Nodular	71	F	7.80			
MEL47	Superficial spreading	59	M	1.20			
MEL48	Superficial spreading	NA	M	0.35			
MEL49	Melanoma nodular	42	M	20.00	V600E		-124 G>A
MEL50	Superficial spreading	61	F	4.30	V600E		
MEL51	Nodular	79	M	22.00		Pos	-146 G>A
MEL52	Lentigo maligna	61	F	3.40			
MEL53	Acral lentiginous	75	M	6.10			
MEL54	Superficial spreading	49	F	2.90	V600E		-146 G>A
MEL55	Acral lentiginous	NA	M	4.40			
MEL56	Lentigo maligna	75	M	0.30			

Supplementary Table S4 - Summary of clinico-pathological and genetic data in 118 gliomas

Case Code	Age	Gender	Diagnosis (Grade)	*TERT*
GLI1	4	F	Pilocytic Astrocytoma (I)	
GLI2	27	M	Pilocytic Astrocytoma (I)	
GLI3	22	M	Pilocytic Astrocytoma (I)	
GLI4	31	F	Pilocytic Astrocytoma (I)	
GLI5	27	M	Pilocytic Astrocytoma (I)	-124 G>A
GLI6	18	M	Pilocytic Astrocytoma (I)	
GLI7	30	F	Pilocytic Astrocytoma (I)	
GLI8	12	F	Pilocytic Astrocytoma (I)	
GLI9	NA	NA	Pilocytic Astrocytoma (I)	
GLI10	NA	NA	Pilocytic Astrocytoma (I)	
GLI11	NA	NA	Pilocytic Astrocytoma (I)	
GLI12	NA	NA	Pilocytic Astrocytoma (I)	
GLI13	NA	NA	Pilocytic Astrocytoma (I)	
GLI14	18	F	Diffuse Astrocytoma (II)	
GLI15	NA	NA	Diffuse Astrocytoma (II)	-124 G>A
GLI16	38	M	Diffuse Astrocytoma (II)	
GLI17	22	M	Diffuse Astrocytoma (II)	
GLI18	50	M	Diffuse Astrocytoma (II)	
GLI19	31	F	Diffuse Astrocytoma (II)	
GLI20	30	M	Diffuse Astrocytoma (II)	
GLI21	59	M	Diffuse Astrocytoma (II)	
GLI22	NA	NA	Diffuse Astrocytoma (II)	
GLI23	53	F	Diffuse Astrocytoma (II)	
GLI24	20	M	Diffuse Astrocytoma (II)	
GLI25	69	M	Diffuse Astrocytoma (II)	-146 G>A
GLI26	42	F	Diffuse Astrocytoma (II)	

GLI27	27	F	Diffuse Astrocytoma (II)	
GLI28	60	F	Diffuse Astrocytoma (II)	-124 G>A
GLI29	NA	NA	Diffuse Astrocytoma (II)	
GLI30	NA	NA	Diffuse Astrocytoma (II)	
GLI31	NA	NA	Diffuse Astrocytoma (II)	
GLI32	NA	NA	Diffuse Astrocytoma (II)	
GLI33	NA	NA	Diffuse Astrocytoma (II)	
GLI34	72	F	Oligodendroglioma (II)	-124 G>A
GLI35	9	M	Oligodendroglioma (II)	
GLI36	33	M	Oligodendroglioma (II)	
GLI37	42	F	Oligodendroglioma (II)	-124 G>A
GLI38	46	F	Oligodendroglioma (II)	
GLI39	45	F	Oligodendroglioma (II)	-124 G>A
GLI40	43	M	Oligodendroglioma (II)	
GLI41	53	M	Oligodendroglioma (II)	-146 G>A
GLI42	53	F	Oligodendroglioma (II)	-124 G>A
GLI43	54	F	Oligodendroglioma (II)	-124 G>A
GLI44	43	F	Oligodendroglioma (II)	-124 G>A
GLI45	34	M	Oligodendroglioma (II)	-146 G>A
GLI46	40	M	Oligodendroglioma (II)	
GLI47	45	F	Oligodendroglioma (II)	-124 G>A
GLI48	NA	NA	Oligodendroglioma (II)	
GLI49	NA	NA	Oligodendroglioma (II)	
GLI50	NA	NA	Oligodendroglioma (II)	
GLI51	NA	NA	Oligodendroglioma (II)	
GLI52	NA	NA	Oligodendroglioma (II)	
GLI53	NA	NA	Oligodendroglioma (II)	
GLI54	NA	NA	Oligodendroglioma (II)	
GLI55	NA	NA	Oligodendroglioma (II)	-124 G>A
GLI56	65	M	Anaplastic Oligodendroglioma (III)	-124 G>A
GLI57	47	F	Anaplastic Oligodendroglioma (III)	-124 G>A
GLI58	65	F	Anaplastic Oligodendroglioma (III)	
GLI59	50	M	Anaplastic Oligodendroglioma (III)	-146 G>A
GLI60	36	F	Anaplastic Oligodendroglioma (III)	-124 G>A
GLI61	53	M	Anaplastic Oligodendroglioma (III)	-146 G>A
GLI62	65	M	Anaplastic Oligodendroglioma (III)	-146 G>A
GLI63	47	M	Anaplastic Oligodendroglioma (III)	-124 G>A
GLI64	50	M	Anaplastic Oligodendroglioma (III)	
GLI65	70	F	Anaplastic Oligodendroglioma (III)	
GLI66	40	M	Anaplastic Oligodendroglioma (III)	-124 G>A
GLI67	67	F	Anaplastic Oligodendroglioma (III)	-124 G>A
GLI68	64	F	Anaplastic Oligodendroglioma (III)	-146 G>A
GLI69	44	M	Anaplastic Oligodendroglioma (III)	
GLI70	42	F	Anaplastic Oligodendroglioma (III)	-124 G>A
GLI71	68	F	Anaplastic Oligodendroglioma (III)	-124 G>A
GLI72	NA	NA	Anaplastic Oligodendroglioma (III)	

GLI73	NA	NA	Anaplastic Oligodendroglioma (III)	
GLI74	NA	NA	Anaplastic Oligodendroglioma (III)	
GLI75	NA	NA	Anaplastic Oligodendroglioma (III)	-124 G>A
GLI76	NA	NA	Anaplastic Oligodendroglioma (III)	
GLI77	NA	NA	Anaplastic Oligodendroglioma (III)	
GLI78	NA	NA	Anaplastic Oligodendroglioma (III)	
GLI79	NA	NA	Anaplastic Oligodendroglioma (III)	
GLI80	56	M	Glioblastoma (IV)	-146 G>A
GLI81	27	F	Glioblastoma (IV)	
GLI82	54	F	Glioblastoma (IV)	-124 G>A
GLI83	46	F	Glioblastoma (IV)	
GLI84	77	M	Glioblastoma (IV)	-124 G>A
GLI85	67	F	Glioblastoma (IV)	-146 G>A
GLI86	50	F	Glioblastoma (IV)	-146 G>A
GLI87	73	M	Glioblastoma (IV)	-146 G>A
GLI88	57	M	Glioblastoma (IV)	-124 G>A
GLI89	28	M	Glioblastoma (IV)	
GLI90	51	F	Glioblastoma (IV)	-124 G>A
GLI91	69	M	Glioblastoma (IV)	-146 G>A
GLI92	53	M	Glioblastoma (IV)	
GLI93	56	F	Glioblastoma (IV)	-124 G>A
GLI94	66	M	Glioblastoma (IV)	-124 G>A
GLI95	68	F	Glioblastoma (IV)	
GLI96	58	F	Glioblastoma (IV)	
GLI97	73	M	Glioblastoma (IV)	-124 G>A
GLI98	61	F	Glioblastoma (IV)	
GLI99	66	F	Glioblastoma (IV)	-124 G>A
GLI100	60	F	Glioblastoma (IV)	-124 G>A
GLI101	54	M	Glioblastoma (IV)	-124 G>A
GLI102	66	F	Glioblastoma (IV)	-124 G>A
GLI103	79	M	Glioblastoma (IV)	-124 G>A
GLI104	31	M	Glioblastoma (IV)	
GLI105	NA	NA	Glioblastoma (IV)	-124 G>A
GLI106	NA	NA	Glioblastoma (IV)	
GLI107	NA	NA	Glioblastoma (IV)	-124 G>A
GLI108	NA	NA	Glioblastoma (IV)	-124 G>A
GLI109	NA	NA	Glioblastoma (IV)	-124 G>A
GLI110	NA	NA	Glioblastoma (IV)	-124 G>A
GLI111	NA	NA	Glioblastoma (IV)	
GLI112	NA	NA	Glioblastoma (IV)	
GLI113	NA	NA	Glioblastoma (IV)	-124 G>A
GLI114	NA	NA	Glioblastoma (IV)	
GLI115	NA	NA	Glioblastoma (IV)	-146 G>A
GLI116	NA	NA	Glioblastoma (IV)	
GLI117	NA	NA	Glioblastoma (IV)	
GLI118	NA	NA	Glioblastoma (IV)	

Supplementary Table S5 – Comparison of the clinico-pathological features of tumours with and without *TERT* mutations

Tumour type	Clinical features	All patients	*TERT* wild type	*TERT* mutated	*p* value
Thyroid* (n=263)	Mean age at diagnosis, yr (±SD)	48±17	46±16	62±13	**<0,0001**
	Gender				
	Male	61 (24%)	50 (22%)	11(42%)	**0,03**
	Female	189 (76%)	174 (78%)	15 (58%)	
	Mean tumour size, cm	3.5±3.4	3.4±3.4	4.6±2.7	**0,008**
CNS (n=118)	Mean age at diagnosis, yr (±SD)	47±18	38±17	57±12	**<0,0001**
	Gender				
	Male	42 (49%)	21 (51%)	20 (47%)	NS
	Female	43 (51%)	20 (49%)	23 (53%)	
Skin melanoma (n=56)	Mean age at diagnosis, yr (±SD)	60±16	60±14	63±12	NS
	Gender				
	Male	26 (46%)	19 (48%)	7 (44%)	NS
	Female	30 (54%)	21 (52%)	9 (56%)	
Bladder (n=82)	Mean age at diagnosis, yr (±SD)	63±10	65±12	63±12	NS
	Gender				
	Male	66 (80%)	24 (70%)	42 (88%)	NS
	Female	16 (20%)	10 (30%)	6 (12%)	

The numbers in parentheses indicate percentages. In some cases information regarding age, gender or tumour size was missing.
*Only follicular cell-derived thyroid carcinomas: FTC, PTC, PDTC and ATC.

Supplementary Table S6 – Clinico-pathological characteristics and *TERT* promoter mutation in the 399 thyroid samples analysed

Histotypes	No. Of cases	Gender ratio (♀:♂)	Mean age (years±SE)	Tumour size (cm±SE)	*BRAF*V600E mutation	*TERT* n (%)
Normal Thyroid	27	3,5:1	47,0 ± 14,8	NA	0	0 (0,0)
Lymphocytic Thyroiditis	9	9:0	44,6 ± 15,7	NA	0	0 (0,0)
Nodular Goiter	12	1,75:1	56,2 ± 13,4	NA	0	0 (0,0)
Follicular Thyroid Adenoma						
Conventional	52	7:1	43,8 ± 12,1	3,5 ± 1,6	0	0 (0,0)
Oncocytic Variant	8	7:0	47,0 ± 14,0	2,7 ± 1,2	0	0 (0,0)
Follicular Thyroid Carcinoma						
Conventional	36	2,5:1	53,7 ± 14,7	4,5 ± 2,8	0	9 (25,0)
Oncocytic Variant	28	5,5:1	51,4 ± 20,2	4,6 ± 3,6	0	0 (0,0)
Papillary thyroid carcinoma						
Conventional	110	3,1:1	43,1 ± 16,2	2,6 ± 1,6	61	12 (10,9)
Follicular Variant	39	3,9:1	45,8 ±14,7	2,6 ± 1,2	2	0 (0,0)
Microcarcinoma	5	5:0	46,0 ±14,4	0,4 ± 0,4	1	0 (0,0)
Mucoepidermoid Carcinoma	4	2:0	43,5 ± 33,2	NA	0	1 (25,0)
Oncocytic Variant of PTC						
Conventional Pattern	4	4:0	45,3 ±11,1	2,8 ± 1,8	4	0 (0,0)
Follicular Pattern	3	2:1	45,3 ±22,5	5,2 ± 3,9	1	0 (0,0)
Warthin-like PTC	4	4:0	55,5 ±11,2	2,0 ± 0,8	4	0 (0,0)
PDTC	14	1:1	57,0 ± 17,4	6,7 ± 2,8	1	2 (14,2)
Anaplastic	16	1,3:1	62,1 ± 12,8	6,9 ± 3,1	5	2 (12,5)
MTC	28	2,3:1	46,4 ± 16,7	3,0 ± 0,9	0	0 (0,0)

Supplementary Table S7 - Summary of clinico-pathological and genetic data in 351 tumour and tumour like thyroid lesions

Case Code	Age	Gender	Diagnosis	*RAS*	*BRAF*	*TERT*
THY1	50	F	FTA			
THY2	50	F	FTA			
THY3	59	M	FTA			
THY4	28	F	FTA			
THY5	45	F	FTA			
THY6	51	F	FTA			
THY7	37	F	FTA			
THY8	53	F	FTA			
THY9	57	F	FTA			
THY10	66	F	FTA			
THY11	63	F	FTA			
THY12	40	F	FTA			
THY13	34	F	FTA			
THY14	65	F	FTA			
THY15	35	F	FTA			
THY16	34	F	FTA			
THY17	18	F	FTA			
THY18	37	F	FTA			
THY19	43	F	FTA			
THY20	53	F	FTA			
THY21	45	F	FTA			
THY22	33	F	FTA			
THY23	34	F	FTA			
THY24	46	M	FTA			
THY25	53	F	FTA			
THY26	65	F	FTA			
THY27	29	F	FTA			
THY28	34	F	FTA			
THY29	34	F	FTA			
THY30	NA	NA	FTA			
THY31	NA	NA	FTA			
THY32	56	F	FTA			
THY33	33	F	FTA			
THY34	47	M	FTA			
THY35	30	F	FTA			
THY36	55	M	FTA			
THY37	NA	F	FTA			

THY38	41	F	FTA			
THY39	45	F	FTA			
THY40	44	F	FTA			
THY41	NA	NA	FTA			
THY42	64	F	FTA			
THY43	NA	NA	FTA			
THY44	61	F	FTA			
THY45	45	F	FTA			
THY46	46	F	FTA			
THY47	29	M	FTA			
THY48	40	F	FTA			
THY49	35	M	FTA			
THY50	42	F	FTA			
THY51	35	F	FTA			
THY52	21	F	FTA			
THY53	36	F	FHCA			
THY54	NA	NA	FHCA			
THY55	25	F	FHCA			
THY56	62	F	FHCA			
THY57	38	F	FHCA			
THY58	57	F	FHCA			
THY59	52	F	FHCA			
THY60	59	F	FHCA			
THY61	54	F	cPTC			
THY62	39	F	cPTC		V600E	
THY63	48	M	cPTC	Pos		
THY64	28	F	cPTC		V600E	
THY65	49	F	cPTC		V600E	
THY66	38	F	cPTC			
THY67	24	F	cPTC		V600E	
THY68	76	F	cPTC		V600E	
THY69	55	F	cPTC			
THY70	28	F	cPTC			
THY71	36	F	cPTC		V600E	
THY72	69	F	cPTC		V600E	
THY73	68	F	cPTC			
THY74	55	F	cPTC		V600E	
THY75	30	F	cPTC	Pos		
THY76	47	F	cPTC		V600E	
THY77	32	F	cPTC	Pos		
THY78	25	F	cPTC		V600E	
THY79	55	F	cPTC			
THY80	31	F	cPTC		V600E	
THY81	64	F	cPTC		V600E	
THY82	30	F	cPTC			

THY83	55	F	cPTC			
THY84	56	F	cPTC			
THY85	25	F	cPTC			
THY86	28	F	cPTC		V600E	
THY87	18	F	cPTC			
THY88	56	F	cPTC			
THY89	14	M	cPTC			
THY90	57	F	cPTC		V600E	
THY91	40	F	cPTC			
THY92	53	M	cPTC		V600E	-124 G>A
THY93	61	F	cPTC			
THY94	44	M	cPTC		V600E	
THY95	82	M	cPTC		V600E	-124 G>A
THY96	42	M	cPTC		V600E	-124 G>A
THY97	46	F	cPTC			
THY98	46	M	cPTC		V600E	
THY99	39	M	cPTC		V600E	
THY100	79	F	cPTC		V600E	-124 G>A
THY101	32	F	cPTC			
THY102	37	F	cPTC		V600E	
THY103	72	F	cPTC		V600E	-124 G>A
THY104	77	M	cPTC		V600E	-124 G>A
THY105	60	M	cPTC		V600E	
THY106	15	M	cPTC			
THY107	38	F	cPTC		V600E	
THY108	38	M	cPTC		V600E	
THY109	38	M	cPTC		V600E	
THY110	27	F	cPTC			
THY111	40	F	cPTC		V600E	
THY112	66	M	cPTC		V600E	-124 G>A
THY113	57	F	cPTC		V600E	
THY114	50	F	cPTC		V600E	
THY115	13	F	cPTC			
THY116	37	F	cPTC		V600E	
THY117	26	F	cPTC		V600E	
THY118	30	F	cPTC			
THY119	52	F	cPTC		V600E	
THY120	42	F	cPTC		V600E	
THY121	NA	NA	cPTC			
THY122	73	F	cPTC			
THY123	54	F	cPTC			
THY124	16	M	cPTC			
THY125	47	F	cPTC		V600E	
THY126	55	F	cPTC		V600E	
THY127	31	F	cPTC	Pos		

THY128	52	F	cPTC			
THY129	25	F	cPTC			
THY130	39	F	cPTC		V600E	
THY131	41	M	cPTC		V600E	
THY132	36	F	cPTC		V600E	
THY133	35	F	cPTC			
THY134	63	F	cPTC		V600E	
THY135	NA	NA	cPTC			
THY136	26	F	cPTC			
THY137	31	F	cPTC			
THY138	30	M	cPTC			
THY139	58	F	cPTC		V600E	-124 G>A
THY140	40	F	cPTC			
THY141	45	M	cPTC		V600E	
THY142	43	M	cPTC		V600E	-124 G>A
THY143	67	M	cPTC		V600E	
THY144	30	F	cPTC			
THY145	31	F	cPTC			
THY146	33	F	cPTC		V600E	
THY147	44	F	cPTC		V600E	
THY148	NA	NA	cPTC			
THY149	61	F	cPTC		V600E	-124 G>A
THY150	54	F	cPTC		V600E	
THY151	72	M	cPTC		V600E	-124 G>A
THY152	52	F	cPTC		V600E	
THY153	20	M	cPTC			
THY154	NA	NA	cPTC			
THY155	47	M	cPTC		V600E	-146 G>A
THY156	36	F	cPTC			
THY157	59	M	cPTC			
THY158	33	F	cPTC			
THY159	30	F	cPTC		V600E	
THY160	29	M	cPTC			
THY161	40	F	cPTC		V600E	
THY162	27	F	cPTC		V600E	
THY163	64	F	cPTC		V600E	
THY164	43	F	cPTC			
THY165	25	F	cPTC			
THY166	42	F	cPTC		V600E	
THY167	53	F	cPTC		V600E	
THY168	22	F	cPTC		V600E	-150 G>A
THY169	41	F	cPTC		V600E	
THY170	7	M	cPTC			
THY171	39	F	fvPTC	Pos		
THY172	46	F	fvPTC			

THY173	36	M	fvPTC	Pos		
THY174	68	F	fvPTC			
THY175	56	F	fvPTC	Pos		
THY176	44	F	fvPTC			
THY177	21	M	fvPTC			
THY178	30	F	fvPTC	Pos		
THY179	61	M	fvPTC			
THY180	41	M	fvPTC	Pos		
THY181	38	F	fvPTC	Pos		
THY182	52	F	fvPTC			
THY183	33	F	fvPTC			
THY184	57	M	fvPTC			
THY185	40	F	fvPTC		V600E	
THY186	75	F	fvPTC			
THY187	47	F	fvPTC			
THY188	57	F	fvPTC			
THY189	57	F	fvPTC			
THY190	22	F	fvPTC		V600E	
THY191	67	F	fvPTC			
THY192	41	F	fvPTC			
THY193	25	F	fvPTC			
THY194	61	F	fvPTC	Pos		
THY195	42	F	fvPTC			
THY196	44	F	fvPTC			
THY197	40	F	fvPTC			
THY198	72	F	fvPTC			
THY199	60	M	fvPTC			
THY200	34	M	fvPTC		K601E	
THY201	38	F	fvPTC			
THY202	76	F	fvPTC			
THY203	36	F	fvPTC			
THY204	48	F	fvPTC			
THY205	30	F	fvPTC			
THY206	53	F	fvPTC			
THY207	38	F	fvPTC			
THY208	21	F	fvPTC			
THY209	42	M	fvPTC			
THY210	30	F	mPTC			
THY211	64	F	mPTC		V600E	
THY212	35	F	mPTC			
THY213	44	F	mPTC			
THY214	57	F	mPTC			
THY215	20	F	MEC			
THY216	67	F	MEC			-124 G>A
THY217	NA	NA	MEC			

THY218	NA	NA	MEC			
THY219	45	F	hcPTC		V600E	
THY220	43	F	hcPTC		V600E	
THY221	33	F	hcPTC		V600E	
THY222	60	F	hcPTC		V600E	
THY223	45	F	hcfvPTC			
THY224	68	F	hcfvPTC		V600E	
THY225	23	M	hcfvPTC			
THY226	68	F	wPTC		V600E	
THY227	55	F	wPTC		V600E	
THY228	41	F	wPTC		V600E	
THY229	58	F	wPTC		V600E	
THY230	55	M	FTC	Pos		
THY231	53	F	FTC			
THY232	82	F	FTC			-124 G>A
THY233	56	F	FTC			
THY234	54	F	FTC	Pos		
THY235	42	F	FTC			
THY236	85	M	FTC			
THY237	78	M	FTC	Pos		-124 G>A
THY238	66	M	FTC	Pos		
THY239	59	F	FTC	Pos		-124 G>A
THY240	41	F	FTC			
THY241	72	M	FTC			
THY242	45	M	FTC			
THY243	51	F	FTC			
THY244	24	M	FTC			
THY245	33	F	FTC			
THY246	42	F	FTC			
THY247	60	F	FTC			-124 G>A
THY248	76	F	FTC			-146 G>A
THY249	27	F	FTC	Pos		
THY250	38	M	FTC			
THY251	49	F	FTC	Pos		-124 G>A
THY252	34	F	FTC			
THY253	53	F	FTC			
THY254	60	F	FTC			
THY255	56	F	FTC			
THY256	56	F	FTC			
THY257	45	F	FTC			-146 G>A
THY258	36	F	FTC			
THY259	NA	NA	FTC			
THY260	64	M	FTC	Pos		
THY261	67	M	FTC			
THY262	58	F	FTC	Pos		-124 G>A

THY263	58	F	FTC	Pos		-124 G>A
THY264	52	F	FTC			
THY265	54	F	FTC	Pos		
THY266	57	F	FHCC			
THY267	55	F	FHCC			
THY268	56	F	FHCC			
THY269	70	F	FHCC			
THY270	NA	NA	FHCC			
THY271	19	F	FHCC	Pos		
THY272	24	F	FHCC			
THY273	59	F	FHCC			
THY274	78	F	FHCC			
THY275	43	F	FHCC			
THY276	63	F	FHCC			
THY277	26	F	FHCC			
THY278	26	F	FHCC			
THY279	NA	NA	FHCC			
THY280	86	F	FHCC			
THY281	53	F	FHCC			
THY282	41	M	FHCC			
THY283	29	M	FHCC			
THY284	68	F	FHCC			
THY285	77	F	FHCC			
THY286	69	F	FHCC			
THY287	41	M	FHCC			
THY288	35	F	FHCC			
THY289	59	F	FHCC			
THY290	57	F	FHCC			
THY291	23	F	FHCC	Pos		
THY292	36	M	FHCC	Pos		
THY293	86	F	FHCC			
THY294	63	F	PDTC			
THY295	NA	NA	PDTC			
THY296	58	M	PDTC		V600E	
THY297	68	F	PDTC			
THY298	NA	NA	PDTC			-124 G>A
THY299	71	F	PDTC			
THY300	52	F	PDTC			
THY301	70	M	PDTC			-124 G>A
THY302	64	M	PDTC			
THY303	38	M	PDTC			
THY304	80	M	PDTC			
THY305	11	M	PDTC			
THY306	52	F	PDTC			
THY307	54	F	PDTC	Pos		-146 G>A

THY308	60	M	Anaplastic		V600E	-124 G>A
THY309	72	M	Anaplastic			
THY310	NA	NA	Anaplastic		V600E	
THY311	74	F	Anaplastic		V600E	
THY312	52	F	Anaplastic			
THY313	55	M	Anaplastic			
THY314	NA	NA	Anaplastic			
THY315	NA	F	Anaplastic			
THY316	56	F	Anaplastic			
THY317	59	F	Anaplastic			
THY318	75	F	Anaplastic		V600E	
THY319	82	F	Anaplastic			
THY320	69	M	Anaplastic		V600E	
THY321	39	M	Anaplastic			
THY322	70	M	Anaplastic			
THY323	44	F	Anaplastic			-146 G>A
THY324	63	M	MTC			
THY325	NA	NA	MTC			
THY326	NA	NA	MTC			
THY327	32	F	MTC			
THY328	NA	NA	MTC			
THY329	NA	NA	MTC			
THY330	NA	NA	MTC			
THY331	NA	NA	MTC			
THY332	NA	NA	MTC			
THY333	NA	NA	MTC			
THY334	68	F	MTC			
THY335	NA	NA	MTC			
THY336	37	F	MTC			
THY337	NA	NA	MTC			
THY338	71	F	MTC			
THY339	40	M	MTC			
THY340	NA	NA	MTC			
THY341	56	F	MTC			
THY342	NA	NA	MTC			
THY343	38	F	MTC			
THY344	NA	NA	MTC			
THY345	NA	NA	MTC			
THY346	23	M	MTC			
THY347	NA	NA	MTC			
THY348	36	F	MTC			
THY349	NA	NA	MTC			
THY350	NA	NA	MTC			
THY351	NA	NA	MTC			

Supplementary Table S8 – Comparison of the clinico-pathological features of conventional PTC with and without *TERT* mutations

Tumour type	Clinical features	All patients	*TERT* wild type	*TERT* mutated	*p* value
Conventional Papillary Thyroid Carcinoma (n=110)	Mean age at diagnosis, yr (±SD)	43±16	41±15	63±14	**<0,0001**
	Gender				
	Male	26 (25%)	18 (19%)	8 (67%)	**0,0012**
	Female	80 (75%)	76 (81%)	4 (33%)	
	Mean tumour size, cm	2,6±1,6	2,4±1,4	4,3±2,2	**0,0004**
	LN metastasis (positive/total)	67 (73%)	56 (68%)	11 (100%)	**0,03**
	BRAF mutation (positive/total)	61 (57%)	49 (50%)	12 (100%)	**0,001**
	NRAS mutation (positive/total)	4(7%)	4 (10%)	0 (0%)	NS

Supplementary Table S9 - Summary of clinico-pathological and genetic data in 82 bladder cancers

Case Code	Age	Gender	Stage	Grade	*TERT*
BC1	66	M	Ta	Low Grade	-146 G>A
BC2	NA	M	T1	Low Grade	
BC3	80	M	Ta	Low Grade	-146 G>A
BC4	70	M	Ta	Low Grade	
BC5	67	M	Ta	Low Grade	-124 G>A
BC6	80	M	Ta	Low Grade	-124 G>A
BC7	65	M	Ta	Low Grade	-124 G>A
BC8	40	M	Ta	Low Grade	-124 G>A
BC9	36	M	T1	Low Grade	-124 G>A
BC10	64	M	Ta	Low Grade	
BC11	65	M	Ta	Low Grade	-124 G>A
BC12	47	F	Ta	Low Grade	
BC13	54	M	Ta	Low Grade	-124 G>A
BC14	41	M	T1	Low Grade	
BC15	50	M	T1	Low Grade	-124 G>A
BC16	67	M	Ta	Low Grade	-124 G>A
BC17	97	M	Ta	Low Grade	-146 G>A
BC18	40	F	Ta	Low Grade	-124 G>A
BC19	60	M	Ta	Low Grade	
BC20	70	M	T1	Low Grade	-146 G>A
BC21	46	F	Ta	Low Grade	
BC22	61	F	Ta	High Grade	-146 G>A
BC23	NA	M	T1	High Grade	-124 G>A
BC24	59	M	T1	High Grade	-124 G>A
BC25	77	M	T1	High Grade	-146 G>A
BC26	65	M	T1	High Grade	-124 G>A
BC27	83	F	T1	High Grade	-124 G>A
BC28	64	M	T1	High Grade	

BC29	NA	M	NA	High Grade	-124 G>A
BC30	NA	M	NA	High Grade	-146 G>A
BC31	67	M	T1	High Grade	-124 G>A
BC32	NA	M	Ta	High Grade	
BC33	NA	M	T1	High Grade	
BC34	NA	M	T1	High Grade	
BC35	NA	M	T1	High Grade	-146 G>A
BC36	74	M	T1	High Grade	-124 G>A
BC37	75	M	Ta	High Grade	
BC38	76	F	T1	High Grade	
BC39	45	M	Ta	High Grade	
BC40	NA	M	T1	High Grade	
BC41	76	F	T1	High Grade	
BC42	NA	M	T1	High Grade	-124 G>A
BC43	72	F	Ta	High Grade	
BC44	NA	F	T1	High Grade	
BC45	67	M	T1	High Grade	-124 G>A
BC46	NA	M	T1	High Grade	-146 G>A
BC47	NA	M	T1	High Grade	-146 G>A
BC48	51	M	T1	High Grade	-146 G>A
BC49	50	M	Ta	High Grade	-124 G>A
BC50	74	M	T1	High Grade	-124 G>A
BC51	70	F	T1	High Grade	-124 G>A
BC52	50	M	T1	High Grade	-146 G>A
BC53	68	M	T1	High Grade	-124 G>A
BC54	56	M	T1	High Grade	
BC55	53	M	T1	High Grade	
BC56	60	F	T1	High Grade	
BC57	74	M	T1	High Grade	
BC58	73	M	T1	High Grade	
BC59	60	F	T1	High Grade	

BC60	64	F	T1	High Grade	
BC61	74	M	T1	High Grade	
BC62	51	M	T1	High Grade	
BC63	63	M	T1	High Grade	-124 G>A
BC64	57	M	Ta	High Grade	-146 G>A
BC65	67	F	Ta	High Grade	-146 G>A
BC66	58	M	Ta	High Grade	-124 G>A
BC67	66	M	T1	High Grade	-124 G>A
BC68	64	M	T1	High Grade	
BC69	70	M	T1	High Grade	-146 G>A
BC70	68	M	Ta	High Grade	-146 G>A
BC71	64	M	T1	High Grade	
BC72	59	F	T1	High Grade	-124 G>A
BC73	63	M	T1	High Grade	-124 G>A
BC74	66	M	Ta	High Grade	
BC75	76	M	T1	High Grade	-124 G>A
BC76	71	M	T1	High Grade	
BC77	61	M	T1	High Grade	-124 G>A
BC78	76	M	T1	High Grade	-124 G>A
BC79	61	M	T1	High Grade	
BC80	68	F	T1	High Grade	
BC81	72	M	T1	High Grade	
BC82	71	M	T1	High Grade	-146 G>A

Supplementary Table S10 - Summary of clinico-pathological and genetic data in 26 kidney cancers

Case code	Diagnosis	Age	Gender	Nuclear grade	Staging	*TERT*
RCC1	CCRCC	68	M			
RCC2	CCRCC	44	M			
RCC3	CCRCC	49	M			
RCC4	CCRCC	49	M	3	pT1a Nx Mx	
RCC5	CCRCC	57	M	2	pT1a Nx Mx	
RCC6	CCRCC	48	F	2	pT1a Nx Mx	
RCC7	CCRCC	48	F	2	pT1a Nx Mx	
RCC8	CCRCC	68	M	2	pT3a Nx Mx	
RCC9	CCRCC	50	M	4	pT3b Nx M0	
RCC10	CCRCC	50	M	4	pT3b Nx M1	
RCC11	CCRCC	62	M	3	pT2 Nx Mx	
RCC12	CCRCC	62	M	3	pT2 Nx Mx	
RCC13	CromRCC	59	M			
RCC14	CromRCC	77	F	2	pT2 Nx Mx	
RCC15	CromRCC	77	F	2	pT2 Nx Mx	
RCC16	CromRCC	72	M	4	pT2 Nx Mx	
RCC17	PRCC	NA	M			
RCC18	PRCC	61	M			
RCC19	PRCC	26	F	2	pT2 N2 MX	
RCC20	PRCC	78	M	2	pT1b Nx Mx	
RCC21	PRCC	34	M	1	pT1a Nx Mx	
RCC22	PRCC	60	M		pT1b Nx Mx	
RCC23	PRCC	60	M		pT1b Nx Mx	
RCC24	PRCC	71	M			
RCC25	PRCC	71	M			
RCC26	PRCC	75	M	3	pT1a Nx Mx	

CCRC – Clear cell renal carcinoma; CromRCC – chromophobe renal cell cancer; PRCC – Papillary renal cell carcinoma;

Supplementary Table S11 - Summary of clinico-pathological and genetic data in 17 phaeochromocytoma

Case code	Age	Gender	Tumor size (cm)	*MEN/NF/VHL*	*TERT*
PHEO1	51	M	4,5	NA	
PHEO2	56	M	7	NA	
PHEO3	54	F	4	NA	
PHEO4	46	F	7	NA	
PHEO5	53	F	2,5	NA	
PHEO6	42	M	8,5	NA	
PHEO7	20	F	1,5	*MEN2*	
PHEO8	55	F	3,5	NA	
PHEO9	19	F	7	NA	
PHEO10	56	M	4,5	NA	
PHEO11	62	M	6	NA	
PHEO12	45	M	7	NA	
PHEO13	73	F	5	NA	
PHEO14	57	M	3,5	NA	
PHEO15	61	M	1,7	NA	
PHEO16	20	F	6	*MEN2*	
PHEO17	46	F	10	*NF1*	

Supplementary Table S12 - Summary of clinico-pathological and genetic data in 36 gastrointestinal stromal tumour

Case code	Age	Sex	Tumor Size (cm)	*KIT*	*PDGFRA*	*TERT*
GIST1	80	F		exon 11 N567K, L576V, 568del575		
GIST2	59	M	1,2	exon 11 V560D		
GIST3	52	M	9,5	exon 11 69997:T>A		
GIST4	67	M	17	exon 11 W557F delK558		
GIST5	58	F	3,5	exon 11 556del557		
GIST6	54	M	19	exon 11 V559D		
GIST7	79	F	7	exon 11 del557-558		
GIST8	46	M	5,5	exon 11 del 550-557, ins550-551		
GIST9	54	M	3,1	exon 11 552del557, K550Q, P551R		
GIST10	76	F	6,7		exon 18 D842V	
GIST11	55	F	6,5	exon 11 del560V		
GIST12	43	M	14,5	exon 11 564del578		
GIST13	73	F	0,8	exon 11 delV559		
GIST14	62	M	2,5	exon 11 del_K558		
GIST15	38	M	3,5	exon 11 V560E		
GIST16	88	F	23	exon 11 L576P		
GIST17	81	F		exon 11 L576P		
GIST18	78	F			exon 12 583del586	
GIST19	40	F	4	exon 9 502-503dup		
GIST20	63	F	9	exon 9 502-503dup		
GIST21	75	M	8	exon 11 Q575H, P577T, delL576		
GIST22	59	F		exon 11 552del570		
GIST23	78	F	24	exon 11 551del553		
GIST24	58	M	13,5	exon 11 557del558		
GIST25	76	M	14	exon 9 502-503dup		
GIST26	20	F	2			
GIST27	77	F	6			
GIST28	74	M	3			
GIST29	58	F	3,5			
GIST30	72	F	8			
GIST31	62	M	6,5			
GIST32	73	M	6			
GIST33	66	F	14			
GIST34	63	F	6,5			
GIST35	55	M	4			
GIST36	82	F	7			

III.2 Targeted expression of BRAF^{V600E} in thyroid cells of transgenic zebrafish induces hyperplasia reverted by loss of WT p53

Abstract

The BRAF^{V600E} mutation is the most common genetic alteration in papillary thyroid carcinomas (PTCs) and are found in 29%-83% of all cases. PTCs harboring B-type Raf kinase (BRAF)^{V600E} are often invasive and this mutation is also present in more advanced stages of the disease such as in poorly differentiated and anaplastic carcinomas arising from PTCs. BRAF^{V600E} kinase activate the mitogen-activated protein kinases (MAPK) pathway, promoting cellular processes such as proliferation, survival, motility and invasion.

To explore the role of BRAF^{V600E} in thyroid cancer pathogenesis, I targeted its expression to thyroid cells of transgenic zebrafish under a thyroid-specific promoter. Fish showed impairment of normal thyroid morphogenesis at early stages of development and they seemed to compensate for BRAF^{V600E}-induced thyroid dysfunction by developing hyperplasia and goiter but not neoplasia. Also, activation of BRAF^{V600E} expression in thyroid cells of transgenic zebrafish during adulthood resulted in a hyperplasic phenotype similar to when BRAF^{V600E} was expressed shortly after birth. In BRAF^{V600E}-expressing animals, upregulation of p53 was observed suggesting a protective mechanism to prevent cancer. Thus, I targeted BRAF^{V600E} expression to thyroid cells of *tp53*^{M214K} zebrafish in order to overcome p53 blockage and progression to cancer. Suprisingly, BRAF^{V600E}-expressing *tp53*^{M214K} fish developed a normal thyroid until adulthood.

In summary, thyroid-specific expression of BRAF^{V600E} induced goiter but not neoplasia which was prevented by loss of WT p53 protein.

Introduction

To create functional follicles, thyroid cells must aggregate, polarize and establish selective permeability barriers between the lumen and the outer compartments. Cellular adhesion, intracellular trafficking, specialized cell-cell junction assembly

and precise regulated morphogenetic cell movements must all be coordinated (Yap et al., 1997).

Disturbances in these cellular processes can be mediated by external factors such as goitrogens or internal factors such as hormonal imbalance or genetic alterations. Ultimately, these factors have important implications in thyroid diseases, mostly characterized by disturbed follicular architecture.

PTCs are characterized by nonoverlapping genetic alterations in more than 70% of the cases. These alterations include rearrangements in the tyrosine kinase (TK) receptors Rearranged-during-transfection (*RET*), Neurotrophic Tyrosine Kinase, Receptor, Type 1 (*NTRK1*), Anaplastic Lymphoma Receptor Tyrosine Kinase (*ALK*) and A Kinase (PRKA) Anchor Protein 9/B-type Raf kinase (*AKAP9*/*BRAF*) and also point mutations in Rat Sarcoma Viral Oncogene Homolog (*RAS*) and *BRAF* genes. Ultimately, most cases will lead to an aberrant activation of the RAS-RAF-MEK-ERK kinase pathway (DeLellis et al., 2004; Kumar et al., 2005; Nikiforov, 2012). Up to 90% of the *BRAF* gene mutations consist in the $BRAF^{V600E}$ (Garnett et al., 2004; Frasca et al., 2008).
The initial evidence that $BRAF^{V600E}$ is required for the cell proliferation, transformation and tumorigenicity of follicular thyroid cells was demonstrated in a xenograft mice model (Liu et al., 2007) even though many studies have supported the role of BRAF mutation in tumor initiation.

Targeted expression of the $BRAF^{V600E}$ in thyroid cells was induced in transgenic FVB/N mice using a bovine thyroglobulin promoter. This study showed that BRAF induced thyroid dysfunction which was compensated by increased levels of thyroid-stimulating hormone (TSH) and goiter development. Also, multifocal tumors involving both lobes of the thyroid gland with mixed papillary and follicular growth pattern were observed in 12 and 22-week-old mice. PTCs presented the classical architecture, tall-cell features and a high potential for invasiveness. Tumors from one of the transgenic lines progressed into poorly differentiated carcinomas (Knauf et al., 2005). PTCs were also observed in a thyrocyte-specific knock-in of $BRAF^{V600E}$ in mice but with a very short latency and complete penetrance by 3 weeks. When this model was crossed with a thyroid stimulating hormone receptor (TshR) knockout mice to genetically ablate TSH signaling, thyroid growth was reduced and low-grade PTCs were observed but only at 9 weeks of age (Franco et al., 2011). More evidence of $BRAF^{V600E}$ involvement in mice thyroid tumorigenesis was perceived when $BRAF^{V600E}$ expression was induced in follicular thyroid cells in a

doxycycline-inducible manner. As early as one week after doxycycline treatment, development of highly penetrant and high-grade papillary thyroid carcinomas with poorly differentiated features and a reversible activation of the MAPK pathway were observed. Upon doxycycline withdrawal, thyroid architecture was reestablished but a second induction not only resulted in hypothyroidism but also reduced thyroid-specific genes expression (Chakravarty et al., 2011).

TP53 mutations are not frequent in thyroid cancer (only 10%) and most have been documented in anaplastic carcinomas. Indeed, well-differentiated thyroid cancers rarely present mutations in *TP53* suggesting a role on cancer progression to poorly differentiated and aggressive phenotypes. Of note, studies on thyroid tumor samples revealed an accumulation of p53 in poorly differentiated and anaplastic forms but also in a few well-differentiated tumors in the absence of any p53 mutation suggesting that p53 inactivation may result from loss of interaction with MDM2 (Soares et al., 1994).

Modeling thyroid cancer in mice have shown that acquired mutations drive tumor progression. In general, $BRAF^{V600E}$ is sufficient to initiate PTCs and *TP53* mutations constrained progression from papillary to anaplastic thyroid carcinoma (McFadden et al., 2014). By generating a thyroid-specific cre recombinase-estrogen receptor (CreER) transgenic mouse and using a Cre-regulated $BRAF^{V600E}$ and a conditional *Trp53*, it was found that p53 loss does enable progression to aggressive anaplastic thyroid cancer but additional events may be required for full anaplastic conversion (McFadden et al., 2014).

Here, I describe the generation of a novel transgenic zebrafish line, tg(*tg*:mCh-T2A-$BRAF^{V600E}$), that expresses $BRAF^{V600E}$ specifically in the thyroid cells allowing imaging of the thyroid development and monitoring of the effect of the oncogene in live animals. By crossing this transgenic line with $tp53^{M214K}$, I generated a second novel zebrafish line providing new insights of the dynamics of $BRAF^{V600E}$ and p53 in zebrafish thyroid. Finally, I used those lines to generate a conditional $BRAF^{V600E}$ expressing line that can be used for future studies and disclose in detail the thyroid phenotypes occurring due to $BRAF^{V600E}$ either in the presence of absence of a WT p53 at different stages of life.

Material and Methods

Zebrafish husbandry and embryo culture

Zebrafish embryos were obtained from natural spawning of adult fish and were raised at 28.5ºC according to Westerfield et al., 2000 and staged in hours post-fertilization (hpf) as described by Kimmel et al., 1995.

Fish strains

The following zebrafish lines were used in this study: tg(*tg*:mCh), tg(*tg*:mCh-T2A-BRAF^{V600E}), tg(*tg*:mCh;*tg*:mCh-T2A-BRAF^{V600E}), *tp53*^{M214K} tg(*tg*:mCh), *tp53*^{M214K} tg(*tg*:mCh-T2A-BRAF^{V600E}), *tp53*^{M214K} tg(*tg*:mCh;*tg*:mCh-T2A-BRAF^{V600E}), tg(*hsp70l*:mCh-T2A-CreER^{T2};*tg*:loxP-CFP-loxP-mCh) and tg(*hsp70l*:mCh-T2A-CreER^{T2};*tg*:loxP-CFP-loxP-mCh-T2A-BRAF^{V600E}), all containing the *cmlc2:EGFP* transgenesis marker. Details on the strategy to generate these lines are briefly described below and in Chapter II.

Generation of plasmids for transgenic lines

A bacterial artificial chromosome (BAC) genomic clone DKEY-97I18 BAC (GenBank CR855311.15) containing the first exon of the zebrafish thyroglobulin (*tg*) gene was obtained from SourceBioScience (Nottingham, UK). An insert corresponding to the region from -2041bp until -1bp relative to the *tg* ATG was amplified and cloned into a p5E-MCS plasmid provided by the Tol2Kit (Kwan et al., 2007). mCherry-T2A-BRAF^{V600E} was amplified and cloned into a pME-entry clone. To build the final constructs, [p5E-*tg* promoter, pME-mCherry and p3E-polyA] or [p5E-*tg* promoter, pME-mCherry-T2A-BRAF^{V600E} and p3E-polyA] were assembled into a pDestTol2pA or a pDestTol2CG2 with *cmlc2:EGFP* cassette. The final constructs used for injection were verified by sequencing and named Tol2*tg*:mCh and Tol2*tg*:mCh-T2A-BRAF^{V600E}. To generate conditional constructs, the loxP-CFP-loxP cassette was cloned downstream of the *tg* promoter using the above-mentioned constructs as backbones.

Transgenesis

For generation of transgenic fish, WT and tg(*hsp70l*:mCherry-T2A-CreER^{T2}) embryos were injected with 30ng/μL of plasmid and 25 ng/μL of capped transposase messenger ribonucleic acid (mRNA) at one-cell stage. Microinjections were performed using a SZX10 Stereo Microscope (Olympus) and PV820 Pneumatic PicoPump (World Precision Instruments, Inc.).

mRNA injections

For mRNA experiments, mCherry, mCherry-T2A-BRAF^{WT} and mCherry-T2A-BRAF^{V600E} were cloned into a pCS2-*CMV* plasmid. Capped mRNA was generated by *in vitro* transcription using the mMessage mMachine SP6 kit (Ambion) linearized with *Hpa*I. Capped mRNA was injected into the yolk of one-cell stage WT or *tp53*^{M214K} embryos at a final concentration of 35ng/μL. Microinjections were performed using a SZX10 Stereo Microscope (Olympus) and PV820 Pneumatic PicoPump (World Precision Instruments, Inc.).

Histology

Zebrafish was fixed in 10% neutral-buffered formalin, decalcified in (ethylenedinitrilo)tetraacetic acid (EDTA) and embedded in paraffin. Details for each stage are described in Chapter II. Three-micrometer-thick sections were prepared and stained with hematoxylin-eosin (HE).

Western blot

Thyroid tissue or embryos were placed in RIPA Buffer (Sigma) supplemented with protease and phosphatase inhibitor cocktail (Sigma) and homogenized with a pestle. Protein lysates were centrifuged and supernatant collected. Lysates were subjected to SDS PAGE, transferred to HyBond-P PVDF membranes (GE Healthcare) and probed with antibodies to BRAF, phospho-ERK1/2, pAKT S473, pAKT T308, PCNA, p16, p53, activated caspase 3, p38 and mCherry (Clontech Lab, Santa Cruz Biotechnology, Cell Signaling, Anaspec and Abcam). Membranes were hybridized with species-specific HRP-conjugated antibodies (Santa Cruz Biotechnology) and bands visualized with Pierce™ ECL Plus Western Blotting Substrate detection system (Thermo Fisher Scientific Inc.). Antibody dilutions are described in Chapter II.

Drug treatment

Fish were heat-shocked in a 37ºC water bath for 30 minutes and immediately a drug treatment was carried out with 2.5μM of 4-hydroxyl-tamoxifen (4-OHT) (H7904, Sigma). Controls were treated with an equivalent amount of 100% ethanol diluted in embryo medium. Fish received treatment at 28ºC for 5 hours in the dark followed by a recovery period in fresh water for 12 hours.

Results

Generation and validation of a thyroid-specific reporter line

A thyroid-specific reporter line allow experimental approaches to study the role of $BRAF^{V600E}$ in zebrafish thyroid. I generated a control reporter construct in which the zebrafish *tg* promoter was used to drive expression of a monomeric red fluorophore mCherry protein. I also generated a reporter construct in which the zebrafish *tg* promoter was used to drive expression of mCherry and $BRAF^{V600E}$ proteins.

The *tg* promoter was chosen because (1) *tg* mRNA expression in zebrafish is detected shortly after thyroid specification at 34hpf; (2) it is exclusive to thyroid cells and not to calcitonin-producing cells, which can be found as distinct glands elsewhere in the fish body (Alt et al., 2006) and; (3) *tg* mRNA is kept at high levels throughout zebrafish thyroid development (Alt et al., 2006; Opitz et al., 2011). The region from -2041bp until -1 relative to the *tg* ATG was cloned because it was expected that the putative regulatory region of the zebrafish *tg* coding sequence would lay between the *tg* ATG and the gene that was immediately upstream of the *tg* (Figure 1). By the same time and for the purpose of generating a thyroid-specific reporter line, Opitz et al., 2012 cloned the region from -3591bp until -518bp relative to the *tg* ATG and reported that this region drove robust reporter expression specifically in thyroid cells of transgenic zebrafish. The -3591bp until -2041bp region was not included in this work because it belonged to the *phf20l1* gene and it was unlikely to harbor a promoter.

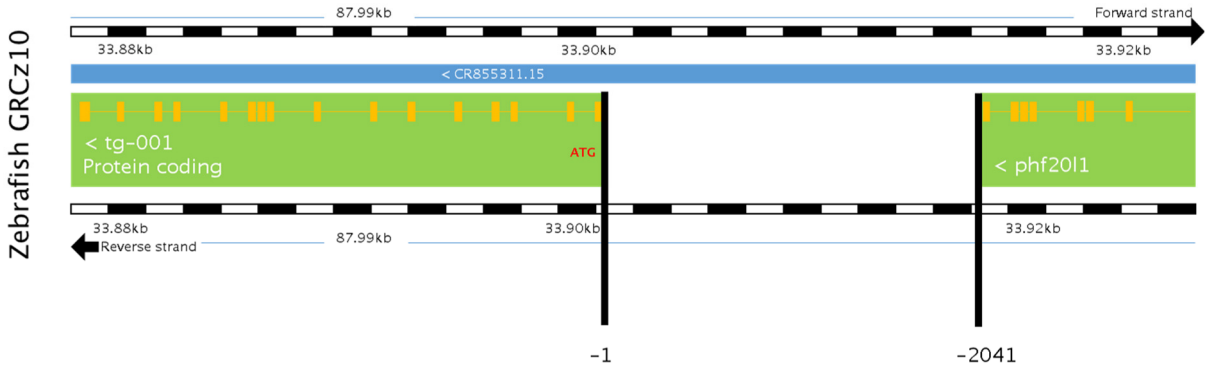

***Figure 1*. Putative *tg* promoter.** Schematic representation of the putative *tg* promoter flanked upstream by the PHD finger protein 20-like 1 (*phf20l1*) gene (encoded in the reverse strand) and downstream by the *tg* gene. The region from -2041bp until -1 relative to the *tg* ATG was chosen to be the *tg* promoter region.

The fluorophore mCherry was chosen as a reporter because a *cmlc2:EGFP* transgenesis marker was to be included in the plasmid backbone. The *cmlc2:EGFP* cassette comprises a ~900-bp enhancer-promoter from the cardiac myosin light chain (cmlc2) gene which drives cytoplasmic EGFP expression specifically in the developing heart (Huang et al., 2003; Auman et al., 2007). This cassette is particularly useful to screen embryos and fish.

mCherry reporter was not fused to BRAF coding sequence, so a self-cleaving 2A peptide (*Thoseaasigna* virus 2A- T2A) that was described to have the highest cleavage efficiency (close to 100%) (Donnelly et al., 2001) was chosen. This allow the cleavage between the upstream gene (mCherry) and the downstream gene (BRAF) of the 2A sequence.

A simian vacuolating virus 40 (SV40) late polyadenylation (polyA) signal sequence derived from the p3E-polyA plasmid was also included because in many systems, including zebrafish, SV40 signal proved to be much more effective in the stabilization of mRNA transcripts and in the promotion of translation (Carswellet al., 1989).

Finally, a Tol2-based destination plasmid was chosen not only because it greatly simplified the generation of expression constructs using the Gateway technology but also because, Tol2 constructs were reported to have a very high transgenesis efficiency (Kawakami et al., 2004). Also, a Tol2Kit containing many entry clones was available for the community (Kwan et al., 2007).

For generation of the two transgenic reporter constructs, a 2.0kb fragment of the putative *tg* promoter was assembled with [mCherry and poly(A)] fragments (Figure 2A) or [mCherry-T2A-BRAF^{V600E} and poly(A)] fragments (Figure 2B) into a pDestTol2pA with a *cmlc2*:EGFP cassette.

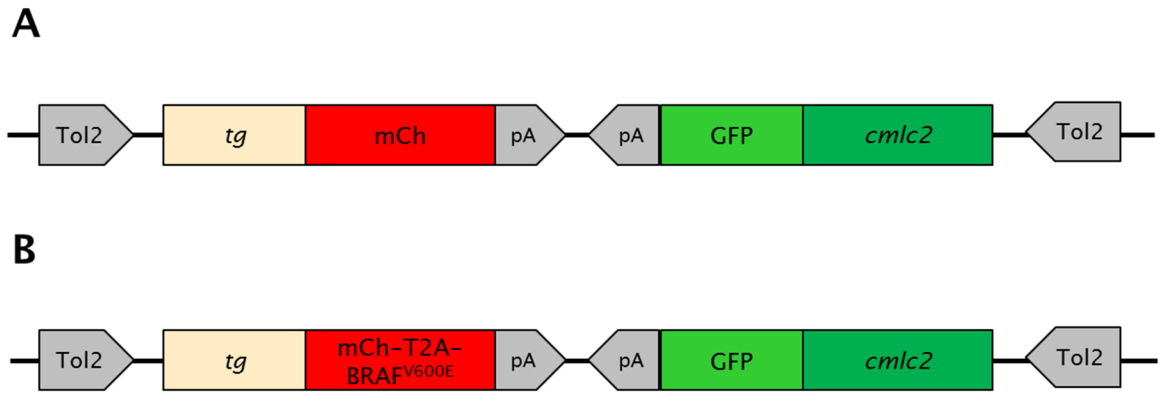

***Figure 2*. Tol2CG2 constructs.** Schematic representation of the (A) Tol2CG2*tg*:mCh-pA (A) and (B) Tol2CG2*tg*:mCh-T2A-BRAF^{V600E}-pA constructs containing Tol2 elements and the *cmlc2*:EGFP-pA cassette. Not shown here is the Tol2*tg*:mCh-pA, also generated in this work.

Tol2*tg*:mCh, Tol2CG2*tg*:mCh or Tol2CG2*tg:mCh*-T2A-BRAF^{V600E} was injected with capped transposase mRNA into one-cell-stage WT zebrafish embryos. By fluorescence microscopy, mosaic mCherry expression was observed in thyroid cells of F0 animals injected with Tol2*tg*:mCh or Tol2CG2*tg*:mCh confirming that the selected 2.0kb *tg* promoter contained regulatory sequences sufficient to drive expression specifically to the thyroid cells. In F0 animals injected with Tol2CG2*tg:mCh*-T2A-BRAF^{V600E}, mosaic mCherry expression was never observed and embryos were always selected for the transgenesis marker.

Embryos presenting mosaic mCherry or EGFP expression in the thyroid or heart, respectively and according to the line, were grown to adulthood and F0 founders were identified by a strong and specific-reporter signal exclusively in those tissues in their progeny. Stable transgenic lines were established using F0 founders. A robust mCherry expression was confirmed to be observed in the thyroid cells of tg(*tg*:mCh) line (Figure 3) but not in the tg(*tg*:mCh-T2A- BRAF^{V600E}).

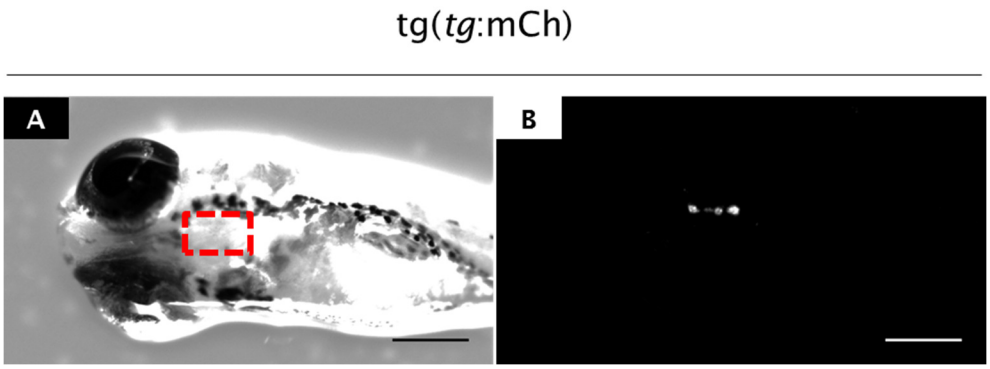

***Figure 3*. tg(*tg*:mCh) line.** (A) 14dpf tg(*tg*:mCh) larvae revealed (B) mCherry protein expression specifically in thyroid cells. Larvae is oriented with anterior to the left. Scale bar: 250μM.

At this point, EGFP reporter expression in the heart was used to select animals from the BRAF^{V600E}-expressing line. By crossing the tg(*tg*:mCh) with the tg(*tg*:mCh-T2A-BRAF^{V600E}) line, a tg(*tg*:mCh;*tg*:mCh-T2A- BRAF^{V600E}) line was generated in order to have a thyroid-specific reporter in the BRAF^{V600E}-expressing line. Embryos showing mCherry expression in the thyroid given by the Tol2*tg*:mCh transgene and EGFP expression in the heart given by the Tol2CG2*tg*:mCh-T2A-BRAF^{V600E} transgene were grown to adulthood.

Because the tg(*tg*:mCh-T2A- BRAF^{V600E}) line was not expressing mCherry, an experiment to determine the protein translation efficiency from mCh-T2A-BRAF^{V600E} was performed in order to exclude possible problems with the 2A cleavage.

A pCS2+ expression plasmid was chosen because it contains a strong enhancer/promoter (simian CMV) followed by a polylinker and a SV40 late polyadenylation site. Also, a SP6 promoter is present in the 5' untranslated region of the mRNA from the sCMV promoter which allows *in vitro* RNA synthesis of sequences cloned into the polylinker. mCherry coding sequence was used as a control and mCh-T2A-BRAF^{WT} was used as a control of T2A efficiency and BRAF toxicity, because BRAF^{wt} proteins do not have an effect on the development of zebrafish embryos (Anastasaki et al., 2012). Capped mRNA was *in vitro* transcribed from the constructs generated: pCS2-*CMV*:mCh, pCS2- *CMV*:mCh-T2A-BRAF^{WT} and pCS2-*CMV*:mCh-T2A-BRAF^{V600E} (Figure 4A).

After injecting capped mCh-T2A-BRAF^{V600E} mRNA in WT embryos, a severe developmental arrest was found at around 4hpi preventing embryos to further develop beyond the blastula stage (Figure 4B). Malformations were found in the majority of injected embryos (90.43%) (Figure 4C) and survival at 24 hours post injection (hpi) was very low (34.8%) (Figure 4D). By fluorescence microscopy, a polka-dot pattern was observed confirming mCherry expression in the cell (Figure 4B). The phenotype produced was believed to be due to expression of mCherry and BRAF^{V600E} because no phenotypes were observed in non-injected WT embryos (Figure 4B). WT embryos injected with capped mCh or mCh-T2A- BRAF^{WT} mRNAs showed no developmental arrest (Figure 4B), a very low frequency of malformations (0.76% and 0.64%, respectively) (Figure 4C) and survival at 24hpi (85.8% and 75.5%, respectively) not significantly different from non-injected WT embryos (Figure 4D). By fluorescence microscopy, it was observed an ubiquitous expression of mCherry in WT embryos injected with capped mCh or mCh-T2A-BRAF^{WT} mRNAs (Figure 4B) which was consistent with the observations reported by Anastasaki et al., 2012. In order to confirm if BRAF^{V600E} was indeed inducing a phenotype, a western blot of embryo lysates was performed by probing with antibodies to mCherry and human BRAF. Blots confirmed the presence of both mCherry and BRAF proteins in embryos injected with mCh-T2A-BRAF^{V600E} mRNA and BRAF probing was similar to those injected with the WT form of BRAF (Figure 4E; E' and E'').

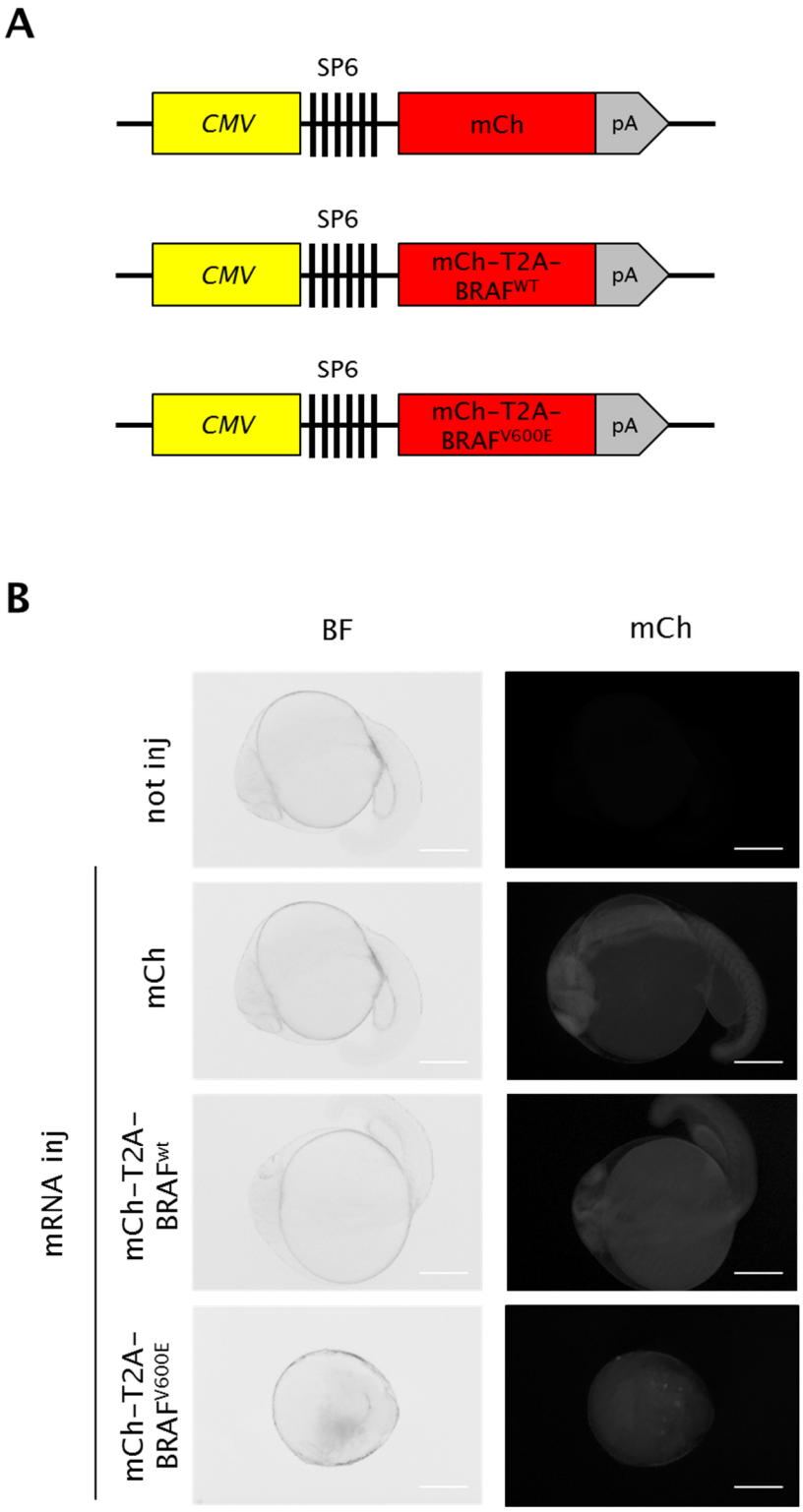
A
SP6
CMV
mCh
pA
SP6
CMV
mCh–T2A–
BRAFWT
pA
SP6
CMV
mCh–T2A–
BRAFV600E
pA
B
BF
mCh
not inj
mRNA inj
mCh
mCh–T2A–
BRAFwt
mCh–T2A–
BRAFV600E

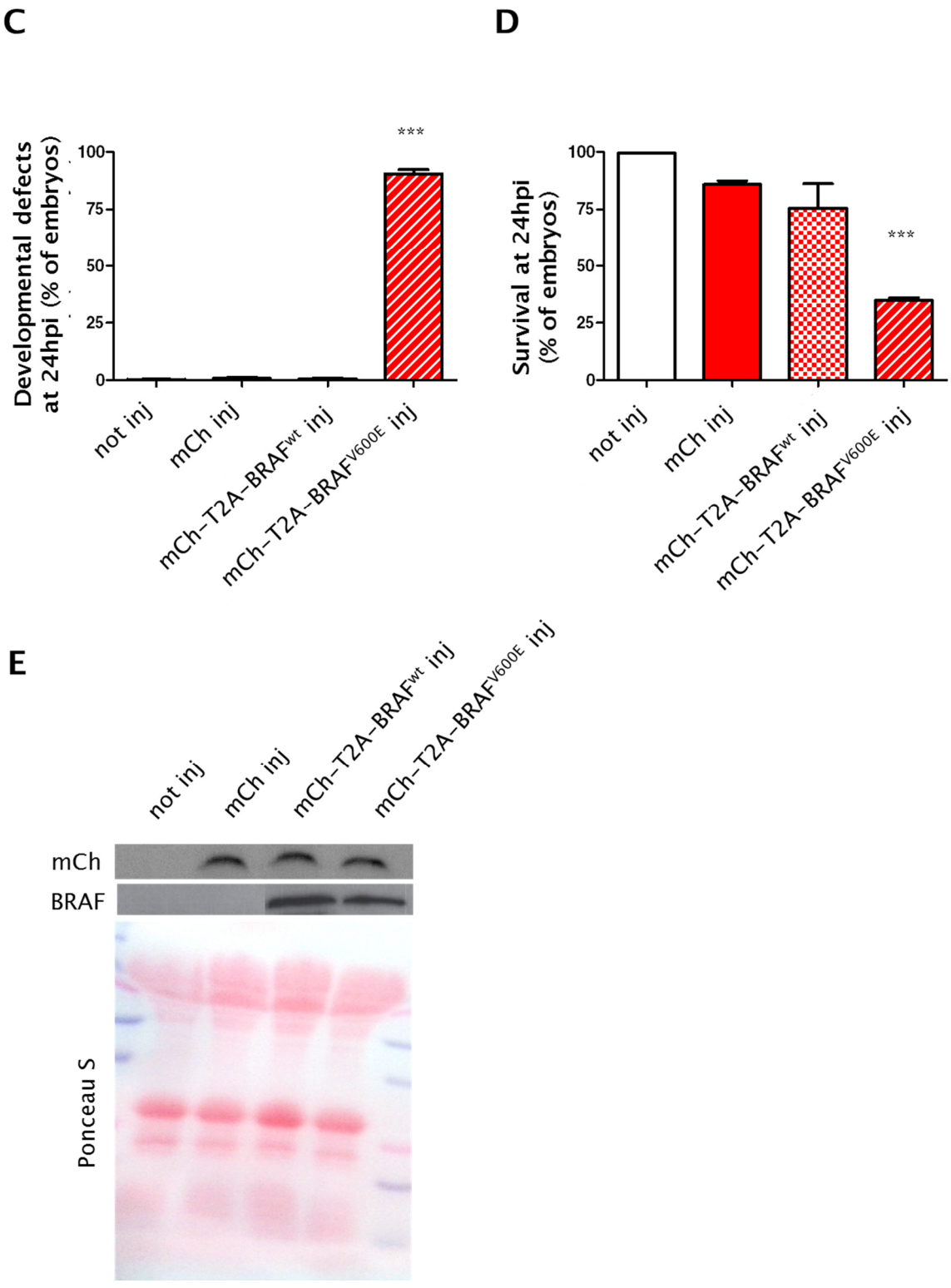
C
Developmental defects at 24hpi (% of embryos)
100
75
50
25
0
***
not inj
mCh inj
mCh–T2A–BRAFwt inj
mCh–T2A–BRAFV600E inj
D
Survival at 24hpi (% of embryos)
100
75
50
25
0
***
not inj
mCh inj
mCh–T2A–BRAFwt inj
mCh–T2A–BRAFV600E inj
E
not inj
mCh inj
mCh–T2A–BRAFwt inj
mCh–T2A–BRAFV600E inj
mCh
BRAF
Ponceau S

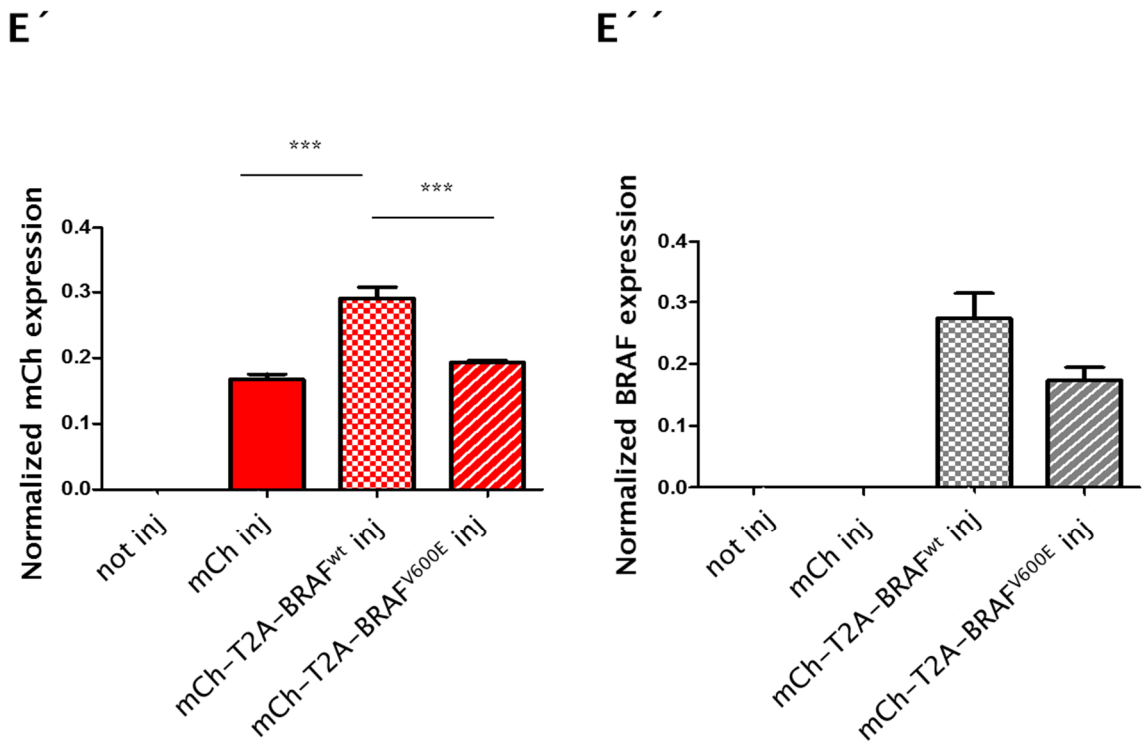

Figure 4. **mRNA experiment in WT embryos.** (A) Schematic representation of the pCS2-*CMV:*mCh, pCS2-*CMV:*mCh-T2A-BRAF^{WT} and pCS2-*CMV:*mCh-T2A-BRAF^{V600E} constructs (top to bottom) containing the SP6 promoter to drive *in vitro* RNA synthesis. (B) Representative images of 24hpf non-injected and 24hpi injected WT embryos with one of the three mRNAs: mCh, mCh-T2A-BRAF^{WT} or mCh-T2A- BRAF^{V600E}. On the left are shown BF images; on the right images acquired with a Texas Red® filter. Scale bar: 300μm. (C) Percentage of developmental defects at 24hpf or 24hpi (statistical analysis only shown for relevant comparisons; $p<0.001$). (D) Survival at 24hpf or 24hpi (statistical analysis only shown for relevant comparisons; $p<0.001$). (E) Western blot analysis of lysates from embryos at 4hpf or 4hpi. 50 embryos were pooled for each condition. Membranes were blotted with mCh and BRAF antibodies. Ponceau S stain showed equal amount of protein in all lanes. (E') mCherry and (E'') BRAF protein levels were quantified and normalized to the amount of protein. Values are shown in bar graphs and represent three independent experiments (statistical analysis only shown for relevant comparisons; $p<0.001$).

To rule out a possible activation of p53-mediated apoptosis due to off-targeting effect of the mRNA injected (Robu et al., 2007), an mRNA experiment was conducted in *tp53*^{M214K} embryos. *tp53*^{M214K} embryos lack apoptosis and cell-cycle arrest responses to deoxyribonucleic acid (DNA) damage because the *tp53*-mediated cell-cycle control is absent (Berghmans et al., 2005).

After injecting capped mCh-T2A-BRAF^{V600E} mRNA in *tp53*^{M214K} embryos, a lower developmental arrest was found in embryos at around 4hpi (Figure 5A) when compared to *tp53*^{M214K} embryos. Malformations were found in injected embryos (39.40%) (Figure 5B) and survival was low (33.00%) (Figure 5C). By fluorescence microscopy, ubiquitous expression of mCherry was observed (Figure 5A). In contrast, *tp53*^{M214K} embryos injected with capped mCh or mCh-T2A- BRAF^{WT} mRNAs showed no developmental arrest (Figure 5A), very low frequency of malformations (1.00% and 0.28%, respectively) (Figure 5B) and survival at 24hpi (92.60% and 85.50%, respectively) (Figure 5C) similar to non-injected *tp53*^{M214K} embryos (0.00% and 98% for malformation frequency and survival, respectively) (Figure 5B and 5C).

Because a less severe phenotype was observed in BRAF^{V600E}-expressing *tp53*^{M214K} embryos, a western blot of embryo lysates was conducted to determine whether the phenotype would be due to a decrease of BRAF expression. Blots confirmed the presence of both mCherry and BRAF proteins in *tp53*^{M214K} embryos injected with mCh-T2A-BRAF^{V600E} mRNA but BRAF protein levels were significantly lower than those found for BRAF^{WT}-expressing *tp53*^{M214K} embryos (Figure 5D; D' and D'') ($p<0.001$) or even BRAF^{V600E}-expressing WT embryos (Figure 4E'').

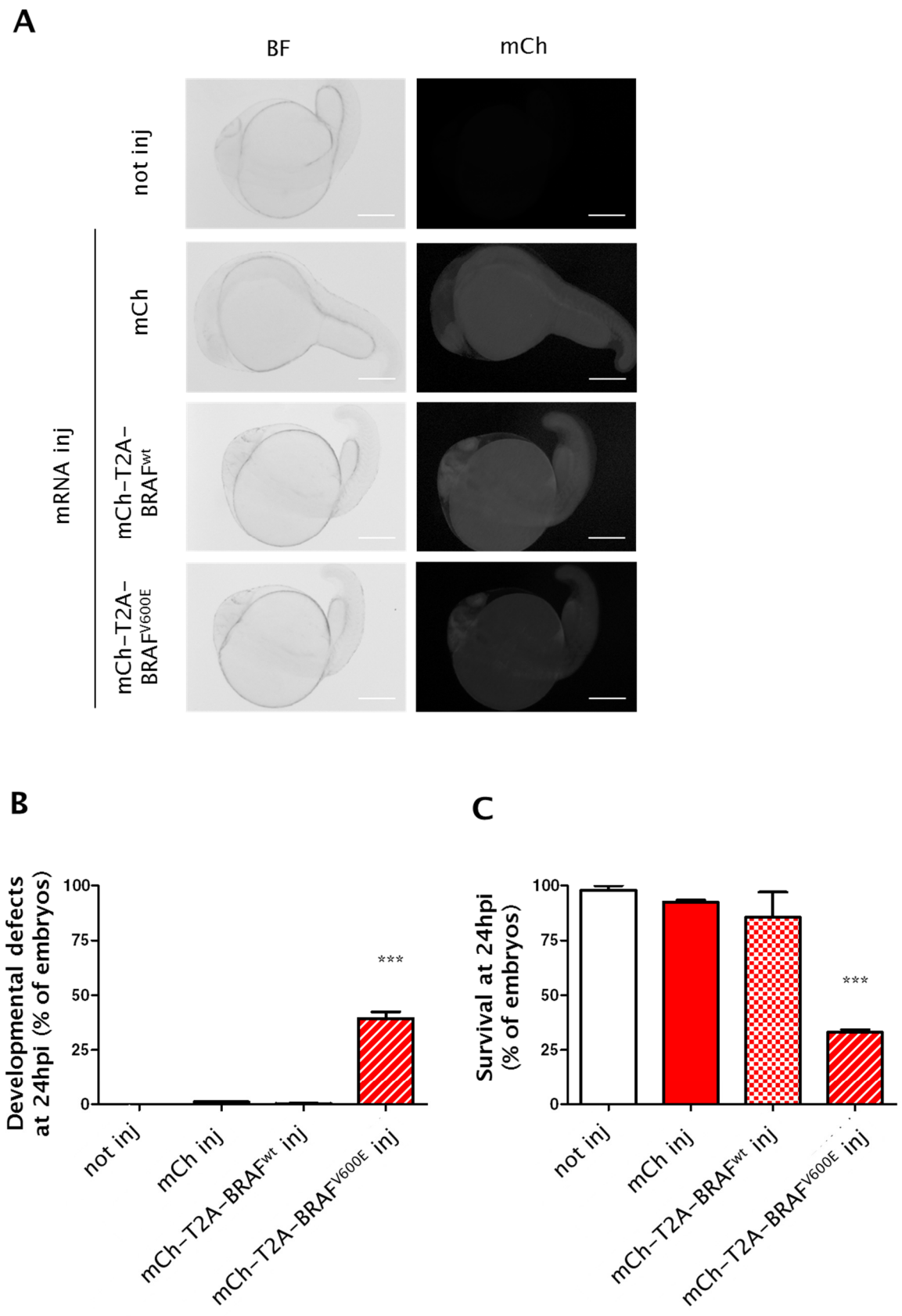
A
BF
mCh
not inj
mRNA inj
mCh
mCh–T2A–BRAFwt
mCh–T2A–BRAFV600E
B
Developmental defects at 24hpi (% of embryos)
100
75
50
25
0
***
not inj
mCh inj
mCh–T2A–BRAFwt inj
mCh–T2A–BRAFV600E inj
C
Survival at 24hpi (% of embryos)
100
75
50
25
0
***
not inj
mCh inj
mCh–T2A–BRAFwt inj
mCh–T2A–BRAFV600E inj

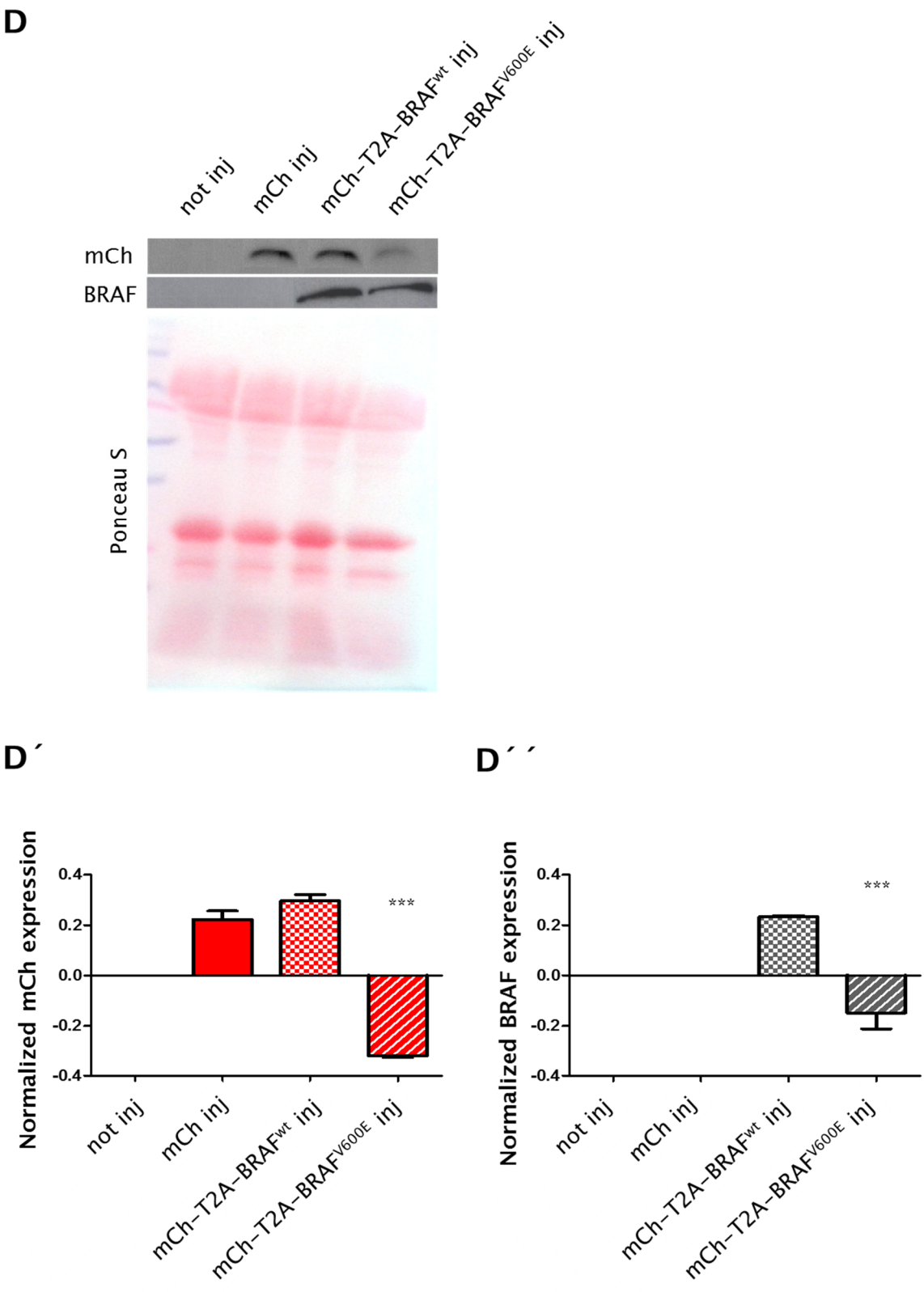

Figure 5. **mRNA experiment in *tp53*^{M214K} embryos.** (A) Representative images of 24hpf non-injected and 24hpi *tp53*^{M214K} embryos injected with one of the three mRNAs: mCh, mCh-T2A-BRAF^{WT} or mCh-T2A-BRAF^{V600E}. On the left are shown BF images; on the right

images acquired with a Texas Red® filter. Scale bar: 300μm. (B) Percentage of developmental defects at 24hpf or 24hpi (statistical analysis only shown for relevant comparisons; $p<0.001$). (C) Survival at 24hpf or 24hpi (statistical analysis only shown for relevant comparisons; $p<0.001$). (D) Western blot analysis of lysates from embryos at 4hpf or 4hpi. 50 embryos were pooled for each condition. Membranes were blotted with mCh and BRAF antibodies. Ponceau S stain showed equal amount of protein in all lanes. (D') mCherry and (D'') BRAF protein levels were quantified and normalized to the amount of protein. Values are shown in bar graphs and represent three independent experiments (statistical analysis only shown for relevant comparisons; $p<0.001$).

Taken together, mRNA experiments showed that $BRAF^{V600E}$-induced phenotype in zebrafish embryos was conditioned by p53 and the presence of a WT p53 protein triggered protective mechanisms (possibly apoptosis and/or cell cycle arrest) against the oncogene.

The mRNA experiments also confirmed an efficient translation of two independent proteins from mCh-T2A-$BRAF^{V600E}$ mRNA. This suggested that, independently of the absence of mCherry expression in the tg(*tg*:mCh-T2A-$BRAF^{V600E}$) fish, the mutant form of BRAF was able to be translated. To confirm BRAF expression in the stable tg(*tg*:mCh-T2A-$BRAF^{V600E}$) line, western blots of protein extracts from thyroid tissues of three month-old fish (Figure 6A) using a BRAF antibody raised against a peptide of human origin were performed. It was confirmed an increase in the levels of BRAF when compared to tg(*tg*:mCh) (Figure 6B). Also, a robust increase in the levels of phospho- Extracellular Regulated Kinase (pERK), a downstream of BRAF, confirmed activation of the MAPK pathway by $BRAF^{V600E}$ (Figure 6B). This suggested that the BRAF protein was indeed functional in thyroid cells of the transgenic line.

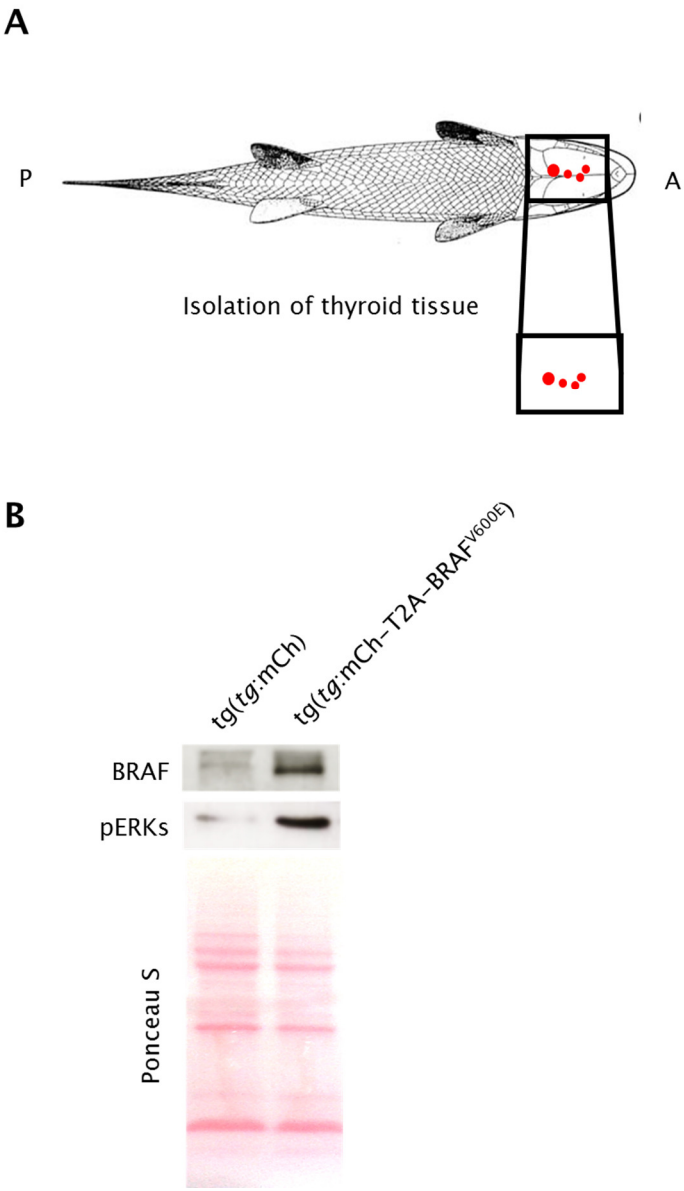

Figure 6. **BRAF and pERK expression in tg(*tg*:mCh-T2A-BRAF^{V600E}) fish.** (A) Schematic representation of the thyroid tissue dissected from mCh-expressing transgenic zebrafish to produce tissue lysates. All follicles were dissected and separated from non-mCh expressing tissues. (B) Western blot analysis of lysates from thyroid tissues of tg(*tg*:mCh) (first lane) and tg(*tg*:mCh-T2A-BRAF^{V600E}) (second lane) fish at 3 months of age. Three fish were pooled for each line. Membranes were blotted with BRAF and pERKs antibodies. Ponceau S showed equal amount of protein in both lanes.

Monitoring BRAF^{V600E}-induced phenotype in transgenic fish

When analyzing live tg(*tg*:mCh;*tg*:mCh-T2A-BRAF^{V600E}) embryos, a robust thyroid-specific reporter signal became detectable at around 34hpf and it was maintained throughout thyroid morphogenesis, similar to tg(*tg*:mCh) embryos.

To study whether BRAF^{V600E} produced an initial phenotype during thyroid growth, mCherry expression was monitored at 60-72hpf, which was the timepoint when conventional fluorescence microscopy was sufficiently sensitive to identify groups of thyroid cells that evaginated from pharyngeal epithelium, and up to 7dpf in tg(*tg*:mCh;*tg*:mCh-T2A-BRAF^{V600E}). It was observed the formation of a unique follicle in the pharyngeal region harboring a main mass of thyroid cells that did not detach to form more follicles as observed in the tg(*tg*:mCh) larvae (Figure 7A). This phenotype was consistent with an impairment of thyroid morphogenesis.

Throughout the screening it seemed that many BRAF^{V600E}-expressing transgenic fish showed abnormal thyroid morphogenesis. When assessing the percentage of larvae displaying such abnormality, 95% (58/61) of tg(*tg*:mCh;*tg*:mCh-T2A-BRAF^{V600E}) but none (0/37) of age-matched controls displayed abnormal morphogenesis (Figure 7B). Therefore, the number of follicles were quantified to further highlight the impaired development in thyroid. In tg(*tg*:mCh;*tg*:mCh-T2A-BRAF^{V600E}) larvae, the number of follicles (1-2 follicles) was much lower than the number observed in tg(*tg*:mCh) larvae (3-7 follicles) ($p<0.0001$) (Figure 7C).

Besides the lower number of follicles, no obvious developmental defects were observed in tg(*tg*:mCh;*tg*:mCh-T2A-BRAF^{V600E}) larvae. Nevertheless, a reduced number of follicles suggested hypoplasia. Larval growth was monitored and standard length (SL) was used as a proxy for developmental stage as described by Parichy et al., 2009. By 7 days post fertilization (dpf), tg(*tg*:mCh-T2A-BRAF^{V600E}) larvae grew marginally faster (2.8% increase in SL) than the controls ($p<0.01$) (Figure 7D).

Since conventional fluorescence microscopy was only able to give an idea of thyroid organization, histological examination of the lower jaw from 7-, 14-, 21- and 28-days-old larvae was performed. tg(*tg*:mCh) revealed thyroid follicles located predominantly in the connective tissue in the lower jaw. Individual follicles were already organized by 7dpf and their number increased with age (Figure 7E). Each follicle was round or oval and was lined by a single-layered epithelium; the center of the follicle was filled with homogenous colloid (Figure 7E). tg(*tg*:mCh-T2A-

BRAF^{V600E}) revealed an unique follicle at very young age that only became organized into a follicular-like structure by 28dpf in the connective tissue in the lower jaw (Figure 7E). This structure remained attached (Figure 7E). Each thyroid follicle was round or oval and was lined by overlapping layers of epithelium consisting of cuboidal cells predominantly basophilic (Figure 7E). Many follicles showed clear vesicles at the periphery and/or lack colloid (Figure 7E).

The abnormal thyroid morphogenesis observed in tg(*tg*:mCh-T2A-BRAF^{V600E}) larvae suggested that it could underly a compromised thyroid function. Disturbance of thyroid hormone (TH) synthesis is known to have fatal consequences as TH action serves important regulatory functions throughout all phases of life (Brix et al., 2011). It did not appear to be the case in tg(*tg*:mCh-T2A-BRAF^{V600E}) larvae as survival registered up to 28dpf was similar to that observed for tg(*tg*:mCh) controls (Figure 7F).

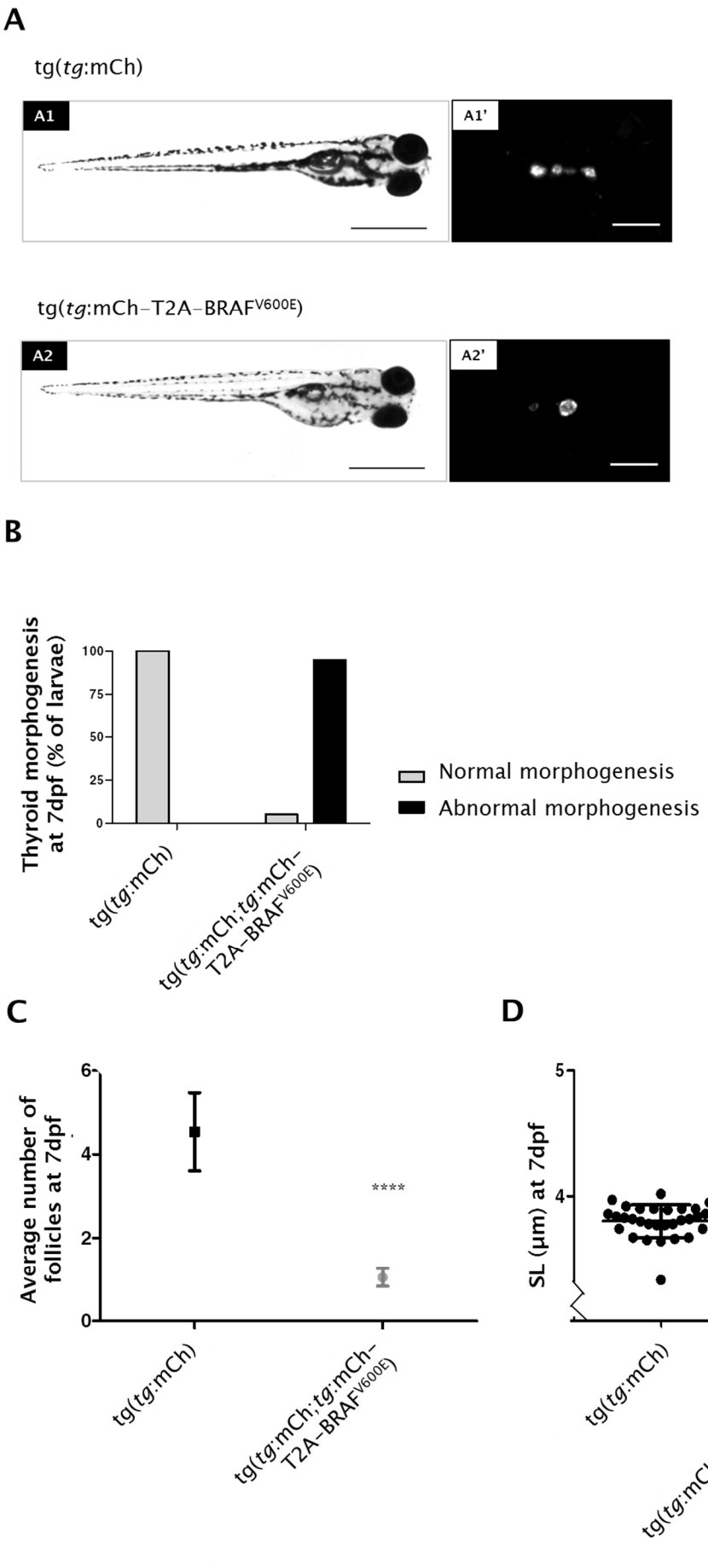
A
tg(tg:mCh)
A1
A1'
tg(tg:mCh–T2A–BRAFV600E)
A2
A2'
B
Thyroid morphogenesis at 7dpf (% of larvae)
100
75
50
25
0
Normal morphogenesis
Abnormal morphogenesis
tg(tg:mCh)
tg(tg:mCh;tg:mCh–T2A–BRAFV600E)
C
Average number of follicles at 7dpf
6
4
2
0
****
tg(tg:mCh)
tg(tg:mCh;tg:mCh–T2A–BRAFV600E)
D
SL (µm) at 7dpf
5
4
**
tg(tg:mCh)
tg(tg:mCh–T2A–BRAFV600E)

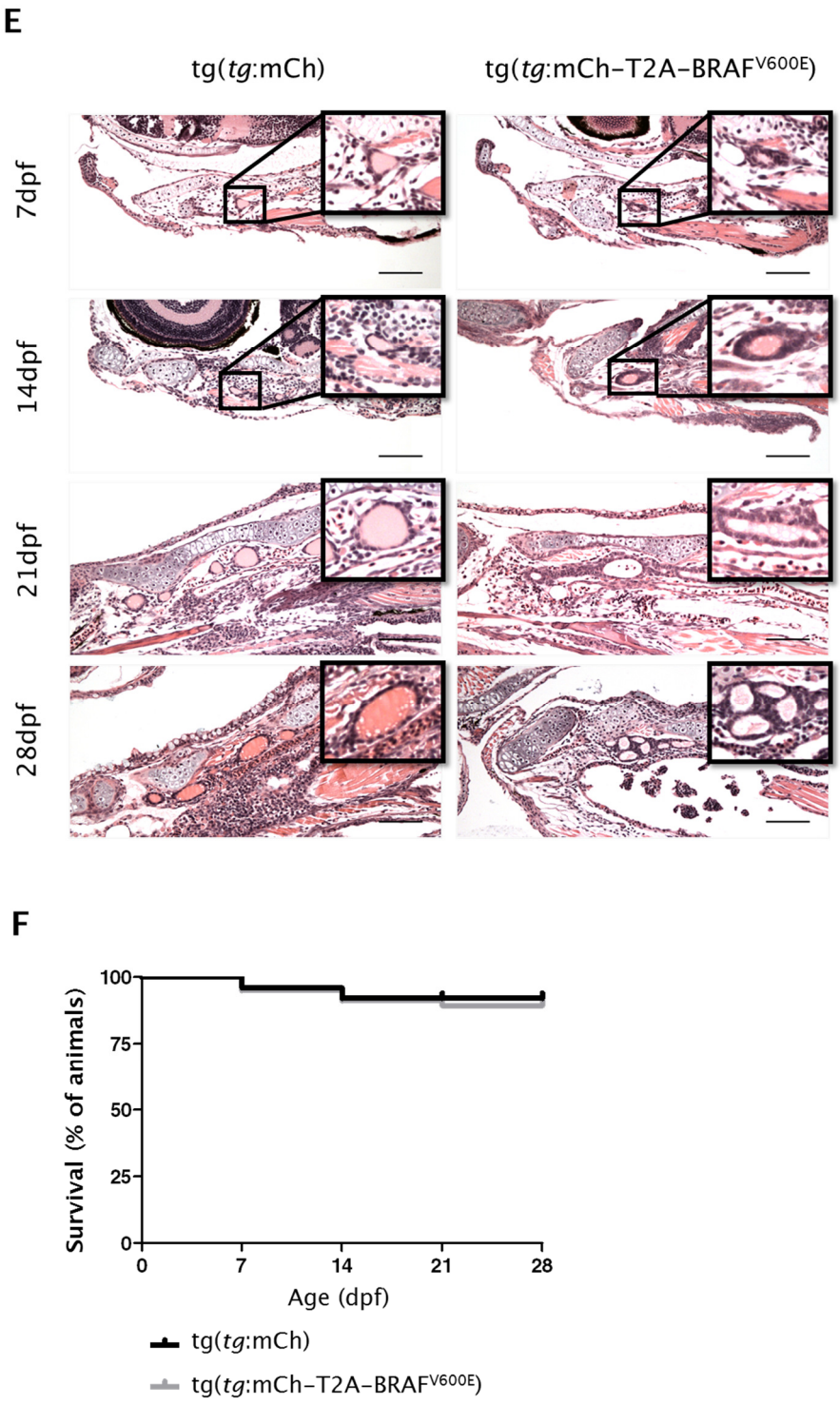

Figure 7. **Characterization of tg(*tg*:mCh-T2A-BRAF^{V600E}) larvae.** (A) Representative phenotypes of (A1) tg(*tg*:mCh) and (A2) tg(*tg*:mCh-T2A-BRAF^{V600E}) at 7dpf and mCherry expression found in thyroid cells (A1' and A2', respectively). Scale bar: 0.5mm (left) and 75μm (right). (B) Frequency of normal and abnormal thyroid morphogenesis at 7dpf assessed in tg(*tg*:mCh) (n=37) and tg(*tg*:mCh;*tg*:mCh-T2A-BRAF^{V600E}) (n=61) ($p<0.0001$).

(C) Average number of follicles at 7dpf quantified in tg(*tg*:mCh) (n=37) and tg(*tg*:mCh;*tg*:mCh-T2A-BRAF^{V600E}) (n=61) ($p<0.0001$). (D) SL measured at 7dpf in tg(*tg*:mCh) (n=31) and tg(*tg*:mCh;*tg*:mCh-T2A-BRAF^{V600E}) (n=31) ($p<0.01$). (E) HE stain of longitudinal sections representative of the lower jaw at 7-, 14-, 21- and 28dpf. Insets show detail of the epithelium. Scale bar: 120μm. (F) Survival curves for tg(*tg*:mCh) (n=25) and tg(*tg*:mCh-T2A-BRAF^{V600E}) (n=25) ($p>0.05$). Values are percentages of fish alive for a certain timepoint.

tg(*tg*:mCh-T2A-BRAF^{V600E}) fish were monitored as they reach the juvenile stage and past sexual maturity in order to understand how thyroid organization and function would be compromised later in life. tg(*tg*:mCh-T2A-BRAF^{V600E}) were found to grow slower than the controls and this was evident by 3 months of age (Figure 8A). Body mass index (BMI) was calculated and a dramatic 25% decrease in body mass was observed in tg(*tg*:mCh-T2A-BRAF^{V600E}) fish when compared to controls (Figure 8B). This suggested that the stunted growth observed could have been due to thyroid dysfunction in the BRAF^{V600E}-expressing line.

At this stage, it was difficult to interpret an increase in mCherry expression observed in living animals from the BRAF^{V600E}-expressing line so histological examination was performed at 2- and 3-months of age. tg(*tg*:mCh) fish displayed thyroid follicles distributed predominantly in the connective tissue along the ventral aorta in the lower jaw (Figure 8C: C1 and C1'). Each follicle was round to oval and was lined by a single-layered epithelium; the center of the follicle was filled with homogenous colloid (Figure 8C: C1''). tg(*tg*:mCh-T2A-BRAF^{V600E}) fish showed signs indicating follicular hyperplasia in the lower jaw (Figure 8C: C2, C2', C3 and C3'). Two major patterns were observed: one of the patterns had relatively large follicles but less numerous than the other pattern and this was evident at 2 months post fertilization (mpf) (Figure 8: C2 *versus* C3) and at 3mpf (Figure 8: C2' *versus* C3'). The follicles were of different shapes and sizes and were lined by variably basophilic cuboidal to columnar epithelial cells (Figure 8C: C2''). Some follicles containing excessive colloid were lined by a flattened layer of epithelial cells, similar epithelium observed in controls. There was formation of focal papillary structures growing into the lumen that lacked fibrovascular cores and showed no complex branching; these papillae were lined by basophilic cuboidal to columnar epithelial cells (Figure 8C: C3'). Taken together, none of the tg(*tg*:mCh)

(0/10) but all tg(*tg*:mCh-T2A-BRAF^{V600E}) fish (10/10) displayed signs of thyroid hyperplasia (hyperplasia incidence at 3mpf: $p<0.0001$) (Figure 8D).

To have a better understanding of the volume occupied by hyperplasic follicles, 3-μm-thick sections covering the whole thyroid of the adult fish were selected to measure a representative thyroid volume. Most tg(*tg*:mCh-T2A-BRAF^{V600E}) fish showed an increase in thyroid volume which must represent enlarged follicles (Figure 8E). Few tg(*tg*:mCh-T2A-BRAF^{V600E}) fish showed similar thyroid volume to that seen in controls which must represent small but numerous hyperplasic follicles (total thyroid volume, $p<0.05$) (Figure 8E).

To understand the molecular mechanisms underlying the hyperplasia observed in tg(*tg*:mCh-T2A-BRAF^{V600E}) fish, thyroid tissue was dissected from both those fish and controls. tg(*tg*:mCh-T2A-BRAF^{V600E}) fish displayed hyperplasia indicating that thyroid cells were proliferating in response to the presence of BRAF^{V600E}. Western blots of protein extracts from thyroid tissues of tg(*tg*:mCh-T2A-BRAF^{V600E}) fish revealed an increase in proliferating cell nuclear antigen (PCNA) levels ($p<0.05$) (Figure 8F and F'), an indicator of proliferation, when compared to tg(*tg*:mCh) fish.

High proliferation suggested that the proliferation-induced pathways were activated. The MAPK pathway includes signaling molecules such as RAF that ultimately lead to the expression of genes that regulate cell proliferation and survival. In BRAF mutated thyroid carcinomas, the MAPK pathway was found to be constitutively activated. MAPK pathway activation was assessed by the protein levels of pERKs, a downstream effector of that pathway. There was a robust increase in pERK protein levels in tg(*tg*:mCh-T2A-BRAF^{V600E}) fish when compared to controls ($p<0.0001$) (Figure 8F and F'). This suggested an activation of the MAPK pathway through BRAF^{V600E}, permissive to cell proliferation and growth.

The phosphatidylinositol-4,5-bisphosphate 3-kinase (PI3K)-V-Akt murine thymoma viral oncogene homolog (AKT) pathway, responsible for signals that reduce apoptosis and allow proliferation was also found to be overactivated in BRAF mutated thyroid carcinomas compared to normal thyroid (Faustino et al., 2012). PI3K-AKT pathway activation was assessed by the protein levels of pAKT S473 and pAKT T308, two important phosphorylation sites that activate the kinase. A consistent increase in the levels of pAKT S473 ($p<0.01$) and pAKT T308 ($p<0.0001$) was found in tg(*tg*:mCh-T2A-BRAF^{V600E}) fish (Figure 8F and F') suggesting that PI3K-AKT activation played a role in the development of hyperplasia.

Paradoxically, $BRAF^{V600E}$ was also found to induce senescence and apoptosis by blocking proliferation (Wajapeyee et al., 2008). In $BRAF^{V600E}$-expressing transgenic animals it was be expected the opposite observation as proliferation was being induced.

p16, an important mediator in blocking cell progression from G1 to S phase, was evaluated to exclude $BRAF^{V600E}$-induced senescence as a restraining factor to malignancy. p16 protein levels were downregulated in tg(*tg*:mCh-T2A-$BRAF^{V600E}$) fish ($p>0.05$) (Figure 8F and F') suggesting that $BRAF^{V600E}$ did not induce senescence.

Activated caspase 3, an important protein in the execution-phase of cell apoptosis, was also evaluated to exclude $BRAF^{V600E}$-induced apoptosis as a mechanism to clear genetically unstable cells. Suprisingly, activated caspase 3 protein levels were increased in tg(*tg*:mCh-T2A-$BRAF^{V600E}$) fish ($p<0.0001$) (Figure 8F and F').

To confirm if caspase activation was induced by p53 as a response to oncogenic stress, p53 protein levels were assessed. Increased levels of p53 protein were found in tg(*tg*:mCh-T2A-$BRAF^{V600E}$) fish ($p<0.0001$) (Figure 8F and F') confirming that apoptosis was triggered in $BRAF^{V600E}$-expressing thyroid cells.

To determine whether p53 activation was mediated indirectly by $BRAF^{V600E}$ through $BRAF^{V600E}$-mediated p38 activation, levels of p38 were assessed. p38 protein levels in tg(*tg*:mCh-T2A-$BRAF^{V600E}$) fish were not different from the controls ($p>0.05$) (Figure 8F and F').

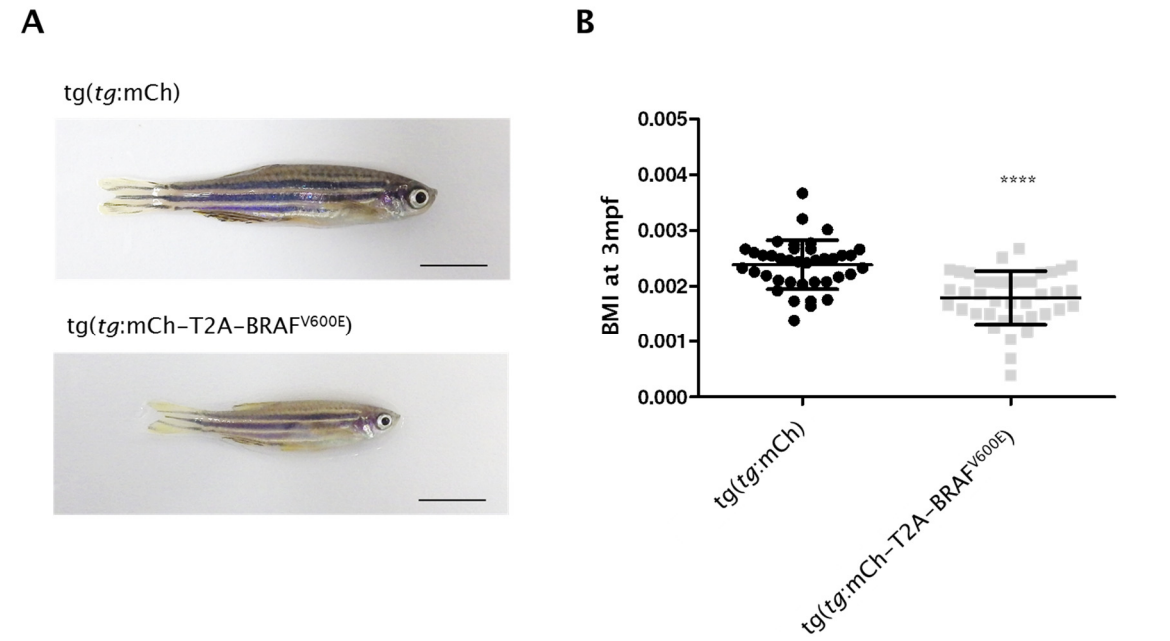
A
tg(tg:mCh)
tg(tg:mCh-T2A-BRAF^{V600E})
B
BMI at 3mpf
0.005
0.004
0.003
0.002
0.001
0.000
****
tg(tg:mCh)
tg(tg:mCh-T2A-BRAF^{V600E})

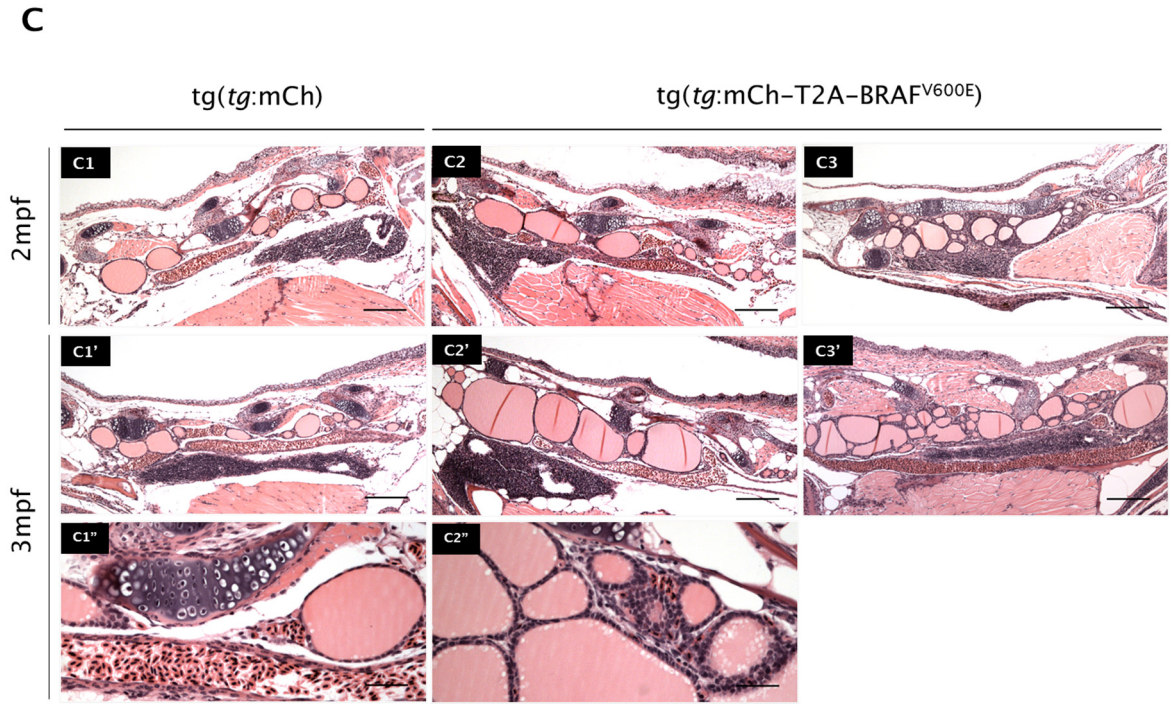
C
tg(tg:mCh)
tg(tg:mCh-T2A-BRAF^{V600E})
2mpf
3mpf
C1
C2
C3
C1'
C2'
C3'
C1"
C2"

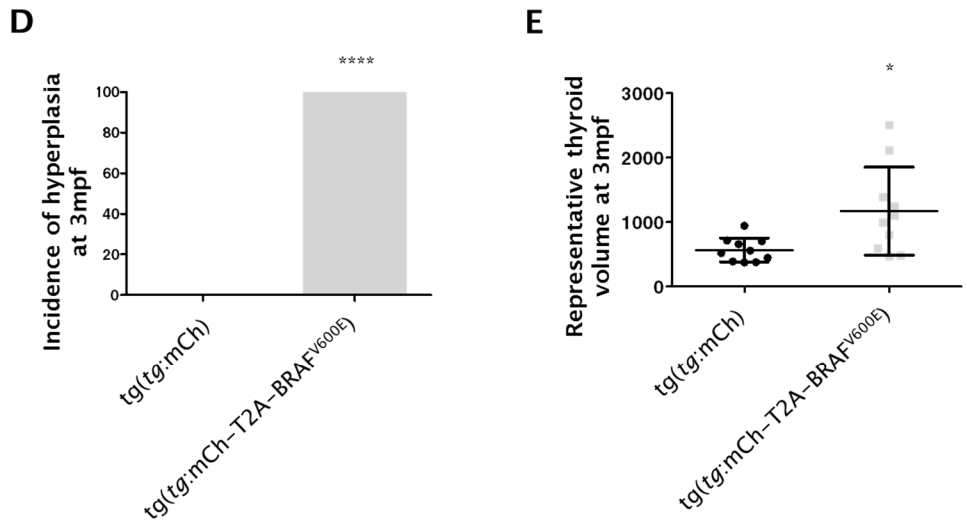
D
Incidence of hyperplasia at 3mpf
100
80
60
40
20
0
****
tg(tg:mCh)
tg(tg:mCh-T2A-BRAFV600E)
E
Representative thyroid volume at 3mpf
3000
2000
1000
0
*
tg(tg:mCh)
tg(tg:mCh-T2A-BRAFV600E)

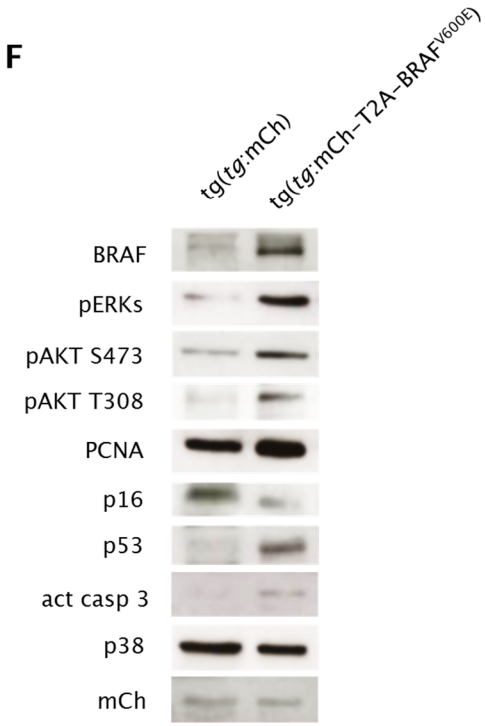
F
tg(tg:mCh)
tg(tg:mCh-T2A-BRAFV600E)
BRAF
pERKs
pAKT S473
pAKT T308
PCNA
p16
p53
act casp 3
p38
mCh

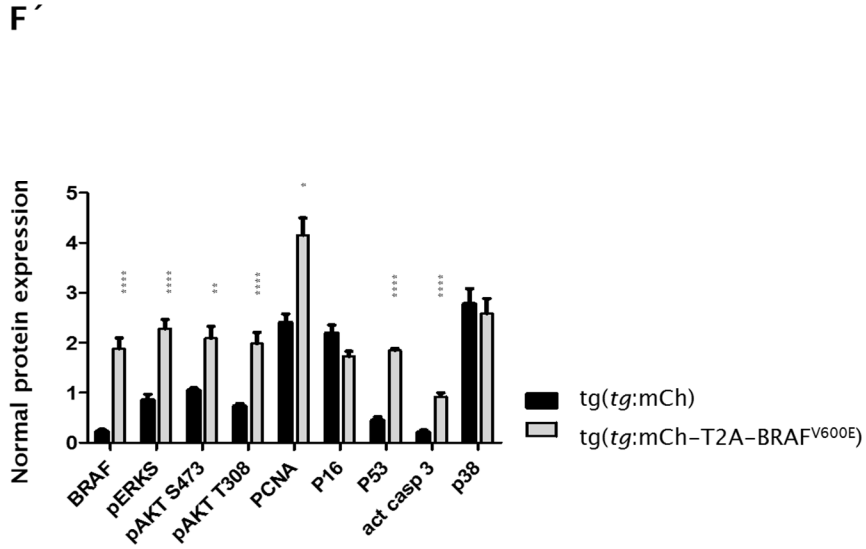
F´
Normal protein expression
5
4
3
2
1
0
BRAF
pERKS
pAKT S473
pAKT T308
PCNA
P16
P53
act casp 3
p38
tg(tg:mCh)
tg(tg:mCh-T2A-BRAFV600E)

Figure 8. **Characterization of tg(*tg*:mCh-T2A-BRAF^{V600E}) juveniles.** (A) Representative phenotypes of tg(*tg*:mCh) and tg(*tg*:mCh-T2A-BRAF^{V600E}) at 3 months of age. Scale bar: 5mm. (B) BMI measured from tg(*tg*:mCh) (n=39) and tg(*tg*:mCh-T2A-BRAF^{V600E}) (n=39) ($p<0.0001$). (C) HE stain of longitudinal sections representative of the lower jaw at 2- and 3mpf. Scale bar: 250μm. C1'' and C2'' are higher magnifications of the follicles. Scale bar: 62μm. (D) Incidence of hyperplasia at 3mpf. Values correspond to the percentage of fish with hyperplasia confirmed by histology (ten fish were studied from each line) ($p<0.0001$). (E) Representative thyroid volume assessed in tissue sections. Values correspond to the volume of each fish studied; ten in total for each line ($p<0.05$). (F) Western blot analysis of lysates from thyroid tissue at 3mpf. Three fish were pooled for each line. Membranes were blotted with relevant antibodies. Ponceau S is shown in Figure 6. (F') Protein levels were quantified and normalized to the amount of protein. Values are shown in bar graphs and represent three independent experiments (statistical analysis only shown for relevant comparisons; $p<0.05$, $p<0.01$ and $p<0.0001$).

tg(*tg*:mCh-T2A-BRAF^{V600E}) fish were monitored until they reach 12 months of age. At this stage, the differences in body weight and body length proved not to be transient (Figure 9A) as reflected by a 11% decrease in body mass when compared to tg(*tg*:mCh) fish ($p<0.001$) (Figure 9B).

At this stage, it was observed a pattern of mCherry expression that suggested enlarged follicles so histological examination was performed to confirm such hypothesis. tg(*tg*:mCh) fish displayed thyroid follicles scattered predominantly in the connective tissue near the ventral aorta (Figure 9C: C1 and C1'). Each follicle was round or oval and was lined by a single-layered epithelium; the center of the follicle was filled with homogenous colloid (Figure 9C: C1 and C1'). tg(*tg*:mCh-T2A-BRAF^{V600E}) fish displayed signs indicating colloid goiter which involved the lower jaw. Follicles were predominantly large or very large close to each other with varying shapes (Figure 9C: C2 and C2'). Small follicles were also observed. Follicles were lined by basophilic and cuboidal epithelial cells and follicles with excessive colloid lined by a flattened layer of epithelial cells (Figure 9C: C2 and C2'). These follicles were well-differentiated and in some cases due to their size, follicles even constricted the ventral aorta. Taken together, none of the tg(*tg*:mCh) (0/20) but most of the tg(*tg*:mCh-T2A-BRAF^{V600E}) fish (18/20) displayed colloid goiter as confirmed by histology (goiter incidence at 12mpf: $p<0.0001$) (Figure 9D).

When examining tissue sections of tg(*tg*:mCh-T2A-BRAF^{V600E}) fish, many exhibited follicles that were markedly larger (Figure 9C: C2 and C2'). In order to determine the extension of the goiterous thyroid, 3-μm-thick sections covering the whole thyroid of the adult fish were selected to determine thyroid volume. On average, tg(*tg*:mCh-T2A-BRAF^{V600E}) fish displayed a 6-fold increase in thyroid volume when compared to controls ($p<0.001$) (Figure 9E).

Although colloid goiter has a good prognosis and survival in humans, thyroid dysfunction without a proper follow-up can result in complications. In tg(*tg*:mCh-T2A-BRAF^{V600E}) fish there was never an experimental interference in the endocrine homeostasis besides the expression of BRAF oncogene by thyroid cells and fish were subjected to the same husbandry conditions as age-matched controls. To verify whether a goiterous state could have influenced the lifespan, all fish from this work that were not used for histological examination were included to determine survival rates. Survival up to 12mpf was similar to that observed for the tg(*tg*:mCh) fish ($p>0.05$) (Figure 9F).

A

tg(*tg*:mCh)

tg(*tg*:mCh-T2A-BRAF^{V600E})

B

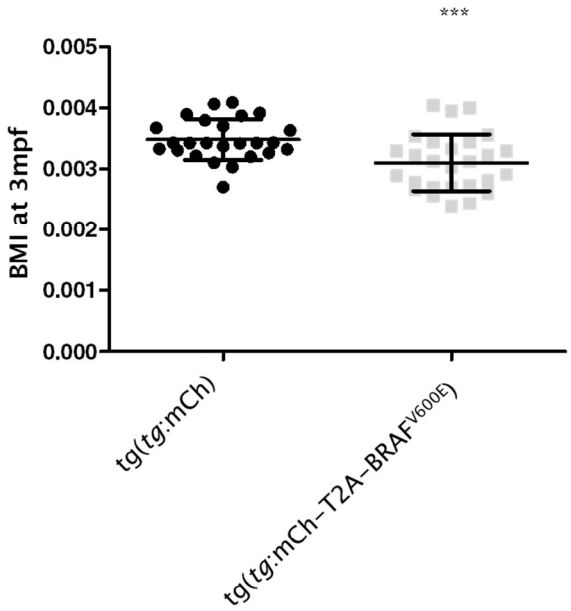

C

tg(*tg*:mCh) tg(*tg*:mCh-T2A-BRAF^{V600E})

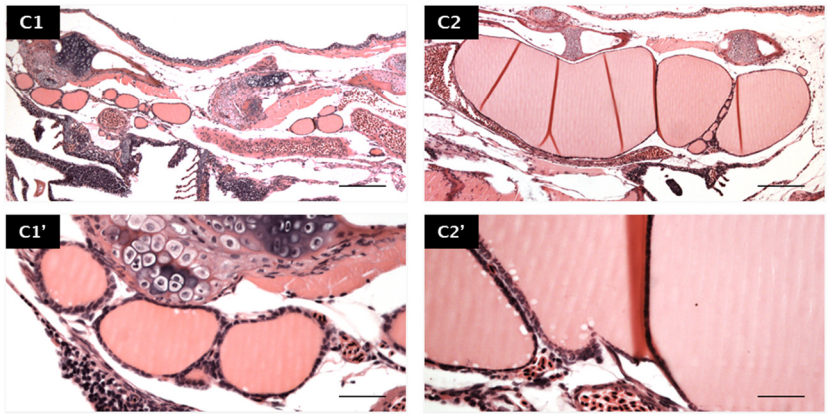

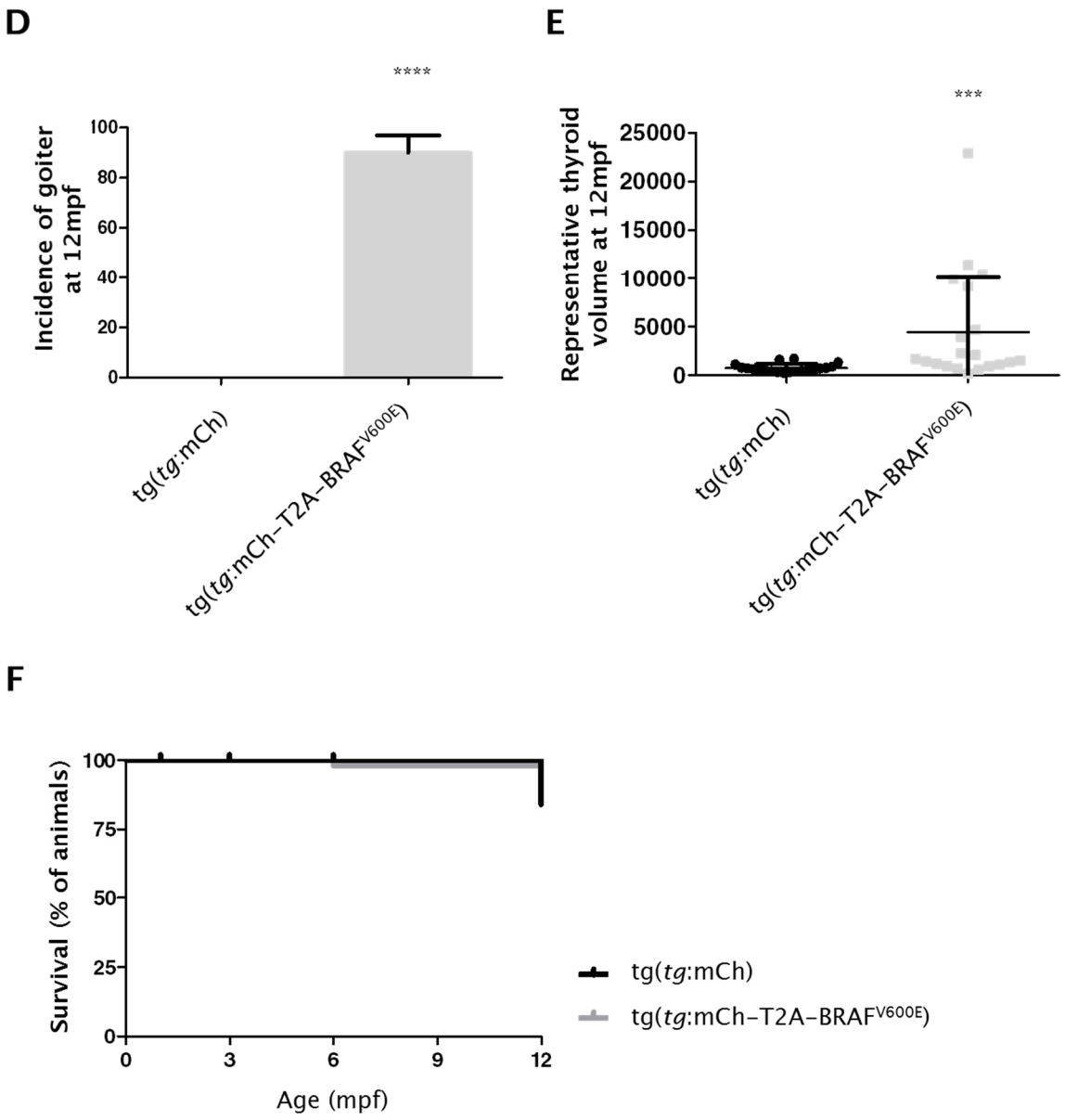

Figure 9. **Characterization of tg(*tg*:mCh-T2A-BRAF^{V600E}) adults.** (A) Representative phenotypes of tg(*tg*:mCh) and tg(*tg*:mCh-T2A-BRAF^{V600E}) at 12 months of age. Scale bar: 7.5mm. (B) BMI measured from tg(*tg*:mCh) (n=25) and tg(*tg*:mCh-T2A-BRAF^{V600E}) (n=28) ($p<0.001$). (C) HE stain of longitudinal sections representative of the lower jaw at 12mpf. Scale bar: 250μm. C1' and C2' are higher magnifications of the follicles. Scale bar: 62μm. (D) Incidence of goiter at 12mpf. Values correspond to the percentage of fish with goiter confirmed by histology (twenty fish were studied from each line) ($p<0.0001$). (E) Representative thyroid volume assessed in tissue sections. Values correspond to the volume of each fish studied; twenty in total for each line ($p<0.001$). (F) Survival curves for tg(*tg*:mCh) (n=25) and tg(*tg*:mCh-T2A-BRAF^{V600E}) (n=25) up to 12mpf ($p>0.05$). Values are percentages of fish alive for a certain timepoint.

Mutating tp53 prevents BRAF^{V600E}-induced thyroid dysfunction in transgenic fish

tg(*tg*:mCh-T2A-BRAF^{V600E}) fish displayed an increase in the protein levels of WT p53 by 3 months of age concomitant with thyroid hyperplasia suggesting that p53 was restraining tumor progression. In order to facilitate cancer development, a *tp53^{M214K}* zebrafish line was used.

tp53^{M214K}-homozygous zebrafish are viable and develop tumors by 16 months of age that histologically resemble malignant peripheral neural shealth tumors not seen in humans and mice with germline mutations of *TP53* (Berghmans et al., 2005; Storer et al., 2010). Of note, zebrafish p53 is highly similar to mammalian p53 in both structure and function sharing 48% homology in amino acid sequence to human p53 (Cheng et al., 1997). p53 is ubiquitously expressed early in zebrafish development (1hpf), at the pharyngula stage (24-48hpf) is predominantly expressed in the head and by 48hpf the protein levels are barely detectable (Cheng et al., 1997; Lee et al., 2008).

tp53^{M214K} missense mutation affects the tp53 protein at an aminoacid position that is orthologous to *TP53* mutations found in human cancer cells. The orthologous human codon for the *tp53^{M214K}* mutation is in exon 7, methionine-246, which was found to be mutated in 124 different human tumors, 8 of which exhibit the same amino acid change (Olivier et al., 2002; Berghmans et al., 2005). This codon is also positioned between other known mutation hot spots in the DNA-binding domain (DBD) of the human *TP53* gene at codons 245, 248, and 249 of exon 7 (Olivier et al., 2002; Berghmans et al., 2005).

tp53^{M214K} mutated protein is not able to activate transcription through the p21 response element and behaves in a dominant-negative manner, inhibiting the ability of the WT tp53 to activate downstream effectors (Berghmans et al., 2005).

Homozygous *tp53^{M214K}* fish were identified from an incross of heterozygous fish. The formed were crossed with tg(*tg*:mCh) fish to produce heterozygous *tp53^{M214K}* tg(*tg*:mCh) or with tg(*tg*:mCh-T2A-BRAF^{V600E}) to produce heterozygous *tp53^{M214K}* tg(*tg*:mCh-T2A-BRAF^{V600E}) fish. Heterozygous fish were incrossed and the homozygous progeny also harboring the transgene were used for all further experiments. These clutches exhibited Mendelian segregation for the *tp53^{M214K}* mutation and embryonic development of the mutant was not affected as described by Berghmans et al., 2005.

When analyzing live *tp53*^{M214K} tg(*tg*:mCh-T2A-BRAF^{V600E}) embryos, a robust thyroid-specific reporter signal became detectable at around 34hpf and it was maintained throughout thyroid morphogenesis similar to *tp53*^{M214K} tg(*tg*:mCh) embryos.

To study whether BRAF^{V600E} would interfere with thyroid morphogenesis in the absence of WT p53 protein in *tp53*^{M214K} tg(*tg*:mCh-T2A-BRAF^{V600E}), mCherry expression was evaluated from 60-72hpf and up to 7dpf. In that line it was observed the organization of follicular-like structures in the pharyngeal region consistent with normal thyroid morphogenesis similarly to *tp53*^{M214K} tg(*tg*:mCh).

Throughout the screening it was obvious that homozygous BRAF^{V600E}-expressing larvae developed normally and were indistinguishable from homozygous controls in terms of viability and fertility (Figure 10A). When assessing the percentage of larvae displaying normal thyroid morphogenesis, 84% (137/163) of *tp53*^{M214K} tg(*tg*:mCh;*tg*:mCh-T2A-BRAF^{V600E}) and 90% (87/96) of controls showed signs indicating no impairment of thyroid morphogenesis ($p>0.05$) (Figure 10B). The number of follicles were quantified in order to confirm that thyroid morphogenesis was indeed normal. In *tp53*^{M214K} tg(*tg*:mCh;*tg*:mCh-T2A-BRAF^{V600E}) larvae the number of follicles (2-5 follicles) was similar to the number found in *tp53*^{M214K} tg(*tg*:mCh) (2 to 6 follicles) ($p>0.05$) (Figure 10C).

A similar growth between both lines was verified when measuring SL at 7dpf ($p>0.05$) (Figure 10D).

By conventional fluorescence microscopy, it was verified that thyroid was developing normally in *tp53*^{M214K} tg(*tg*:mCh;*tg*:mCh-T2A-BRAF^{V600E}) larvae. However, it was important to clarify whether thyroid cells were organized similarly to *tp53*^{M214K} controls so histological examination of the lower jaw was performed from 7-, 14-, 21- and 28-days-old larvae. *tp53*^{M214K} tg(*tg*:mCh) revealed thyroid follicles located predominantly in the connective tissue of the lower jaw. The individual follicles were round or oval and were lined by a single-layered cuboidal epithelium; the center of the follicle was filled with colloid and vesicles were seen (Figure 10E). *tp53*^{M214K} tg(*tg*:mCh-T2A-BRAF^{V600E}) larvae displayed the same histology features described above (Figure 10E).

The survival in *tp53*^{M214K} tg(*tg*:mCh-T2A-BRAF^{V600E}) was similar to the controls which was consistent with normal thyroid growth during the larval stage ($p>0.05$) (Figure 10F).

A

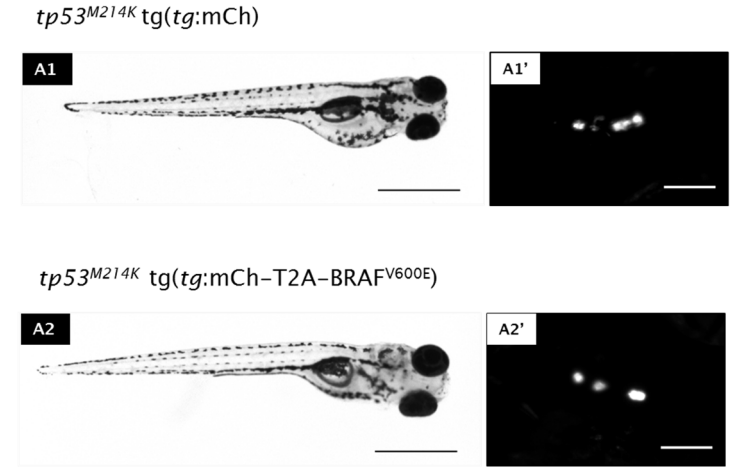
tp53M214K tg(tg:mCh)
A1
A1'
tp53M214K tg(tg:mCh-T2A-BRAFV600E)
A2
A2'

B

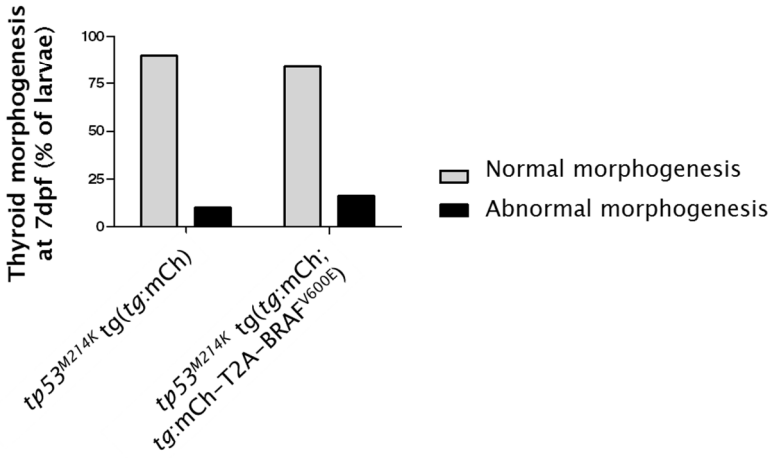
Thyroid morphogenesis at 7dpf (% of larvae)
100
75
50
25
0
Normal morphogenesis
Abnormal morphogenesis
tp53M214K tg(tg:mCh)
tp53M214K tg(tg:mCh; tg:mCh-T2A-BRAFV600E)

C

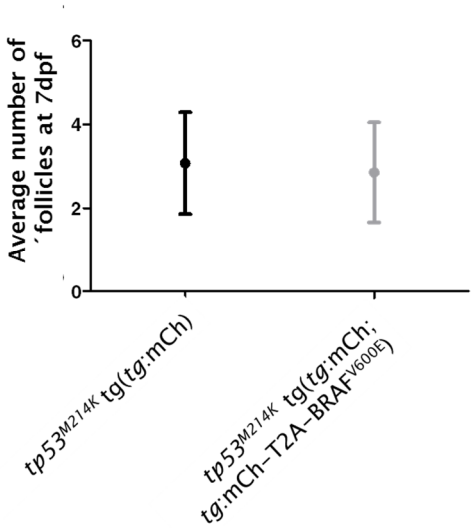
Average number of follicles at 7dpf
6
4
2
0
tp53M214K tg(tg:mCh)
tp53M214K tg(tg:mCh; tg:mCh-T2A-BRAFV600E)

D

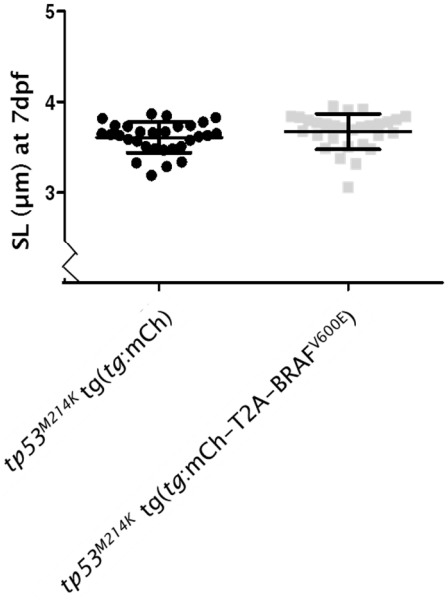
SL (µm) at 7dpf
5
4
3
tp53M214K tg(tg:mCh)
tp53M214K tg(tg:mCh-T2A-BRAFV600E)

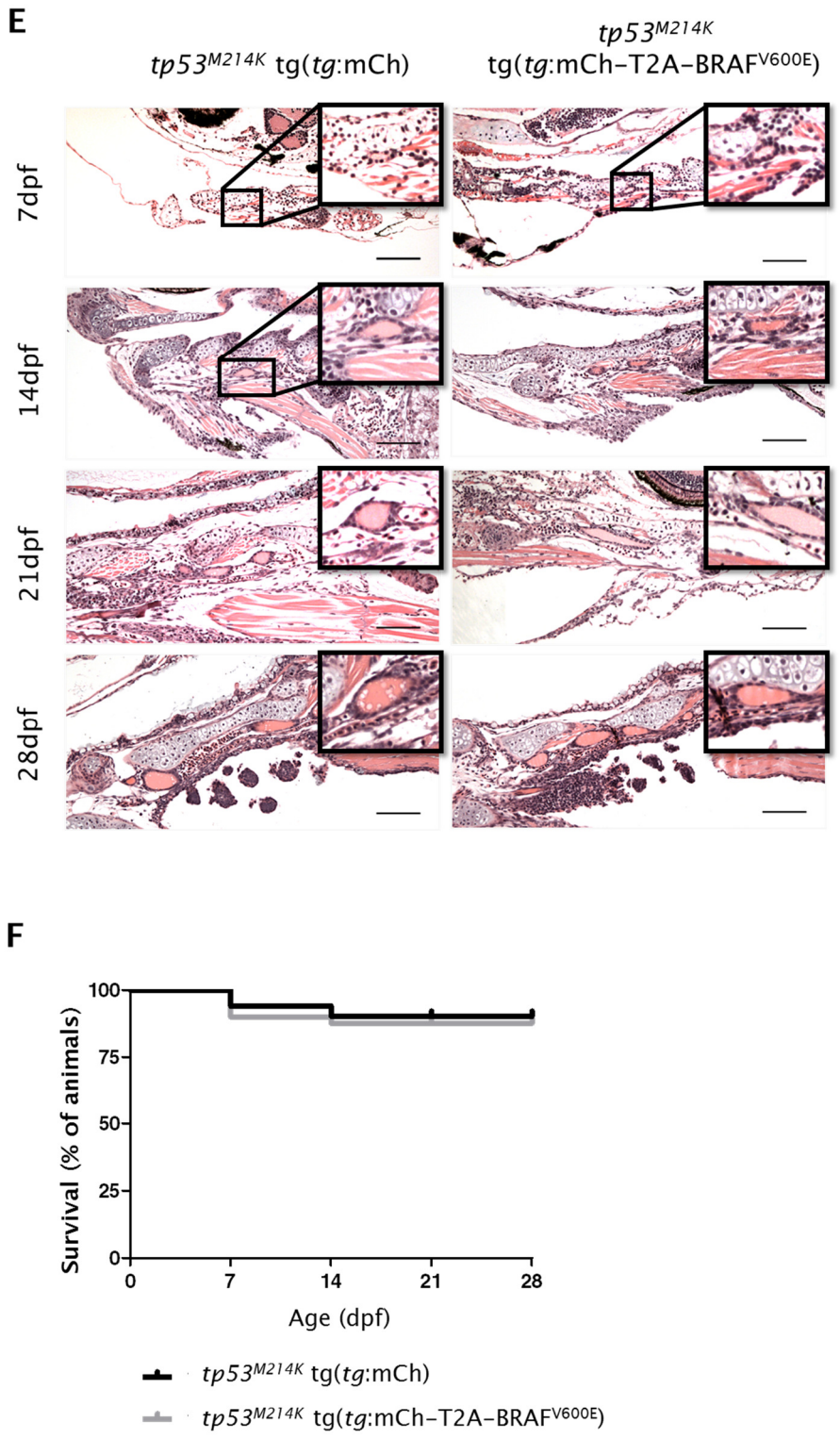

Figure 10. **Characterization of *tp53*^{M214K} tg(*tg*:mCh-T2A-BRAF^{V600E}) larvae.** (A) Representative phenotypes of (A1) *tp53*^{M214K} tg(*tg*:mCh) and (A2) *tp53*^{M214K} tg(*tg*:mCh-T2A-BRAF^{V600E}) at 7dpf and mCherry expression found in thyroid cells (A1' and A2', respectively). Scale bar: 0.5mm (left) and 75μm (right). (B) Frequency of normal and abnormal thyroid

morphogenesis at 7dpf assessed in *tp53*^{M214K} tg(*tg*:mCh) (n=96) and *tp53*^{M214K} tg(*tg*:mCh;*tg*:mCh-T2A-BRAF^{V600E}) (n=163) (p>0.05). (C) Average number of follicles at 7dpf quantified in *tp53*^{M214K} tg(*tg*:mCh) (n=96) and *tp53*^{M214K} tg(*tg*:mCh;*tg*:mCh-T2A-BRAF^{V600E}) (n=163) (p>0.05). (D) SL measured at 7dpf in *tp53*^{M214K} tg(*tg*:mCh) (n=30) and *tp53*^{M214K} tg(*tg*:mCh-T2A-BRAF^{V600E}) (n=29). (p>0.05). (E) HE stain of longitudinal sections representative of the lower jaw at 7-, 14-, 21- and 28dpf. Insets show the detail of the epithelium. Scale bar: 120μm. (F) Survival curves for *tp53*^{M214K} tg(*tg*:mCh) (n=25) and *tp53*^{M214K} tg(*tg*:mCh-T2A-BRAF^{V600E}) (n=25) (p>0.05). Values are percentages of fish alive for a certain timepoint.

tp53^{M214K} tg(*tg*:mCh-T2A-BRAF^{V600E}) were monitored as they reach the juvenile stage and past sexual maturity. They grew indistinguishable from *tp53*^{M214K} tg(*tg*:mCh) controls (Figure 11A). It was observed a similar BMI between the two lines at 3 months of age (p>0.05) (Figure 11B). It was also confirmed that *tp53*^{M214K} fish had a similar BMI to that of *tp53*^{wt} fish (p>0.05) (Supplementary Figure 1A).

Assuming that a normal thyroid development would not promote tissue dysfunction later on, histological examination was performed to confirm this hypothesis. *tp53*^{M214K} tg(*tg*:mCh-T2A-BRAF^{V600E}) and controls displayed similar histology. Thyroid follicles were located in the connective tissue near the ventral aorta (Figure 11C: C1, C1', C2 and C2'); each follicle was round to oval and was lined by a single-layered cuboidal epithelium while the center of the follicle was filled with homogeneous colloid (Figure 11C: C1'' and C2''); sometimes vesicles were seen. None of the *tp53*^{M214K} tg(*tg*:mCh-T2A-BRAF^{V600E}) displayed signs of thyroid hyperplasia nor did the controls.

Importantly, some *tp53*^{M214K} tg(*tg*:mCh) displayed follicles larger than the BRAF^{V600E}-expressing mutant line. This was confirmed when measuring the thyroid volume by selecting 3-μm-thick-sections representative of the whole thyroid of adult fish; but it was not significantly different from the volume found for BRAF^{V600E}-expressing line (p>0.05) (Figure 11D).

No hyperplasia or neoplasia was observed by 3 months of age in *tp53*^{M214K} tg(*tg*:mCh-T2A-BRAF^{V600E}) fish. Protein extracts from thyroid tissues were used to understand whether the reversion of the BRAF^{V600E}-induced phenotype would be explained by low proliferation. A low increase in PCNA levels was found in *tp53*^{M214K} tg(*tg*:mCh-T2A-BRAF^{V600E}) (p<0.05) (Figure 11E and E') suggesting that proliferation was not suppressed but it may have not be sufficient to induce hyperplasia.

Low protein levels of pERKs ($p>0.05$) in *tp53*^{M214K} tg(*tg*:mCh-T2A-BRAF^{V600E}) fish (Figure 11E and E') confirmed that the MAPK pathway was downregulation even in the presence of BRAF^{V600E}. This suggested the presence of an inhibitory factor acting downstream of BRAF, restraining MAPK pathway activation. Similar pAKT S473 protein levels were found in *tp53*^{M214K} tg(*tg*:mCh-T2A-BRAF^{V600E}) when compared to the controls ($p>0.05$) (Figure 11E and E') but the protein levels of pAKT T308 were lower in the former line ($p<0.05$) (Figure 11E and E'). This suggested that suppression of AKT phosphorylation at residue T308 was due to inhibition of PDK1.

Absence of WT p53 was expected to not activate senescence and/or apoptosis. Protein levels of p16 ($p<0.05$) and activated caspase 3 ($p<0.0001$) were very low and concomitant with low levels of p53 ($p<0.05$). This confirmed the inability of the *p53*^{M214K} protein to induce a programmed cell death (Figure 11E and E'). Strikingly, high levels of *tp53*^{M214K} protein in *tp53*^{M214K} tg(*tg*:mCh) controls were found and should represent an accumulation of the mutant protein, but not the WT tetramer. The protein levels of p38 were assessed to understand if downregulation of ERK would suppress p38 activity. Similar protein levels of p38 to that found for the controls were observed ($p>0.05$) (Figure 11E and E'). Furthermore, the protein levels of BRAF in in *tp53*^{M214K} tg(*tg*:mCh-T2A-BRAF^{V600E}) fish were consistently upregulated confirming the expression of this oncogene.

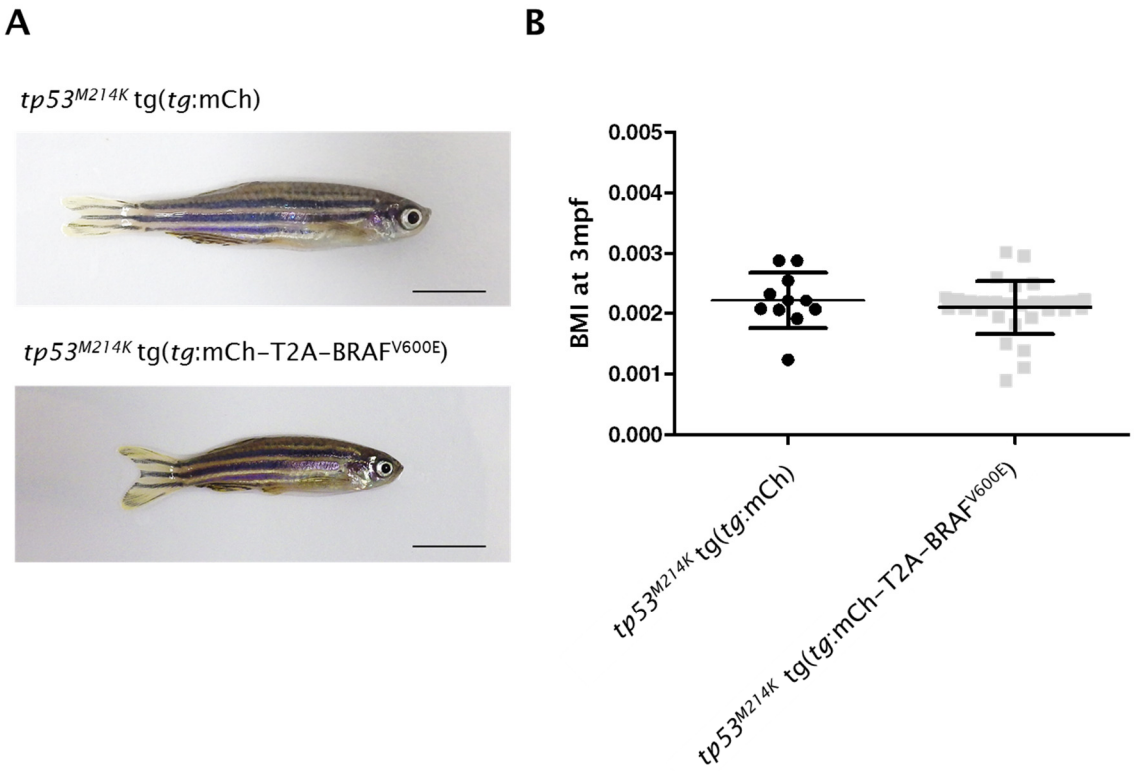
A
tp53M214K tg(tg:mCh)
tp53M214K tg(tg:mCh-T2A-BRAFV600E)
B
BMI at 3mpf
0.005
0.004
0.003
0.002
0.001
0.000
tp53M214K tg(tg:mCh)
tp53M214K tg(tg:mCh-T2A-BRAFV600E)

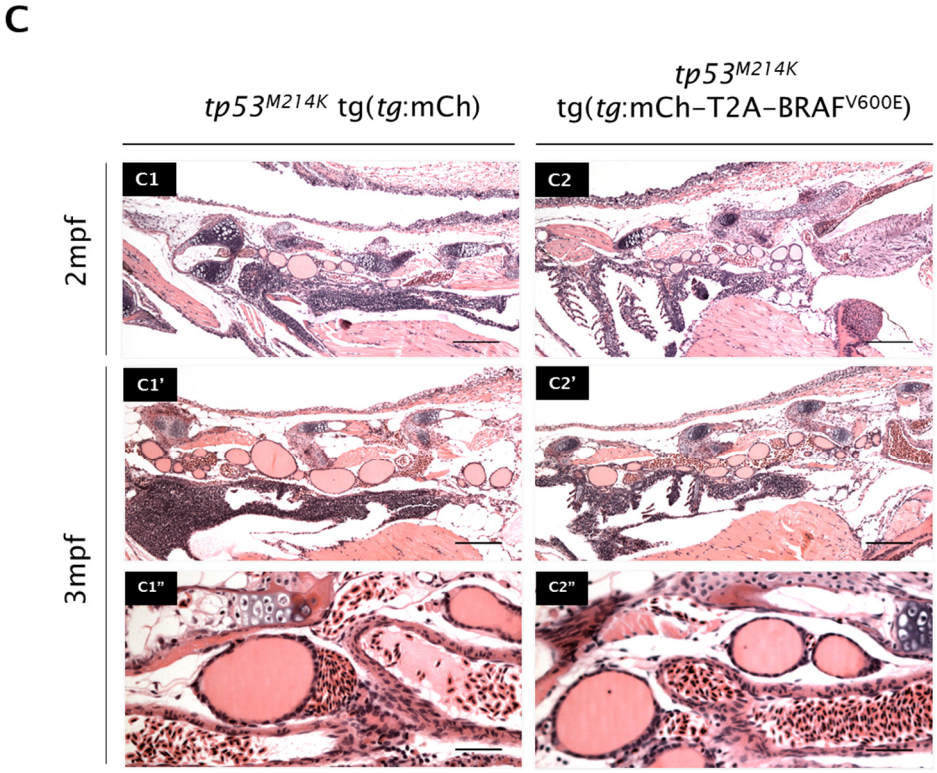
C
tp53M214K tg(tg:mCh)
tp53M214K
tg(tg:mCh-T2A-BRAFV600E)
2mpf
3mpf
C1
C2
C1'
C2'
C1"
C2"

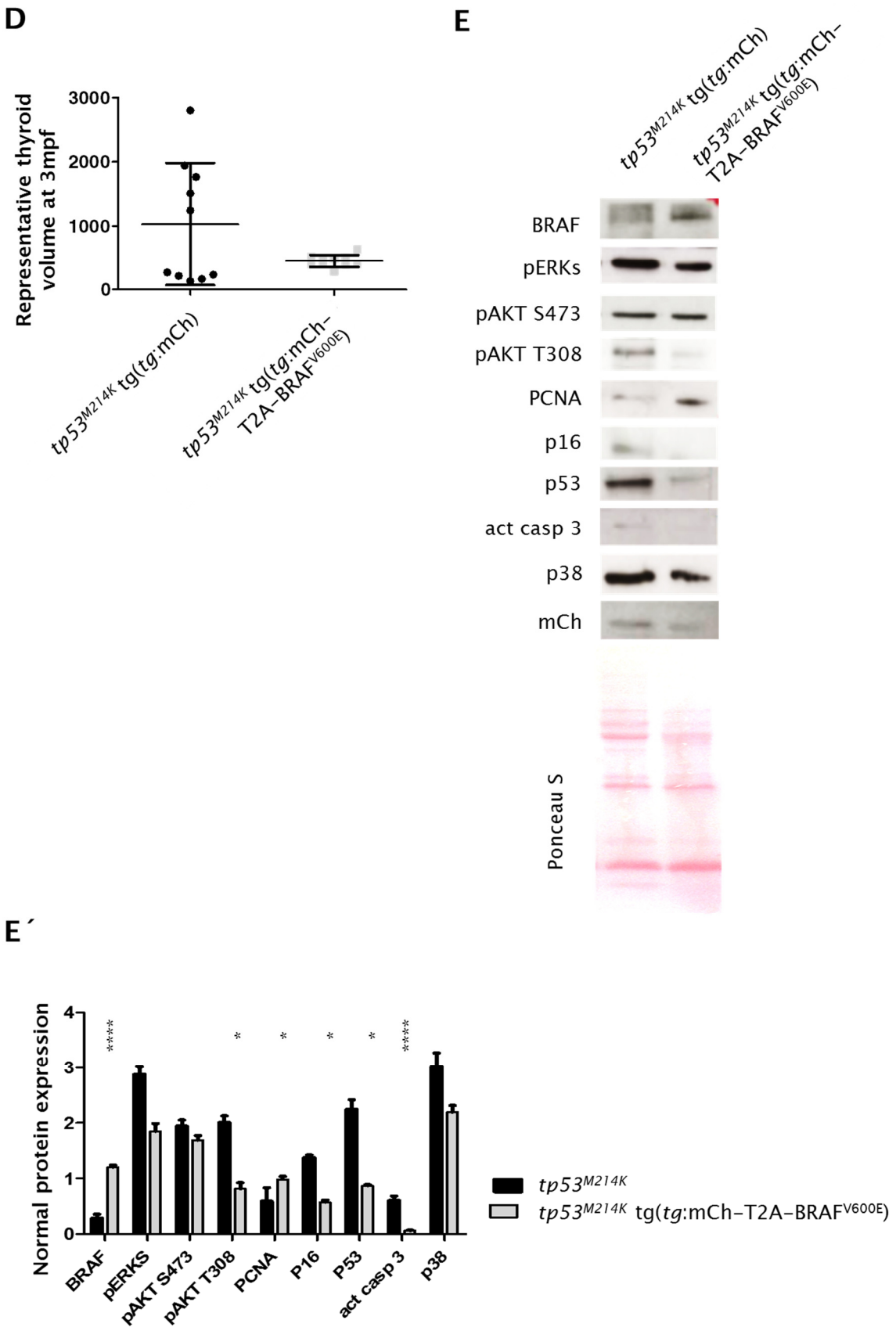
D
Representative thyroid volume at 3mpf
3000
2000
1000
0
tp53M214K tg(tg:mCh)
tp53M214K tg(tg:mCh–T2A–BRAFV600E)
E
tp53M214K tg(tg:mCh)
tp53M214K tg(tg:mCh–T2A–BRAFV600E)
BRAF
pERKs
pAKT S473
pAKT T308
PCNA
p16
p53
act casp 3
p38
mCh
Ponceau S
E´
Normal protein expression
4
3
2
1
0
****
*
*
*
*
****
BRAF
pERKS
pAKT S473
pAKT T308
PCNA
P16
P53
act casp 3
p38
tp53M214K
tp53M214K tg(tg:mCh–T2A–BRAFV600E)

Figure 11. **Characterization of *tp53*^{M214K} tg(*tg*:mCh-T2A-BRAF^{V600E}) juveniles.** (A) Representative phenotypes of *tp53*^{M214K} tg(*tg*:mCh) and *tp53*^{M214K} tg(*tg*:mCh-T2A-BRAF^{V600E}) at 3 months of age. Scale bar: 5mm. (B) BMI measured from *tp53*^{M214K} tg(*tg*:mCh) (n=11) and *tp53*^{M214K} tg(*tg*:mCh-T2A-BRAF^{V600E}) (n=30) ($p>0.05$). (C) HE stain of longitudinal sections representative of the lower jaw at 2-and 3mpf. Scale bar: 250μm. C1'' and C2'' are higher magnifications of the follicles. Scale bar: 62μm. (D) Representative thyroid volume assessed in tissue sections. Values correspond to the volume of each fish studied; ten in total for each line ($p>0.05$). (E) Western blot analysis of lysates from thyroid tissue at 3mpf. Three fish were pooled for each line. Membranes were blotted with relevant antibodies. Ponceau S showed equal amount of protein in both lanes. (E') Protein levels were quantified and normalized to the amount of protein. Values are shown in bar graphs and represent three independent experiments (statistical analysis only shown for relevant comparisons; $p<0.05$ and $p<0.0001$).

tp53^{M214K} tg(*tg*:mCh-T2A-BRAF^{V600E}) fish were monitored until they reach 12 months of age. At this stage, those fish grew indistinguishable from the controls (Figure 12A). Because a late thyroid dysfunction was yet to be verified, the BMI was calculated. Similar BMI was found in BRAF^{V600E}-expressing mutant fish comparing to controls ($p>0.05$) (Figure 12B). It was also confirmed that *tp53*^{M214K} fish had a similar BMI to that of *tp53*^{wt} fish ($p>0.05$) (Supplementary Figure 1B).

To discard a possible late BRAF^{V600E} thyroid dysfunction in the *tp53*^{M214K} line, histological examination was performed. *tp53*^{M214K} tg(*tg*:mCh) fish displayed thyroid follicles scattered predominantly in the connective tissue near the ventral aorta. Each follicle was round or oval and was lined by a single-layered cuboidal epithelium; the center of the follicle was filled with homogenous colloid (Figure 12C: C1 and C1'). These features were also found in *tp53*^{M214K} tg(*tg*:mCh-T2A-BRAF^{V600E}) although a conspicuous enlargement of thyroid follicles was observed (Figure 12C: C2 and C2'). In one fish (1/11), the follicles were larger suggesting colloid goiter but goiter was never found in any of the controls (0/9) (goiter indicence at 12mpf: $p>0.05$) (Figure 12D).

Tissue sections of *tp53*^{M214K} tg(*tg*:mCh-T2A-BRAF^{V600E}) fish were measured in order to understand if the enlargement would be similar to that found for the WT p53 line, both expressing the BRAF oncogene under the same conditions. On average, *tp53*^{M214K} tg(*tg*:mCh-T2A-BRAF^{V600E}) fish displayed a 3-fold increase in follicle

volume when compared to controls ($p<0.001$) (Figure 12E), still lower that the volume measured in tg(*tg*:mCh-T2A-BRAF^{V600E}) for the same age.

To evaluate survival, all fish from this work that were not used for histological examination were included. Survival up to 12mpf was similar to that observed for controls ($p>0.05$) (Figure 12F).

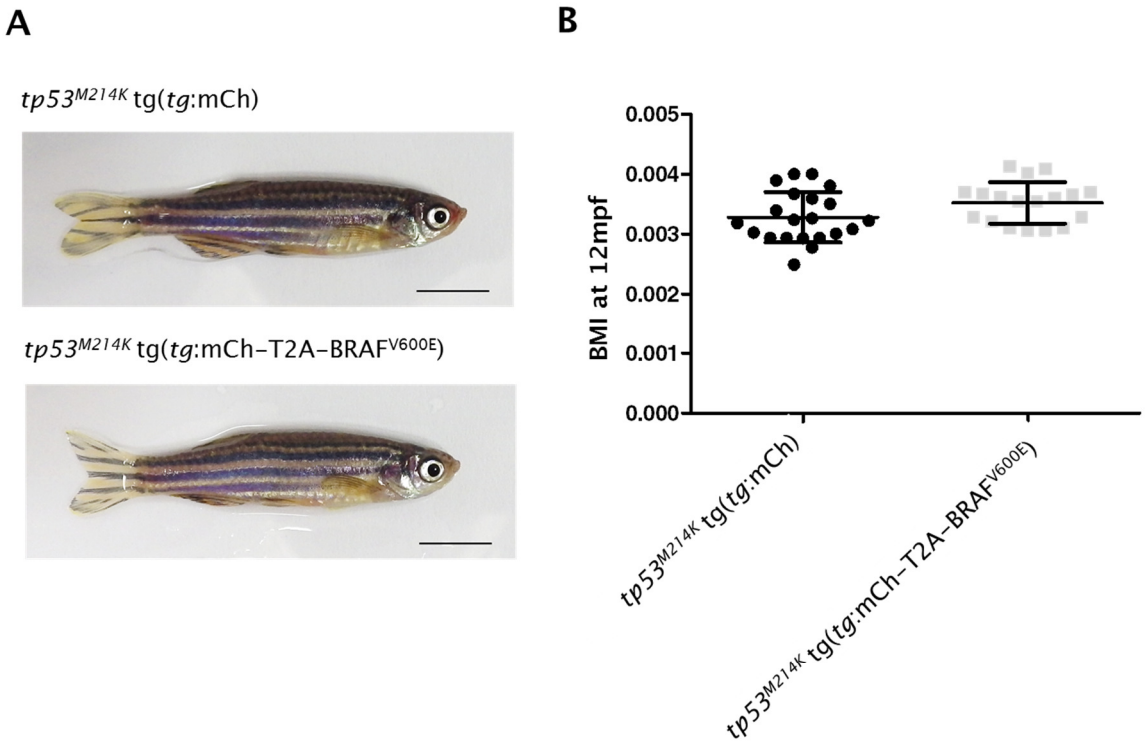

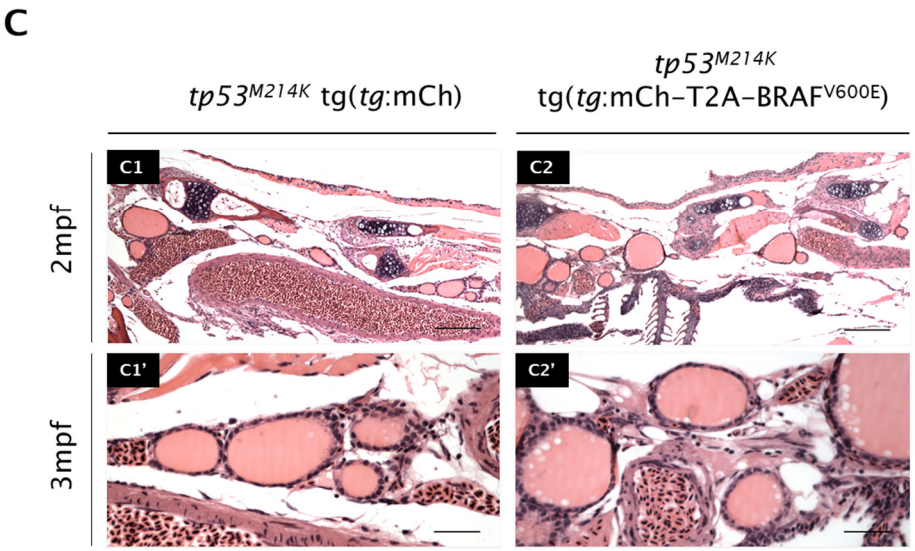

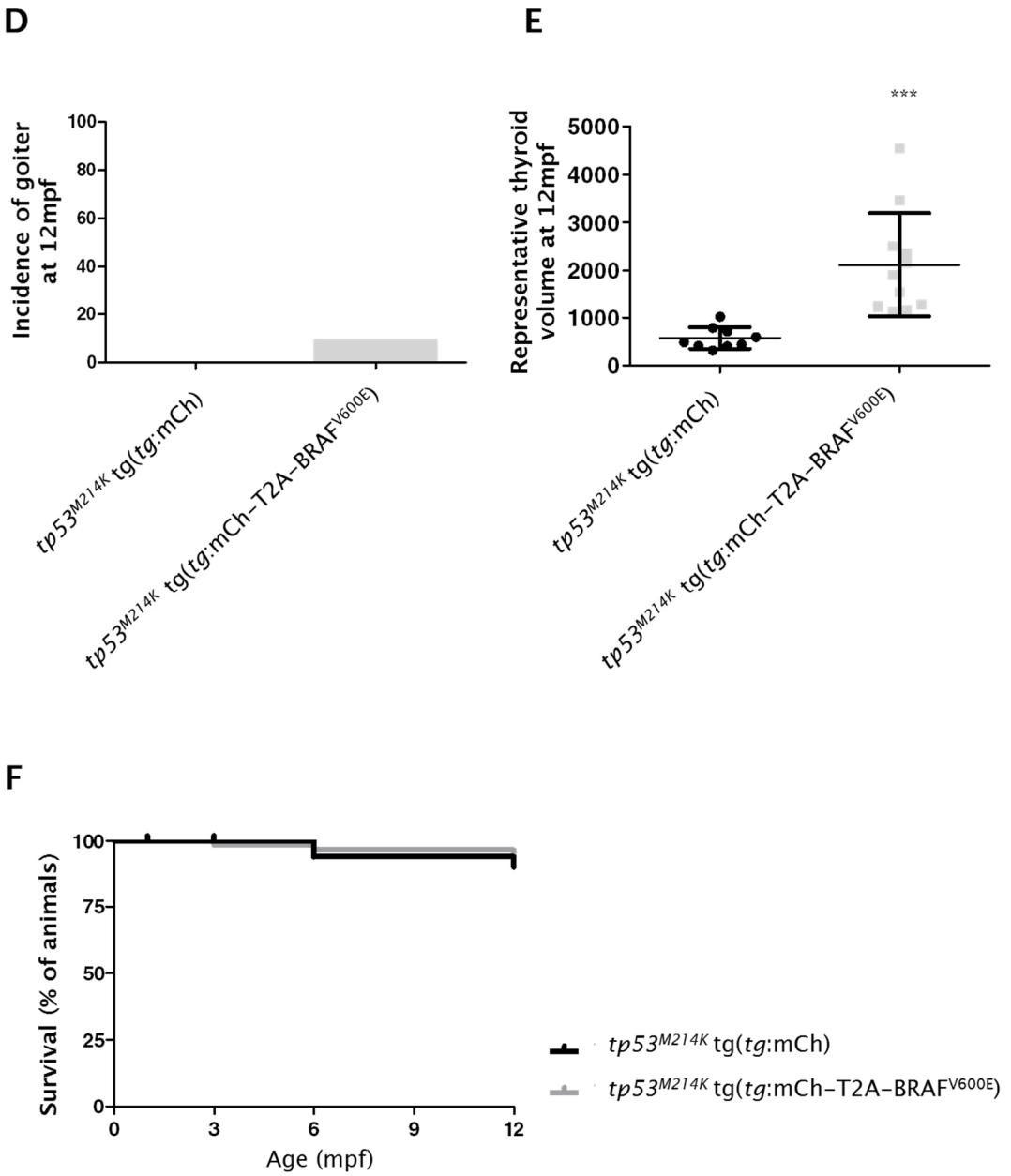

Figure 12. **Characterization of *tp53*^{M214K} tg(*tg*:mCh-T2A-BRAF^{V600E}) adults.** (A) Representative phenotypes of *tp53*^{M214K} tg(*tg*:mCh) and *tp53*^{M214K} tg(*tg*:mCh-T2A-BRAF^{V600E}) at 12 months of age. Scale bar: 7.5mm. (B) BMI measured from *tp53*^{M214K} tg(*tg*:mCh) (n=25) and *tp53*^{M214K} tg(*tg*:mCh-T2A-BRAF^{V600E}) (n=28) ($p>0.05$). (C) HE stain of longitudinal sections representative of the lower jaw at 12mpf. Scale bar: 250μm. C1' and C2' are higher magnifications of the follicles. Scale bar: 62μm. (D) Incidence of goiter at 12mpf. Values are percentages of fish with goiter confirmed by histology (eleven and nine fish were studied from BRAF^{V600E} and control line, respectively) ($p>0.05$). (E) Representative thyroid volume assessed by tissue sections. Values correspond to the volume of each fish studied; eleven and nine fish were studied from BRAF^{V600E} and control line, respectively ($p<0.001$). (F)

Survival curves for *tp53*^{M214K} tg(*tg*:mCh) (n=25) and *tp53*^{M214K} tg(*tg*:mCh-T2A-BRAF^{V600E}) (n=25) up to 12mpf ($p>0.05$). Values are percentages of fish alive for a certain timepoint.

Reduced BRAF^{V600E} expression in tp53^{M214K} fish may explain absence of BRAF-induced phenotype

It was observed an abnormal thyroid morphogenesis in tg(*tg*:mCh-T2A-BRAF^{V600E}) larvae by 7dpf and accelerated growth that was not seen in age-matched *tp53*^{M214K} tg(*tg*:mCh-T2A-BRAF^{V600E}) fish ($p<0.0001$) (Figure 13A). tg(*tg*:mCh-T2A-BRAF^{V600E}) fish developed thyroid hyperplasia by 3 months of age and colloid goiter was observed at 12 months of age as well as a delay in growth (BMI at 3mpf: $p<0.01$ and at 12mpf: $p<0.01$), concomitant with BRAF^{V600E} expression in thyroid cells (Figure 13B). Hyperplasia and reduced growth were not observed in age-matched *tp53*^{M214K} tg(*tg*:mCh-T2A-BRAF^{V600E}) fish (Figure 13B). This suggested that in the absence of WT p53, the BRAF^{V600E}-induced phenotypes in fish were not sustained.

In one hand, BRAF^{V600E} expression at 3 months of age in tg(*tg*:mCh-T2A-BRAF^{V600E}) fish is consistent with activation of MAPK and PI3K-AKT pathways through pERKs and pATKs, respectively (Figure 13D). This suggested a role of these pathways in the hyperplasia observed. On the other hand, upregulation of p53 and activated caspase 3 (Figure 13D) suggested that p53 put a brake in BRAF-expressing cells. When compared to the *tp53*^{M214K} tg(*tg*:mCh-T2A-BRAF^{V600E}) fish, BRAF^{V600E} expression is reduced concomitant with low levels of pERKs and pATKs (Figure 13D). This suggested that even in the absence of the brake that would favor progression to malignancy, the downregulation of important pathways have contributed to produce no evidences of hyperplasia or cancer until 12 months of age in the BRAF^{V600E}-expressing *tp53*^{M214K} line.

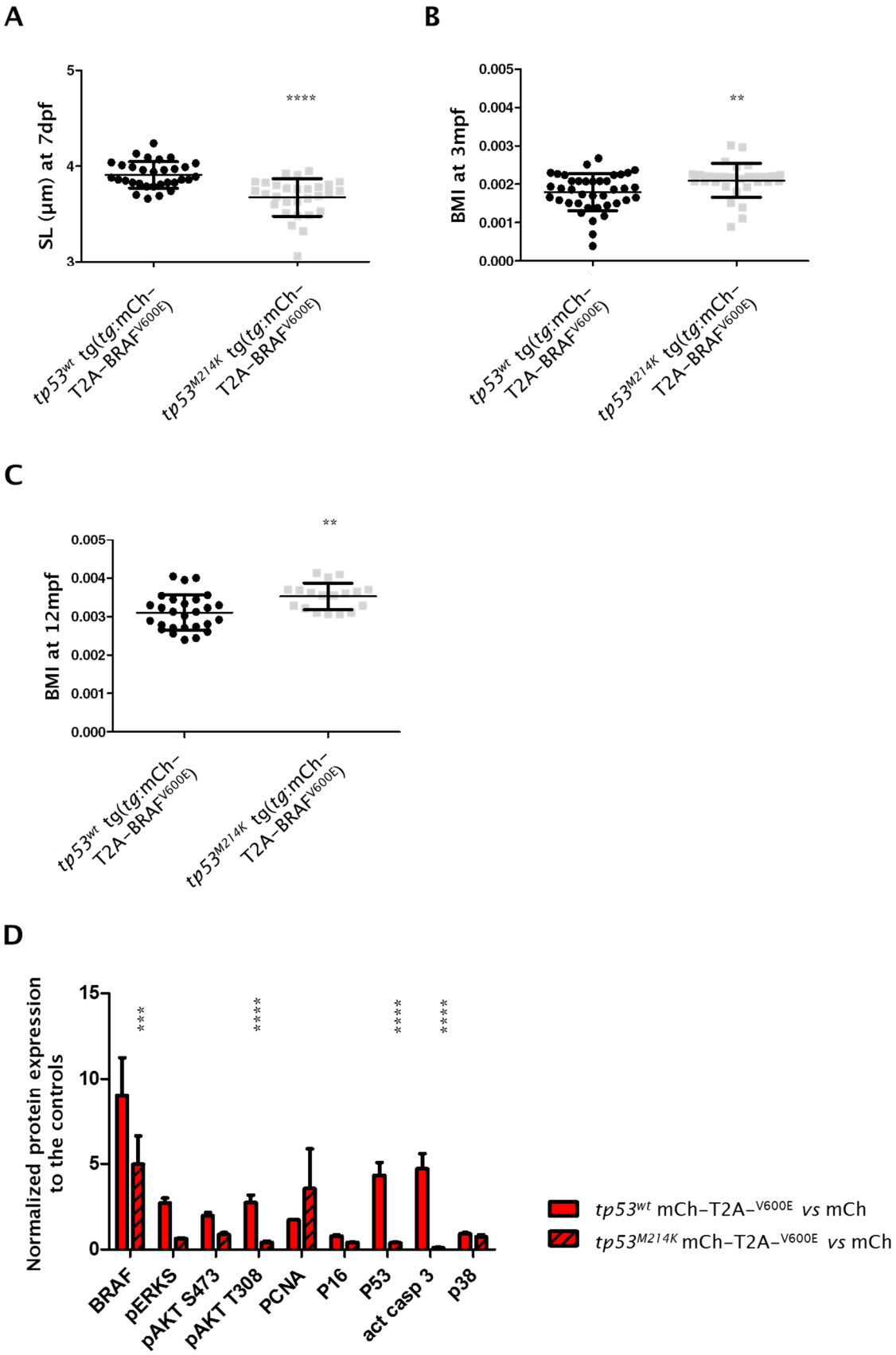
A
SL (µm) at 7dpf
5
4
3
****
tp53wt tg(tg:mCh-T2A-BRAFV600E)
tp53M214K tg(tg:mCh-T2A-BRAFV600E)
B
BMI at 3mpf
0.005
0.004
0.003
0.002
0.001
0.000
**
tp53wt tg(tg:mCh-T2A-BRAFV600E)
tp53M214K tg(tg:mCh-T2A-BRAFV600E)
C
BMI at 12mpf
0.005
0.004
0.003
0.002
0.001
0.000
**
tp53wt tg(tg:mCh-T2A-BRAFV600E)
tp53M214K tg(tg:mCh-T2A-BRAFV600E)
D
Normalized protein expression to the controls
15
10
5
0
***
****
****
****
BRAF
pERKS
pAKT S473
pAKT T308
PCNA
P16
P53
act casp 3
p38
tp53wt mCh-T2A-V600E vs mCh
tp53M214K mCh-T2A-V600E vs mCh

Figure 13. **Comparison between BRAF^{V600E}-expressing tp53^{wt} and tp53^{M214K} lines.** (A) SL measured at 7dpf from *tp53^{wt}* tg(*tg*:mCh-T2A-BRAF^{V600E}) (n=31) and *tp53^{M214K}* tg(*tg*:mCh-T2A-BRAF^{V600E}) (n=29) ($p<0.0001$). (B) BMI measured at 3 months of age from *tp53^{wt}* tg(*tg*:mCh-T2A-BRAF^{V600E}) (n=39) and *tp53^{M214K}* tg(*tg*:mCh-T2A-BRAF^{V600E}) (n=30) ($p<0.01$). (C) BMI measured at 12 months of age from *tp53^{wt}* tg(*tg*:mCh-T2A-BRAF^{V600E}) (n=27) and *tp53^{M214K}* tg(*tg*:mCh-T2A-BRAF^{V600E}) (n=18) ($p<0.01$). (D) Western blot analysis of lysates from thyroid tissue at 3mpf. Values are shown in bar graphs and represent three independent experiments, each corresponding to a pool of three fish (statistical analysis only shown for relevant comparisons; $p<0.001$ and $p<0.0001$).

Conditional targeted expression of BRAF^{V600E} in thyroid cells of transgenic zebrafish (preliminary data)

Expressing BRAF^{V600E} in thyroid cell lines and in the thyroid of mice models have shown contradictory data. Mitsutake et al., 2005 showed that *in vitro* conditional BRAF^{V600E} expression failed to transform rat differentiated thyroid PCCL3 cells and induce apoptosis in parallel with increased DNA synthesis, dedifferentiation and chromosomal instability (Mitsutake et al., 2005). Moreover, Vizioli et al., 2011 demonstrated that primary cultures of thyroid transfected with BRAF^{V600E} promote oncogene-induced senescence but not oncogenic transformation (Vizioli et al., 2011). In mice, Shimamura et al., 2013 described that conditional BRAF^{V600E} expression did not induce tumor formation and engineered postnatal expression of BRAF^{V600E} in a small number of thyroid cells did not initiate tumorigenesis in thyroid (Shimamura et al., 2013) despite of mice modeled to thyroid-specific expression of BRAF^{V600E} developed goiter and invasive PTCs early in life (Knauf et al., 2005; Mercer et al., 2005; Franco et al., 2011).

In tg(*tg*:mCh-T2A-BRAF^{V600E}) fish, a very early impairment of thyroid morphogenesis and development of hyperplasia was observed by 2 months of age. In order to model sporadic thyroid cancer, a transgenic model was developed in which BRAF^{V600E} was expressed late in life and controlled in a very efficient manner under physiological serum TSH concentrations.

In the past decade, the Cre-loxP technology, when combined with inducible systems, has allowed a controlled spatial and/or temporal expression of mutations from tumor suppressor genes and oncogenes.

The tg(*hsp70l*:mCherry-T2A-CreER^{T2}) transgenic line is a non-leaky conditional line that has a bicistronic mRNA coding for mCherry and CreER^{T2} separated by a viral T2A peptide sequence under the control of the zebrafish heat shock cognate 70-kd protein, like (*hsp70l*) promoter (Hans et al., 2011). In the absence of tamoxifen (TAM), Cre-loxP-site-specific recombination does not occur whereas in the presence of TAM and after heat shock full recombination can be achieved. A construct, in which BRAF^{V600E} expression would be normally suppressed by the presence of a floxed gene but induced when this gene was rearranged by Cre, was developed.

To facilitate cloning, the following previous constructs were used: Tol2CG2*tg:*mCh and Tol2CG2*tg:*mCh-T2A-BRAF^{V600E}. The loxP-CFP-loxP cassette was cloned downstream of the *tg* promoter and upstream of the mCh or mCh-T2A-BRAF^{V600E} (Figure 14A and 14B, respectively). CFP reporter was chosen because it would allow to monitor the recombination process in thyroid cells upon heat shock and TAM treatment.

Tol2CG2*tg:*loxP-CFP-loxP-mCh or Tol2CG2*tg:*loxP-CFP-loxP-mCh-T2A-BRAF^{V600E} was injected with capped transposase mRNA into one-cell-stage tg(*hsp70l*:mCherry-T2A-CreER^{T2}) embryos. By fluorescence microscopy, mosaic CFP expression was observed in thyroid tissue of F0 animals injected with Tol2CG2*tg:*loxP-CFP-loxP-mCh or Tol2CG2*tg*:loxP-CFP-loxP-mCh-T2A-BRAF^{V600E}. This was the confirmation that the construct was functional and *tg* promoter was sufficient to drive expression of CFP specifically to the thyroid cells.

Embryos presenting mosaic CFP or EGFP expression in the thyroid or the heart, respectively were grown to adulthood and F0 founders were identified by a specific-reporter signal exclusively in those tissue of their progeny. Stable transgenic lines were established using F0 founders. A robust CFP expression was confirmed in thyroid cells of both F0-*hsp70l:*mCherry-T2A-CreER^{T2};*tg:*loxP-CFP-loxP-mCh and F0-*hsp70l:*mCherry-T2A-CreER^{T2};*tg:*loxP-CFP-loxP-mCh-T2A-BRAF^{V600E} lines.

When analyzing live embryos from the lines above-mentioned, a robust thyroid specific reporter signal became detectable at around 34hpf and it was maintained throughout thyroid growth similar to tg(*tg*:mCh) embryos.

A preliminary experiment was conducted by inducing Cre-loxP-mediated recombination in tg(*hsp70l*:mCherry-T2A-CreER^{T2};*tg*:loxP-CFP-loxP-mCh-T2A-BRAF^{V600E}) fish at 2 ½ months of age. This age was chosen not only because recombination during larval stage would not portrayed the sporadic cancer but also because fish would handle better the anesthesia, performed in order to monitor the reporter expression.

The recombination was induced by heat shock followed by exposure to the active metabolite of TAM, 4-Hydroxyl-Tamoxifen (4-OHT). Recombination efficiency was assessed by a gradual loss of CFP expression and gradual gain of mCherry expression, which was ubiquitous in the initial hours after the heat shock and specifically to the thyroid cells in the days that followed (Figure 14C).

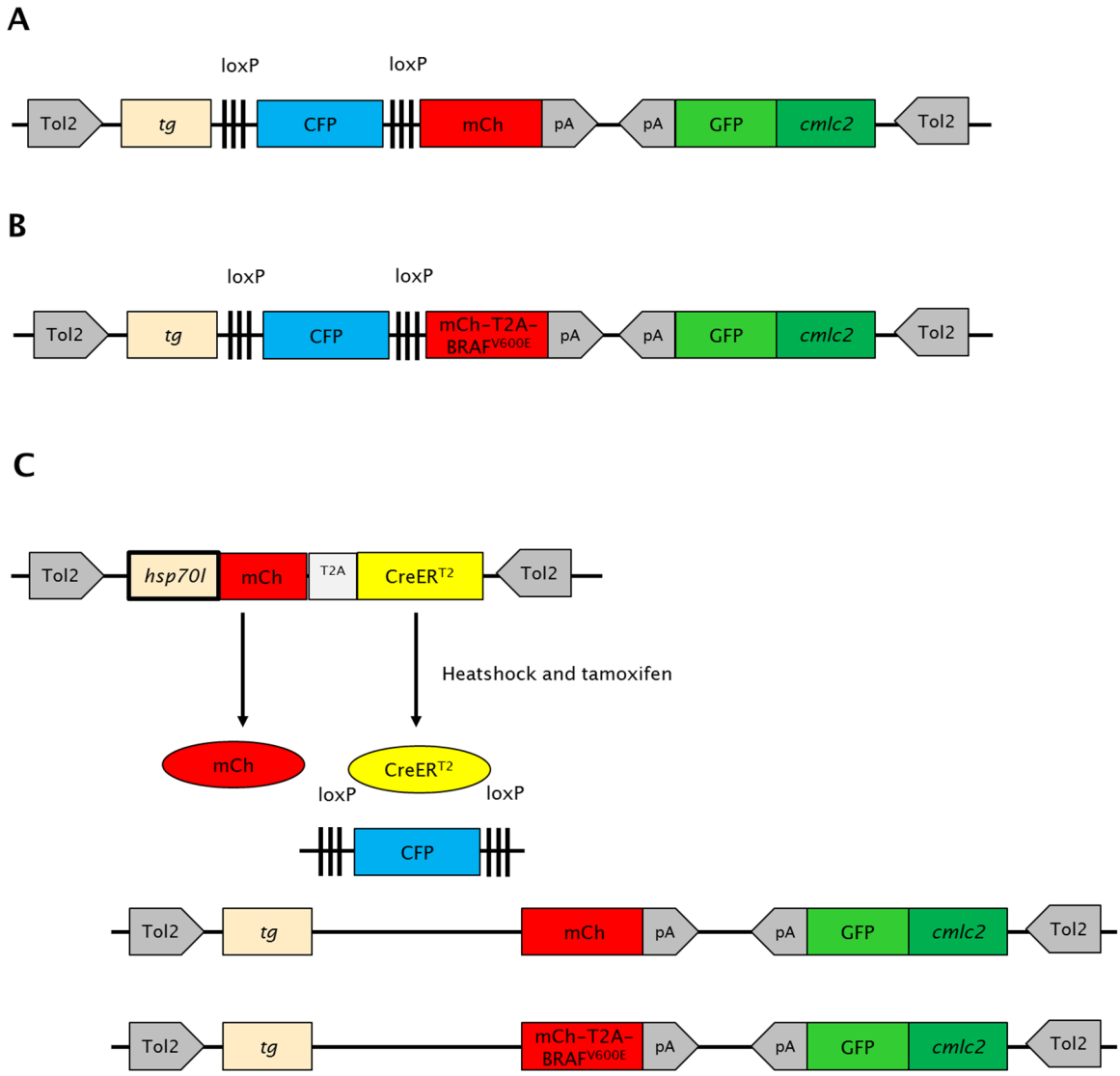

Figure 14. **Conditional constructs** (A) Schematic representation of the (A) Tol2*tg*:loxP-CFP-loxP-mCh and (B) Tol2*tg*:loxP-CFP-loxP-mCh-T2A-BRAF^{V600E} constructs containing Tol2 elements and the *cmlc2*:EGFP-pA cassette. (C) Schematic representation of the Cre-mediated recombination of the *hsp70l*:mCh-T2A-CreER^{T} allele in the blue-to-red reporter *tg*:loxP-CFP-loxP-mCh/mCh-T2A-BRAF^{V600E} line in the presence of heat and 4-OHT exposure and final transgenes kept in the genome.

Transgenic embryos carrying the CFP reporter and the tg(*hsp70l*:mCh-T2A-CreER^{T2}) allele displayed a strong CFP signal until 2 ½ months of age. Heat shock and exposure to 4-OHT led shortly after to a strong ubiquitous mCherry expression

indicating successful induction of CreER^{T2} expression. Fish were monitored and CFP expression was completely lost during the first weeks after induction. This confirmed the successful recombination event in most or all thyroid cells. mCherry expression was never detected; observation that corroborated with the absent mCherry expression in tg(*tg*:mCh-T2A-BRAF^{V600E}) fish.

Without having an expressing reporter that would help to monitor thyroid morphology, fish were grown until they reached 4 months of age and then histological examination was performed. tg(*hsp70l*:mCherry-T2A-CreER^{T2};*tg*:loxP-CFP-loxP-mCh-T2A-BRAF^{V600E}) fish, in which recombination was not induced, displayed thyroid follicles scattered predominantly in the connective tissue near the ventral aorta (Figure 15 A). Follicles were round to oval and were lined by a single-layered epithelium confining a very homogenous colloid (Figure 15 A'). Fish in which recombination was induced showed follicular hyperplasia in the lower jaw (Figure 15B). The follicles were either big or very small and were very close. The epithelium lining the follicles was variably basophilic cuboidal to columnar (Figure 15B'). There was a marked inflammatory infiltrate likely to be of lymphocytic origin surrounding the follicles and inside the blood vessels nearby (Figure 15: B'' and B'''). Because the hyperplasia described resembled that found in tg(*tg*:mCh-T2A-BRAF^{V600E}) fish, it suggested that expression of BRAF^{V600E} was induced successfully.

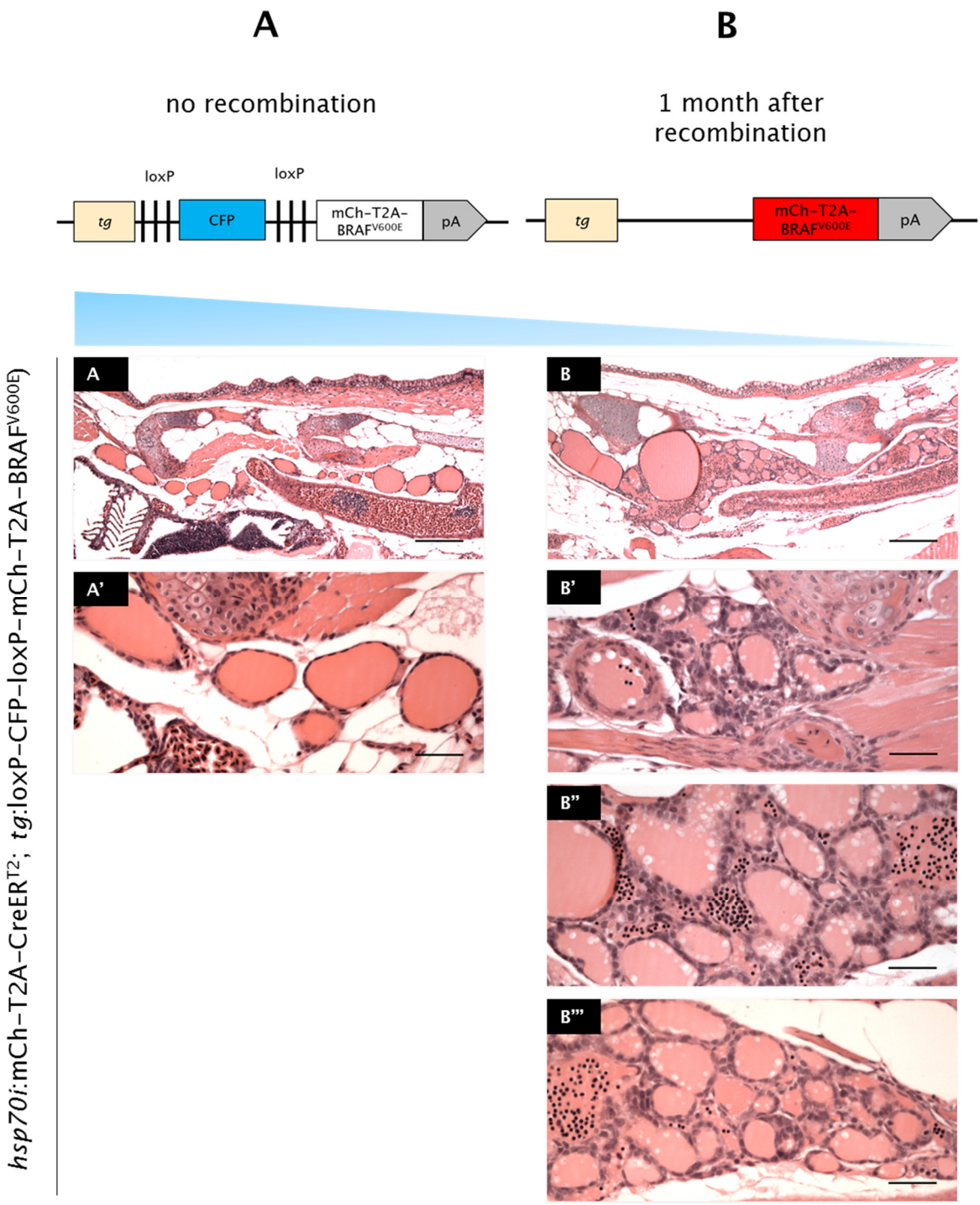

***Figure 15*. Cre-mediated recombination of the *hsp70i*:mCh-T2A-CreER^{T2} allele in the blue-to-red reporter tg(*tg*:loxP-CFP-loxP-mCh-T2A-BRAF^{V600E}) line in the absence and presence of heat and 4-OHT exposure.** (A) Scheme of the transgene in the absence of recombination and HE stain of longitudinal sections representative of the lower jaw. Scale bar: 250μm. (B) Higher magnification of the follicles. Scale bar: 62μm. B: Scheme of the

transgene upon recombination and HE stain of longitudinal sections representative of the lower jaw. Scale bar: 250μm. B'-B''': Higher magnification of the follicles. Scale bar: 62μm.

This experiment was not performed on tg(*hsp70l*:mCherry-T2A-CreER^{T2};*tg*:loxP-CFP-loxP-mCh) fish because no age-matched adults were available at that time. Instead, an experiment similar to the one described for the tg(*hsp70l*:mCherry-T2A-CreER^{T2};*tg*:loxP-CFP-loxP-mCh-T2A-BRAF^{V600E}) was performed on 14dpf larvae. Successful recombination event was confirmed by the loss of CFP and gain of mCherry expression one week after heat shock and 4-OTH treatment (Figure 16). This was also the confirmation that the blue-to-red reporter lines were working upon heat shock and 4-OTH treatment. Of note, blue-to-red recombination was not seen in all larvae suggesting that Cre-mediated recombination was not successful in some cases. On the contrary, the experiment on adults resulted in blue loss in all fish studied. This suggested the presence of WTs in larvae from incrosses; in the absence of the tg(*hsp70l*:mCh-T2A-CreER^{T2}) allele recombination did not occur. All tg(*hsp70l*:mCherry-T2A-CreER^{T2};*tg*:loxP-CFP-loxP-mCh-T2A-BRAF^{V600E}) adults were screened for the tg(*hsp70l*:mCh-T2A-CreER^{T2}) allele and recombination was always efficient.

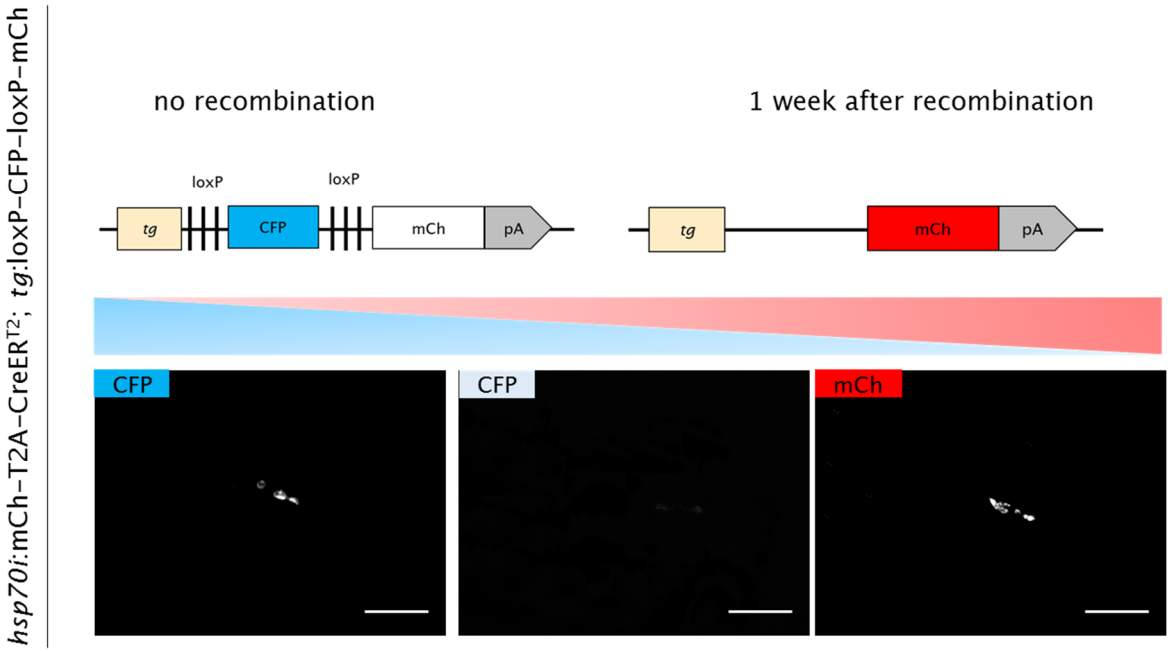

***Figure 16*. Cre-mediated recombination of the *hsp70i*:mCh-T2A-CreER^{T2} allele in the blue-to-red reporter tg(*hsp70i*:mCherry-T2A-CreER^{T2};*tg*:loxP-CFP-loxP-mCh) line in the absence and presence of heat and 4-OHT exposure.** Scheme of the transgene in the absence and one week after recombination (top) and live imaging of the follicles losing CFP and gaining mCh expression. Larvae is oriented with anterior to the right. Scale bar: 250μm.

Discussion

The BRAF^{V600E} is by far the most common genetic event associated to an oncogene found in PTCs and many believe that it is present at the early stage of these carcinomas. Because there is almost no concomitance of BRAF with RET/PTC or RAS in PTCs, a single oncogenic hit may be sufficient to activate the MAPK pathway and, when combined with other events, results in cell transformation (Soares et al., 2003; Xing, 2005; Frasca et al., 2008).

Our results showed that the most common human BRAF mutation is capable of inducing a dramatic change in zebrafish thyroid tissue. Thyroid-specific expression of BRAF^{V600E} led to an impaired thyroid morphogenesis that was permissive to the development of hyperplasia and colloid goiter found in virtually all transgenic fish from the tg(*tg*:mCh-T2A-BRAF^{V600E}) line.

We propose a contribution to thyroid cell proliferation by $BRAF^{V600E}$ (Liu et al., 2007) in our transgenic model. We found in juvenile thyroids that overexpression of $BRAF^{V600E}$ was concomitant with an overexpression of pERKs and pAKTs, representing an activation of the MAPK and PI3K-AKT pathways, respectively. This observation corroborate with the fact that (1) $BRAF^{V600E}$ can gain up to 500-fold increased activation stimulating the MAPK pathways in cells that harbor the BRAF mutation, even in the absence of any extracellular stimuli (Cantwell-Doris et al., 2011) and (2) constitutive activation of effectors along the MAPK and PI3K-AKT pathways are essential in thyroid cancer (Mitsutake et al., 2005; Palona et al., 2006; Faustino et al., 2012; Xing., 2013). Upregulation of proliferation may have been due to phosphorylation and stabilization of genes responsible for cell-cycle entry promoted by a sustained ERK signaling (Chambard et al., 2007). This was key to a successful development of hyperplasia by 3 months of age. Also, high levels of ERKs could have possibly induced cell-cycle arrest by expression of cylin-dependent kinases (CDK)-inhibitor proteins such as p21 and p27 (Chambard et al., 2007), however activation of AKT indicated that the arrest was counteracted allowing cells to engage in active proliferation. We also found high levels of p53 and activated caspase 3 which indicated that an apoptotic machinery could have been suppressing tumors at this stage. This observation is consistent with Mitsutake et al., 2005 that reported that $BRAF^{V600E}$ expression allowed activation of apoptosis (Mitsutake et al., 2005). We propose that apoptosis possibly reduced the number of cells that were dependent on the RAF signaling and likely to acquire genomic instability. This must have restrained tumor development in tg(*tg*:mCh-T2A-$BRAF^{V600E}$) fish by 3 months of age.

Furthermore, we propose that thyroid-specific expression of $BRAF^{V600E}$ induced dysfunction in this tissue possibly due to repression of sodium iodide symporter (NIS) expression which is tighly regulated by the thyroid-stimulating hormone (TSH)- thyroid stimulating hormone receptor (THSR)-cyclic adenosine monophosphate (AMP)-protein kinase A (PKA) signaling pathway. Our hypothesis is supported by data showing that $BRAF^{V600E}$ induce transforming growth factor beta (TGFβ) secretion leading to NIS repression in a MEK-ERK-independent manner but cooperating with the pathway (Riesco-Eizaguirre et al., 2009). Upon NIS repression, we propose that the iodide uptake mediated by this symporter was compromised and so was the TH synthesis. In turn, homeostatic compensation could have been achieved through increased TSH released by the pituitary. TSH levels enabled thyroid to reach a steady state through development of goiter. Our hypothesis is

consistent with the mice model of thyroid cancer described by Knauf et al., 2005. Thyroid-specific expression of BRAF^{V600E} induced thyroid dysfunction which was compensated through increased TSH levels and goiter development at 5 weeks of age (Knauf et al., 2005).

Altogether, these observations indicate that BRAF^{V600E} promoted thyroid cell transformation in zebrafish but contrarily to human and mice PTCs, differentiated or poorly differentiated carcinomas were not observed at least until 12 months of age. The difference may simply represent a limitation of this particular zebrafish model as previously seen in some mice models of thyroid cancer (Chakravarty et al., 2011; Shimamura et al., 2013).

Lower body weight in the tg(*tg*:mCh-T2A-BRAF^{V600E}) juveniles and adult zebrafish suggested that thyroid of these fish may have failed at some point of development to produce enough TH. Insufficient TH could have been due to either an impairment in the TH synthesis or transport. TH or TSH levels were not measured but because no other phenotype associated with TH deficit was observed during development, it is tempting to speculate that TH levels were near normal at all times; TSH levels may have been elevated. This hypothesis was supported by the gradual thyroid enlargement which by 2 months of age was 2-fold and by 12 months was 6-fold greater than controls. This suggested that thyroid enlargement resulted from a transient hypothyroid state arising due to BRAF^{V600E} effect in thyroid cells which was then compensated by high levels of TSH that eventually promoted in part the development of a steady goiterous state.

As transgene expression was driven by the *tg* promoter and cell dedifferentiation promoted by BRAF^{V600E} is known to reduce the activity of the *tg* promoter, that may have led to a discrete decrease in BRAF^{V600E} expression that conveniently attenuated its full-oncogenic effect yet enough to induce proliferation. Although transgene copy number was not measure, it can not be excluded as one of the reasons that may have conditioned the amount of BRAF^{V600E} expression, independently of the mechanisms regulating the *tg* promoter and subsequently the transgene expression.

Our data indicated that although expression of BRAF^{V600E} can cause the transformation of thyroid cells, additional mutations must be required for the progression to cancer in our model. Molecularly, loss of p53, in addition to activating mutation in the *BRAF* gene, is a genetic signature of thyroid tumor progression (Soares et al., 1994; Bai et al., 2006; Morita et al., 2008). Suprisingly,

tp53^{M214K} tg(*tg*:mCh-T2A-BRAF^{V600E}) fish did not readily develop neoplasia. This indicated that this particular oncogenic stimulus proved to be insufficient for tumorigenesis initiation in our model. Additional genetic alterations other that p53 loss must be required for thyroid tumorigenesis in zebrafish. Also, many key proteins involved in cancer have unknown or non-canonical functions, and thus the multihit nature of some models can result in unpredictable outcomes.

In summary, thyroid-specific expression of BRAF^{V600E} induced abnormal thyroid morphogenesis which transitied to hyperplasia and colloid goiter during adulthood. These phenotype supported an important role of BRAF^{V600E} in thyroid cells and indicated that the tg(*tg*:mCh-T2A-BRAF^{V600E}) model should be useful to understand further phenotypes promoted by BRAF^{V600E}. Furthermore, WT p53 loss in a thyroid-specific expression of BRAF^{V600E} transgenic zebrafish did not cooperate with BRAF^{V600E} expression in the genesis of tumors. These two models will be useful tools for the study of thyroid cancer pathogenesis namely to disclose which promoting and/or suppressing signals are ultimately preventing neoplasia.

Supplementary data

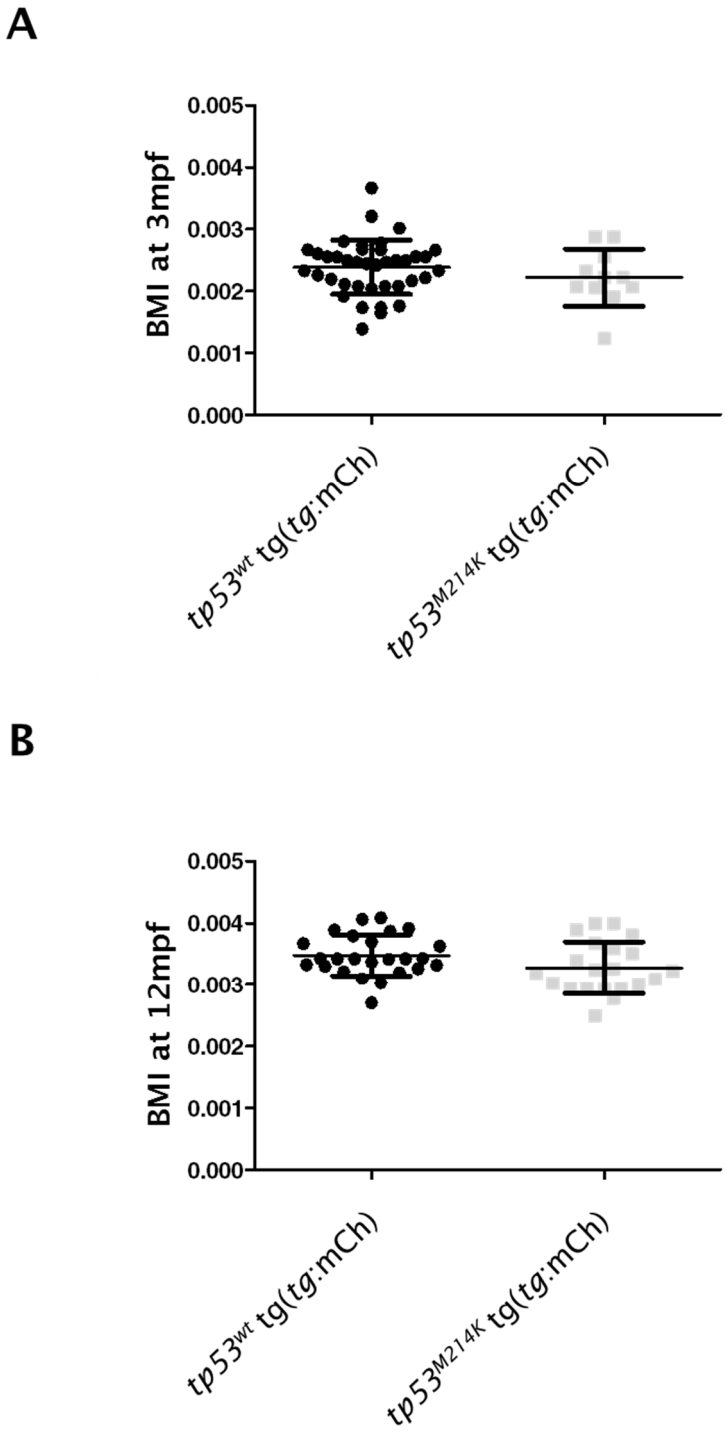

Supplementary figure 1. **BMI in p53^{wt} and tp53^{M214K} fish.** (A) BMI measured at 3 months of age from *tp53*^{wt} tg(*tg*:mCh) (n=39) and *tp53*^{M214K} tg(*tg*:mCh) (n=11) ($p>0.05$). (B) BMI measured at 12 months of age from *tp53*^{wt} tg(*tg*:mCh) (n=25) and *tp53*^{M214K} tg(*tg*:mCh) (n=21) ($p>0.05$).

Chapter IV

Discussion

The RAS/BRAF/MEK/ERK pathway is mutated in about 30% of all cancers (Garnett et al., 2004) and mutations in the B-type Raf kinase (*BRAF*) gene are found in approximately 7% of cancers (Davies et al., 2002), including thyroid cancer (Soares et al., 2003). The predominant mutation in the *BRAF* gene involves a thymidine to adenosine transversion accounting for the majority of the observed mutations in *BRAF* (Davies et al., 2002). Nevertheless, *BRAF* mutation may be complemented by other genetic events (Woodman et al., 2010). A classical example is melanocytic nevi that frequently harbor oncogenic *BRAF* mutations, but only a minority progress to melanoma. In human melanocytes, persistent $BRAF^{V600E}$ expression triggers oncogene-induced senescence. This implies that bypass of oncogene-induced senescence by additional genetic events is necessary for malignant transformation of melanocytes (Yu et al., 2009). In zebrafish, transgenic expression of human $BRAF^{V600E}$ was sufficient to develop ectopic f-nevi that are only highly melanoma prone when combined with a p53 null background (Patton et al., 2005).

The purpose of this thesis was to identify additional genetic events that contribute to thyroid tumorigenesis and have a close relation with $BRAF^{V600E}$. We focused on the recently identified telomerase reverse transcriptase (*TERT*) promoter mutations and disclosed that thyroid $BRAF^{V600E}$ mutation-positive carcinomas harbored those mutations (Vinagre et al., 2013). Predicting the necessity of an animal model to study additional genetic alterations that in cooperation with $BRAF^{V600E}$ promote tumor development in thyroid, we developed a novel model in zebrafish. We generated a transgenic zebrafish expressing $BRAF^{V600E}$ in thyroid cells and disclosed its relation with p53 mutation which is frequently found in undifferenciated thyroid carcinomas. These zebrafish models will be useful tools for the study of genetic alterations in thyroid in a biological context.

IV.1 Frequency of TERT promoter mutations in human cancers

Regulation of promoters is known to be one of the many mechanisms playing an important role in human tumorigenesis but until very recently there were only few studies addressing the presence of mutations in promoter regions of human tumors. For example, a polymorphism in the human *SURVIVIN* gene promoter located at cell cycle-dependent element/cell cycle genes homology region (CDE/CHR) repressor binding motifs was found at high frequency in cancer cell lines (Xu et al., 2004).

Mutations in regulatory parts of the genome, in addition to those in protein-coding sequences gained relevance when it was identified two somatic mutations in the *TERT* promoter (Horn et al., 2013; Huang et al., 2013). Until then, the failure to discover recurrent mutations or gene rearrangements that would activate TERT expression was inconsistent with TERT role in cancer.

In my lab, we subsequently described the presence of *TERT* promoter mutations in other human cancers and validated the findings reported by others (Horn et al., 2013; Huang et al., 2013).

In skin melanomas, we found *TERT* promoter mutations in a similar frequency to that reported (Horn et al., 2013) in primary melanomas (33%), but lower than the frequency found by others in metastatic melanomas (85%) (Horn et al., 2013; Huang et al., 2013). We have analysed very few metastatic melanomas that did not show a significantly higher frequency of *TERT* promoter mutations. We have also confirmed a significant association between TERT and $BRAF^{V600E}$ mutations in melanomas, as previously reported (Horn et al., 2013). Interestingly, in benign nevi, which also frequently harbour $BRAF^{V600E}$ mutations, no *TERT* promoter mutations were found.

In the central nervous system (CNS) tumours, we found that *TERT* promoter mutations were frequent events in gliomas, particularly in glioblastomas (GBM) (62%). Our results were in accordance with studies reporting that *TERT* promoter mutations were detected in 55% (Nonoguchi et al., 2013) or in 51% (Kilella et al., 2013) of the glioblastomas analysed. Another study described that 60% of GBMs were positive for TERT mRNA and telomerase activity but *TERT* promoter mutations were not assessed (Lotsch et al., 2013). Our findings also indicated that *TERT* mutations were associated with older patients, in accordance with another report (Killela et al., 2013).

In bladder cancer, we find a very high frequency of *TERT* promoter mutations which is consistent with increased telomerase activity found in bladder tumors (Sanchini et al., 2005) but those mutations were not found in our series of kidney cancer, neuroendocrine tumors (phaeochromocytoma) or gastrointestinal stromal tumor (GIST).

In thyroid cancer, *TERT* mutations were found in follicular cell-derived cancers (PTC, FTC, poorly differentiated and anaplastic thyroid carcinomas) but not in medullary thyroid carcinomas, which was consistent with other studies (Killela et

al., 2013; Landa et al., 2013) nor in goiter, adenomas or in thyroiditis. These findings are in accordance with telomerase expression that is less frequent in normal tissue and in hyperplastic lesions than in malignant thyroid lesions (Capezzone et al., 2011).

In classical PTCs, *TERT* promoter mutations were associated with $BRAF^{V600E}$ mutation, as observed in melanomas, and coexistence of mutations in both genes was associated with increased expression of the TERT mRNA in thyroid cancer. These findings suggest a cooperative effect of $BRAF^{V600E}$ and *TERT* promoter mutations. In one hand, cells acquiring genetic alterations such as the $BRAF^{V600E}$ mutation begin to reply to the oncogenic stimuli by inducing proliferation. Very short telomeres upon several cell divisions may trigger telomere dysfunction which may be compensated by telomerase reactivation via *TERT* promoter mutations (Londoño-Vallejo JA 2008, Muzza M 2015). In the other hand, activation of the mitogen-activated protein kinase (MAPK) pathway by $BRAF^{V600E}$ is known to upregulate the erythroblast transformation-specific (ETS) system (Janknecht et al., 1995; Whitmarsh et al., 1995; Strahl et al., 1996). Having *de novo* consensus binding sites for ETS factors promoted by *TERT* promoter mutations, the lifespan of BRAF-driven clones is extended. Further accumulation of additional genetic defects is suported which in turn allows progression to advanced tumor stages (Pratilas CA 2009, Huang FW 2013, Horn S 2013, Liu X 2013). Thus, the coexistence of $BRAF^{V600E}$ and $TERT^{C228T}$ must form a unique mechanism upregulating the expression of *TERT*. This oncogenic cooperation of TERT with *BRAF* mutation is interestingly similar to the findings in a transgenic mouse model in which *TP53* mutation and induced overexpression of TERT cooperatively promoted cancer development (González-Suárez et al., 2002).

The presence of *TERT* promoter mutations in thyroid cancer led to further studies by our group. *TERT* promoter mutations were found to be an indicator of clinical aggressiveness of follicular cell-derived thyroid carcinomas, being associated with distant metastases, worse response to treatment, and poor outcome. The detection of *TERT* promoter mutations appears to be, per se, a promising prognostic indicator in DTCs and PTCs (Melo et al., 2014; Melo et al., 2015).

Our series were small to draw a definitive conclusion but recently a large-scale study of multiple tumor types supported the evidence that *TERT* promoter mutations differentially enhanced the transcriptional activity of the *TERT* core promoter (Huang et al., 2015). At the time of our study, many speculated that

mutations in the *TERT* promoter, rather than the coding region of the gene, were creating additional binding sites for ETS transcription factors. A recent study implicated GA-Binding Protein (GABP) as a relevant ETS factor (Bell et al., 2015) as it was identified the recruitment of the multimeric GABP transcription factor specifically to the mutant *TERT* promoter. Although many ETS factors can bind similar deoxyribonucleic acid (DNA) sequence motifs, the GABP is a unique factor that binds to neighboring ETS motifs as a heterotetrameric complex.

In summary, our work identified *TERT* mutations as common events in human cancers and supported the assumption that *TERT* promoter mutations may be one of the mechanisms that underlies telomerase reactivation in several types of human tumours. However, the pathway by which an epigenetically silenced *TERT* gene is activated by one of two cancer-specific somatic mutations on its promoter remains largely unknown.

IV.2 Targeted expression of BRAF^{V600E} in thyroid cells of transgenic zebrafish induces hyperplasia reverted by loss of WT p53

Oncogenic BRAF plays an important role in maintaining the transformed and progressive state of neoplastic thyroid cells (Liu et al., 2007).

Targeted expression of BRAF^{V600E} in thyroid cells of a living animal allows to model thyroid cancer and it is a novel approach to study the relationship between *BRAF* mutation and those found in the *TERT* promoter.

The development of two fluorescent reporter lines, tg(*tg*:mCh) and tg(*tg*:mCh-T2A-BRAF^{V600E}), has given an opportunity to visualize and study the effect of BRAF^{V600E} in early thyroid growth and organization in zebrafish. These transgenic lines combine an early onset of transgene expression specific to the thyroid, with live imaging of thyroid growth, from thyroid budding to formation of follicles.

Apart from the demonstration of the effect of BRAF^{V600E} expression in cell lines and thyroid gland of mice, very little is known about its role in other organisms. Our observation that BRAF^{V600E} expression does not result in thyroid cancer in zebrafish, even in the absence of WT p53, highlights a unique capacity of this line to serve as an *in vivo* tool to screen thyroid dysfunction mediated by BRAF^{V600E} and to identify potential mechanisms that do not allow the development of cancer. In this regard,

our observations argue that BRAF^{V600E} expression in the context of *tp53*^{M214K} might be particularly interesting for further studies.

Concerning the BRAF^{V600E} expression in the developing thyroid of larvae, our results demonstrated an abnormal thyroid morphogenesis and accelerated larval growth as early as 7dpf. The first observation is particularly relevant as it shows that BRAF^{V600E} expression affects the spatial organization and migration of developing follicles in zebrafish.

We did not study this effect in detail, however we propose that BRAF^{V600E}-induced phenotype in the first days of development may have contributed to a downregulation of thyroid-specific genes that mediate thyroid differentiation and growth. In zebrafish, these processes are mediated by NK2 homeobox 1a (*nk2.1a*), paired box gene 2.1 (*pax 2.1*) and hematopoietically expressed homeobox (*hhex*) (Wendl et al., 2002; Alt et al., 2006). In one particular study, reduction in *pax2a* and loss of *nkx2.1a* expression in zebrafish was concomitant with a reduction of thyroid primordium volume and a decreased number of thyroid cells as a result of overexpression of Notch intracellular domain (NICD) in embryos (Porazzi et al., 2012). Although we did not explore the Notch signaling, we propose that downregulation of thyroid-specific genes might have been mediated by BRAF^{V600E} *via* activation of MAPK pathway which in turn might have upregulated Notch signaling (Ferretti et al., 2008; Yamashita et al., 2013). Nevertheless, this hypothesis needs further investigation. Because the phenotype prevailed during the larval development, it also indicated that BRAF^{V600E} expression may have enabled downregulation of solute carrier family 5 (sodium/iodide cotransporter), Member 5 (*slc5a5)* and cathepsin B (*ctsb*), two important proteins in thyroid hormone (TH) biosynthesis (Bizhanova et al., 2009). These hypothesis are in accordance with data showing that BRAF^{V600E} is associated with silencing of multiple thyroid-specific iodine-metabolizing genes *in vitro* and in human tumors (Erhardt et al., 1999; Riesco-Eizaguirre et al., 2006; Liu et al., 2007b; Tang et al., 2010; Cantwell-Dorris et al., 2011). In our transgenic model, downregulation of these genes may have allowed a delay in embryonic thyroid growth which is consistent with the observed phenotype. We can not conclude whether protein synthesis of thyroglobulin (*tg*) was affected but, because there was no retardation of body growth, it suggested that thyroid function was not severly disturbed at this stage. Also, maternal contribution of the TH might have compensated for a possible compromised

thyroid function during the first days of development (Brown., 1997; Elsaline et al., 2003b).

Regarding the $BRAF^{V600E}$-induced phenotype in the thyroid of juvenile fish, our results showed thyroid hyperplasia and retardation of fish growth by 2-3 months of age (see below). The first observation suggested a contribution to thyroid cell proliferation by $BRAF^{V600E}$ (Liu et al., 2007). When examining thyroid tissue, it was found an overexpression of $BRAF^{V600E}$ concomitant with an overexpression of pERKs and pAKTs, representing an activation of the MAPK and PI3K-AKT pathways, respectively. This observation corroborate with the fact that (1) $BRAF^{V600E}$ can gain up to 500-fold increased activation stimulating the MAPK pathways in cells that harbor the BRAF mutation, even in the absence of any extracellular stimuli, allowing those cells to become self-sufficient in growth signals within the pathway (Cantwell-Doris et al., 2011) and (2) constitutive activation of effectors along the MAPK and PI3K-AKT pathways are essential in thyroid cancer (Mitsutake et al., 2005; Palona et al., 2006; Faustino et al., 2012; Xing., 2013). Our data also showed an upregulation of proliferation which we believe was due to phosphorylation and stabilization of genes responsible for cell-cycle entry and repressing genes responsible for inhibiting proliferation promoted by a sustained ERK signaling (Chambard et al., 2007). This was key to a successful development of hyperplasia. Also high levels of ERKs could have possibly induced cell-cycle arrest by expression of cylin-dependent kinases (CDK)-inhibitor proteins such as p21 and p27 (Chambard et al., 2007), however activation of AKT suggested that the arrest was counteracted enabling cells to engage in active proliferation.

In melanocytes, senescence has been proposed to play a major role in preventing malignant transformation of melanocytic nevi. Evidence pointed out that $BRAF^{V600E}$ expression in mouse models resulted in induction of senescence in melanocytes and senescent markers are highly expressed in human melanocytic nevi (Collado et al., 2010; Dhomen et al., 2009). Our data showed a downregulation of senescence which must have contributed to prevent growth arrest by BRAF oncogene-induced senescence (Vizioli et al., 2011). We believe that in our model senescence did not play a role in preventing malignant transformation of thyroid cells due to mechanisms that overcame arrest of cell proliferation.

We found in the juvenile thyroid high levels of p53 and activated caspase 3 which can indicated that an apoptotic machinery was behind tumor suppression at this stage. This observation is consistent with Mitsutake et al., 2005 that reported that

BRAF^{V600E} expression allowed activation of apoptosis (Mitsutake et al., 2005). Also, Wapapeyee et al., 2008 reported that expression of BRAF^{V600E} in primary cells lead to synthesis and secretion of insulin-like growth factor-binding protein 7 (IGFBP7) which, by acting through autocrine/paracrine pathways to inhibit BRAF-MEK-ERK signaling, induced apoptosis by upregulating pro-apoptotic B-cell lymphoma 2 (BCL2) family proteins (Wapapeyee et al., 2008). We propose that apoptosis possibly reduced the number of cells that were dependent on the RAF signaling and likely to acquire genomic instability which in turn significantly decreased the likehood of tumor development in those fish by 3 months of age.

It should be noted that at this stage, hyperplasia was a possible phenotype in the thyroid of transgenic fish. Appreciating other models in mice, human neuroblastoma RAS viral (v-ras) oncogene homolog (*NRAS*) with a mutation at codon 61, which is an upstream activator of RAF, targeted to thyroid cells lead to the development of thyroid hyperplasia characterized by large, indistinct areas of small follicles with scant colloid and tall epithelial cells by 6 months of age (Vitagliano et al., 2006). Targeting the Paired Box 8 (*PAX8)/*Peroxisome Proliferator-Activated Receptor (*PPAR Gamma*) rearrangement to mice thyroid cells also led to thyroid hyperplasia and enlarged follicles at 1 year of age (Diallo-Krou et al., 2009).

Regarding the BRAF^{V600E}-induced phenotype in the thyroid of 12-month old fish, our results have shown that these fish displayed signs resembling colloid goiter and kept the growth retardation observed while juveniles. We propose that thyroid-specific expression of BRAF^{V600E} induced dysfunction in this tissue possibly due to repression of sodium iodide symporter (NIS) expression which is tighly regulated by the thyroid-stimulating hormone (TSH)- thyroid stimulating hormone receptor (THSR)-cyclic adenosine monophosphate (AMP)-protein kinase A (PKA) signaling pathway. This hypothesis is supported by a study that reported that BRAF^{V600E} induced transforming growth factor beta (TGFβ) secretion leading to NIS repression in a MEK-ERK-independent manner but cooperating with the pathway (Riesco-Eizaguirre et al., 2009).

We also propose that upon NIS repression, the iodide uptake mediated by this symporter was compromised and so was the TH synthesis. In turn, homeostatic compensation could have been achieved through increased TSH released by the pituitary. TSH levels enabled thyroid to reach a steady state through development of colloid goiter. This possible compensation was only possible if TSH receptor

expression was not affected by BRAF^{V600E}, allowing adequate TSH responsiveness. Our hypothesis is consistent with the mice models of thyroid cancer. Thyroid-specific expression of BRAF^{V600E} induced thyroid dysfunction which was compensated through increased TSH levels and goiter development at 5 weeks of age (Knauf et al., 2005). Tamoxifen treated Thyro::CreERT2;BRAF^{CA} mice also developed enlarged, goiterous, hypercellular thyroid that was up to 10 times larger than controls one month only after BRAF^{V600E} expression was induced and up to 300 times larger after 12 months (Charles et al., 2011). In these models activated BRAF^{V600E} ultimately elicited PTCs in the adult mouse (Knauf et al., 2005; Charles et al., 2011). Also, compensation mediated by TSH is indeed a plausible hypothesis as TSH signaling pathway cooperate with oncogenic-BRAF, in part by cAMP signaling. A study showed that deletions in Gsα, a protein which couples hormonal stimulation of several cell membrane receptors to the activation of adenylyl cyclase, did not prevent formation of thyroid tumors in *LSL-Braf^{V600E}/TPO-Cre/Gnas-E1$^{fl/fl}$* mice (Franco et al., 2011).

We propose that retardation in growth found from 3 to 12 months of age in tg(*tg*:mCh-T2A-BRAF^{V600E}) fish is likely to be a consequence of thyroid dysfunction. This suggests that fish could have been hypothyroid at some point during development and eventually compensated by becoming euthyroid. Knauf et al., 2005 showed that one particular mice line with thyroid-specific expression of BRAF^{V600E} initially grew marginally slower than nontransgenic littermates but proved to be transient as it was not observed after eight weeks (Knauf et al., 2005). Nevertheless, we cannot exclude the maintenance of a hypothyroid state in transgenic fish as judged by the phenotype found in a model of *tg* mutants of zebrafish (Jao et al., 2008). These fish were reported to be homozygous insertional mutants for the putative *tg* gene and as they entered adulthood, they developed a goiter-like phenotype in the absence of *tg* and THs synthesis (Jao et al., 2008). Further mechanistic and functional studies are clearly needed to clarify the nature of the BRAF^{V600E} interaction in zebrafish thyroid.

Besides the plausible explanations from molecular and functional perspectives, we understand that thyroid-specific expression of BRAF^{V600E} in thyroid cells was due to a transgene and its expression and regulation were certainly dependent on many genetic factors. We do not exclude the hypothesis that tumor development was not successful in tg(*tg*:mCh-T2A-BRAF^{V600E}) fish because (1) the oncogene dosase was

not sufficient to full transformation of thyroid cells and/or (2) downregulation of the *tg* promoter upon BRAF-induced silencing of thyroid-specific genes.

The first assumption is supported by observations in transgenic mice. In doxycycline-inducible transgenic mice, that allowed RAS activation to be titrated, high-level but not low-level of RAS activation induced tumor suppressor pathways and triggers an irreversible senescent growth arrest in vivo (Sarkisian et al., 2007). In one of the two mice transgenic lines with targeted expression of the $BRAF^{V600E}$ in thyroid cells, $BRAF^{V600E}$ levels were low enough to induce a very weak increase in pERK levels in mice thyroids (Knauf et al., 2005). Oncogene dosage in our transgenic model may have been dependent on the transgene copy number.

The second point is not less important. If the *tg* promoter was downregulated at some level by the mutant form of BRAF or downstream effectors, it might have restrained $BRAF^{V600E}$ levels enough to induce cell proliferation to a limited extent. Indeed, a study found that expression of thyroid-specific genes and their transcription factors is lost in thyroid cells derived from follicular, papillary and anaplastic human carcinomas and in these cells, thyroid-specific promoter activities such as the *tg* promoter were absent. Only re-expression of transcription factors was able to stimulate transcription from the promoters at some extent (Ros et al., 1999).

One intriguing observation was that neoplasia was not observed in tg(*tg*:mCh-T2A-$BRAF^{V600E}$) fish until 12 months of age, instead these fish developed colloid goiter. In the light of these findings, we hypothesize that in our model $BRAF^{V600E}$ would only elicit neoplasia if the p53 pathway was downregulated. Melanocyte-specific expression of $BRAF^{V600E}$ in zebrafish induced a dramatic change in fish pigmentation patterns and it was found to be sufficient to promote fish nevi development but not melanomas. Indeed, melanoma only developed in a $tp53^{M214K}$ background (Patton et al., 2005). This observation is of particular relevance because *TP53* mutations are not frequently found in well-differentiated thyroid carcinomas and are associated with tumor progression to anaplastic forms of cancer (Soares et al., 1994). Also, using a thyroid-specific Cre recombinase-estrogen receptor (CreER) transgenic mouse with a Cre-regulated $BRAF^{V600E}$ and a conditional *Trp53* it was found that p53 loss enabled progression to aggressive anaplastic thyroid cancer but additional events were required for full anaplastic conversion (McFadden et al., 2014)

Suprisingly, *tp53*^{M214K} tg(*tg*:mCh-T2A-BRAF^{V600E}) fish showed normal thyroid morphogenesis during larval growth with proper follicle migration and invididualization. Hyperplasia and/or growth retardation was not observed in juveniles and neoplasia was also not found by 12 months of age. When examining thyroid tissue at 3 months of age, it was found a decrease in BRAF^{V600E} expression concomitant with downregulation of pERKs and pAKTs, representing lack of activation of the MAPK and PI3K-AKT pathways, respectively. Also, proliferation was not extensively promoted as judged by a comparison with the controls. We propose that in this transgenic model, inneficient activation of the MAPK and PI3K-AKT pathways may have supported a normal thyroid phenotype even in absence of a tumor suppressor gene and/or activation of apoptosis. Studies have shown that activation of the MAPK pathway leads to increased levels of p53 and subsequent stimulation of p53-dependent physiological responses including apoptosis and cell-cycle arrest (Agarwal et al., 2001; Wu et al., 2004). Also, the MAPK pathway is regulated in response to p53, as p53 is believed to stimulate the secretion of growth factors that activate the pathway (Lee et al., 2000; Wu et al., 2004).

Without understanding the final mechanisms, we propose that loss of WT p53 has prevented BRAF^{V600E}-induced thyroid dysfunction by an unclarified mechanism, possibly implicating the MAPK pathway. This might have resulted in reexpression and/or restablishment of thyroid-specific genes favoring normal thyroid growth and function in zebrafish. In turn, fish did not develop neoplasia by lack or insufficient pro-oncogenic signals.

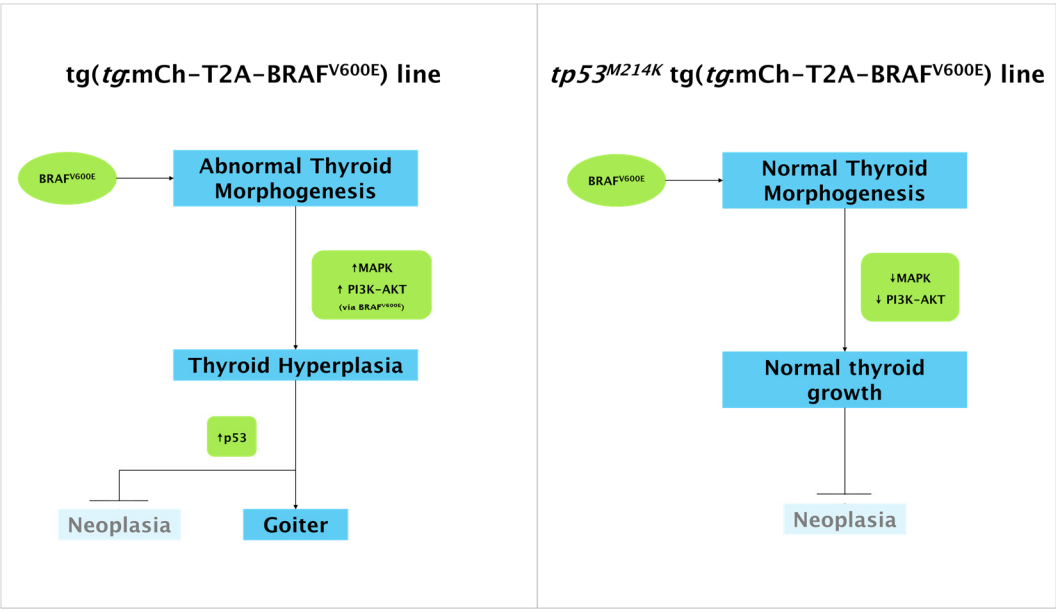

Figure 1. **Working hypothesis.** In the tg(*tg*:mCh-T2A-BRAF^{V600E}) line, BRAF^{V600E} induced abnormal thyroid morphogenesis and thyroid hyperplasia as a result of upregulation of the MAPK and PI3K-AKT signaling pathways. Upregulation of WT p53 restrained cancer and BRAF-induced dysfunction was compensated by increased levels of TSH leading to the development of goiter. In the *tp53*^{M214K} tg(*tg*:mCh-T2A-BRAF^{V600E}) line, BRAF^{V600E} was not able to upregulate the MAPK and PI3K-AKT signaling pathways and in the absence of WT p53, thyroid developed similarly to WT.

Chapter V

Conclusion

For the past half century, research have led us to believe that cancer has its origin in a single cell that acquire mutation(s) and this paradigm was established by the fact that cancers often harbor a large number of mutations and also chromosomal abnormalities and many carcinogens are indeed mutagens (Prehn, 2005).

Numerous genetic alterations have an important role in the tumorigenesis of thyroid tumors and a prominent example is the T1799A point mutation on the B-type Raf kinase (*BRAF*) gene. *BRAF* mutations along with other classical mutations have been extensively studied for many years including the cellular processes that these proteins, when mutated, mediated (Woodman et al., 2010).

The human genome is far richer and complex than once thought and it is not surprising that it is not just the gene but the network that makes the genome so dynamic. Translating to cancer, this dynamics creates too many opportunities for tumorigenesis initiation that go beyond a simple mutation. No wonder cancer is more diverse that its genetics and this explains why researchers are still committed in understanding and control cancer.

In contrast to coding regions, the functional impact of noncoding regions is more difficult to evaluate, due to the lack of knowledge those regions from the genome. Indeed, the non-protein-coding sequences, which accounts for over 98% of the human genome, remain widely unexplored in cancer.

Human model-oriented, my thesis has shown for the first time the presence of mutations in the promoter region of telomerase reverse transcriptase (*TERT*) in different histotypes of thyroid cancer (Vinagre et al., 2013) and the results validated the findings reported by others in melanoma, bladder and gliomas (Horn et al., 2013; Huang et al., 2013; Killela et al., 2013). Also, it seemed that activated BRAF enhanced the effects of *TERT* promoter mutations. Evidence showed that TERT promoter mutations were significantly associated with increased TERT mRNA expression in thyroid cancers and that TERT mRNA was particularly high in cases harbouring both *TERT* and *BRAF* mutations (Vinagre et al., 2013). The location of these mutations in the *TERT* promoter, rather than in the coding region of the gene, creates additional binding sites for transcription factors and represents also a novel mechanism of genetic activation in cancer. Further observational and mechanistic studies are needed to clarify these points.

Animal model-oriented, my thesis has shown that targeted $BRAF^{V600E}$ expression in thyroid cells of transgenic zebrafish induced abnormal thyroid morphogenesis

followed by hyperplasia and colloid goiter but not neoplasia (Almeida et al., submitted). BRAF-induced thyroid dysfunction could be related to repression of sodium iodide symporter (NIS) and homeostatic compensation was achieved through increased thyroid-stimulating hormone (TSH) levels (Almeida et al., submitted). High TSH levels must have been required to reach a new steady state which was arrived in part through development of colloid goiter and not carcinomas. Remarkably, activated BRAF alone or in p53-deficient zebrafish did not induce formation of cancer during the set of experiments (Almeida et al., submitted). Loss of the wild-type (WT) p53 possibly prevented BRAF-induced thyroid dysfunction by restoring at some level thyroid function and restraining cancer development by controlling the propagation of genetically-unstable cells.

References

Agarwal ML, Ramana CV, Hamilton M, Taylor WR, DePrimo SE, Bean LJ, Agarwal A, Agarwal MK, Wolfman A, Stark GR. 2001. Regulation of p53 expression by the RAS-MAP kinase pathway. Oncogene. 20(20):2527-36.

Airaksinen MS, Saarma M. 2002. The GDNF family: signaling, biological functions and therapeutic value. Nature reviews: Neuroscience. 3(5):383-394.

Almeida AL, Boaventura P, Soares P, Clinical Management of Thyroid Cancer: Etiopathogenic factors of thyroid cancer, Pages 46-62, Future Medicine. 2013

Alt B, Reibe S, Feitosa NM, Elsalini OA, Wendl T, Rohr KB. 2006. Analysis of origin and growth of the thyroid gland in zebrafish. Developmental Dynamics. 235(7):1872-83.

Amatruda JF, Shepard JL, Stern HM, Zon LI. 2002. Zebrafish as a cancer model system. Cancer Cell. 1(3):229-31.

Anastasaki C, Rauen KA and Patton EE. 2012. Continual low-level MEK inhibition ameliorates cardio-facio-cutaneous phenotypes in zebrafish. Disease Models & Mechanisms. 5, 546-552.

Auman HJ, Coleman H, Riley HE, Olale F, Tsai H-J, Yelon D. 2007. Functional Modulation of Cardiac Form through Regionally Confined Cell Shape Changes. PLoS Biology. 5(3), e53.

Bai L, Zhu W-G. 2006. p53: Structure, Function and Therapeutic Applications. Journal of Cancer Molecules. 2(4): 141-153.

Begum S, Rosenbaum E, Henrique R, Cohen Y, Sidransky D, Westra WH. 2004. BRAF mutations in anaplastic thyroid carcinoma: implications for tumor origin, diagnosis and treatment. Modern Pathology. 17:1359–1363.

Bell RJA, Rube HT, Kreig A, Mancini A, Fouse SD, Nagarajan RP, Choi S, Hong C, He D, Pekmezci M, Wiencke JK, Wrensch MR, Chang SM, Walsh KM, Myong S, Song JS, Costello JF. 2015. The transcription factor GABP selectively binds and activates the mutant TERT promoter in cancer. Science. 348(6238), 1036–1039.

Berghmans S, Murphey RD, Wienholds E, Neuberg D, Kutok JL, Fletcher CDM, Morris JP, Liu TX, Schulte-Merker S, Kanki JP, Plasterk R, Zon LI, Look AT. 2005. tp53 mutant zebrafish develop malignant peripheral nerve sheath tumors. Proceedings of the National Academy of Sciences of the United States of America. 102(2), 407–412.

Bizhanova A, Kopp P. 2009. The Sodium-Iodide Symporter NIS and Pendrin in Iodide Homeostasis of the Thyroid. Endocrinology. 150(3), 1084–1090.

Brix K, Führer D, Biebermann H. 2011. Molecules important for thyroid hormone synthesis and action – known facts and future perspectives. Thyroid Research. *4*(Suppl 1), S9.

Brousset P, Chaouche N, Leprat F, Branet-Brousset F, Trouette H, Zenou RC, Merlio JP, Delsol G. 1997. Telomerase activity in human thyroid carcinomas originating from the follicular cells. The Journal of Clinical Endocrinology & Metabolism. 82(12):4214-6.

Brown DD. 1997. The role of thyroid hormone in zebrafish and axolotl development. Proceedings of the National Academy of Sciences of the United States of America. 94(24), 13011–13016.

Cantwell-Dorris ER, O'Leary JJ, Sheils OM. 2011. BRAFV600E: implications for carcinogenesis and molecular therapy. Molecular Cancer Therapeutics. 10(3):385-94.

Capezzone M, Cantara S, Marchisotta S, Busonero G, Formichi C, Benigni M, Capuano S, Toti P, Pazaitou-Panayiotou K, Caruso G, Carli AF, Palummo N, Pacini F. 2011. Telomere length in neoplastic and nonneoplastic tissues of patients with familial and sporadic papillary thyroid cancer. The Journal of Clinical Endocrinology & Metabolism. 96, E1852–E1856.

Capezzone M, Marchisotta S, Cantara S, and Pacini F. 2009. Telomeres and Thyroid Cancer. Current Genomics. 10(8), 526–533.

Carswell S, Alwine JC. 1989. Efficiency of utilization of the simian virus 40 late polyadenylation site: effects of upstream sequences. Molecular and Cellular Biology. 9(10), 4248–4258.

Castro P, Rebocho AP, Soares RJ, Magalhães J, Roque L, Trovisco V, Vieira de Castro I, Cardoso-de-Oliveira M, Fonseca E, Soares P, Sobrinho-Simões M. 2006. PAX8-PPARGamma Rearrangement Is Frequently Detected in the Follicular Variant of Papillary Thyroid Carcinoma. The Journal of Clinical Endocrinology & Metabolism. 91:1, 213–220.

Ceol CJ, Houvras Y, Jane-Valbuena J, Bilodeau S, Orlando DA, Battisti V, Fritsch L, Lin WM, Hollmann TJ, Ferré F, Bourque C, Burke CJ, Turner L, Uong A, Johnson LA, Beroukhim R, Mermel CH, Loda M, Ait-Si-Ali S, Garraway LA, Young RA, Zon LI. 2011. The SETDB1 histone methyltransferase is recurrently amplified in and accelerates melanoma. Nature. 471(7339), 513–517.

Chakravarty D, Santos E, Ryder M, Knauf JA, Liao X-H, West BL, Fagin JA. 2011. Small-molecule MAPK inhibitors restore radioiodine incorporation in mouse thyroid cancers with conditional BRAF activation. The Journal of Clinical Investigation. 121(12), 4700–4711.

Chambard JC, Lefloch R, Pouysségur J, Lenormand P. 2007. ERK implication in cell cycle regulation. Biochimica et Biophysica Acta . 1773(8):1299-310.

Charles RP, Iezza G, Amendola E, Dankort D, McMahon M. 2011. Mutationally activated $BRAF^{V600E}$ elicits papillary thyroid cancer in the adult mouse. Cancer Research. 71(11), 3863–3871.

Cheng R, Ford BL, O'Neal PE, Mathews CZ, Bradford CS, Thongtan T, Barnes DW, Hendricks JD, Bailey GS. 1997. Zebrafish (Danio rerio) p53 tumor suppressor gene: cDNA sequence and expression during embryogenesis. Molecular Marine Biology and Biotechnology. 6(2):88-97.

Clark DP, Pazdernik NJ. 2013. Molecular Biology. Oxford: Academic Press.

Collado M, Serrano M. 2010. Senescence in tumours: evidence from mice and humans. Nature Reviews: Cancer. 10(1), 51–57.

Davies H, Bignell GR, Cox C, Stephens P, Edkins S, Clegg S, Teague J, Woffendin H, Garnett MJ, Bottomley W, Davis N, Dicks E, Ewing R, Floyd Y, Gray K, Hall S, Hawes R, Hughes J, Kosmidou V, Menzies A, Mould C, Parker A, Stevens C, Watt S, Hooper S, Wilson R, Jayatilake H, Gusterson BA, Cooper C, Shipley J, Hargrave D, Pritchard-Jones K, Maitland N, Chenevix-Trench G, Riggins GJ, Bigner DD, Palmieri G, Cossu A, Flanagan A, Nicholson A, Ho JW, Leung SY, Yuen ST, Weber BL, Seigler HF, Darrow TL, Paterson H, Marais R, Marshall CJ, Wooster R, Stratton MR, Futreal PA. 2002. Mutations of the BRAF gene in human cancer. Nature. 417:949–54.

DeLellis RA, Lloyd RV, Heitz PU, Eng C. 2004. World Health Organization Classification of Tumours, Pathology and Genetics of Tumours of Endocrine Organs. Lyon: IARC Press.

Dhillon AS, Hagan S, Rath O, Kolch W. 2007. MAP kinase signaling pathways in cancer. Oncogene. 26, 3279–3290.

Dhillon AS, Kolch W. 2004. Oncogenic B-Raf mutations: crystal clear at last. Cancer Cell. 5(4):303–304.

Dhomen N, Reis-Filho JS, da Rocha Dias S, Hayward R, Savage K, Delmas V, Larue L, Pritchard C, Marais R. 2009. Oncogenic Braf induces melanocyte senescence and melanoma in mice. Cancer Cell. 15(4):294–303.

Diallo-Krou E, Yu J, Colby LA, Inoki K, Wilkinson JE, Thomas DG, Giordano TJ, Koenig RJ. 2009. Paired Box Gene 8-Peroxisome Proliferator-Activated Receptor-Gamma Fusion Protein and Loss of Phosphatase and Tensin Homolog Synergistically Cause Thyroid Hyperplasia in Transgenic Mice. Endocrinology. 150(11), 5181–5190.

Donnelly ML, Hughes LE, Luke G, Mendoza H, ten Dam E, Gani D, Ryan MD. 2001. The cleavage activities of foot-and-mouth disease virus 2A site-directed mutants and naturally occurring 2A-like sequences. Journal of General Virology. 82(Pt 5): 1027–41.

Dooley K, Zon LI. 2000. Zebrafish: a model system for the study of human disease. Current Opinion in Genetics & Development. 10(3):252–6.

Elsalini OA, Rohr KB. 2003b. Phenylthiourea disuprts thyroid function in developing zebrafish. Development Genes and Evolution. 212: 593–598.

Elsalini OA, von Gartzen J, Cramer M, Rohr KB. 2003. Zebrafish hhex, nk2.1a, and pax2.1 regulate thyroid growth and differentiation downstream of Nodal-dependent transcription factors. Developmental Biology. 263(1):67–80.

Erhardt P, Schremser EJ, Cooper GM. 1999. B-Raf Inhibits Programmed Cell Death Downstream of Cytochrome c Release from Mitochondria by Activating the MEK/Erk Pathway. Molecular and Cellular Biology. 19(8), 5308–5315.

Farahati J, Geling M, Mader U, Mortl M, Luster M, Muller JG, Flentje M, Reiners C. 2004. Changing trends of incidence and prognosis of thyroid carcinoma in lower Franconia, Germany, from 1981–1995. Thyroid. 14 141–147.

Faustino A, Couto JP, Pópulo H, Rocha AS, Pardal F, Cameselle-Teijeiro JM, Lopes JM, Sobrinho-Simões M, Soares P. 2012. mTOR pathway overactivation in BRAF mutated papillary thyroid carcinoma. The Journal of Clinical Endocrinology & Metabolism. 97(7):E1139–49.

Ferlay J, Soerjomataram I, Ervik M. 2013. GLOBOCAN 2012 v1.0, Cancer Incidence and Mortality Worldwide: IARC CancerBase No. 11. Lyon, France: International Agency for Research on Cancer.

Ferretti E, Tosi E, Po A, Scipioni A, Morisi R, Espinola MS, Russo D, Durante C, Schlumberger M, Screpanti I, Filetti S, Gulino A. 2008. Notch signaling is involved in expression of thyrocyte differentiation markers and is down-regulated in thyroid tumors. The Journal of Clinical Endocrinology & Metabolism. 93(10):4080–7.

Fournie JW, Wolfe MJ, Wolf JC, Courtney LA, Johnson RD, Hawkins WE. 2005. Diagnostic criteria for proliferative thyroid lesions in bony fishes. Toxicologic Pathology. 33(5):540–51.

Franco AT, Malaguarnera R, Refetoff S, Liao X-H, Lundsmith E, Kimura S, Pritchard C, Marais R, Davies TF, Weinstein LS, Chen M, Rosen N, Ghossein R, Fagin JA. 2011. Thyrotrophin receptor signaling dependence of Braf-induced thyroid tumor

initiation in mice. Proceedings of the National Academy of Sciences of the United States of America. 108(4), 1615–1620.

Frasca F, Nucera C, Pellegriti G, Gangemi P, Attard M, Stella M, Loda M, Vella V, Giordano C, Trimarchi F, Mazzon E, Belfiore A, Vigneri R. 2008. BRAF(V600E) mutation and the biology of papillary thyroid cancer. Endocrine-Related Cancer. 15(1):191–205.

Galleani J, Miranda C, Pierotti MA, Greco A. 2009. H2AX phosphorylation and kinetics of radiation-induced DNA double strand break repair in human primary thyrocytes. Thyroid. 3:257–64.

Gandolfi G, Ragazzi M, Frasoldati A, Piana S, Ciarrocchi A, Sancisi V. 2015. TERT promoter mutations are associated with distant metastases in papillary thyroid carcinoma. European Journal of Endocrinology. 172(4):403–13.

Garnett MJ, Marais R. 2004. Guilty as charged: BRAF is a human oncogene. Cancer Cell. 6:313–319.

Giordano TJ, Kuick R, Thomas DG, Misek DE, Vinco M, Sanders D, Zhu Z, Ciampi R, Roh M, Shedden K. 2005. Molecular classification of papillary thyroid carcinoma: distinct BRAF, RAS, and RET/PTC mutationspecific gene expression profiles discovered by DNA microarray analysis. Oncogene. 24:6646–6656.

González-Suárez E, Flores JM, Blasco MA. 2002. Cooperation between p53 mutation and high telomerase transgenic expression in spontaneous cancer development. Molecular and Cellular Biology. 22(20):7291–301.

Grunwald DJ, Eisen JS. 2002. Headwaters of the zebrafish – emergence of a new model vertebrate. Nature Reviews Genetics. 3(9):717–24.

Guerra A, Sapio MR, Marotta V, Campanile E, Rossi S, Forno I, Fugazzola L, Budillon A, Moccia T, Fenzi G, Vitale M. 2012. The primary occurrence of BRAF(V600E) is a rare clonal event in papillary thyroid carcinoma. The Journal of Clinical Endocrinology & Metabolism. 97(2):517–24.

Gymnopoulos M, Elsliger M-A, Vogt PK. 2007. Rare cancer-specific mutations in PIK3CA show gain of function. Proceedings of the National Academy of Sciences of the United States of America. 104(13), 5569–5574.

Hanahan D, Weinberg RA. 2011. Hallmarks of Cancer: The Next Generation. Cell. 144(5):646–74.

Hans S, Freudenreich D, Geffarth M, Kaslin J, Machate A, Brand M. 2011. Generation of a non-leaky heat shock-inducible Cre line for conditional Cre/lox strategies in zebrafish. Developmental Dynamics. 240(1):108–15.

Horn S, Figl A, Rachakonda PS, Fischer C, Sucker A, Gast A, Kadel S, Moll I, Nagore E, Hemminki K, Schadendorf D, Kumar R. 2013. TERT promoter mutations in familial and sporadic melanoma. Science. 339(6122):959–61.

Hou P, Liu D, Shan Y, Hu S, Studeman K, Condouris S, Wang Y, Trink A, El-Naggar AK, Tallini G, Vasko V, Xing M. 2007. Genetic alterations and their relationship in the phosphatidylinositol 3-kinase/Akt pathway in thyroid cancer. Clinical Cancer Research. 13(4):1161–70.

Huang CJ, Tu CT, Hsiao CD, Hsieh FJ, Tsai HJ. 2003. Germ-line transmission of a myocardium-specific EGFP transgene reveals critical regulatory elements in the cardiac myosin light chain 2 promoter of zebrafish. Developmental Dynamics. 228(1):30–40.

Huang D-S, Wang Z, He X-J, Diplas BH, Yang R, Killela PJ, Meng Q, Ye ZY, Wang W, Jiang XT, Xu L, He XL, Zhao ZS, Xu WJ, Wang HJ, Ma YY, Xia YJ, Li L, Zhang RX, Jin T, Zhao ZK, Xu J, Yu S, Wu F, Liang J, Wang S, Jiao Y, Yan H, Tao H-Q. 2015. Recurrent TERT promoter mutations identified in a large-scale study of multiple tumor types are associated with increased TERT expression and telomerase activation. European Journal of Cancer. 51(8), 969–976.

Huang FW, Hodis E, Xu MJ, Kryukov GV, Chin L and Garraway LA. 2013. Highly recurrent TERT promoter mutations in human melanoma. Science. 339(6122), 957–959.

Janknecht R, Ernst WH, Nordheim A. 1995. SAP1a is a nuclear target of signaling cascades involving ERKs. Oncogene. 10:1209–1216.

Jao L-E, Maddison L, Chen W, Burgess SM. 2008. Using retroviruses as a mutagenesis tool to explore the zebrafish genome. Briefings in Functional Genomics and Proteomics. 7(6), 427–443.

Jovanovic L, Delahunt B, McIver B, Eberhardt NL, Grebe SK. 2008. Most multifocal papillary thyroid carcinomas acquire genetic and morphotype diversity through subclonal evolution following the intra-glandular spread of the initial neoplastic clone. The Journal of Pathology. 215(2):145–54.

Kawakami K, Takeda H, Kawakami N, Kobayashi M, Matsuda N, Mishina M. 2004. A transposon-mediated gene trap approach identifies developmentally regulated genes in zebrafish. Developmental Cell. 7(1):133–44.

Killela PJ, Reitman ZJ, Jiao Y, Bettegowda C, Agrawal N, Diaz LA, Friedman AH, Friedman H, Gallia GL, Giovanella BC, Grollman AP, He TC, He Y, Hruban RH, Jallo GI, Mandahl N, Meeker AK, Mertens F, Netto GJ, Rasheed BA, Riggins GJ, Rosenquist TA, Schiffman M, Shih IeM, Theodorescu D, Torbenson MS, Velculescu VE, Wang TL, Wentzensen N, Wood LD, Zhang M, McLendon RE, Bigner DD, Kinzler KW, Vogelstein B, Papadopoulos N, Yan H. 2013. TERT promoter mutations occur frequently in gliomas and a subset of tumors derived from cells with low rates of self-renewal. Proceedings of the National Academy of Sciences of the United States of America. 110(15), 6021–6026.

Kimmel CB, Ballard WW, Kimmel SR, Ullmann B, Schilling TF. 1995. Stages of embryonic development of the zebrafish. Developmental Dynamics. 203(3):253–310.

Kimura S. 2011. Thyroid-Specific Transcription Factors and Their Roles in Thyroid Cancer. Journal of Thyroid Research. 710213.

Knauf JA, Fagin JA. 2009. Role of MAPK pathway oncoproteins in thyroid cancer pathogenesis and as drug targets. Current Opinion in Cell Biology. 21(2):296–303.

Knauf JA, Ma X, Smith EP, Zhang L, Mitsutake N, Liao XH, Refetoff S, Nikiforov YE, Fagin JA. 2005. Targeted expression of BRAFV600E in thyroid cells of transgenic mice results in papillary thyroid cancers that undergo dedifferentiation. Cancer Research. 15;65(10):4238-45.

Kroll TG, Sarraf P, Pecciarini L. 2000. PAX8-PPARGamma1 fusion in oncogene human thyroid carcinoma. Science. 289(5483):1357–1360.

Kumar V, Abbas AK, Fausto N, Robbins SL, Cotran RS. 2005. Robbins and Cotran pathologic basis of disease. Philadelphia: Elsevier Saunders.

Kuroda H, Basu S. 2003. RET/PTC-induced dedifferentiation of thyroid cells is mediated through Y1062 signaling through SHC–RAS–MAP kinase. Oncogene 22:4406–4412.

Kwan KM, Fujimoto E, Grabher C, Mangum BD, Hardy ME, Campbell DS, Parant JM, Yost HJ, Kanki JP, Chien CB. 2007. The Tol2kit: a multisite gateway-based construction kit for Tol2 transposon transgenesis constructs. Developmental Dynamics. 236(11):3088-99.

Lam S, Lang BH-H. 2014. A Review of the Pathogenesis and Management of Multinodular Goiter, Thyroid Disorders - Focus on Hyperthyroidism, Dr. Gonzalo Diaz Soto (Ed.).

Landa I, Ganly I, Chan TA, Mitsutake N, Matsuse M, Ibrahimpasic T, Ghossein RA, Fagin JA. 2013. Frequent Somatic TERT Promoter Mutations in Thyroid Cancer: Higher Prevalence in Advanced Forms of the Disease. The Journal of Clinical Endocrinology and Metabolism. 98(9), E1562–E1566.

Langenau DM, Traver D, Ferrando AA, Kutok JL, Aster JC, Kanki JP, Lin S, Prochownik E, Trede NS, Zon LI, Look AT. 2003. Myc-induced T cell leukemia in transgenic zebrafish. Science. 299(5608):887-90.

Lee KC, Goh WL, Xu M, Kua N, Lunny D, Wong JS, Coomber D, Vojtesek B, Lane EB, Lane DP. 2008. Detection of the p53 response in zebrafish embryos using new monoclonal antibodies. Oncogene. 27(5):629-40.

Lee SW, Fang L, Igarashi M, Ouchi T, Lu KP and Aaronson SA. 2000. Sustained activation of Ras/Raf/mitogen-activated protein kinase cascade by the tumor suppressor p53. Proceedings of the National Academy of Sciences of the United States of America. 97, 8302-8305.

Link V, Shevchenko A, Heisenberg C-P. 2006. Proteomics of early zebrafish embryos. BMC Developmental Biology. 6, 1.

Liu D, Hu S, Hou P, Jiang D, Condouris S, Xing M. 2007b. Suppression of BRAF/MEK/MAP kinase pathway restores expression of iodide-metabolizing genes in thyroid cells expressing the V600E BRAF mutant. Clinical Cancer Research. 13(4):1341-9.

Liu D, Liu Z, Condouris S, and Xing M. 2007. BRAF V600E Maintains Proliferation, Transformation, and Tumorigenicity of BRAF-Mutant Papillary Thyroid Cancer Cells. The Journal of Clinical Endocrinology and Metabolism. 92(6), 2264-2271.

Liu S, Leach SD. 2011. Zebrafish models for cancer. Annual Review of Pathology. 6:71-93.

Liu T, Brown TC, Juhlin CC, Andreasson A, Wang N, Bäckdahl M, Healy JM, Prasad ML, Korah R, Carling T, Xu D, Larsson, C. 2014. The activating TERT promoter mutation C228T is recurrent in subsets of adrenal tumors. Endocrine-Related Cancer. 21(3), 427-434.

Liu X, Bishop J, Shan Y, Pai S, Liu D, Murugan AK, Sun H, El-Naggar AK, Xing M. 2013. Highly prevalent TERT promoter mutations in aggressive thyroid cancers. Endocrine-Related Cancer. 20(4), 603-610.

Liu X, Qu S, Liu R, Sheng C, Shi X, Zhu G, Murugan AK, Guan H, Yu H, Wang Y, Sun H, Shan Z, Teng W. Xing, M. 2014. TERT Promoter Mutations and Their Association with *BRAF* V600E Mutation and Aggressive Clinicopathological Characteristics of Thyroid Cancer. The Journal of Clinical Endocrinology and Metabolism. *99*(6), E1130-E1136.

Liu Y, Kulesz-Martin M. 2001. p53 protein at the hub of cellular DNA damage response pathways through sequence-specific and non-sequence-specific DNA binding. Carcinogenesis. 22(6):851-60.

Lloyd RV, Buehler D, Khanafshar E. 2011. Papillary Thyroid Carcinoma Variants. Head and Neck Pathology. *5*(1), 51–56.

Lodish H, Berk A, Zipursky SL, et al. 2000. Molecular Cell Biology. 4th edition. New York: W. H. Freeman. Section 20.4, Receptor Tyrosine Kinases and Ras.

Londoño-Vallejo JA. 2008. Telomere instability and cancer. Biochimie. 90(1):73-82.

Lötsch D, Ghanim B, Laaber M, Wurm G, Weis S, Lenz S, Webersinke G, Pichler J, Berger W, Spiegl-Kreinecker, S. 2013. Prognostic significance of telomerase-associated parameters in glioblastoma: effect of patient age. Neuro-Oncology. *15*(4), 423–432.

Manie S, Santoro M, Fusco A, Billaud M. 2001. The RET receptor: function in development and dysfunction in congenital malformation. Trends in genetics: TIG. 17(10):580-589.

Manson R, Wilkinson JS. 1973. The thyroid gland – a review. Australian Veterinary Journal. 49, 44–49.

Marais R, Light Y, Paterson HF, Manson CS, Marshall CJ. 1997. Differential regulation of Raf-1, A-Raf, and B-Raf by oncogenic ras and tyrosine kinases. The Journal of Biological Chemistry. 272(7):4378-4383.

McFadden DG, Vernon A, Santiago PM, Martinez-McFaline R, Bhutkar A, Crowley DM, McMahon M, Sadow PM, Jacks T. 2014. p53 constrains progression to anaplastic thyroid carcinoma in a Braf-mutant mouse model of papillary thyroid cancer. Proceedings of the National Academy of Sciences of the United States of America. 111(16), E1600–E1609.

McKay MM, Morrison DK. 2007. Integrating signals from RTKs to ERK/MAPK. Oncogene. 26(22):3113-3121.

Melo M, da Rocha AG, Vinagre J, Batista R, Peixoto J, Tavares C, Celestino R, Almeida A, Salgado C, Eloy C, Castro P, Prazeres H, Lima J, Amaro T, Lobo C, Martins MJ, Moura M, Cavaco B, Leite V, Cameselle-Teijeiro JM, Carrilho F, Carvalheiro M, Máximo V, Sobrinho-Simões M, Soares P. 2014. TERT Promoter Mutations Are a Major Indicator of Poor Outcome in Differentiated Thyroid Carcinomas. The Journal of Clinical Endocrinology and Metabolism. 99(5), E754–E765.

Mercer K, Giblett S, Green S, Lloyd D, Dias SD, Plumb M, Marais R, Pritchard C. 2005. Expression of Endogenous Oncogenic ^{V600E}B-raf Induces Proliferation and Developmental Defects in Mice and Transformation of Primary Fibroblasts. Cancer Research. 65(24), 11493–11500.

Mione MC, Trede NS. 2010. The zebrafish as a model for cancer. Disease Models & Mechanisms. 3(9-10), 517–523.

Mitsutake N, Knauf JA, Mitsutake S, Mesa C Jr, Zhang L, Fagin JA. 2005. Conditional BRAFV600E expression induces DNA synthesis, apoptosis, dedifferentiation, and chromosomal instability in thyroid PCCL3 cells. Cancer Research. 65(6):2465-73.

Morita N, Ikeda Y, Takami H. 2008. Clinical significance of p53 protein expression in papillary thyroid carcinoma. World Journal of Surgery. 32(12):2617-22.

Muzza M, Colombo C, Rossi S, Tosi D, Cirello V, Perrino M, De Leo S, Magnani E, Pignatti E, Vigo B, Simoni M, Bulfamante G, Vicentini L, Fugazzola L. 2015. Telomerase in differentiated thyroid cancer: promoter mutations, expression and localization. Molecular and Cellular Endocrinology. 5;399:288-95.

Nikiforov YE. 2002. RET/PTC rearrangement in thyroid tumors. Endocrine Pathology. 13 3–16.

Nikiforov YE. 2008. Thyroid Carcinoma: Molecular Pathways and Therapeutic Targets. Modern Pathology : An Official Journal of the United States and Canadian Academy of Pathology, Inc. 21(Suppl 2), S37–S43.

Nikiforov YE. 2012. Thyroid tumors: classification, staging and general considerations. In: , Nikiforov Y , Biddinger PW , Thompson LDR, eds. Diagnostic pathology and molecular genetics of the thyroid. Baltimore: Lippincott Williams &Wilkins. 108–118.

Nikiforova MN, Kimura ET, Gandhi M, Biddinger PW, Knauf JA, Basolo F, Zhu Z, Giannini R, Salvatore G, Fusco A, Santoro M, Fagin JA, Nikiforov YE. 2003. BRAF mutations in thyroid tumors are restricted to papillary carcinomas and anaplastic or poorly differentiated carcinomas arising from papillary carcinomas. The Journal of Clinical Endocrinology & Metabolism. 88:5399–404.

Nonoguchi N, Ohta T, Oh JE, Kim YH, Kleihues P, Ohgaki H. 2013. TERT promoter mutations in primary and secondary glioblastomas. Acta Neuropathology. 126(6):931–7.

Olivier M, Eeles R, Hollstein M, Khan MA, Harris CC, Hainaut P. 2002. The IARC TP53 database: new online mutation analysis and recommendations to users. Human Mutation. 19(6):607–14.

Opitz R, Maquet E, Huisken J, Antonica F, Trubiroha A, Pottier G, Janssens V, Costagliola S. 2012. Transgenic zebrafish illuminate the dynamics of thyroid morphogenesis and its relationship to cardiovascular development. Developmental Biology. 372(2):203–16.

Opitz R, Maquet E, Zoenen M, Dadhich R, Costagliola S. 2011. TSH receptor function is required for normal thyroid differentiation in zebrafish. Molecular Endocrinology. 25(9):1579–99

Palona I, Namba H, Mitsutake N, Starenki D, Podtcheko A, Sedliarou I, Ohtsuru A, Saenko V, Nagayama Y, Umezawa K, Yamashita S. 2006. BRAFV600E promotes invasiveness of thyroid cancer cells through nuclear factor kappaB activation. Endocrinology. 147(12):5699–707.

Parichy DM, Elizondo MR, Mills MG, Gordon TN, Engeszer RE. 2009. Normal Table of Post-Embryonic Zebrafish Development: Staging by Externally Visible Anatomy

of the Living Fish. Developmental Dynamics : An Official Publication of the American Association of Anatomists. 238(12), 2975–3015.

Park YJ, Kim YA, Lee YJ, Kim SH, Park SY, Kim KW, Chung JK, Youn YK, Kim KH, Park do J, Cho BY. 2010. Papillary microcarcinoma in comparison with larger papillary thyroid carcinoma in BRAF(V600E) mutation, clinicopathological features, and immunohistochemical findings. Head Neck. 32:38–45.

Patton EE, Widlund HR, Kutok JL, Kopani KR, Amatruda JF, Murphey RD, Berghmans S, Mayhall EA, Traver D, Fletcher CD, Aster JC, Granter SR, Look AT, Lee C, Fisher DE, Zon LI. 2005. BRAF mutations are sufficient to promote nevi formation and cooperate with p53 in the genesis of melanoma. Current Biology. 15(3):249–54.

Phay JE, Shah MH. 2010. Targeting RET receptor tyrosine kinase activation in cancer. Clinical Cancer Research. 16(24):5936–5941.

Pliss GB, Zabezhinski MA, Petrov AS, Khudoley VV. 1982. Peculiarities of N-nitramines carcinogenic action. Arch Geschwulstforsch. 52(8):629–34.

Porazzi P, Calebiro D, Benato F, Tiso N, Persani L. 2009. Thyroid gland development and function in the zebrafish model. Molecular and Cellular Endocrinology. 27;312(1–2):14–23

Porazzi P, Marelli F, Benato F, de Filippis T, Calebiro D, Argenton F, Tiso N, Persani L. 2012. Disruptions of global and JAGGED1-mediated notch signaling affect thyroid morphogenesis in the zebrafish. Endocrinology. 153(11):5645–58.

Pratilas CA, Taylor BS, Ye Q, Viale A, Sander C, Solit DB, and Rosen N. 2009. ^{V600E}BRAF is associated with disabled feedback inhibition of RAF–MEK signaling and elevated transcriptional output of the pathway. Proceedings of the National Academy of Sciences of the United States of America. 106(11), 4519–4524.

Prehn RT. 2005. The role of mutation in the new cancer paradigm. Cancer Cell International. 5, 9.

Preto A, Singhrao SK, Haughton MF, Kipling D, Wynford-Thomas D, Jones CJ. 2004. Telomere erosion triggers growth arrest but not cell death in human cancer cells

retaining wild-type p53: implications for antitelomerase therapy. Oncogene. 23(23):4136-45.

Riesco-Eizaguirre G, Gutiérrez-Martínez P, García-Cabezas MA, Nistal M, Santisteban P. 2006. The oncogene BRAF V600E is associated with a high risk of recurrence and less differentiated papillary thyroid carcinoma due to the impairment of Na+/I- targeting to the membrane. Endocrine-Related Cancer. 13(1):257-69.

Riesco-Eizaguirre G, Rodríguez I, De la Vieja A, Costamagna E, Carrasco N, Nistal M, Santisteban P. 2009. The BRAFV600E oncogene induces transforming growth factor beta secretion leading to sodium iodide symporter repression and increased malignancy in thyroid cancer. Cancer Research. 69(21):8317-25.

Robu ME, Larson JD, Nasevicius A, Beiraghi S, Brenner C, Farber SA, Ekker SC. 2007. p53 Activation by Knockdown Technologies. PLoS Genetics. *3*(5), e78.

Rohr KB, Concha ML. 2000. Expression of nk2.1a during early development of the thyroid gland in zebrafish. Mechanisms of Development. 95(1-2):267-70.

Ros P, Rossi DL, Acebrón A, Santisteban P. 1999. Thyroid-specific gene expression in the multi-step process of thyroid carcinogenesis. Biochimie. 81(4):389-96.

Rudner LA, Brown KH, Dobrinski KP, Bradley DF, Garcia MI, Smith AC, Downie JM, Meeker ND, Look AT, Downing JR, Gutierrez A, Mullighan CG, Schiffman JD, Lee C, Trede NS, Frazer JK. 2011. Shared acquired genomic changes in zebrafish and human T-ALL. Oncogene. 30(41):4289-96.

Saad AG, Kumar S, Ron E, Lubin JH, Stanek J, Bove KE, Nikiforov YE. 2006. Proliferative activity of human thyroid cells in various age groups and its correlation with the risk of thyroid cancer after radiation exposure. The Journal of Clinical Endocrinology & Metabolism. 91(7):2672-7.

Saji M, and Ringel MD. 2010. The PI3K-AKT-mTOR pathway in initiation and progression of thyroid tumors. Molecular and Cellular Endocrinology. 321(1), 20-28.

Saji M, Xydas S, Westra WH, Liang CK, Clark DP, Udelsman R, Umbricht CB, Sukumar S, Zeiger MA. 1999. Human telomerase reverse transcriptase (hTERT) gene expression in thyroid neoplasms. Clinical Cancer Research. 5:1483–1489.

Samuels Y, Wang Z, Bardelli A, Silliman N, Ptak J, Szabo S, Yan H, Gazdar A, Powell SM, Riggins GJ, Willson JK, Markowitz S, Kinzler KW, Vogelstein B, Velculescu VE. 2004. High frequency of mutations of the PIK3CA gene in human cancers. Science. 304(5670):554.

Sanchini MA, Gunelli R, Nanni O, Bravaccini S, Fabbri C, Sermasi A, Bercovich E, Ravaioli A, Amadori D, Calistri D. 2005. Relevance of urine telomerase in the diagnosis of bladder cancer. JAMA. 294, 2052–2056.

Santarpia L, Myers JN, Sherman SI, Trimarchi F, Clayman GL, El-Naggar AK. 2010. Genetic alterations in the RAS/RAF/mitogen-activated protein kinase and phosphatidylinositol 3-kinase/Akt signaling pathways in the follicular variant of papillary thyroid carcinoma. Cancer. 15;116(12):2974-83.

Santoro M, Melillo RM, Carlomagno F, Fusco A, Vecchio G. 2002. Molecular mechanisms of RET activation in human cancer. Annals of the New York Academy of Sciences. 963:116–121.

Sarkisian CJ, Keister BA, Stairs DB, Boxer RB, Moody SE, Chodosh LA. 2007. Dose-dependent oncogene-induced senescence in vivo and its evasion during mammary tumorigenesis. Nature Cell Biology. 9(5):493–505.

Shimamura M, Nakahara M, Orim F, Kurashige T, Mitsutake N, Nakashima M, Kondo S, Yamada M, Taguchi R, Kimura S, Nagayama Y. 2013. Postnatal expression of BRAFV600E does not induce thyroid cancer in mouse models of thyroid papillary carcinoma. Endocrinology.154(11):4423–30.

Skvortzov DA, Rubzova MP, Zvereva ME, Kiselev FL, and Donzova OA. 2009. The Regulation of Telomerase in Oncogenesis. Acta Naturae. 1(1), 51–67.

Soares P, Cameselle-Teijeiro J, Sobrinho-Simões M. 1994. Immunohistochemical detection of p53 in differentiated, poorly differentiated and undifferentiated carcinomas of the thyroid. Histopathology. 24(3):205-10.

Soares P, Lima J, Preto A, Castro P, Vinagre J, Celestino R, Couto JP, Prazeres H, Eloy C, Máximo V, Sobrinho-Simões M. 2011. Genetic alterations in poorly differentiated and undifferentiated thyroid carcinomas. Current Genomics. 12(8):609-17.

Soares P, Lima J, Preto A, Castro P, Vinagre J, Celestino R, Couto JP, Prazeres H, Eloy C, Máximo V, Sobrinho-Simões, M. 2011. Genetic Alterations in Poorly Differentiated and Undifferentiated Thyroid Carcinomas. Current Genomics. 12(8), 609–617.

Soares P, Trovisco V, Rocha AS, Feijão T, Rebocho AP, Fonseca E, Vieira de Castro I, Cameselle-Teijeiro J, Cardoso-Oliveira M, Sobrinho-Simões M. 2004. BRAF mutations typical of papillary thyroid carcinoma are more frequently detected in undifferentiated than in insular and insular-like poorly differentiated carcinomas. Virchows Arch. 444(6):572-6.

Soares P, Trovisco V, Rocha AS, Lima J, Castro P, Preto A, Maximo V, Botelho T, Seruca R, Sobrinho-Simões M. 2003. BRAF mutations and RET/PTC rearrangements are alternative events in the etiopathogenesis of PTC. Oncogene. 22:4578–4580.

Storer NY, Zon LI. 2010. Zebrafish models of p53 functions. Cold Spring Harb Perspect Biol. 2(8):a001123.

Strahl T, Gille H, Shaw PE. 1996. Selective response of ternary complex factor Sap1a to different mitogen-activated protein kinase subgroups. Proceedings of the National Academy of Sciences of the United States of America. 93:11563–11568.

Sun H, Lesche R, Li, D-M, Liliental J, Zhang H, Gao J, Gavrilova N, Mueller B, Liu X, Wu H. 1999. PTEN modulates cell cycle progression and cell survival by regulating phosphatidylinositol 3,4,5,-trisphosphate and Akt/protein kinase B signaling pathway. Proceedings of the National Academy of Sciences of the United States of America. 96(11), 6199–6204.

Tang KT, Lee CH. 2010. BRAF mutation in papillary thyroid carcinoma: pathogenic role and clinical implications. Journal of the Chinese Medical Association. 73(3):113-28.

Teng KK, Hempstead BL. 2004. Neurotrophins and their receptors: signaling trios in complex biological systems. Cellular and Molecular Life Sciences. 61:35-48.

Tronko MD, Howe GR, Bogdanova TI, Bouville AC, Epstein OV, Brill AB, Likhtarev IA, Fink DJ, Markov VV, Greenebaum E et al. 2006. A cohort study of thyroid cancer and other thyroid diseases after the Chornobyl accident: thyroid cancer in Ukraine detected during first screening. Journal of the National Cancer Institute. 98:897-903.

Trovisco V, Soares P, Preto A, Castro P, Máximo V, Sobrinho-Simões M. 2007. Molecular genetics of papillary thyroid carcinoma: great expectations. Arquivos Brasileiros de Endocrinologia & Metabologia. 51(5):643-53.

Trovisco V, Soares P, Soares R, Magalhães J, Sá-Couto P, Sobrinho-Simões M. 2005. A new BRAF gene mutation detected in a case of a solid variant of papillary thyroid carcinoma. Human Pathology. 36(6):694-7.

Umbricht CB, Saji M, Westra WH, Udelsman R, Zeiger MA, Sukumar S. 1997. Telomerase activity: a marker to distinguish follicular thyroid adenoma from carcinoma. Cancer Research. 57(11):2144-7.

VanPutte C, Regan J, Russo A. 2000. Seeley's Anatomy & Physiology, ed 9, McGraw-Hill.

Vinagre J, Almeida A, Pópulo H, Batista R, Lyra J, Pinto V, Coelho R, Celestino R, Prazeres H, Lima L, Melo M, da Rocha AG, Preto A, Castro P, Castro L, Pardal F, Lopes JM, Santos LL, Reis RM, Cameselle-Teijeiro J, Sobrinho-Simões M, Lima J, Máximo V, Soares P. 2013. Frequency of TERT promoter mutations in human cancers. Nature Communications. 4:2185.

Vinagre J, Pinto V, Celestino R, Reis M, Pópulo H, Boaventura P, Melo M, Catarino T, Lima J, Lopes JM, Máximo V, Sobrinho-Simões M, Soares P. 2014. Telomerase

promoter mutations in cancer: an emerging molecular biomarker? Virchows Archive. 465(2):119-33.

Vitagliano D, Portella G, Troncone G, Francione A, Rossi C, Bruno A, Giorgini A, Coluzzi S, Nappi TC, Rothstein JL, Pasquinelli R, Chiappetta G, Terracciano D, Macchia V, Melillo RM, Fusco A, Santoro M. 2006. Thyroid targeting of the N-ras(Gln61Lys) oncogene in transgenic mice results in follicular tumors that progress to poorly differentiated carcinomas. Oncogene. 25(39):5467-74.

Vizioli MG, Possik PA, Tarantino E, Meissl K, Borrello MG, Miranda C, Anania MC, Pagliardini S, Seregni E, Pierotti MA, Pilotti S, Peeper DS, Greco A. 2011. Evidence of oncogene-induced senescence in thyroid carcinogenesis. Endocrine-Related Cancer. 18(6):743-57.

Wajapeyee N, Serra RW, Zhu X, Mahalingam M, Green MR. 2008. Oncogenic BRAF Induces Senescence and Apoptosis through Pathways Mediated by the Secreted Protein IGFBP7. Cell. 132(3), 363-374.

Wan PT, Garnett MJ, Roe SM, Lee S, Niculescu-Duvaz D, Good VM, Jones CM, Marshall CJ, Springer CJ, Barford D, Marais R; Cancer Genome Project 2004. Mechanism of activation of the RAF-ERK signaling pathway by oncogenic mutations of B-RAF. Cell. 116:855-867.

Wang N, Liu T, Sofiadis A, Juhlin CC, Zedenius J, Höög A, Larsson C, Xu D. 2014. TERT promoter mutation as an early genetic event activating telomerase in follicular thyroid adenoma (FTA) and atypical FTA. Cancer. 120(19):2965-79.

Wang Y, Hou P, Yu H, Wang W, Ji M, Zhao S, Yan S, Sun X, Liu D, Shi B, Zhu G, Condouris S, Xing M. 2007. High prevalence and mutual exclusivity of genetic alterations in the phosphatidylinositol-3-kinase/akt pathway in thyroid tumors. The Journal of Clinical Endocrinology & Metabolism. 92(6):2387-90.

Wangari-Talbot J, Chen S. 2012. Genetics of melanoma. Frontiers in Genetics. 3, 330.

Wendl T, Lun K, Mione M, Favor J, Brand M, Wilson SW, Rohr KB. 2002. Pax2.1 is required for the development of thyroid follicles in zebrafish. Development. 129(15):3751–60.

Westerfield M. 2000. The zebrafish book. A guide for the laboratory use of zebrafish (Danio rerio). 4th ed., Univ. of Oregon Press, Eugene

White R, Rose K, Zon L. 2013. Zebrafish cancer: the state of the art and the path forward. Nature Reviews Cancer. 13(9):624–36.

Whitmarsh AJ, Shore P, Sharrocks AD, Davied RJ. 1995. Integration of MAP kinase signal transduction pathways at the serum response element. Science. 269:403–407.

Woodman SE, Mills GB. 2010. Are oncogenes sufficient to cause human cancer? Proceedings of the National Academy of Sciences of the United States of America. 107(48), 20599–20600.

Wu GS. 2004. The functional interactions between the p53 and MAPK signaling pathways. Cancer Biology & Therapy. 3(2):156–61.

Xing M, Liu R, Liu X, Murugan AK, Zhu G, Zeiger MA, Pai S, Bishop, J. 2014. BRAF V600E and TERT Promoter Mutations Cooperatively Identify the Most Aggressive Papillary Thyroid Cancer With Highest Recurrence. Journal of Clinical Oncology, 32(25), 2718–2726.

Xing M. 2005. BRAF mutation in thyroid cancer. Endocrine-Related Cancer. 12:245–262.

Xing M. 2010. Genetic Alterations in the Phosphatidylinositol-3 Kinase/Akt Pathway in Thyroid Cancer. Thyroid. 20(7), 697–706.

Xing M. 2012. $BRAF^{V600E}$ Mutation and Papillary Thyroid Cancer: Chicken or Egg? The Journal of Clinical Endocrinology and Metabolism. 97(7), 2295–2298.

Xing M. 2013. Molecular pathogenesis and mechanisms of thyroid cancer. Nature Reviews: Cancer. 13(3), 184–199.

Xu X, Quiros RM, Gattuso P, Ain KB, Prinz RA. 2003. High prevalence of BRAF gene mutation in papillary thyroid carcinomas and thyroid tumor cell lines. Cancer Research. 63:4561–4567.

Xu Y, Fang F, Ludewig G, Jones G, Jones D. 2004. A mutation found in the promoter region of the human survivin gene is correlated to overexpression of survivin in cancer cells. DNA and Cell Biology. 23(7): 419–429.

Yamamoto T, Ebisuya M, Ashida F, Okamoto K, Yonehara S, Nishida E. 2006. Continuous ERK activation downregulates antiproliferative genes throughout G1 phase to allow cell-cycle progression. Current Biology. 16(12):1171–82.

Yamashita, AS, Geraldo, MV, Fuziwara, CS, Kulcsar, MAV, Friguglietti, CUM, da Costa, RB, Baia GS, Kimura, E. T. 2013. Notch Pathway Is Activated by MAPK Signaling and Influences Papillary Thyroid Cancer Proliferation. Translational Oncology. 6(2), 197–205.

Yap AS, Brieher WM, Gumbiner BM. 1997. Molecular and functional analysis of cadherin-based adherens junctions. Annual Review of Cell and Developmental Biology. 13:119–46.

Yu H, McDaid R, Lee J, Possik P, Li L, Kumar SM, Elder DE, Van Belle P, Gimotty P, Guerra M, Hammond R, Nathanson KL, Dalla Palma M, Herlyn M, Xu X. 2009. The Role of *BRAF* Mutation and p53 Inactivation during Transformation of a Subpopulation of Primary Human Melanocytes. The American Journal of Pathology. 174(6), 2367–2377.

Zhu Z, Gandhi M, Nikiforova MN, Fischer AH, Nikiforov YE. 2003. Molecular profile and clinical-pathologic features of the follicular variant of papillary thyroid carcinoma: An unusually high prevalence of ras mutations. American Journal of Clinical Pathology. 120:71.

Appendix A

Chapter 4

Etiopathogenic factors of thyroid cancer

Ana Lourenço Almeida, Paula Boaventura & Paula Soares

Thyroid cancer is the most common endocrine malignancy, with more deaths annually than all of the other endocrine cancers combined [1]. In the last few years, its frequency has been rising, with the highest rate of increase for small and localized thyroid cancers. This led many authors to suggest that this increase is attributable to better cancer detection and early diagnosis through ultrasonography and fine-needle aspiration biopsies [1,2]. However, it is most likely that this is not the sole reason and other factors probably play a role, namely radiation exposure (therapeutic and fallout) [1,2], chemical environment carcinogens, autoimmune phenomena and alterations in iodine intake [1]. In this chapter, environmental risk factors for thyroid cancer will be addressed, giving a particular emphasis on ionizing radiation and endocrine disruptors.

doi:10.2217/EBO.13.37

Aa Ionizing radiation: type of radiation (e.g., x-rays or γ-rays) that has the ability to penetrate material inducing a process called ionization (any process by which a neutral atom or molecule gains or loses electrons, acquiring a net charge). It comes from radioactive materials or radiation generators.

Ionizing radiation

Ionizing radiation is a major risk factor for thyroid cancer and particularly for papillary thyroid cancer (PTC), the most common type of thyroid cancer [2]. The thyroid is unusually sensitive to external and internal radiation, and it is, in fact, an organ with a documented rise in cancer incidence after radiation exposure, especially during childhood [1]. The pathophysiology of radiation-induced thyroid damage includes:

- Short-term effects, related to direct damage of the parenchymal cells that causes an inhibition of follicular epithelial function;
- Late sequelae caused by cell death, autoimmune reactions, chronic inflammation, vascular toxicity, fibrous organization and partial epithelial regeneration [3,4]. Thyroid cancer can be a long-term consequence of radiation. This risk is modulated by other factors, such as age, gender, dose and type of radiation.

Thyroid exposure to irradiation (internal vs external radiation)

Exposure of the thyroid to radiation can result from exposure to an external source (external radiation) or to radioactive material that enters the body (internal radiation).

Internal radiation exposure results from radioactive isotopes that enter the body by ingestion, inhalation or absorption. The radioactive isotopes recognized as the most important in this context are iodine isotypes, namely Iodine-131 and Iodine-133.

Most of the information on thyroid cancer risk and internal radiation came from studies on the health effects of nuclear power tests/accidents, notably the Chernobyl accident; before this evidence, internal radiation was believed to have relatively low potential risk [5]. The first years after the Chernobyl accident allowed several striking epidemiological observations, namely an increased incidence in thyroid cancer, particularly pronounced among the youngest at the time of exposure (0–4 years of age). Given the huge amount of radioiodine isotopes released, the radiation dose to the thyroid gland was estimated to be 1000–10,000-times higher than to any other organ [6], and the thyroid of young children was revealed to be extremely sensitive to those radioiodines [5]. Moreover, it was possible to detect that iodine deficiency and radiation dose from the Chernobyl fallout acted jointly, with a twofold higher excess relative risk observed in areas of

Gray (Gy) is the unit of the International Unit System. Radiation dose absorbed by a specific organ or tissue per unit of mass.

severe iodine deficiency compared with iodine-sufficient areas [5]. Thirty-six years after the accident, thyroid cancer risk in exposed young people continues to be significantly elevated.

Curiously, diagnostic or therapeutic use of radioiodine did not show evidence of increased risk of thyroid cancer; this may simply be related to radiation exposure at an older age when the thyroid has a lower sensitivity to the carcinogenic effects of radiation [6,7], or to the dose applied, which results mainly in a cytotoxic effect.

Evidence for the etiopathogenic role of external radiation for thyroid cancer came from studies of atomic bomb survivors and from cohorts of individuals subjected to therapeutic or esthetic external radiation. Between 1920 and 1960, external radiation was used for a variety of head and neck benign conditions, namely x-ray scalp epilation for tinea capitis treatment. This kind of procedure has been shown to increase the risk for thyroid cancer [8,9]. By conducting a retrospective and prospective study in a Portuguese cohort subjected to x-ray scalp epilation for tinea capitis treatment, we observed an increased prevalence (2.6%) of thyroid cancer [9]. Sadetzki *et al.*, in a retrospective study performed in a similar cohort from Israel, found a thyroid cancer prevalence of 0.95% in the irradiated individuals compared with 0.35% in two matched nonirradiated groups [8].

Presently, people still can be exposed to (external or internal) radiation, namely in the setting of incidental nuclear accidents (as recently verified in Fukushima, Japan), radiotherapy, diagnostic examinations and selected occupations (e.g., radiologists).

Among the atomic bomb survivors, thyroid cancer was one of the earliest solid cancers linked to external radiation exposure [1,10]. Radiotherapy for head and neck cancers, thorax cancers, lymphomas, breast cancers and whole-body irradiation may expose the thyroid to radiation due to its anatomical position [4]. Treatment-related secondary cancers are becoming a disturbing problem as survival from the majority of childhood cancers is relatively high and is continuing to improve [11]. An update from the Childhood Cancer Survivor Study confirmed the previously established dose–response relationships and estimated odds ratios for the development of thyroid cancer after high-dose therapy in childhood (odds ratio: 9.8; 95% CI: 3.2–34.8), as well as the fall-off risk at doses exceeding 20–25 Gy, thought to be attributable to cell killing [12].

Presently, diagnostic computed tomography (CT) scanning is the major source of x-ray exposure by medical means [13]. CT involves much larger radiation doses compared with conventional x-ray imaging procedures;

the typical organ dose from a CT scan is 0.01–0.02 Gy [11]. There is increasing concern regarding radiation exposure to the thyroid gland from pediatric CT scans, especially if an iodinated contrast is used. It appears that many physicians are ill-informed about the risks of diagnostic examinations using radiation, so there is a clear need to educate the medical profession and the general public about the risks regarding CT imaging [11].

Although there are some differences between internal and external radiation exposure, the magnitude of excess cancer risk and the findings for effect modification by age at exposure and gender are generally compatible.

Risk factors for irradiation-induced thyroid cancer: age, gender & dose

A major risk factor for radiation-induced thyroid cancer is young age at exposure – the maximum risk is when the exposure occurs below the age of 5 years; above the age of 15–25 years the risk is only slightly increased compared with adults [6]. Importantly, the excess risk persists for at least 40 years after exposure [8,14].

It has been suggested that children develop radiation-related cancer more often than adults because their tissues are actively growing and cells are dividing more rapidly, so they are more susceptible to the mutagenic effects of radiation [1,11]. Moreover, children have a longer life expectancy compared with adults, therefore presenting a longer period for the expression of radiation-induced cancers. Consequently, the adverse effects of radiation are much greater in children than in adults. Keeping this line of thought, one could expect the fetus to be highly vulnerable to radiation exposure. However, information about thyroid cancer risks associated with *in utero* exposure to Chernobyl fallout is very limited [5]. Clearly, this issue will need additional research to establish the relative radiosensitivity of the prenatal versus the postnatal versus the adult thyroid gland [11].

PTC affects women more than men, although until puberty the sex ratio is relatively equal [1]. It is predicted that, in the near future, thyroid cancer will be one of the five leading causes of new cancers in women, representing 5% of all cancers [15], and the fastest growing cancer in this gender [2]. The additional risk of thyroid cancer in radiation-exposed individuals was estimated to be 4–12-times higher in females than in males [6]. A higher radiosensitivity in women has been discussed but the mechanisms underlying that radiosensivity are not yet established.

The question of gender as a risk factor for thyroid cancer has been puzzling since, in spite of the clearly increased risk in women, it seems that the

disease may be more aggressive in men [1]. It is also important to refer to the fact that prepubertal and postmenopausal incidence rates are no greater in women than in men, so it has been repeatedly suggested that the female preponderance may be due to estrogen or other gender-related hormonal factors.

Any irradiation to the thyroid involving more than 0.5 Gy, in particular during childhood, should be viewed with concern [3]; for some authors, doses as low as 0.05–0.1 Gy may cause apprehension [8,14]. With the data presently reported in the literature, there remains uncertainty about the doses of irradiation that the thyroid tolerates, as well as about the dose–volume and dose–time relationships [4]. Therefore, it is recommended that the radiation dose that the thyroid will receive in the diagnostic and/or therapeutic context is limited.

Radiation-induced thyroid cancer: biological & genetic aspects

The mechanisms through which radiation induces thyroid tumors are still poorly understood [6]. Moreover, it is not known with certainty whether radiation-related thyroid cancer has the same clinical behavior as sporadic thyroid cancer [11]. Some studies find radiation-related thyroid tumors as being frequently multifocal, although they do not demonstrate that these differences imply a different tumor behavior; on the contrary, other studies suggest that these tumors present a more aggressive clinical course [11].

Histological differences have also been reported. PTC was the most common histological type found among post-Chernobyl cases and the tumors were more often of the solid/follicular subtype than of the classical papillary type [5]. The solid architecture, exclusively or admixed with other architectural patterns, commonly observed in the post-Chernobyl cases, is less frequent in thyroid tumors without history of radiation exposure [2].

Concerning molecular alterations, the most common mutational mechanism in radiation-induced thyroid tumors consists of chromosomal rearrangements, notably the *RET/PTC* rearrangements, which can be found, in some series, in up to 80% of these tumors **(Table 4.1)** [2,6]. In sporadic nonirradiated thyroid tumors, the frequency of these rearrangements can be as low as 5–15% [6]. In sporadic tumors, the most prevalent mutation mechanism is point mutation, typically involving the *BRAF* and *RAS* genes [2]. *BRAF* mutations are infrequent events in thyroid cancers from subjects exposed to radiation, both internal and external [16,17]. *BRAF* mutations and *RET/PTC* rearrangements are usually alternative events in the etiopathogenesis of PTC [18], but recently Dinets *et al.* found the co-occurrence of *RET/PTC* and *BRAF* mutation in four PTCs from post-Chernobyl cases [19].

Table 4.1. The most frequent genetic alterations in sporadic versus radiation-associated thyroid cancer.

Cancer type	*BRAF* mutations (%)	*NRAS* mutations (%)	*RET/PTC* rearrangements (%)
Sporadic thyroid cancer	30–69	10–20	5–40
Radiation-associated thyroid cancer	4–24	ND	50–80

ND: Not defined.

Efforts are being made to develop strategies that would distinguish a thyroid carcinoma caused by radiation from one that is not, as neither the histological features nor the genetic alterations observed in these tumors have shown to be specific fingerprints of exposure to radiation [20]. Ory *et al.*, using microarray transcriptome profiles, identified a signature of 322 genes that allowed the discrimination of postradiotherapy-induced tumors from their sporadic counterparts, with an efficacy of 90% [20]. They suggest that the same strategy could be applied to classify post-Chernobyl thyroid tumors.

Clinical management of radiation-related thyroid tumors

All subjects exposed to radiation during childhood should be submitted to a life-long follow-up that will take into account the risk factors for developing a thyroid carcinoma: female gender, a young age at irradiation, high irradiation dose, and personal or family history of radiation-associated tumors [6]. In this follow-up, neck palpation and neck ultrasonography should be performed every 1–3 years, depending on the risk factors. Thyroid nodules ≤1 cm only need to be controlled with ultrasonography 6–12 months later. Any thyroid nodule ≥1 cm should be submitted to a fine-needle aspiration biopsy; the results will decide on the need for further treatment (including surgery).

Imaizumi *et al.*, in a long-term follow-up study, demonstrated a high risk for thyroid cancer in atomic bomb survivors with solid thyroid nodules compared with nodule-free survivors [21]. Therefore, in accordance with what was reported by Rubino *et al.* [6], they proposed that irradiated individuals with thyroid nodules should be followed carefully, not only by ultrasonography but also by biopsy, irrespective of age, sex, thyroglobulin level, thyroid-stimulating hormone (TSH) level, thyroid radiation dose or nodule volume, because none of these factors predicted the development of cancer. They recommend at least biennial follow-up, even if the nodules are diagnosed as benign [21].

Endocrine disruptors

Aa Endocrine disruptors: substances in the environment, food and consumer products that interfere with the synthesis, secretion, transport, metabolism, binding action or elimination of the hormones responsible for homeostasis.

The relationship between thyroid dysfunction and cancer has been studied for years and there is now evidence that points to a bilateral association linking both. Thyroid dysfunction triggered by factors such as endocrine disruptors may ultimately contribute to cancer, whereas thyroid cancer may induce dysfunction of the thyroid gland.

The endocrine disruptor hypothesis was postulated in the early 1990s, when a report linked fetal exposure to the synthetic estrogen diethylstilbestrol with the development of a very rare clear-cell carcinoma of the vagina. It did not take long to realize the complexity of the effects upon exposure to endocrine disruptors.

The group of molecules identified as endocrine disruptors is very heterogeneous and can adversely impact a number of hormonal systems. In a scientific statement published by The Endocrine Society, the endocrine disruptors are defined as "compounds natural or synthetic which through environmental or inappropriate developmental exposures alter the hormonal and homeostatic systems that enable the organism to communicate with and respond to its environment" [22]. The statement supports the relationship connecting environmental exposure to the disruptors with effects not only on the endocrine but also on the nervous system.

Concerning the thyroid, it has been shown that thyroid disruptors (TDs), ranging from industrial chemicals to natural substances, may interfere with the complex regulatory system of the thyroid. Broadly defined, TDs are capable of altering the structure and function of the thyroid gland and of the regulatory enzymes associated with thyroid homeostasis, or changing the circulating and tissue concentrations of thyroid hormones [22]. Howdeshell [23] and Bruker-Davis [24] extensively reviewed many TDs and summarized the effects of these chemicals on thyroid metabolism by citing wildlife and experimental animal and human studies. We will next focus on the more relevant TDs.

Perchlorates & polychlorinated biphenyls as TDs

Perchlorate is a chemical found naturally in the soil that has been used as an oxidant in solid rocket propellants, ordnance, fireworks and airbag systems, for example. Its environmental stability has led to contamination in drinking and irrigation waters and in food [25]. The effects of perchlorate as a TD were extensively studied in animal models, and the main effect is

competitive inhibition of the sodium iodide symporter (NIS), leading to triiodothyronine (T3) and thyroxine (T4) suppression [24,26]. In fact, perchlorate has been used in the treatment of hyperthyroidism. Blount *et al.* reported that increased levels of urinary perchlorate were found to be predictive of significantly lower levels of serum T4 and significantly higher levels of serum TSH in women with urine iodine concentrations below 100 µg/l (median level that indicates a prevalence of goiter in a population due to dietary iodine insufficiency). Nevertheless, urine perchlorate was only a significant positive predictor of serum TSH, but not serum T4, in females with urinary iodine above 100 µg/l. The same study observed a significantly greater effect of perchlorate on serum T4 in smokers, which may reflect a cumulative effect of perchlorate and thiocyanate, the latter being a metabolite of the goitrogen substance cyanide found in cigarettes [27]. Of note, increased levels of thiocyanate are associated with an increased thyroid volume and a higher risk for goiter development [28].

Exposure to perchlorate and other NIS competitors including nitrate and thiocyanate may have a significant effect on thyroid hormones, particularly in an iodine-insufficient dietary environment. Since infants are vulnerable to thyroid hormone insufficiency, and because breast milk is believed to have high levels of perchlorate, it was of concern that this chemical may affect thyroid hormone signaling in early developmental stages, although consistent studies failed to show such a relationship [22]. Other studies were less successful in finding a significant relationship between perchlorate exposure and thyroid parameters.

Polychlorinated biphenyls (PCBs) are industrial organochlorine compounds that exist in a variety of congeners, paired phenyl rings with various degrees of chlorination; their effect is congener-specific (dependent on the number and structural relation of chlorine atoms in the molecule). PCBs were phased out in the mid 1970s owing to their carcinogenic potential but these chemicals still persist in the environment by resisting to molecular degradation. The most threatening PCBs are those with a higher degree of chlorination at meta- and para-positions, owing to its structural resemblance to T4 and its persistence in human and animal tissues [29]. PCBs were shown to affect thyroid function on many levels: reduce the ability of thyroid hormones to bind to transthyretin (TTR), since they are a potent competitive inhibitor; upregulate liver enzymes that metabolize thyroid hormones; inhibit or upregulate the production of deiodinases, which convert T4 to T3; and act as an agonist or antagonist on the thyroid receptor site [30]. Most studies have shown an inverse relationship between PCB exposure levels and serum levels of total T3,

total T4 and TSH; however, not all studies have agreed on the extent of the effects of thyroid disruption by PCBs. Unquestionably, PCBs are directly implicated in lower circulating levels of thyroid hormones, especially T4, and in thyroid toxicity [29], but the consequences of PCB exposure appear to be more complex given the 209 possible different chlorine substitution patterns on the bisphenyl backbone and derived metabolites [22].

PCB congeners can also affect gene expression in the brain by mimicking the effect of thyroid hormone, and can exert neurotoxic effects on the developing brain by causing a state of relative hypothyroidism [22]. Thus, the PCB effect is not directly restricted to the thyroid gland.

2,3,7,8-tetra-chloro-dibenzo-p-dioxin (TCDD) is thought to be the most toxic polychlorinated dibenzo-para-dioxin congener. In mice and rats, TCDD decreases T4 and increases TSH, and causes follicular cell adenomas of the thyroid gland, as well as carcinomas and fibrosarcomas in different sites [26,31]. Data from humans are scarce and come from cohort studies of populations exposed to industrial exposures and accidents, but the evidence is still limited. A cohort study revealed two cases of thyroid cancer out of 104 cancer cases, on an area contaminated with less than 5 µg/m^2 of 2,3,7,8-TCDD, due to an industrial accident. Other studies showed a significant increase of thyroid cancer in workers exposed to 2,3,7,8-TCDD compared with those nonexposed [31] and a significant increase in TSH levels for the group of war veterans with the highest exposure to 2,3,7,8-TCDD [26].

Impact of TDs on the thyroid axis

TDs may interfere with the regulatory network of thyroid hormone synthesis, metabolism and distribution, and affect various levels of endocrine regulation and feedback control **(Table 4.2)**, namely by:

- Inhibiting the iodide uptake at the follicular cell membrane
- Compromising the production and interconversion of thyroid hormones
- Disturbing the transport of thyroid hormones in the bloodstream
- Altering the enzyme-regulated metabolism of thyroid hormones
- Changing the thyroid receptor activity

Therefore, major targets of endocrine disruptors within the thyroid axis are the NIS, hemoprotein thyroperoxidase (TPO), the T4 distributor protein TTR, the deiodinases, the thyroid hormone-conjugating enzymes and the thyroid hormone receptor family **(Figure 4.1)**.

Table 4.2. The most important thyroid disruptors, their mechanisms of action and effects on thyroid hormones.

Thyroid disruptor	Mechanism	Effect on THs
Perchlorate, thiocyanate, bromate, nitrate	Competition with NIS	Decreased T3 and T4 synthesis
Methilmazole, amitrole, ehylenothiourea, mancozeb, benzophenone-2 and methylmercaptoimidazole, isoflavones and flavonoids	Blocking production and inhibition of TPO	Decreased T3 and T4 synthesis
PCBs, flame retardants, phthalates, the pesticide metabolite pentachlorophenol, synthetic flavonoids and plasticizers including bisphenol A	Competitive binding to TTR	Decreased T4 levels and compromise of fetal brain T4 production
Hydroxyl PCBs, flame retardants, tetrabromobisphenol A and bisphenol A and dioxins	Altering binding to thyroid receptor	Altered activation of thyroid hormone-dependent gene transcription
PCBs, FD&C red dye #3, octyl-methoxycinnamate, the pesticide methoxychlor and the toxic metals cadmium and lead	Inhibition of deiodinase activity	Decreased peripherical T3 synthesis
Hydroxylated PCBs, triclosan, pentachlorophenol, dioxins, acetochlor, phenobarbital, 3-methylcoanthrene and bisphenol A	Inhibition of diphosphoryl-glucuronosyl- and sulfo-transferases and enhanced hepatic metabolism	Deregulation of peripherical levels of T3 and increased biliary excretion of T3 and T4
Dichlorodiphenyltrichloroethane, PCBs	Inhibition of TSH receptor	Decreased T3 and T4 production

FD&C: Food, Drug and Cosmetics; NIS: Sodium iodide symporter; PCB: Polychlorinated biphenyl; T3: Triiodothyronine; T4: Thyroxine; TH: Thyroid hormone; TPO: Thyroperoxidase; TSH: Thyroid-stimulating hormone; TTR: Transthyretin.

The first step in thyroid hormone biosynthesis is the uptake of iodide into the follicular cell, which is mediated by the plasma membrane transport protein, the NIS. NIS (and possibly other auxiliary proteins responsible for building up the sodium gradient across the cell membrane) can be affected by TDs such as perchlorate, thiocyanate, bromate and nitrate, which, by competing with iodine for binding to the NIS, inhibit the uptake of iodide. It is likely that their disruptor effect on iodide uptake is dependent on the presence and concentration of other NIS inhibitors as well as iodine itself,

Figure 4.1. Major targets of disruption by endocrine disruptors within the thyroid hormone axis.

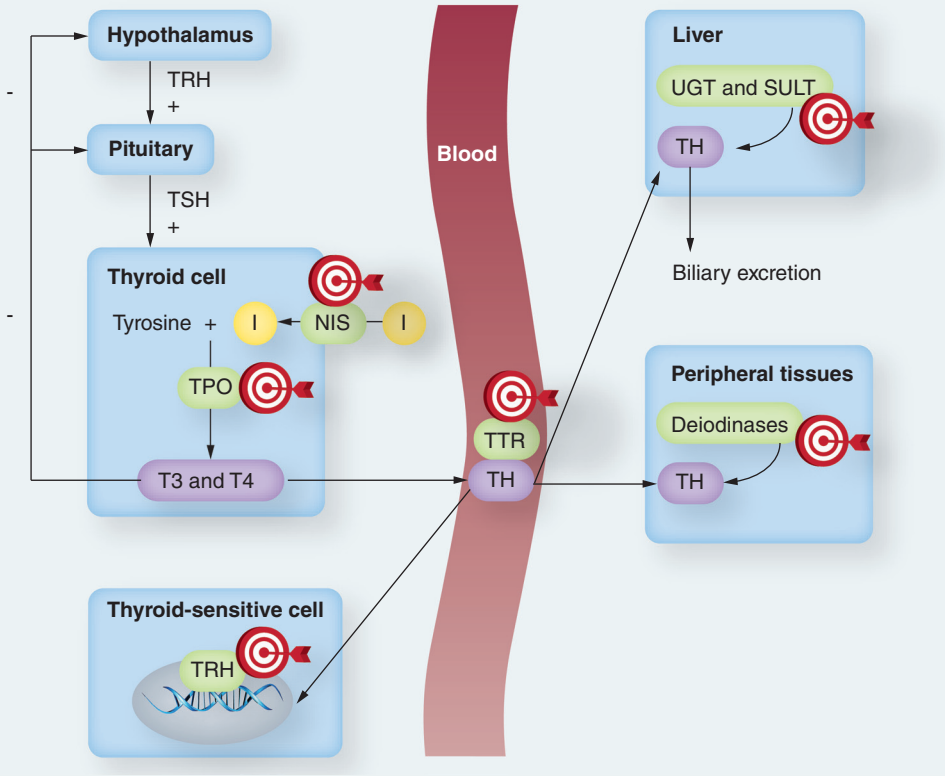

The NIS, the hemoprotein TPO, the T4 distributor protein TTR, the deiodinases, thyroid hormone-conjugating enzymes UGT and SULT, and the thyroid hormone receptor family are major targets of endocrine disruptors.
I: Iodine; NIS: Sodium iodide symporter; SULT: Sulfotransferase; T3: Triiodothyronine; T4: Thyroxine; TH: Thyroid hormone; TPO: Thyroperoxidase; TRH: Thyrotropin-releasing hormone; TSH: Thyroid-stimulating hormone; TTR: Transthyretin; UGT: Uridine 5'-diphospho-glucuronosyltransferase.

as it has been observed for perchlorate [32]. The effect of NIS disruptors is a decrease of T3 and T4 synthesis and they may exacerbate problems of iodine deficiency [25]. Of note, iodine deficiency, which has been associated with the risk of thyroid cancer and downregulation of NIS expression (observed in thyroid adenomas and carcinomas), when combined with the effect of disruptors of NIS activity can also be relevant in the carcinogenesis process.

TPO is an enzyme that plays a central role during thyroid hormone (T3 and T4) synthesis and is stimulated by the presence of TSH. Some TDs, namely

Aa Goitrogens: substances that inhibit the synthesis of the thyroid hormones. This results in increased levels of thyrotropin, which excessively stimulates thyroid cell growth, thereby causing goiter.

methilmazole, amitrole, ehylenothiourea, mancozeb, benzophenone-2 and methylmercaptoimidazole, appear to be able to inactivate TPO in one of at least three ways:

- By a reversible interaction that does not involve covalent binding;
- By an irreversible interaction requiring *de novo* synthesis of enzyme to restore its activity;
- By inhibiting the production of TPO. Thus, the synthesis of thyroglobulin and the production of T3 and T4 are compromised [33,34].

Furthermore, TPO seems to be a target of goitrogens, which are present in nutritive sources such as isoflavones, especially those found in soy protein, and also flavonoids. There is evidence of a mutual enhancement of the effects of iodine deficiency and nutritional or environmental goitrogens, probably via the inhibition of TPO, thus promoting goiter development, which has been related to thyroid neoplasia [28,30].

To maintain an extrathyroidal pool of thyroid hormones available for cellular use, transporter proteins bind to the T4 released in the bloodstream by the follicular cells. One of the transporter proteins is TTR. TTR binds to only 15–20% of the circulating T4 but it is crucial to deliver T4 across the blood–brain barrier and through the placenta. T4 binding to TTR is known to be very sensitive to the interference of endocrine disruptors, such as PCBs, flame retardants, phthalates, the pesticide metabolite pentachlorophenol, synthetic flavonoids and plasticizers including bisphenol A (some have higher affinity to TTR than T4 does itself). Disruptors binding to TTR may not only decrease the levels of T4 and the availability of thyroid hormones to various tissues, but also be targeted for transport and uptake [26]. As for TPO, flavonoids are also known to be potent competitors for T3 and T4 binding to TTR [28].

To exert its biological function, T3 binds to nuclear thyroid receptors inside the target cells, and those receptors act as signal transducers to initiate intranuclear changes in the metabolism of the cell. Hydroxyl PCBs, flame retardants (tetrabromobisphenol A and bisphenol A) and dioxin can activate or inhibit the cellular uptake of thyroid hormones, therefore altering the nuclear thyroid receptor activity and gene transcription. Biliary excretion of both T3 and T4 could also possibly be increased [26,30].

Deiodinase enzymes, which control the production and recycling of thyroid hormones, are sensitive to the interference of PCBs, Food, Drug and Cosmetics (FD&C) red dye #3, octyl-methoxycinnamate, the pesticide

methoxychlor and the toxic metals cadmium and lead. By altering the enzymatic activity, these disruptors lead to a decrease of peripheral synthesis of T3 [26].

Besides deiodinases, a number of diphosphoryl-glucuronosyl transferase or sulfotransferase isoenzymes are responsible for the metabolism of thyroid hormones in the liver, enabling the biliary clearance of glucuronide or sulfate conjugates of T4 or T3 [30]. Once again, hydroxylated PCBs, triclosan, pentachlorophenol, dioxins, acetochlor, phenobarbital, 3-methylcoanthrene and bisphenol A inhibit the enzymes responsible for detoxification reactions of thyroid hormones, thus deregulating the peripheral levels of T3 and T4 and increasing their biliary excretion [26,30]. An increase in both the metabolism and clearance of T3 could also result in a goiter, as the thyroid gland compensates to maintain proper hormone levels [24].

Finally, both TSH and thyrotropin-releasing hormone were found to be affected by TDs, mainly through receptor-binding inhibition mechanisms, compromising the upregulation of metabolism and T3 and T4 production [26]. Of note, one of the most sensitive determinants of thyroid dysfunction is the measurement of serum TSH. Triggered by TDs, elevated TSH levels, as well as iodine deficiency, may induce both goiter growth and the development of thyroid nodules [35]. To date, some epidemiological studies have reported a strong association between serum TSH levels and the risk of malignancy in thyroid nodules and have shown that serum TSH concentration, even within the normal range, is an independent predictor of the presence of thyroid malignancy [36–38]. This could be explained by the trophic effect of TSH on thyroid cancer growth, which is likely to be mediated by the TSH receptors present on tumor cells [36]. Moreover, a lesser degree of TSH suppression is associated with an increased incidence of relapse of differentiated thyroid tumors since these usually retain responsiveness to TSH [39,40]. Therefore, TSH suppression is also an independent predictor of relapse-free survival, and the prognosis is improved with a greater level of TSH suppression on well-differentiated tumors [39,40], which seems to slow down tumor progression.

To summarize, TDs can elicit their own spectrum of alterations on nearly every step of the production and metabolism of thyroid hormones by altering the gland function and regulation **(Table 4.2)** [24]. A prolonged disruption of the pituitary–thyroid axis may be linked to thyroid neoplasia [34]. However, not every TD promotes the development of thyroid neoplasia, as some compensatory mechanisms may ensure a still normal thyroid function, probably as long as the iodine supply is adequate [28].

Financial & competing interests disclosure

This work was supported, in part, by a grant from the Calouste Gulbenkian Foundation (ref. 76636) and Portuguese Foundation for Science and Technology (project: PIC/IC/83154/2007), and further funding from the Portuguese Foundation for Science and Technology by a grant to P Boaventura (SFRH /BPD/34276/2007) and AL Almeida (SFRH/BD/79135/2011). The Institute of Molecular Pathology and Immunology of the University of Porto is an Associate Laboratory of the Portuguese Ministry of Science, Technology and Higher Education and is partially supported by the FCT. The authors have no other relevant affiliations or financial involvement with any organization or entity with a financial interest in or financial conflict with the subject matter or materials discussed in the manuscript apart from those disclosed.

No writing assistance was utilized in the production of this manuscript.

Summary.

- Ionizing radiation is a major risk factor for thyroid cancer.
- Exposure at a young age is a major risk factor for radiation-induced thyroid cancer, and the risk is maximal when exposure occurs below the age of 5 years.
- Any irradiation involving more than 0.5 Gy to the thyroid, especially in childhood, should be viewed with concern.
- Thyroid function, thyroid hormone action in the periphery and feedback regulation could be disrupted by thyroid disruptors at the same time.
- Endocrine disruptor effect can occur in a tissue-specific manner and/or affect more than one target within the thyroid hormone axis.

References

1 Wartofsky L. Increasing world incidence of thyroid cancer: increased detection or higher radiation exposure? *Hormones* (*Athens*) 9(2), 103–108 (2010).

2 Nikiforov YE. Is ionizing radiation responsible for the increasing incidence of thyroid cancer? *Cancer* 116(7), 1626–1628 (2010).

3 Massimino M, Gandola L, Mattavelli F *et al.* Radiation-induced thyroid changes: a retrospective and a prospective view. *Eur. J. Cancer* 45(14), 2546–2551 (2009).

4 Berges O, Belkacemi Y, Giraud P. Normal tissue tolerance to external beam radiation therapy: thyroid. *Cancer Radiother.* 14(4–5), 307–311 (2010).

5 Cardis E, Hatch M. The Chernobyl accident – an epidemiological perspective. *Clin. Oncol.* (*R. Coll. Radiol.*) 23(4), 251–260 (2011).

6 Rubino C, Cailleux AF, De Vathaire F, Schlumberger M. Thyroid cancer after radiation exposure. *Eur. J. Cancer* 38(5), 645–647 (2002).

7 Dickman PW, Holm LE, Lundell G, Boice JD Jr, Hall P. Thyroid cancer risk after thyroid examination with ^{131}I: a population-based cohort study in Sweden. *Int. J. Cancer* 106(4), 580–587 (2003).

8 Sadetzki S, Chetrit A, Lubina A, Stovall M, Novikov I. Risk of thyroid cancer after childhood exposure to ionizing radiation for tinea capitis. *J. Clin. Endocrinol. Metab.* 91(12), 4798–4804 (2006).

9 Boaventura P, Soares P, Pereira D, Teixeira-Gomes J, Sobrinho-Simoes M. Head and neck lesions in a cohort

irradiated in childhood for tinea capitis treatment. *Lancet Infect. Dis.* 11(3), 163–164 (2011).

10 Hayashi Y, Lagarde F, Tsuda N *et al.* Papillary microcarcinoma of the thyroid among atomic bomb survivors: tumor characteristics and radiation risk. *Cancer* 116(7), 1646–1655 (2010).

11 Sinnott B, Ron E, Schneider AB. Exposing the thyroid to radiation: a review of its current extent, risks, and implications. *Endocrine Rev.* 31(5), 756–773 (2010).

12 Bhatti P, Veiga LH, Ronckers CM *et al.* Risk of second primary thyroid cancer after radiotherapy for a childhood cancer in a large cohort study: an update from the Childhood Cancer Survivor Study. *Radiat. Res.* 174(6), 741–752 (2010).

13 Baker SR, Hsieh YH, Maldjian PD, Scanlan MT. Inadvertent thyroid irradiation in protocol-driven trauma CT: a survey of hospital ERs. *Emerg. Radiol.* 16(3), 203–207 (2009).

14 Ron E, Lubin JH, Shore RE *et al.* Thyroid cancer after exposure to external radiation: a pooled analysis of seven studies. *Radiat. Res.* 141(3), 259–277 (1995).

15 Siegel R, Naishadham D, Jemal A. Cancer statistics, 2012. *CA Cancer J. Clin.* 62(1), 10–29 (2012).

16 Collins BJ, Schneider AB, Prinz RA, Xu X. Low frequency of *BRAF* mutations in adult patients with papillary thyroid cancers following childhood radiation exposure. *Thyroid* 16(1), 61–66 (2006).

17 Lima J, Trovisco V, Soares P *et al.* Reply to: low prevalence of *BRAF* mutations in radiation-induced thyroid tumors in contrast to sporadic papillary carcinomas. *Cancer Lett.* 230(1), 149–150 (2005).

18 Soares P, Trovisco V, Rocha AS *et al. BRAF* mutations and *RET/PTC* rearrangements are alternative events in the etiopathogenesis of PTC. *Oncogene* 22(29), 4578–4580 (2003).

19 Dinets A, Hulchiy M, Sofiadis A *et al.* Clinical, genetic, and immunohistochemical characterization of 70 Ukrainian adult cases with post-Chornobyl papillary thyroid carcinoma. *Eur. J. Endocrinol.* 166(6), 1049–1060 (2012).

20 Ory C, Ugolin N, Levalois C *et al.* Gene expression signature discriminates sporadic from post-radiotherapy-induced thyroid tumors. *Endocr. Relat. Cancer* 18(1), 193–206 (2011).

21 Imaizumi M, Usa T, Tominaga T *et al.* Long-term prognosis of thyroid nodule cases compared with nodule-free controls in atomic bomb survivors. *J. Clin. Endocrinol. Metab.* 90(9), 5009–5014 (2005).

22 Diamanti-Kandarakis E, Bourguignon JP, Giudice LC *et al.* Endocrine-disrupting chemicals: an endocrine society scientific statement. *Endocr. Rev.* 30(4), 293–342 (2009).

23 Howdeshell KL. A model of the development of the brain as a construct of the thyroid system. *Environ. Health Perspect.* 110(Suppl. 3), S337–S348 (2002).

24 Brucker-Davis F. Effects of environmental synthetic chemicals on thyroid function. *Thyroid* 8(9), 827–856 (1998).

25 Wolff J. Perchlorate and the thyroid gland. *Pharmacol. Rev.* 50(1), 89–105 (1998).

26 Boas M, Main KM, Feldt-Rasmussen U. Environmental chemicals and thyroid function: an update. *Curr. Opin. Endocrinol. Diabetes Obes.* 16(5), 385–391 (2009).

27 Blount BC, Pirkle JL, Osterloh JD, Valentin-Blasini L, Caldwell KL. Urinary perchlorate and thyroid hormone levels in adolescent and adult men and women living in the United States. *Environ. Health Pers.* 114(12), 1865–1871 (2006).

28 Köhrle J. Environment and endocrinology: the case of thyroidology. *Ann. Endocrinol. (Paris)* 69(2), 116–122 (2008).

29 Langer P. Persistent organochlorinated pollutants (PCB, DDE, HCB, dioxins, furans) and the thyroid – review 2008. *Endocr. Regul.* 42(2–3), 79–104 (2008).

30 Patrick L. Thyroid disruption: mechanisms and clinical implications in human health. *Altern. Med. Rev.* 14(4), 326–346 (2009).

31 No authors listed. IARC Working Group on the Evaluation of Carcinogenic Risks to Humans. Polychlorinated dibenzo-para-dioxins and polychlorinated dibenzofurans. *IARC Monogr. Eval. Carcinog. Risks Hum.* 69, 33–344 (1997).

32 De Groef B, Decallonne BR, Van der Geyten S, Darras VM, Bouillon R. Perchlorate versus other environmental sodium/iodide symporter inhibitors: potential thyroid-related health effects. *Eur. J. Endocrinol.* 155(1), 17–25 (2006).

33 Crofton KM. Thyroid disrupting chemicals: mechanisms and mixtures. *Int. J. Androl.* 31(2), 209–223 (2008).

34 Hard GC. Recent developments in the investigation of thyroid regulation and thyroid carcinogenesis. *Environ. Health Pers.* 106(8), 427–436 (1998).

35 Verburg FA. The association between multinodular goiter and thyroid cancer. *Minerva Endocrinol.* 35(3), 187–192 (2010).

36 Boelaert K, Horacek J, Holder RL, Watkinson JC, Sheppard MC, Franklyn JA. Serum thyrotropin concentration as a novel predictor of malignancy in thyroid nodules investigated by fine-needle aspiration. *J. Clin. Endocrinol. Metab.* 91(11), 4295–4301 (2006).

37 Haymart MR, Repplinger DJ, Leverson GE *et al.* Higher serum thyroid stimulating hormone level in thyroid nodule patients is associated with greater risks of differentiated thyroid cancer and advanced tumor stage. *J. Clin. Endocrinol. Metab.* 93(3), 809–814 (2008).

38 Polyzos SA, Kita M, Efstathiadou Z *et al.* Serum thyrotropin concentration as a biochemical predictor of thyroid malignancy in patients presenting with thyroid nodules. *J. Cancer Res. Clin. Oncol.* 134(9), 953–960 (2008).

39 Biondi B, Filetti S, Schlumberger M. Thyroid-hormone therapy and thyroid cancer: a reassessment. *Nat. Clin. Pract. Endocrinol. Metab.* 1(1), 32–40 (2005).

40 Pujol P, Daures JP, Nsakala N *et al.* Degree of thyrotropin suppression as a prognostic determinant in differentiated thyroid cancer. *J. Clin. Endocrinol. Metab.* 81(12), 4318–4323 (1996).